



**HAL**  
open science

## Impression 3D sans Coffrage de Structures en Terre.

Mahan Motamedi

► **To cite this version:**

Mahan Motamedi. Impression 3D sans Coffrage de Structures en Terre.. Mécanique des matériaux [physics.class-ph]. Université Paris-Est, 2023. Français. NNT : 2023PESC1001 . tel-04579517

**HAL Id: tel-04579517**

**<https://hal.science/tel-04579517v1>**

Submitted on 1 Oct 2024

**HAL** is a multi-disciplinary open access archive for the deposit and dissemination of scientific research documents, whether they are published or not. The documents may come from teaching and research institutions in France or abroad, or from public or private research centers.

L'archive ouverte pluridisciplinaire **HAL**, est destinée au dépôt et à la diffusion de documents scientifiques de niveau recherche, publiés ou non, émanant des établissements d'enseignement et de recherche français ou étrangers, des laboratoires publics ou privés.

# THÈSE DE DOCTORAT



## Scaffold-Free 3D Printing of Earthen Shells Impression 3D de Structures en Terre sans l'Usage de Coffrage

**Thèse de doctorat de l'Université Paris-Est,**

École doctorale n° 528, Ville, Transports et Territoires – VTT  
Champ disciplinaire du doctorat : Architecture, Conception Computationnelle et Construction Robotique

Thèse préparée dans la unité de recherche **GSA de l'École Nationale d'Architecture Paris-Malaquais**  
sous la direction de **Oliver BAVEREL**, Professeur,  
le co-encadrement de **Romain MESNIL**, Docteur,

**Thèse soutenue à l'École des Ponts ParisTech le 29 novembre 2023, par**

**Mahan MOTAMEDI**

### **Composition du jury**

Membres du jury avec voix délibérative :

**Emmanuel DUFRASNES**, Professeur, ENSA, Strasbourg  
**Kristina SHEA**, Professeure, ETH  
**José PINTO DUARTE**, Titre, Penn-State, SCDC  
**Romain ANGER**, Professeur, ENSA, Lyon

Président  
Rapporteuse  
Rapporteur  
Examineur

باشد تا خاک را با نظر بپايديم ...

*Qu'il en soit ainsi, que nous transformions la terre  
en or par notre regard...*

*Let it be so, that we turn the earth into gold  
through our gaze ...*

# Dedication

This dissertation is dedicated to Maurizio, our laboratory director, who sadly passed away. His support was instrumental in my research journey. Maurizio's hospitality and cool attitude will always be remembered, especially when he invited the laboratory researchers to his hometown in Catania, Sicily. Thank you for everything, Maurizio. This work is a tribute to you and your contribution to our laboratory's research efforts.

# Acknowledgement

I want to express my sincere gratitude to my supervisor, Olivier Baverel, for his invaluable support and guidance throughout my thesis journey. His expertise, dedication, and passion for the field have been invaluable in shaping my research and inspiring me to achieve my goals. Olivier's willingness to go above and beyond to provide feedback on my work, offer helpful suggestions, and encourage me has been instrumental in completing my dissertation. His constant support and encouragement have been an irreplaceable source of motivation, and I cannot thank him enough for his time, expertise, and mentorship.

I would also like to thank my friend, colleague, and advisor, Robin Oval. His keen and sharp outlook towards my ideas and research has been an invaluable asset throughout my journey. Robin's insightful feedback, constructive criticism, and helpful suggestions have helped me to better structure my pathway through complex ideas and problems. His support and encouragement have been a driving force behind my success, and I cannot thank him enough for his time, dedication, and guidance.

I am also deeply grateful to my co-supervisor, Romain Mesnil, for his invaluable contributions to my research. Romain's sharp intellect, deep knowledge, and expertise in the field have been instrumental in guiding my research and helping me to overcome some challenges. His constant availability, steadfast support, and insightful advice have been invaluable in shaping my ideas and research. I have had the privilege of working with Romain on several projects since 2018, and I have always benefited from his leads and guidance. I cannot thank him enough for his support, dedication, and mentorship throughout my thesis journey.

Romain Duballet is a highly accomplished researcher in concrete 3D printing whom I had the privilege of working alongside for six months while fabricating his final thesis prototype. Our collaboration was incredibly valuable, providing me with the foundational skills and knowledge necessary to pursue my thesis work. I am extremely grateful to Romain for his mentorship and guidance during this period, and I credit much of my success to the invaluable experience gained through our work together.

I want to extend my heartfelt gratitude to my friend and research assistant, Malo Charrier, for his dedication, support, and sacrifices throughout my research. Malo played a pivotal role in the initial attempts of 3D printing vaults with kaolin clay. I still remember the first successful squinch vault we printed together in 2020 when we had to stay until 9 p.m. at the school. Malo's commitment, hard work, and passion for the project were key to our success. His tireless efforts to work extra hours and his patience and persistence in troubleshooting various issues helped me immensely in overcoming the challenges of the fabrication process. Together, we printed several amazing prototypes, including the prototype of the Multi-vault with

three patches. Malo's contributions to my research are invaluable, and I could not have completed this dissertation without his support.

I also express my sincere gratitude to my colleague and researcher at Navier MSA, Leo Demont, for his technical support during my research period. He has always been there to help me solve problems, especially with the moody robotic arms when they did not feel like working for no reason sometimes. Leo's full-hearted support and guidance have been instrumental in shaping my research and inspiring me to achieve my goals. His dedication and commitment to my success are truly inspiring, and I am incredibly grateful for his support throughout my journey. I also had the privilege of working with Leo on the HOLCIM Hackathon competition project, where we guided the students of Ecole des Ponts Paris tech for the prototype of a reinforced concrete 3D printed block as a component of a building slab. Leo's technical knowledge and experience in the field were invaluable in guiding the students in the project. Working with Romain and Leo on various projects has been a great learning experience for me and I am grateful for their guidance and support throughout my research journey.

I am grateful to have had the support of Krittika Wallia, my friend and research assistant. Krittika took over Malo's role after he departed from Build'in lab, and she was just as supportive and helpful to me. Krittika also sacrificed her extra working hours to help me overcome the challenges of printing overhangs and achieving the right balance with gravity. We experienced numerous failures together, and it was disheartening to see all of our hard work disappear in seconds. However, Krittika was always there to motivate and encourage me to develop new ideas to solve the fabrication problems and push the prototypes further. Her positive attitude and perseverance were essential in keeping me focused and inspired to achieve my goals. I am truly grateful for her support and dedication throughout my research journey.

I also express my gratitude to the rest of the Ecole des Ponts staff, who provided essential support throughout my research journey. In particular, I would like to thank Marie Francois for her kindness and assistance with administrative processes. Her guidance and support made the administrative procedures much smoother, allowing me to focus on my research. I am truly grateful for her help and support.

# Contents

<b>1</b>	<b>Introduction</b>	<b>16</b>
1.1	Motivation . . . . .	16
1.2	Literature Review . . . . .	17
1.2.1	Automation in Construction . . . . .	17
1.2.2	Additive Manufacturing:Implementation in Construction . . . . .	17
1.2.3	Concrete 3D Printing (C3DP) . . . . .	19
1.2.4	Earth 3D Printing (E3DP) . . . . .	23
1.2.5	C3DP vs E3DP . . . . .	26
1.2.6	Shells and Vaults . . . . .	26
1.2.7	Adapting Ancient Vaulting Techniques to 3D Printing: Valuable Lessons Learned . . . . .	28
1.2.8	Minimising Formwork in Construction . . . . .	31
1.2.9	Comparison of the 3D Printing Methods . . . . .	32
1.2.10	Modular Construction and Additive Manufacturing . . . . .	33
1.3	Problem Statement . . . . .	35
1.4	Research Objectives and Methodology . . . . .	36
1.4.1	Objectives . . . . .	36
1.4.2	SF3DP Setups . . . . .	37
1.4.3	Research Methodology . . . . .	38
1.5	Outline . . . . .	39
<b>2</b>	<b>Topological &amp; Geometrical Design: Introduction to Patching design grammar</b>	<b>41</b>
2.1	Introduction . . . . .	41
2.1.1	Outline . . . . .	42
2.2	Funicular Form-Finding . . . . .	42
2.3	From Geometry to Robotic Orders . . . . .	45
2.3.1	Slicing Methods . . . . .	45
2.3.2	Creation of Robotic Trajectories . . . . .	45
2.4	Developing Vault Designs for Structures with Quadrilateral Boundaries	46
2.4.1	Quad Boundaries Typology . . . . .	46
2.5	Patching Design Grammar . . . . .	48
2.5.1	Introduction . . . . .	49
2.5.2	Grammars vs Parametric Design . . . . .	50
2.5.3	Patching Grammar . . . . .	51
2.5.4	Terms of Patching Grammar . . . . .	52
2.5.5	Support Types . . . . .	52

2.5.6	Patch Print Direction . . . . .	53
2.5.7	Supports Junctions . . . . .	54
2.5.8	Patching Grammar Rules . . . . .	55
2.5.9	Rules Naming . . . . .	57
2.6	Design Strategies Utilising Patching Grammar . . . . .	58
2.6.1	Generative Design Strategy . . . . .	58
2.6.2	Analytical Design Strategy . . . . .	62
2.6.3	Topology Finding of the Patches Using the Delaunay Analytical Tool . . . . .	64
2.6.4	Topology Finding of the Patches Using Heat Analytical Tool	64
2.7	Geometry Tuning . . . . .	68
2.8	Roofing the Conventional 3D Printed Houses . . . . .	71
2.9	Conclusion . . . . .	73
<b>3</b>	<b>Material, Mechanics &amp; Structural Analysis</b>	<b>77</b>
3.1	Introduction . . . . .	77
3.2	Methods to Increase the Mechanical Performance of Earth-Based Mortars . . . . .	78
3.3	Rheological Requirements For Clay 3D Printing . . . . .	80
3.3.1	Pumpability, Workability and Buildability . . . . .	80
3.3.2	Stiffness Requirements . . . . .	81
3.3.3	Yield Criterion of Soils and Rocks . . . . .	83
3.3.4	Influence of Water Content on the Mechanical Properties of Soils . . . . .	85
3.3.5	Drying Mechanism of Soils . . . . .	88
3.4	Analytical Consideration . . . . .	89
3.4.1	Geometrical Effects . . . . .	89
3.4.2	Drying and Increase in Mechanical Performance . . . . .	93
3.4.3	Characteristic Structuration Time . . . . .	94
3.4.4	Impact of Heating on Crust Layer Formation . . . . .	94
3.4.5	Effect of Environment and Energy Consumption . . . . .	95
3.5	Experiments . . . . .	96
3.5.1	Wind-Tunnel Experiment . . . . .	96
3.5.1.1	Experimentation Environment . . . . .	97
3.5.1.2	Experiment Protocol . . . . .	97
3.5.1.3	Experiment Results . . . . .	98
3.5.2	Squeeze Test . . . . .	102
3.5.3	Slug Test . . . . .	104
3.5.4	Vane Test . . . . .	105
3.5.5	Printing Cylinders with Different Heating Methods . . . . .	106
3.6	Structural Analysis . . . . .	109
3.6.1	Mixture Properties . . . . .	110
3.6.2	Step-Wise Elastic Buckling Analysis . . . . .	110
3.6.3	Step-Wise Plastic Buckling Analysis . . . . .	114
3.6.4	Slicing Pattern Effect on Structural Behaviour . . . . .	114
3.6.5	Cross-Section Design . . . . .	115
3.6.6	Finite Element Analysis . . . . .	117
3.7	Conclusion . . . . .	120



<b>4</b>	<b>Fabrication &amp; Automation</b>	<b>122</b>
4.1	Introduction . . . . .	122
4.2	Geometric Data to Robotic Commands . . . . .	123
4.3	Small . . . . .	123
4.4	Medium . . . . .	127
4.5	Large . . . . .	135
4.5.1	U Shape Wall ( $120 \times 90 \times 23h$ cm) . . . . .	139
4.5.2	Squinch on a Wooden Wall . . . . .	140
4.5.3	Interlocking Module . . . . .	146
4.5.4	How to Bind Fresh Clay to an Air-Dried Clay? . . . . .	148
4.5.5	Conclusion . . . . .	149
<b>5</b>	<b>Conclusion</b>	<b>152</b>
5.1	Key Findings . . . . .	152
5.2	Limitations and Future Work . . . . .	153

# List of Figures

1.1	Detailed Classification of Digital Fabrication Methods in Construction, Showcasing the Spectrum of Technologies from Additive to Subtractive Manufacturing. . . . .	18
1.2	The Solar Sinter System in Action: Utilizing Solar Energy for 3D Printing with Sand. This innovative approach demonstrates the potential for sustainable manufacturing processes in arid environments [137]. . . . .	25
1.3	Squinch Vault . . . . .	29
1.4	Barrel Vault . . . . .	30
1.5	Ground-Supported Barrel Vault . . . . .	30
1.6	Dome . . . . .	31
1.7	Overview of Various Scenarios for Scaffold-Free 3D Printing Methods, Demonstrating the Range of Applications and Techniques in the Context of Earthen Architecture. . . . .	38
2.1	Evolution of Construction Techniques: From Mason-Laid Brick Layers to Six-Axis Robot-Printed Layers. This comparison illustrates the transformative shift towards automation, showcasing advancements in precision and efficiency in building methods. . . . .	43
2.2	Replicating Vaulting Techniques with a Six-Axis Mobile Robot: Bridging Traditional Craftsmanship and Robotic Precision . . . . .	43
2.3	Surface Bond Comparison: (a) 2.5D Printing Topology vs. (b) 3D Printing Topology - Analyzing Layer Adhesion and Structural Integrity	44
2.4	Funicular Form-Finding Process . . . . .	44
2.5	Characteristics of Different Slicing Methods for Geometry - A Comparative Analysis of Techniques and Outcomes . . . . .	45
2.6	Four-Step Process from Geometry to Printing a Shell: Conceptualization, Design, Slicing, and Fabrication . . . . .	46
2.7	Steps of Converting a Quad Boundary into a Circular Boundary: Sequential Transformation . . . . .	47
2.8	Comparison of Two Patching Methods for Quad Boundaries . . . . .	47
2.9	Four Patching Strategies for Different Types of Quads: A Comprehensive Analysis of Techniques and Applications . . . . .	49
2.10	Patching Design Process Overview . . . . .	50
2.11	Elements of Multi-Vault Structures: Identifying Key Components and Their Interconnections . . . . .	52
2.12	Types of Supports in Patching Grammar - A Detailed Classification and Their Functional Roles . . . . .	53

2.13	Comparative Analysis of Two Squinch Geometries with Varied Support Conditions: Effects on Print Direction . . . . .	54
2.14	Illustration of a Pole in a Quad Mesh: Highlighting Pseudo Quad Faces and Mesh Topology . . . . .	55
2.15	Examples of Support Junctions in Boundary Design: A Visual Guide to Types and Connections . . . . .	56
2.16	Laws Governing the Combination of Supports and Their Classification	56
2.17	Support Configurations . . . . .	57
2.18	Pole Positioning Strategies in Support Boundary Configuration . . . . .	58
2.19	Catalogue of Primary Rules in Patching Design Grammar . . . . .	59
2.20	Catalogue of Hybrid Rules in Patching Design Grammar . . . . .	60
2.21	Comparative Analysis of Generative vs. Analytical Design Approaches in Patching Grammar . . . . .	61
2.22	The Generative Design Process:A Step-by-Step Overview . . . . .	62
2.23	Three Instances of User-Designed Decomposition for Target Boundaries via Generative Design Approach: Showcasing Customisation and Innovation by users through Patching Design Grammar . . . . .	63
2.24	Application of the Analytical Design Approach via Delaunay Method on User-Defined Geometries . . . . .	65
2.25	Application of the Analytical Design Approach via Delaunay Method on User-Defined Boundaries . . . . .	66
2.26	Topology-Finding Process Across Four Different Boundaries Using the Delaunay Analytical Method . . . . .	66
2.27	Analytical Design Using the Heat Method for Two Different Boundaries: Application of Heat Method Geodesic Distance in Patching Design Grammar - A Comparative Study . . . . .	67
2.28	Analytical Design Utilising the Heat Method for Geometries with Voids	68
2.29	Tuning Multi-Vault Patches' Geometries in Three Different Manners: A Comparative Analysis of Adjustments and Outcomes . . . . .	69
2.30	Analytical Comparison of Three Geometry Tuning Methods: Evaluating Structural Integrity . . . . .	70
2.31	Step-by-Step Increase of Curvature on a Selected Patch of a Multi-Vault by Applying Force in Normal Direction: Process and Structural Transformation . . . . .	72
2.32	Effects of Patch Curvature on Stresses Generated in Its Ribs: Analysing the Relationship Between Curvature and Structural Integrity	72
2.33	The ICON-3D Printed House: Illustrating the Conventional Use of 3D Printing in Residential Construction with Roofs Constructed by Labour Force . . . . .	73
2.34	Proposed Roof Design for the ICON-3D Printed House: Integrating Patching Technique in the 3D Printing Process for Residential Buildings	74
3.1	Different Methods of Applying Heat to Fresh Mortar in the 3D Printing Process . . . . .	78
3.2	(a) Nominal Printing Regime vs. (b) Free Deposition Due to Material Settling . . . . .	82

3.3	Comparative Representation of Undrained vs. Drained Conditions in the 3D Printing Process . . . . .	85
3.4	Stages of Water Content and Compaction in a 3D Printed Layer of Kaolin Clay Mixture: Analyzing the Evolution of Material Properties . . . . .	86
3.5	The Wall Considered in This Study . . . . .	89
3.6	Comparative Analysis of Three Walls with Equivalent Material Volume: Assessing Design Efficiency, Structural Performance . . . . .	92
3.7	Structural Analysis Data for Three Walls with Equivalent Material Volume . . . . .	92
3.8	Strength Evolution of Speswhite Kaolin Clay Over Time with a Drying Rate of $\Delta = 2kg/m^2/hour$ . . . . .	93
3.9	Appearance of Crust Layer Due to Overheating . . . . .	95
3.10	Wind Tunnel Setup for Clay Evaporation Experiment . . . . .	97
3.11	Wind-Tunnel Experimentation Setup . . . . .	98
3.12	Fabricated Wind Tunnel Inside an Oven . . . . .	99
3.13	Results of the Drying Experiment . . . . .	101
3.14	Comparison Between Theoretical Predictions and Experimental Results . . . . .	102
3.15	Mould for Casting Material Samples for Squeeze Test . . . . .	103
3.16	Squeeze Steps of a Material Sample . . . . .	103
3.17	Slug mass measurements as a function of flow rate. Error bars indicate standard deviation, and the dashed line corresponds to the average of all measurements. . . . .	105
3.18	Vane Test for In-Field Measurement of Critical Shear Strength . . . . .	106
3.19	3D Printed Cylinders Using Different Heating Methods . . . . .	106
3.20	Designed Cylinder for Layer Heating Experiment . . . . .	108
3.21	Possible Failure Modes During the 3D Printing Process of Funicular Forms with Fresh Unreinforced Mortars . . . . .	110
3.22	Impact of Geometry and Boundary Modifications on the Structural Buckling of a Squinch: Comparative Analysis of Design Variations and Their Effects . . . . .	113
3.23	Step-Wise Analysis of Thrust Network in the Section of a Shell . . . . .	114
3.24	Impact of Slicing Patterns on the Inter-Layer Bonding of a Printed Overhang Structure . . . . .	115
3.25	Slicing Patterns and Their Effect on Structural Integrity . . . . .	116
3.26	Characteristics of a Shell's Cross-Section Design . . . . .	117
3.27	Different Infill Patterns for the Cross-Section of a Shell . . . . .	118
3.28	The FEA process in KARAMBA . . . . .	119
3.29	Material Component of Karamba Plugin and the Input Parameters . . . . .	120
4.1	Creating Robotic Procedures in the Hal Robotics Plugin for Grasshopper: A Step-by-Step Workflow Illustration . . . . .	124
4.2	Robot's Inability to Reach the Target Plane . . . . .	125
4.3	Robot Self-Clashes Due to Close Target Constraint . . . . .	125
4.4	Robot-Tool Clashes Due to Improper Orientation of the Target Plane . . . . .	126
4.5	Small Prototyping Setup . . . . .	126
4.6	Prototype of a Multi-Vault Constructed Using a Small Prototyping Setup and Wood-Based Material . . . . .	128
4.7	The Medium Scale Prototyping Environment . . . . .	129

4.8	Schema of the Clay Extruding System . . . . .	130
4.9	The First Medium Prototype: A Double-Layered Squinch - Detailed View of Construction and Layering Technique . . . . .	132
4.10	Displacement Occurring in the Last Layers of the Printing Process . .	133
4.11	The Buckled Squinch . . . . .	134
4.12	Second Medium Prototype: A Multi-Vault with Two Squinches and One Pendentive . . . . .	135
4.13	3D Printing of an Intermediate Patch (Pendentive) Between Self-Supporting Independent Patches (Squinches): Fabrication of a Custom-Made Nozzle to Minimize Robot Movement Constraints . . .	136
4.14	The Large-Scale Prototyping Environment . . . . .	138
4.15	The Material Extrusion System . . . . .	138
4.16	Components of the MAI 4MultiMix 3D Pump: An Exploded View Diagram Highlighting Key Parts . . . . .	139
4.17	Prototype of The U-Shape Wall . . . . .	141
4.18	Comparison of Two Squinch Geometries . . . . .	142
4.19	Wooden Wall as Support for Squinch Prototype . . . . .	143
4.20	Print Process of the Squinch with Straight Crest . . . . .	144
4.21	Print Process of the Squinch with Positive Curvature Crest . . . . .	145
4.22	3D Representation of the Printing Process for the Squinch with Positive Curvature Crest . . . . .	147
4.23	Process of Planting Screws to Prevent The Layers Detachment . . . .	148
4.24	3D Printing an Interlocking Module with Heat Assistance: A Comparative View Using One vs. Two Heat Guns for Enhanced Structural Build-Up . . . . .	149

# List of Tables

1.1	Showcasing State-of-the-Art 3D Printing Systems in Construction . .	20
1.1	Showcasing State-of-the-Art 3D Printing Systems in Construction . .	21
1.2	Comparative Overview of Concrete vs. Clay 3D Printing Aspects . .	27
1.3	Comparative Analysis of 3D Printed Projects . . . . .	33
1.4	Comparison of 3D Printing Regimes . . . . .	34
1.5	Comprehensive Classification of 3D Printing Setups for Scaffold-Free 3D Printing (SF3DP) . . . . .	37
2.1	Analytical Comparison of Geometrically Tuned Patches Using Three Different Methods: Assessing Structural Analysis Results . . . . .	70
3.1	Drying rate of Speswhite kaolin clay in the wind tunnel experiment (in $\frac{gr}{min}$ ). . . . .	100
3.2	Results of the Squeeze Test on Four Cylindrical Speswhite Kaolin Clay Mixture samples.(Water content = 56% . . . . .	103
3.3	Printing Process Without Heat or Wind Flow . . . . .	107
3.4	Printing Process with Two Ventilators . . . . .	107
3.5	Printing Process with Two Industrial Heaters . . . . .	108
3.6	Printing Process with One Heat Gun . . . . .	109

# Résumé

Cette thèse présente une enquête complète sur le domaine émergent des techniques d'impression 3D pour les structures en terre dans la construction, en fusionnant les anciennes techniques de voûtes issues de l'architecture du désert avec les technologies modernes d'impression 3D. L'étude est motivée par le besoin croissant de solutions de construction durables et rentables. Elle commence par une revue de la littérature approfondie qui contextualise le travail dans le paysage plus large de l'impression 3D dans la construction et la science des matériaux.

La recherche introduit de nouvelles considérations de conception, en se concentrant spécifiquement sur la grammaire de conception de Patching et la recherche de formes funiculaires, afin d'optimiser l'intégrité structurelle et la qualité esthétique des structures en terre. Une analyse rigoureuse de la mécanique des matériaux est menée, examinant la résistance des mortiers à base de terre et les exigences rhéologiques pour l'impression 3D d'argile.

Le manuscrit explore en outre les méthodes d'automatisation et de fabrication, en employant la création d'ordres robotiques et le prototypage à diverses échelles pour valider les résultats théoriques. Le travail aboutit à des idées clés qui ont le potentiel de faire progresser considérablement le domaine de l'impression 3D dans la construction, en particulier avec des matériaux terrestres. Des recommandations pour des travaux futurs sont également fournies, décrivant les prochaines étapes pour des applications pratiques et des recherches supplémentaires. Dans l'ensemble, ce travail présente une approche novatrice pour la construction durable dans l'industrie AEC en mariant des anciennes techniques de voûtes avec une technologie de pointe.

# Abstract

This dissertation explores the fusion of ancient vaulting techniques from desert architecture with modern 3D printing technologies, specifically focusing on earth-based materials. By leveraging state-of-the-art fabrication and computational design tools, the study aims to minimise material usage and the construction footprint on the environment. The first chapter lays the groundwork, covering automation in construction, additive manufacturing, and scaffold-free building methods. The second chapter delves into design strategies for creating scaffold-free vaults, employing the 'Patching' design grammar for design variations. The third chapter tackles material considerations in clay 3D printing, introducing the "Layer Heating" method for 3D printing with saturated earth-based mortars and discussing finite element analysis techniques tailored for this material. The fourth chapter presents the practical challenges and opportunities encountered when 3D printing prototypes at various scales. The dissertation concludes by summarising key insights and outlining avenues for future research. Overall, this work presents a novel approach to sustainable construction in the AEC industry by marrying ancient vaulting techniques with cutting-edge technology.<sup>1</sup>

---

1. The video of the defence of this dissertation can be found at [96]



# Chapter 1

## Introduction

### 1.1 Motivation

Today, the planet Earth is becoming warmer and warmer as time passes. We can't help to make it less warm than it is, but we can keep it as it is and stop it from becoming warmer. The main reason for this global warming is the carbon emission from human activities such as agriculture, farming, factories, buildings, cars, and planes. Building and construction activities are responsible for 30-38% of emitted carbon worldwide [29, 78]. In addition, the construction sector heavily relies on valuable natural resources like raw materials and potable water. Furthermore, it generates construction waste by utilising these raw material resources, such as the remains of wooden scaffolds following construction [47, 14, 119]. Consequently, the construction industry must prioritise sustainable development practices for cities and buildings to safeguard our planet.

Construction is a large industry worldwide. It consists of 6% of global GDP<sup>1</sup> and is going to have 14.7% of global GDP by 2030 [133, 29]. Construction companies consistently seek productiveness and solutions for reducing costs. On the other hand, the studies strongly suggest that productivity in the construction industry has been declining in recent decades worldwide[12] due to numerous reasons such as labourer's resistance to change, declining actual labourer costs and poor data interoperability [82].

During the last decade, additive manufacturing has been studied abundantly to be integrated into the construction industry, promising increased construction efficiency and lowering construction costs. In other words, additive manufacturing can give construction companies what they search for, reducing construction costs and increasing productivity by automation in construction. Although the construction industry so far has managed to develop highly productive systems without the help of robots, there are specific areas of application that the industry would benefit from the robot application. The main ones are the application of robots in the construction process, which can produce better quality with faster production [72]. On the other hand, clay and earth-based materials are of great interest as 3D printing materials thanks to their ease of use, recyclability and reusability [3], which gives an additional advantage to additive manufacturing as a construction method. Therefore, this research addresses sustainable construction development through the additive manufacturing of earth-based materials.

---

1. Gross domestic product

## 1.2 Literature Review

### 1.2.1 Automation in Construction

The idea of automation in construction is not very recent. The first research on automation in construction dates back to the 1970s in the former Soviet Union [138]. Despite being one of the oldest and most economically influential industries, until very recently, the construction industry was one of the most unfamiliar fields to the robotics and automation community and slowed in response to innovation. Although a very advanced industry historically, construction is not considered the most sophisticated sector today [6]. Throughout history, ancient civilisations have demonstrated remarkable innovation in construction, evident in structures like pyramids, the Acropolis, Persepolis, ziggurats, and cathedrals. This highlights the pioneering nature of the construction field. However, over the past eight centuries, the construction industry has not experienced a substantial evolution, apart from adopting industrial construction tools over manual ones. While there have been minor changes in the building erection process, such as the replacement of old pulleys with gantry cranes and the substitution of human force for diesel trucks, the underlying principles of construction have largely remained unchanged. The transition from wooden or earthen structures to steel and concrete is another notable shift. Nevertheless, the industry has not fully harnessed the potential of digitisation, and as a result, construction remains one of the least digitalised sectors in the global economy to date [6, 78]. On the other hand, industries such as automobiles, electronics, trains, aircraft, farming, etc., have increased their productivity several times more than construction by exploiting the advantages of computer-integrated manufacturing (CIM). Furthermore, studies show that the labourer productivity in manufacturing industries is continuously rising, whereas the labourer productivity in the construction industry has been decreasing [12]. Automation in construction can significantly reduce the cost of buildings and increase the quality of construction by reducing construction discrepancies. since the 80s, pioneer construction companies have transitioned from manual to semi-automated construction. The application of robotics in construction is mostly applied to finishing the building interior, such as ceiling and floor panel installation, plumbing positioning, robot for setting concrete walls, erection of the building skeleton, construction of walls and vertical elements or other applications in civil infrastructure such as tunnels and bridges [89, 72]. Digital fabrication is a sub-field of automation in construction. *Digital fabrication* is a common name used in AEC<sup>2</sup> for describing the fabrication of building elements using CAM<sup>3</sup> tools. Figure 1.1 shows different principal recognised digital fabrication methods that are used in the construction industry [80]. The focus of this research is on the Additive method of digital fabrication using digitally controlled nozzles.

### 1.2.2 Additive Manufacturing: Implementation in Construction

Additive manufacturing is a rapidly growing technology that is being integrated into manufacturing and our day-to-day lives. The term additive manufacturing

---

2. Architecture, engineering and construction  
3. Computer aided manufacturing

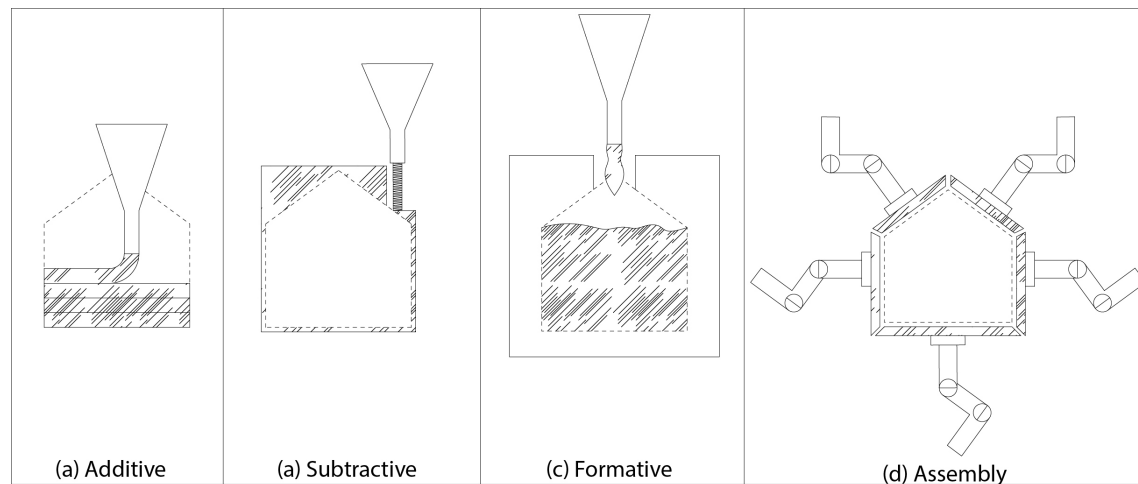


Figure 1.1 – Detailed Classification of Digital Fabrication Methods in Construction, Showcasing the Spectrum of Technologies from Additive to Subtractive Manufacturing.

is also labelled by a variety of names such as three-dimensional (3D) printing, rapid prototyping (RP), layered manufacturing (LM) or solid free-form fabrication (SFF) in commercial environment[13]. Additive manufacturing is attributed to the objects' fabrication with the material layer's deposition wisely. With the aid of 3D modelling software, users can design their objects. Then they can use STL<sup>4</sup> file producing software<sup>5</sup> to convert their geometry into triangular faces or a list of connected x,y and z coordinates<sup>6</sup>. The smaller the triangular faces, the more precise the geometry approximation will be. Then, the approximated geometry should be sliced into planar contours in which the geometry is approximated for the second time. Again, the lower the distance between these planar contours, the more precise and close to the initial geometry the approximation will be.

Additive manufacturing (AM) was developed in 1980 with the first form of 3D printing called stereolithography (SLA). Since then, many other additive manufacturing systems such as SLS<sup>7</sup> and FDM<sup>8</sup> have been developed. Many other developed systems of additive manufacturing can be found in [150].

Until the last decade, additive manufacturing has been practised in many industries, such as industrial design, medicine, automotive, aeronautics, aerospace, etc. Contrary to other industries, construction has been slow to take advantage of automated additive manufacturing techniques. Nevertheless, additive manufacturing was used in architecture to fabricate architectural models as supplementary material to architectural blueprints [106]. since the last decade, with the emergence of additive manufacturing systems on a large scale, such as D-shape and contour crafting, the construction sector is making a breakthrough among other industries. Since the last decade, additive manufacturing using digital fabrication tools such as industrial arms, gantry cranes and cable-driven robots has taken the attention of construction companies as a substitute for conventional construction

4. Stereolithography or Standard Tessellation Language or standard triangulation language

5. In 3D Printing community this software are known as slicers

6. Mesh

7. selective laser sintering

8. fused deposition modelling

techniques such as casting concrete with the aid of wooden or steel pallets and moulds executed by labourers [111, 87, 52]. The advantages of automated additive manufacturing over traditional construction techniques can be listed as follows:

1. saving material resources by fabrication of structurally efficient buildings in which the material is only placed where it is needed.
2. significantly reducing the construction and demolish waste.
3. Reducing construction cost and waste for formwork.
4. Economically interesting by the decrease of on-site labourers thanks to automation with digital CAM<sup>9</sup> tools.
5. Safety is another advantage of using robots instead of labourers on construction sites.
6. Productivity in time and quality of the construction.
7. Handling complex tasks which can not be done by human labourer .
8. Reducing the delays of the project.
9. Possibility of individualisation and customisation.

For all the above-mentioned points, the additive manufacturing technique, especially using concrete, has been practised among the pioneer construction companies.

### 1.2.3 Concrete 3D Printing (C3DP)

Concrete is used worldwide as the most used construction material. It is considered the second most frequently used material on our planet. This is due to its several benefits as a construction material, including low production cost, mouldability into various shapes, high thermal resistance and relatively high durability [113]. In concrete 3D Printing, a digitally controlled nozzle precisely extrudes concrete layer by layer. This technique has been extensively researched by several research institutions and companies over the last decade. The first pioneer of this technique was B.Khoshnevis, who developed a 3D Printing process using a gantry crane and named it Contour Crafting in 2004, intending to print buildings on the scale of dwellings.

In the present day, numerous companies across the globe are engaged in concrete printing for building construction. Some prominent examples include Winsun (China), Total Kustom, Wasp, and Apis cor. For a comprehensive list of concrete 3D printing practitioners in the construction industry and their respective records of 3D-printed projects, please refer to the source [58]. It provides detailed information on the subject.

The main advantage of the concrete 3D printing approach in construction is that it can manufacture complex, nonstandard geometries and details rapidly. The concrete 3D printed houses are economically interesting and fast in production; For example, a 38 square meters 3D Printed house by Apis cor company only cost 10k dollars which means 275 dollars per square meter, and it took only 24 hours to be constructed [136].

The most common challenges in concrete 3D printing are as follows:

- 
9. Computer-aided manufacturing

Table 1.1 – Showcasing State-of-the-Art 3D Printing Systems in Construction

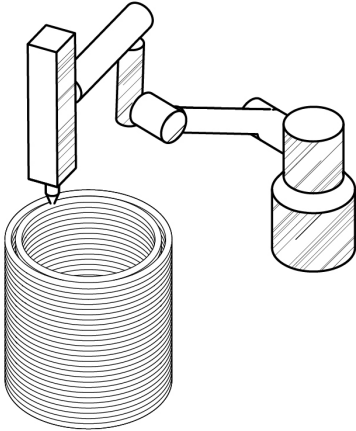
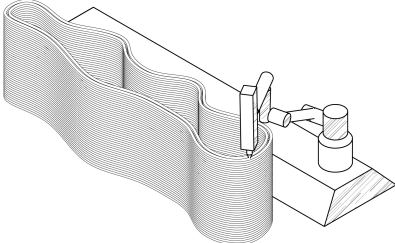
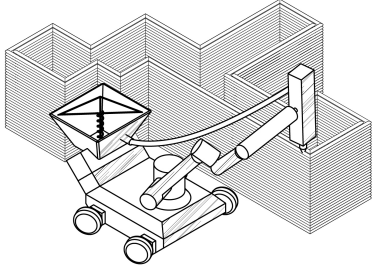
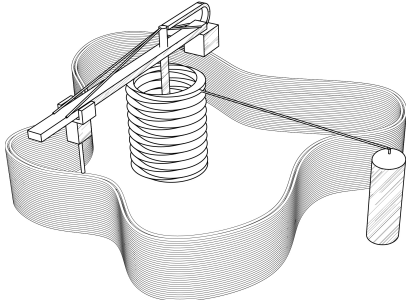
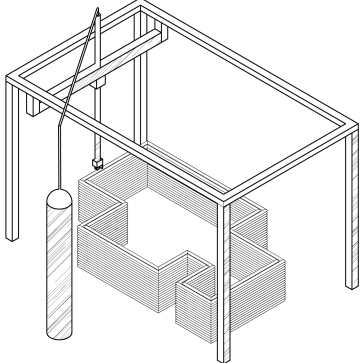
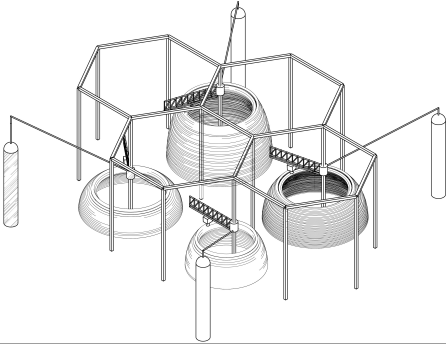
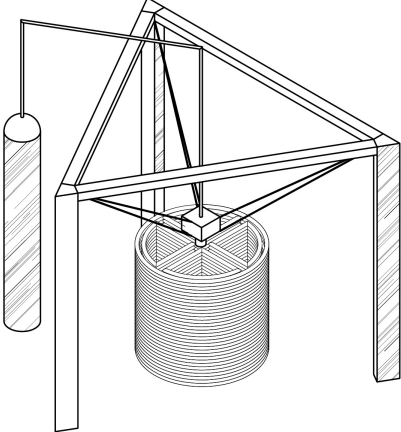
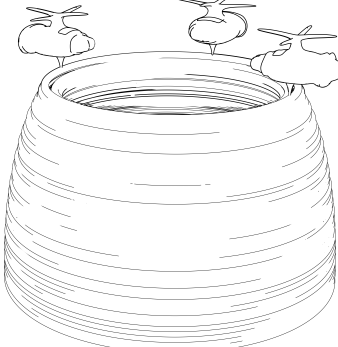
System	Demonstration	Pros	Cons
Robotic arm		High flexibility in orientation of the extrusion head	- Limited size - Not suitable for in-situ printing
Robotic arm on a track		- High flexibility in orientation of the extrusion head. - Ability to print in large scale in one direction (Track).	- Limited size - Not suitable for in-situ printing
Mobile robotic arm		- High flexibility in orientation of the extrusion head. - No restriction in printing scale (Except for the vertical dimension).	- Possible calibration and precision discrepancies
Crane		- Suitable for in-situ construction	- Limited size - Limited in joints position (Only X,Y,Z) - Stays inside the building after the printing process
Gantry crane		- Suitable for in-situ construction	- Limited size - Limited in joints position (Only X,Y,Z)

Table 1.1 – Showcasing State-of-the-Art 3D Printing Systems in Construction

System	Demonstration	Pros	Cons
Multi-crane		- Scalability	- Long installation time. - Limited in head orientation. - Limited in Z dimension
Cable-driven robot		- Low cost installation - High flexibility	- Limited dimension
Swarm drones		- Unlimited dimensions. - Possibility of print in not accessible environments.	- Low precision

1. **Scalable printing setup:** Depending on the structure scale, 3D printing requires a modular, transportable printer that must be as large as the produced structure.
2. **Occurrence of cold joints in between layers:** Another challenge for the printing of the concrete is controlling the rheology and printing process speed to avoid the occurrence of the cold joint. [44],[74].
3. **Challenge in reinforcement by induced fibres:** One of the most challenging aspects of concrete 3D printing is the integration of induced reinforcing fibres in printing to increase the tensile resistance of printed elements. There are researchers such as [19] that are working on this subject.
4. **Surface quality and finishing:** The fourth challenge is about the surface finishes and quality of the print. To have consistency in the shape and geometry of the layers, the printing parameters and the material's rheology must be continuously controlled and tuned to have an acceptable surface

finishing result. However, even if the rheology and printing parameters are perfectly respected, due to the nature of layer-by-layer printing, the finishing surfaces must be post-processed to have a competitive surface quality with moulded concrete.

### 5. Controlling the material deformation.

The list of 3D Printing systems for construction and their features are represented in table 1.1. Four main concrete 3D printing setups are typically used in research centres and 3D printing companies:

1. **6-axis arms:** The 6-axis robots can perform complex tasks and are highly flexible in joint position. However, the dimension of these robots is typically fixed, making the printing scale limited. There is research on developing mobile robots for 3D Printing purposes, such as [33] and [154]. Such projects will lead to setups that are flexible in movement and scalability.
2. **Gantry cranes:** These setups are mostly used by construction companies to print vertical elements of the buildings, such as walls and columns. These setups are convenient for large-scale printing. However, gantry cranes are not as flexible as 6-axis- robots as they have the freedom to move only in 3 or 4-axis. The assembly of these setups are considered to be costly.
3. **Crane:** Similar to gantry cranes, simple cranes work on a 3-4 axis. The difference between the cranes and gantry cranes is that the cranes are typically installed in one pile and are positioned in the centre of the working space, whereas the gantry cranes are installed on two piles and surround the working area. The cranes are mostly used to print buildings with circular plans.
4. **Cable driven robots:** These setups are similar to gantry cranes concerning the surrounding working area. However, these setups are easier to install and usually cover larger working spaces. Furthermore, if the cable-driven robots have 6-axis arms at head level, they can have compelling reachability and flexibility. The implementation of the cable-driven robots is discussed in some research such as [7],[69],[153]

From a material perspective, concrete 3D printing has undergone extensive study over the past decade. One crucial aspect is the pumpability of fresh concrete mortar, which requires sufficient fluidity to be pumped from the concrete reservoir to the head of the concrete printing system. Subsequently, the material needs to gain enough strength to support its weight without deforming (workability) and withstand the weight of additional layers (buildability). Therefore, the material must be thoroughly examined from both fluid mechanics and solid mechanics perspectives to ensure its suitability for the printing process. This entails understanding and optimising the material's rheological properties during the printing operation.

To manipulate and adjust the structuration rate of fresh concrete for optimal printability, the use of admixtures is a common practice. These admixtures play a crucial role in controlling the rate at which the material's yield strength increases, considering various printing parameters such as robot speed, printing vertical speed, extrusion rate, layer thickness, and height. By carefully selecting and adjusting the admixtures, it becomes possible to fine-tune the rheological properties of the concrete mix to meet the specific requirements of the printing process. This allows for better

control over the material's flowability and strength development, ensuring successful and efficient concrete 3D printing operations.

### 1.2.4 Earth 3D Printing (E3DP)

Nowadays, raw earth has become a privileged material for the construction of contemporary ambitious projects [127]. Indeed, the earth is a material which does not degrade [46]. The wood deteriorates, the metal rusts, the stone and cement can be attacked chemically, and in general, all the materials alter over time. But the earth remains the same since it is already an altered material [46]. This character makes the earth special and valuable for construction. Furthermore, Construction using earth materials is a great solution to reduce the environmental impact of construction. Earth is one of the oldest and, till now, intensively used natural building materials [135]. Around 30% of the world's population still lives or works in buildings constructed from the earth. Most of them dwell in simple huts of rural communities or traditionally hand-crafted buildings. In addition, many people looking for healthy, environmentally friendly buildings in so-called developed societies experience the benefits of earthen construction materials [135]. Moreover, unlike reinforced concrete, the earth can be recycled and returned to nature after the building's lifetime if the material is used in raw condition. Construction with earth-based materials can significantly reduce construction waste and exploitation of virgin materials such as wood, steel or cement from nature, the embodied energy of buildings and increasing thermal comfort [9] in the buildings. According to a study highlighted in [56], 3D-printed earth structures demonstrate enhanced thermal conductivity when compared to traditionally constructed earth structures of the same dimensions. This finding suggests that the thermal performance of 3D-printed earth buildings is more efficient, potentially offering benefits in terms of energy efficiency and thermal comfort. Despite efforts to reintroduce earthen structures into modern construction, they are less prevalent than concrete structures in developed societies. As a result, the earth extracted for building and infrastructure purposes often goes to waste due to the lack of a viable solution for utilising it as a primary construction material. The diminished use of earthen structures can be attributed to two main factors. Firstly, these structures are susceptible to adverse weather conditions such as rain, floods, and earthquakes. Raw earth has lower yield strength and mechanical properties compared to industrial materials. However, there are examples of earthen structures that have demonstrated stability, durability, and the ability to span large distances when properly designed and constructed. The second reason is the inherent weight and material consumption associated with earthen structures. This made them less desirable than alternative construction methods using lighter materials like concrete and steel. The recent advancement in numerical software and hardware can help the earthen material return to the construction industry, primarily through 3D printing [55]. Additive manufacturing is a construction method in which we can use material wisely. It offers the potential to design and build lightweight and resistant structures against imposing loads through topology and geometrical optimisation. Using earth in additive manufacturing is an excellent solution for developing a sustainable and low-environment-impacting construction solution. Furthermore, to reduce the carbon footprint related to housing construction, a large part of the scientific community considers the



replacement of cement concrete by unfired earth-based materials as a promising route. CRAterre [28] is one of the most advanced institutions that promote the earth as a contemporary material for construction. Indeed, it is a building material with very low embodied energy [118]. However, raw earth suffers from a poor image and difficulty meeting modern productivity standards and passing some durability tests designed for industrial materials [147]. Many researchers are studying the low reliability of earth-based material for industrial construction usage by increasing the mechanical performance of earth using stabilisation and fibres for construction with rammed earth technique [99] and recently with 3D printing technique. The earth is an omnipresent material which can be extracted locally for construction, reducing the embodied energy of the material for transportation [102]. The raw earth can return to nature after the life cycle of the building and make the construction demolition waste zero [73]. Integrating digital fabrication and the earth is a new solution for the sustainable development of cities. However, this domain is still in its infancy. The attempts for digital manufacturing of earth-based materials can be categorised by type of material as follows:

1. Clay and ceramics
2. Rammed earth
3. Sand
4. Adobe/cob

### **Clay and Ceramics**

In recent decades, the advent of a novel technology for the 3D printing of clay opened up new sustainable possibilities in construction [132]. The earth-based material such as clay has been used in additive manufacturing for the fabrication of decorative elements falling into the category of ceramics [20], [120]. These elements are processed and cooked after printing. The buildings also could be cooked after the printing process to have an increase in compressive strength if needed. A variety of additive processing methods for ceramic masses have been researched. Study in [122] reviews the integration of parametric design with clay 3D printing.

### **Rammed Earth**

One of the examples of constructing with earth using advanced techniques is the off-site crane-based production of rammed earth in the projects of Martin Rauch and Herzog and Demeuron architects for the construction of the Ricola's herb centre in Laufen [51].

### **Sand**

An example of an attempt at digital fabrication using sand can be attributed to the nominal work of Markus Kyser for printing objects using his special SLS printer for sintering the sands of the desert and printing objects without any temporary support thanks to the nature of SLS printing system [137].

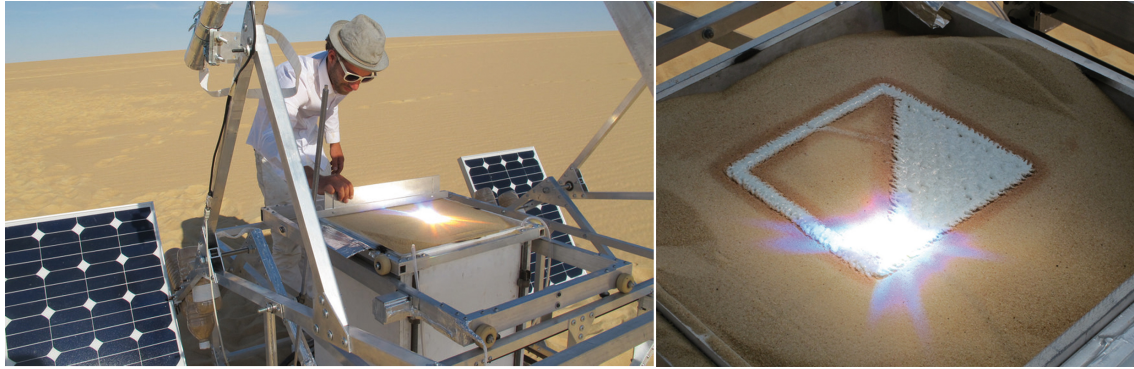


Figure 1.2 – The Solar Sinter System in Action: Utilizing Solar Energy for 3D Printing with Sand. This innovative approach demonstrates the potential for sustainable manufacturing processes in arid environments [137].

### Adobe/Cob

Cob, a traditional earth construction method, has been historically employed worldwide. This technique involves mixing subsoil (earth), water, and a fibrous material, often straw, to create a cohesive mixture [54]. This combination of materials forms a robust and durable structure, allowing cob to be utilised in various architectural applications throughout history.

The first fully printed earth shell, named "Tecla," has been successfully designed by Francesca Moretti and executed by the Wasp company using crane-based 3D printers [22]. This innovative house features circular shells and serves as an inspiration for future sustainable buildings. As reported in [67], Tecla comprised 150 printed layers and took approximately 200 hours to fabricate. With a fabrication cost of \$900, this house is considered economically affordable, making it particularly suitable for low-income societies. Furthermore, it took two weeks after the printing process to have the house dry. The Wasp company has recently unveiled its latest offering, the "Maker Economy Starter Kit." This comprehensive kit encompasses all the tools required for 3D printing a house using earth as the primary material. Included in the kit are essential components such as a crane, mixing pump, extrusion head, and recycling tool [98]. With this kit, users can access the equipment needed to embark on earth-based construction projects.

Another example of fully 3D printed earthen shells is *Casa Covida* by Ronald Rael, a designer and architect and Virginia San Fratello[128]. However, these two shells have some differences in their 3D printing patterns. Another example of 3D Printed clay shell is explored by Gramazio Kohler research studio for the fabrication of *Clay Rotunda* as a music lab in 2021 [57], which used a different fabrication technique than *Casa Covida* and *Tecla*. This technique is not classical 3D Printing based on continuous material extrusion from the numerically controlled nozzle. This technique to fabricate the *Clay Rotunda* is based on assembling the fresh material units, which could be imitated by spot-wise printing patterns using 3D Printing setups. However, this technique looks more advanced than the technique used for *Casa Covida* and *Tecla*, which is vertical extrusion of the material or 2.5 D printing technique [35], since the material is posed in different directions(3D printing) and was not restricted to only vertical extrusion. These various examples showcase the evolving possibilities and techniques within 3D printing of earthen structures, each

offering unique approaches to construction. The next section compares Earth 3D printing to Concrete 3D printing and highlights their pros and cons.

### 1.2.5 C3DP vs E3DP

The comparison between Earth 3D printing and Concrete 3D printing reveals distinct advantages and disadvantages of each technique. The processes of Concrete 3D printing and Earth 3D printing are similar in principle. However, key differences result in advantages and disadvantages for each of them. The main difference lies in the rheology of the materials used. The rheological properties of cementitious materials need to be controlled differently than earth-based materials.

For example, the yield stress of cement and earth increases over time after deposition. However, the increase in material strength does not follow the same patterns for both earth and cementitious materials. In cementitious materials, the yield stress increases through chemical reactions between the molecules of the cement, while in the earth, the yield stress of fresh mortar increases due to the evaporation of water, which is not a chemical reaction. To elaborate, evaporation is a physical process, not a chemical one. It involves the phase change of a liquid (water) into a gas (water vapour) due to an increase in temperature or a decrease in pressure. During evaporation, the water molecules gain enough energy to overcome intermolecular forces and escape into the air, leaving behind the solid components of the clay mixture. The composition and chemical properties of the clay and water remain unchanged during evaporation. In E3DP, the geometry of the printing structure influences the development of the material's properties, while in C3DP, the geometry of the printing structure does not directly affect the evolution of the printing mortar properties. This aspect will be discussed in more detail in Chapter 3.

Furthermore, considering the evolution of mechanical properties in concrete and earth-based materials, the 3D printing speed in C3DP is higher than in Earth E3DP. A study by Tarhan et al. [141] shows that replacing a 3D-printed concrete sample with an earthen-based one would achieve half the number of layers. However, using appropriate methods to enhance the mechanical properties of earth-based materials can improve E3DP.

Table 1.2 compares the different aspects of Concrete 3D printing and Earth 3D printing in more detail, where clay is chosen as the earth-based material. The term "concrete" also refers to high-performance cement typically used in the concrete 3D printing process.

### 1.2.6 Shells and Vaults

A shell is a structure defined by a curved surface. It is thin in the direction perpendicular to the surface, but there is no absolute rule regarding how thin it has to be [2]. In most cases, the shells must be fabricated with the help of temporary elements such as wooden formwork to support the shell. The fabrication of doubly-curved shells using conventional techniques and formwork consumes a massive amount of material as temporary supports. In addition, the conventional method of erecting scaffolds is labourer-intensive. The study in [49] shows that

Table 1.2 – Comparative Overview of Concrete vs. Clay 3D Printing Aspects

Comparison criteria	Concrete 3D printing	Clay 3D Printing
<b>3D printing setups</b>	Pump + Extrusion head. The extrusion head only pushes the material with a step motor.	Pump + Extrusion head. The extrusion head can work with step motor or pneumatic jacks.
<b>3D Printing techniques</b>	Obligation for continues printing since the concrete can get hard inside the extrusion head and ruin the head.	Possibility of pausing the printing process
<b>Structuration / Drying rate</b>	The material gain strength after deposition by the time due to chemical reaction in cement molecules.	The material gain strength after deposition by the time due to the water evaporation from the mixture which is not a chemical reaction
<b>Shrinkage / Cracks</b>	Low level of shrinkage / Vulnerable to cracks	High level of shrinkage / Vulnerable to cracks
<b>Layers bond adhesion and cold joints</b>	Prone to the occurrence of cold joints	Prone to occurrence of cold joints
<b>Rheology control using admixtures</b>	Using chemical admixtures for pumpability and buildability.	Using air flow-heat- alcohol or chemical admixtures for buildability.
<b>Reinforcement technique</b>	Using fibres in printing process for increasing the material tensile strength of the material	Using natural substances such as straws or corks to material mixture to increase the tensile strength of the material
<b>Structural performance</b>	Works in compression	Works in compression

the material cost for fabrication of a complex concrete wall with conventional construction technique was three times higher than robotic fabrication due to the need for special formwork in the traditional construction method.

Shells and vaults are suitable types of sustainable and efficient structures to be 3D printed without scaffolding due to the following reasons:

1. Shells do not have to be covered with horizontal elements such as slabs and roofs, making their fabrication possible without formwork by printing overhangs.
2. The vault structures work in compression only, and this feature aligns well with the constraint of unreinforced fresh mortars such as concrete and earth.
3. Shells are thin in thickness and consequently lightweight, producing less internal stress, which is required for 3D printing with low-strength fresh material.
4. Shells can cover long spans without being supported by columns.

The following section explores different methods and strategies to reduce reliance on formwork in fabricating shells and vaults.

### 1.2.7 Adapting Ancient Vaulting Techniques to 3D Printing: Valuable Lessons Learned

The ancient vaulting techniques for indigenous desert architecture are a great inspiration for scaffold-free construction methods. The masons in arid areas such as Iran's deserts, due to the lack of wood and stone resources, had to invent solutions for the construction using mainly earth, water and sun. However, some other material, such as gypsum and lime, was also common for the fabrication of interior finishing and ornaments. There are several types of vaulting techniques without scaffolding in the history of earthen vaults. There are also some vaulting techniques with stay-in-place scaffolding in which the scaffolding does not only have a temporary role in the construction process but becomes a structural element after being used as a support. These supports were mainly in the form of arches made out of gypsum mortar. Here we mention only the vaulting techniques without the use of any formwork, scaffolding or temporary supports, which can be transformed into a method for scaffold-free 3D printing method (SF3DP).

#### 1. Filpoosh Vaulting Method (Squinch Vault):

During the Sasanid era, Persian masons devised the Filpoosh vaulting method, also known as the Squinch Vault. This method covered rectangular boundaries using self-standing elements called squinches and pendentives, using a vaulting technique called Filpoosh. One of the earliest structures constructed using this technique is the Niasar temple, which served as a praying space for Zoroastrians. Figure 1.3(a) [75] depicts a mason creating a squinch while another mason works on a pendentive to construct a Filpoosh vault. Figure 1.3(b) [75] shows the placement of a squinch on the corner of a rectangular boundary, which is the first step in fabricating a Filpoosh vault. Figure 1.3(c) [114] shows a representation of four squinches positioned at the corners of a quadrilateral boundary, waiting for the pendentives to be placed in between them.

2. **Barrel Vaulting Method:** The barrel vaulting method was extensively used for constructing wide-span vaults. It involved inclined first layers of the vaults, supported by straight walls or short arc walls historically referred to as "Espar" in Persian vaulting vocabulary. Subsequent layers of bricks or mud blocks were progressively added at increasing angles in a linear direction to shape the vault. Figure 1.4(a) [75] shows a mason placing a brick block onto a previous layer of a barrel vault situated on a rectangular boundary. Figure 1.4(b) [42] depicts a mason laying the initial layers of a barrel vault supported by a straight wall. Figure 1.4(c) [75] shows an "Espar," which traditionally serves as a support for barrel vaults.

3. **Ground Supported Barrel Vault:** The ground-supported barrel vault, although less prevalent compared to the two aforementioned vaulting systems, possesses distinct characteristics. In the fabrication process of conventional barrel vaults, the initial layers of brick units are supported by a straight vault

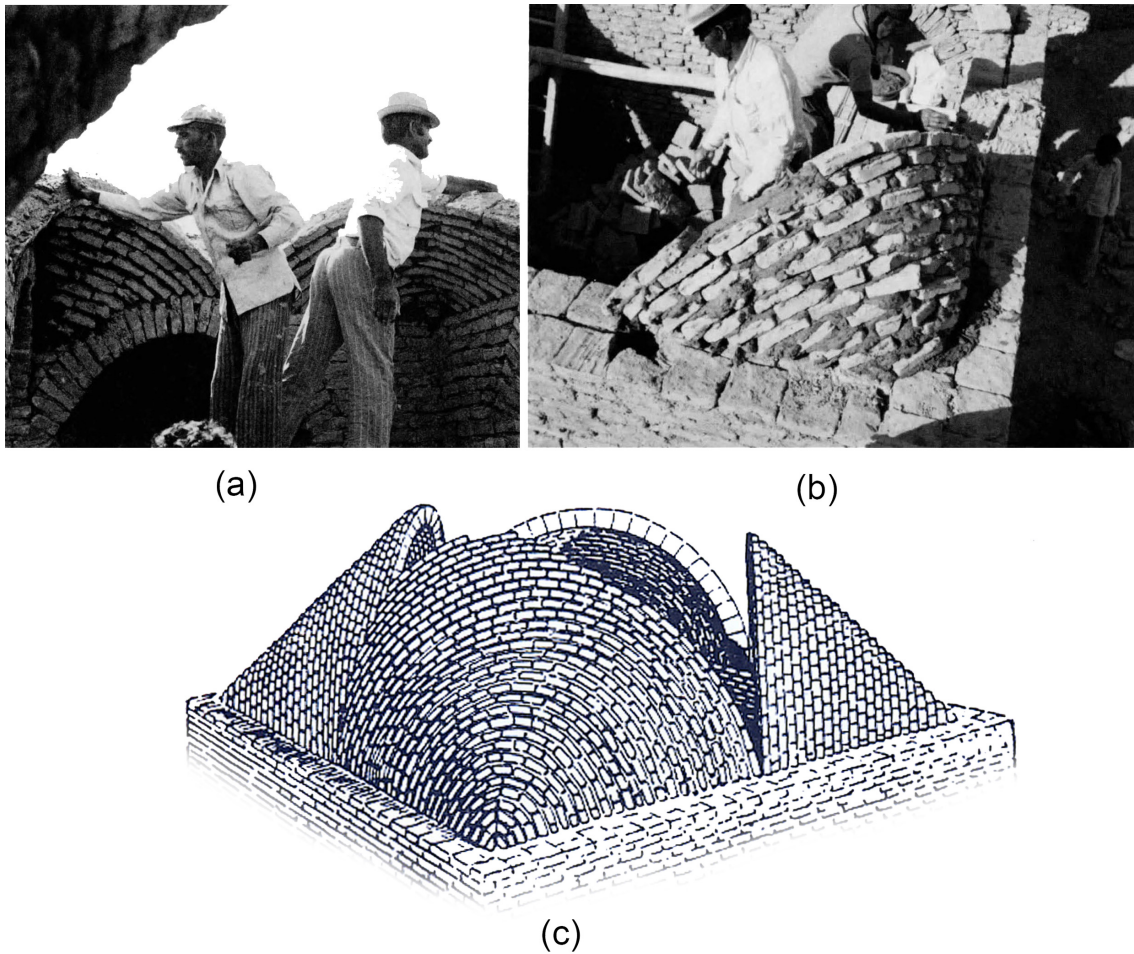


Figure 1.3 – Squinch Vault

(vertical support). However, in the fabrication process of ground-supported barrel vaults, the first layers are supported by the ground or horizontal support. Figure 1.5(a) [42] shows a mason constructing the second half of a ground-supported barrel vault, placed on a rectangular boundary from the opposite side of the first part. Figure 1.5(b) [42] illustrates a ground-supported barrel vault where the initial bricklayer is directly supported by the ground.

4. **Domes:** Domes are the most common structures that can be built without formwork and have a worldwide historical presence. Domes typically have a circular base, and their geometry can vary from spheres to catenary-based geometries. Figure 1.6(a,b) [75] demonstrates the fabrication process of a brick dome. Figure 1.6(c) [68] showcases another dome that was used as a refrigerator in the middle of the desert to preserve ice blocks.

Later in chapter 2, it is discussed how these historical vaulting techniques can be used in 3D printing systems to print shells without any scaffolding. In addition, the transition of these historical techniques into design grammar is discussed in this research.

The combination of accumulated knowledge of ancient masons with the computation power of digital design software and cutting-edge digital fabrication technology can open a broad opportunity for the construction of highly efficient and sustainable

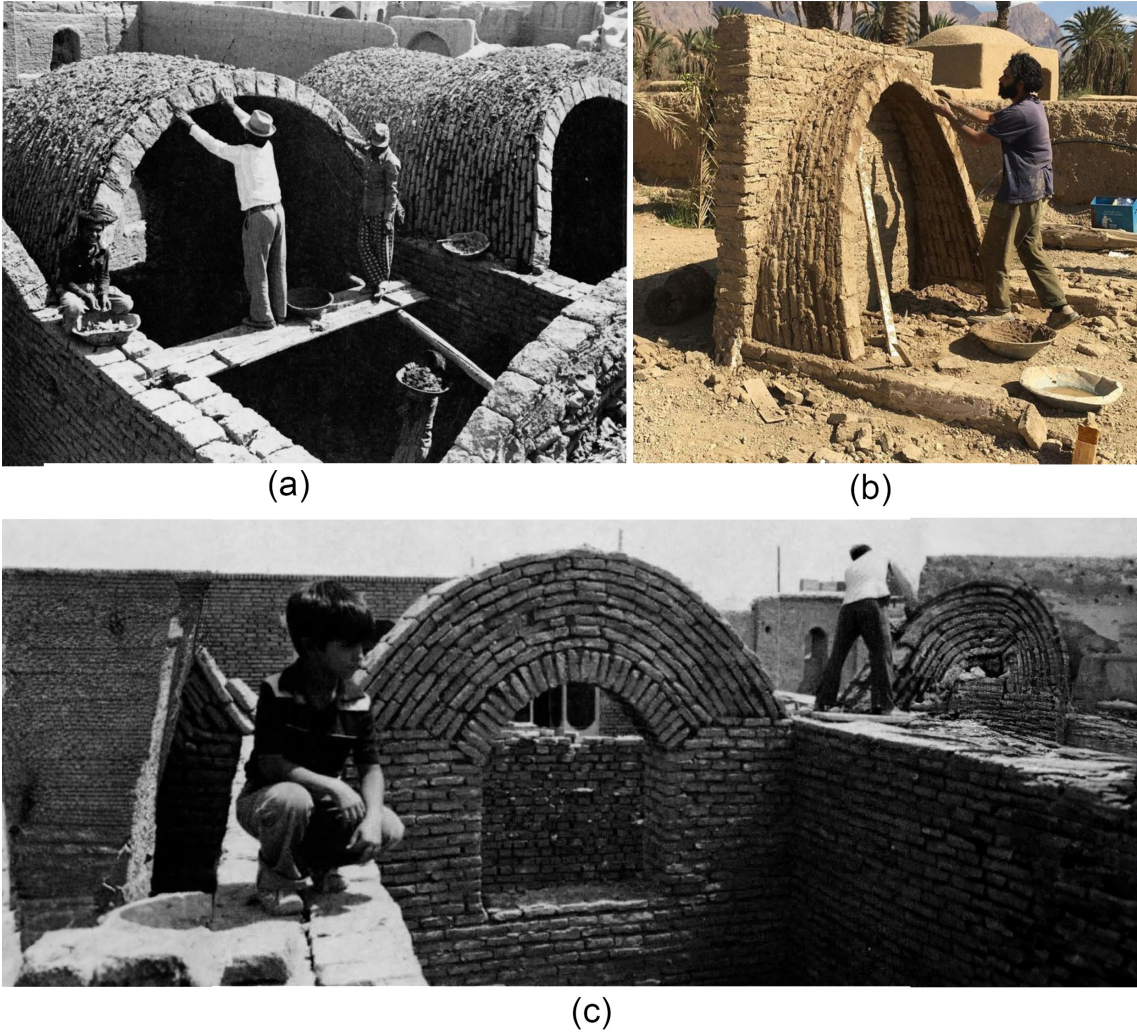


Figure 1.4 – Barrel Vault



Figure 1.5 – Ground-Supported Barrel Vault

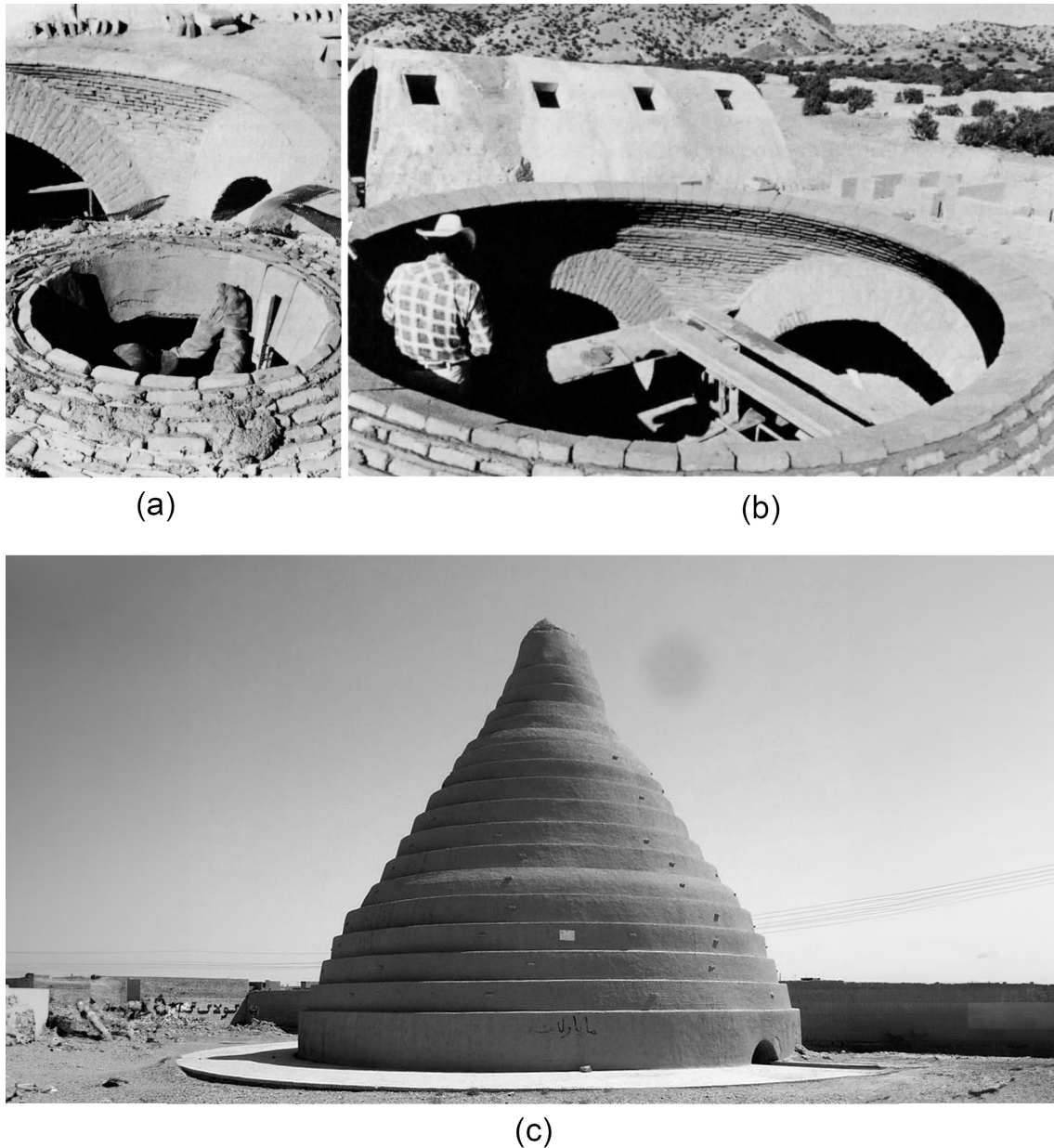


Figure 1.6 – Dome

structures that are adapted to the needs of humans in this era.

This research studies profoundly the methods used by the ancient masons to fabricate earth vaults without formwork and transform these techniques into digital design and fabrication processes using a variety of disciplines such as computer graphics, mechanical engineering, rheological science, computation design, Mesh topologies and robotics.

### 1.2.8 Minimising Formwork in Construction

The construction sector uses various terms interchangeably with "formwork," such as falsework, scaffold, temporary support, pallets, mould, centring, and others. While these terms may have different nuances in execution, they all serve the same purpose: holding the structure temporarily during construction. The term



"falsework" itself suggests temporary or redundant work. Formwork can constitute 35-54% of the total construction cost and consume 50-75% of the construction time [107]. Therefore, reducing or eliminating the need for formwork is a significant concern in construction due to its cost and time implications. Various methods are employed in conventional projects to address the challenge of costly formwork:

1. **Reusable Formwork:** This type of formwork can be utilized in different projects and adapted to various configurations. For example, Felix Candela used reusable, adaptable formwork made of straight elements to construct the "Los Manantiales" shell, which could be employed in another project with a different geometry [94].
2. **Stay-in-Place Formwork:** This method involves fabricating brick vaults using gypsum arches that support stacking the brick layers. Eventually, the arches transform into rib-like structural elements within the vaults.
3. **Formwork-Free Construction:** Ancient masons in arid regions constructed vaults without formwork. (Refer to Section 1.2.7 for more details.)

In automated construction methods, the formwork challenge is addressed through the following methods:

1. **Stay-in-Place Formwork:** For instance, the mesh mould technique is employed for fabricating curved reinforced concrete walls [59] or constructing space truss walls using polystyrene blocks [36].
2. **Dynamic Formwork:** Examples include the Smart Dynamic Casting (SDC) system [91], or the assembly of glass vault structures using two robots, where one robot supports other robots in stacking the glass bricks [112].
3. **Binder Jetting Technique:** This 3D printing technique employs the printing material as support for the printed structure. Examples include the D-Shape system by Enrico Dini for 3D printing concrete structures [93] and selective sintering of sands using the SLS system developed by Markus Kyser [123].
4. **Reusable Fabric Formwork:** Fabric or cable net formwork finds extensive use in constructing double-curved concrete shells [101, 148].


With an understanding of the challenges posed by traditional formwork, the next section will explore and compare different 3D printing methods used in the construction of architectural-scale units.

### 1.2.9 Comparison of the 3D Printing Methods

In the AEC (Architecture, Engineering, and Construction) industry, 3D printing methods can be categorised based on various aspects, including printing regime [34, 130], construction method, 3D printing setup, and printing material. Table 1.3 categorises existing solutions for printing buildings and shells, along with their respective advantages and disadvantages in terms of formwork usage, design flexibility, automation level, and scalability. To control the geometry of the printing layer, the practitioners have used different printing regimes. The Printing regimes differ based on the printing strategy and the printing mortar rheology. Based on the classification in [130], all 3D Printing regimes stand between two main printing regime categories. First is the **Infinite brick extrusion** where the printing mortar

yield strength is so high that it's not sheared under the stresses imposed by the pumping pressure. Therefore, in this regime, the material exits the extrusion nozzle unsheared. The shape of the extruding nozzle governs the layer's form in this method. For example, the material exiting from a nozzle with a circular hole with a diameter of 15 mm forms a cylindrical layer with the cross-section of a circle with a diameter of 15 mm. Second is the Free-deposition regime in which the printing mortar has a very low yield stress. Consequently, the exiting material from the extrusion nozzle is sheared, and the shape of the depositing layer is governed by the competition between gravity, pumping pressure, material yield strength and the distance of the nozzle from the printing bed or the previously printed layer. The free deposition technique is abundantly practised in Clay 3D Printing for decorative objects to form curly patterns formed naturally in the 3D Printing process. However, on an architectural scale, this regime is practised to fabricate space truss masonry walls by Duballet et al. [36]. Other printing regimes can be classified as slip forming [91], layer pressing and oriented layer pressing [17]. Table 1.4 compares different 3D printing regimes.

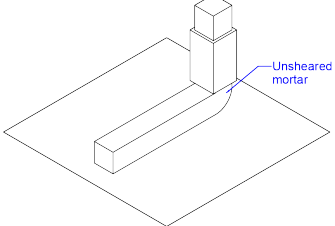
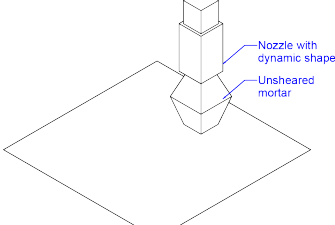
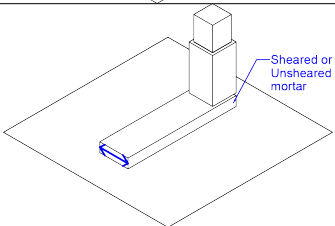
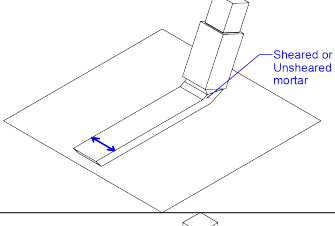
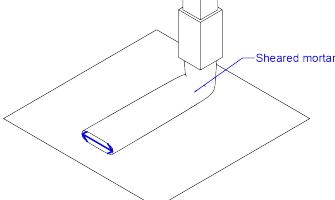
Table 1.3 – Comparative Analysis of 3D Printed Projects

Fabrication Method	Vertical Printing	Cantilevered Printing	Modular Printing
Fabrication Setup	Crane / Gantry Crane	Crane / Gantry Crane	Robotic Arms
Utilisation of formwork	For openings and roofs	Only for openings	For Assembly
Scability	Only in vertical dimension for crane setups	Only in vertical dimension for crane setups	High freedom for scability
Design Flexibility	Vertical Elements / Constrained Cantilevers	Plans are restricted to circular configuration	High flexibility for design configuration
Automation Level	Semi-Automated	Almost fully automated except for the openings	Semi automated (In case if assembly is done manually)
Automation Complexity Level	Low Complexity	Low Complexity	High Complexity
Project Example			
Description	The first 3D printed house in Germany [115]		

### 1.2.10 Modular Construction and Additive Manufacturing

A modular building is a building that consists of several prefabricated identical elements called a module. For example, the *Nakagin* capsule tower by Kisho Kurokawa, inspired by the Metabolism architectural movement [88] is one of the

Table 1.4 – Comparison of 3D Printing Regimes

Printing regime	Demonstration	Depositing Material state	Layer Geometry controlling factor
Infinite brick extrusion		Unsheared	Nozzle geomtery
Slip forming		Unsheared	Dynamic nozzle geometry
Layer Pressing		Sheared or unsheared	Nozzle geometry (If not sheared) Nozzle distance from the printing bed
Oriented Layer Pressing		Sheared or unsheared	Nozzle geometry (If not sheared) Nozzle distance from the printing bed Nozzle orientation angle
Free-Deposition		Sheared	Material Yield strength Gravity and self weight

most remarkable examples of modular construction where capsules as the living units were inserted inside a concrete structure. Another example is the *Habitat 67* by Moshe Safdie. This building consists of precast concrete boxes as living modules [131]. The advantages of modular construction are as follows:

1. **Reducing the construction cost by equalising the building elements:** Since the building elements in modular buildings are identical, the final cost for the fabrication of the elements can be significantly reduced due to the reduction of the fabrication complexity.
2. **Reducing the building maintenance cost:** A module can be replaced by a new one if a flaw or damage occurs in a part of the structure.
3. **Rapid construction:** Modular buildings can be installed in a few days, depending on the module's complexity.
4. **Producing less construction waste:** The offsite prefabrication produces

significantly less waste than in-situ construction.

Modular construction in additive manufacturing has been practised in several projects. An example of modular construction by additive manufacturing is to divide a building or shell into pieces print the pieces individually, and assemble those pieces on site, such as the proposal in [41] for modular 3D printed ceramic shelter or research by University of Waterloo architecture students for the fabrication of hexagonal 3D printed modular shelter [24]. However, this technique can also add up to the construction complexities for assembly, fabrication discrepancies, and the problem of weak bonds between the elements. The modular 3D printing technique is also practised by the Blocks research group for the fabrication of *Striatus* bridge [11]. For this project, although the modules have been printed without support, the assembly of the bridge elements required the erection of the form-works making the process less automated and less productive and more material-consuming. Another example is the project by Wu Hao et al. for printing the modules of a funicular spatial structure [151]. The advantages of modular construction in additive manufacturing are as follows:

1. **Addressing the restricting dimensions of printers:** In additive manufacturing of buildings using fixed setups such as arms on pedestals, cranes and gantry cranes, the dimension of the building is restricted by the dimension of the printing setup. The bigger the building, the larger the fabrication setup must be, and this adds to the building cost. Instead, the building can be divided into several smaller components, and those components can be printed with smaller and cheaper printing setups and finally be assembled on-site.
2. **Reducing the building risk:** In the 3D printing process, it is possible to malfunction the printing setup or any other unexpected issue which can interrupt the printing process and, in some cases, damage the whole printed object until the time interruption occurs. However, using modular 3D printing, the risk of damaging the whole printed part can be reduced to only one module.

### 1.3 Problem Statement

The implementation of additive manufacturing in construction is still in its infancy despite being vastly studied by researchers. There are many aspects to improve and technical problems to address to exploit the full advantages of this technique in the construction sector. Concrete 3D printing companies practising the implementation of additive manufacturing in their projects still use this technique only to construct vertical elements such as walls and columns. The rest of the building components, such as foundations, roofs, and openings, are still constructed traditionally. This issue will make the construction process less automated and consequently less productive.

On the other hand, several projects such as *Casa Covida* or *Tecla* have taken advantage of shell-like structures to address the problem of horizontal elements in buildings and embed the fabrication of roof elements in the additive manufacturing process by printing cantilevered structures. However, their fabrication setup is still based on cranes that print structures with circular plans. This is due to the necessity of covering the circular plan with a dome-like structure as roofing. Aside from restricting the design of circular buildings from an architectural point of

view, the dimension of the shell is governed by the dimension of the printing crane. Furthermore, these shells have been printed continuously, where the structure is considered one piece, and the printing layers are continuously printed on top of each other to shape the shell envelope. This construction technique can restrict the maximum achievable span and design freedom.

Modular step-wise 3D Printing is a method to tackle the aforementioned problem. However, there is still a lack of a printing strategy that can fully transform the building construction into a fully automated process without requiring highly complicated fabrication setups.

The list of problems that this research is addressing is as follows:

1. Removing the formwork from the 3D printing process of the shells.
2. Establish a fabrication-aware design method for shells that can be 3D printed without any scaffolding or temporary support.
3. Establishing design methods for SF3DP shell with various boundary conditions.
4. Addressing the challenges of using low-impact construction material, specifically earth-based material, for shell construction.
5. Controlling the rheological properties of earth-based materials in the 3D printing process without using chemical additives.
6. Proposing a 3D printing approach that can be fully automated without using highly complex fabrication setups.

## 1.4 Research Objectives and Methodology

### 1.4.1 Objectives

This research aims to explore the feasibility of fabricating shell-like structures through 3D printing, utilising earth-based printing paste, and eliminating the need for scaffolding. This objective arises from the following reasons:

#### 1. Reasons for 3D printing :

- (a) Reducing the material consumption in construction by deposition material where needed.
- (b) Fully automate the construction process to:
  - i. Reduce the time needed to install the scaffold and support.
  - ii. Reduce the number of labourers needed for construction to save time and expenses (construction productivity).
  - iii. Minimise fabrication discrepancies.
  - iv. Ability to build shells in harsh environments where the existence of humans is not safe.
  - v. Increase the safety of the labourer and reduce the risks

#### 2. Reasons for removing the scaffolds in construction process

- (a) Reduce construction waste by eliminating formwork.
- (b) Accelerating the construction process.
- (c) Reduce construction complexity and facilitate the automation process.

### 3. Reasons for using earth-based material for shells construction

- (a) Reducing the building’s construction’s embodied energy (emitted carbon).
- (b) The earth-based materials are recyclable and get back to nature after the life cycle of the building
- (c) The earth-based materials have efficient thermal conductivity and acoustic resistance.

The primary focus of this research is to develop a fabrication-aware design method for SF3DP (Scaffold-Free 3D Printed) shells. This design method aims to facilitate the exploration of diverse geometries within pre-established boundaries, which can subsequently be optimised according to the specific objectives and constraints of a particular printing project. Additionally, a secondary objective of this research is to investigate the impact of applying heat to the printing mortar during the 3D printing process. This examination aims to assess how heat affects the buildability and structural stability of the printed structure.

#### 1.4.2 SF3DP Setups

This section presents different possible 3D printing setups and processes mostly adaptable to scaffold-free 3D printing of the shells. As described above in Table 1.1, different available setups in the market can be used for both off-site and in situ 3D printing scenarios. We can categorise the printing setups into two classes. The mobile setups and fixed setups are presented in the table below:

Table 1.5 – Comprehensive Classification of 3D Printing Setups for Scaffold-Free 3D Printing (SF3DP)

Mobile Setups	Mobile arms
	Drones
Fixed setups	Robotic arms
	Cranes
	Gantry Cranes
	Multi-Cranes
	Cable-driven robots

The SCF3D can be performed in two main methods. First, we have modular printing, and the second is monolithic printing. The patches can be printed separately and assembled at the target site in modular printing. In this method, only patches fully supported by the ground, such as squinches and domes supported by the ground (only those with ground support), can be printed separately. The pendentives must be printed when the primary ground-supported elements are placed in the target place. Another scenario is that several interconnected Patches can be printed separately and be assembled later. On the other hand, in monolithic printing, the entire multivault is printed in one place.

Figure 1.7 classifies different printing scenarios using different setups for 3CF3DP. Each 3D printing environment(A, B) and printing method (a,b) are labelled. Furthermore, each 3D printing setup is given a number (1,2,3, etc.). For example, (B). (a). (3) means Off-site modular 3D Printing using a crane.

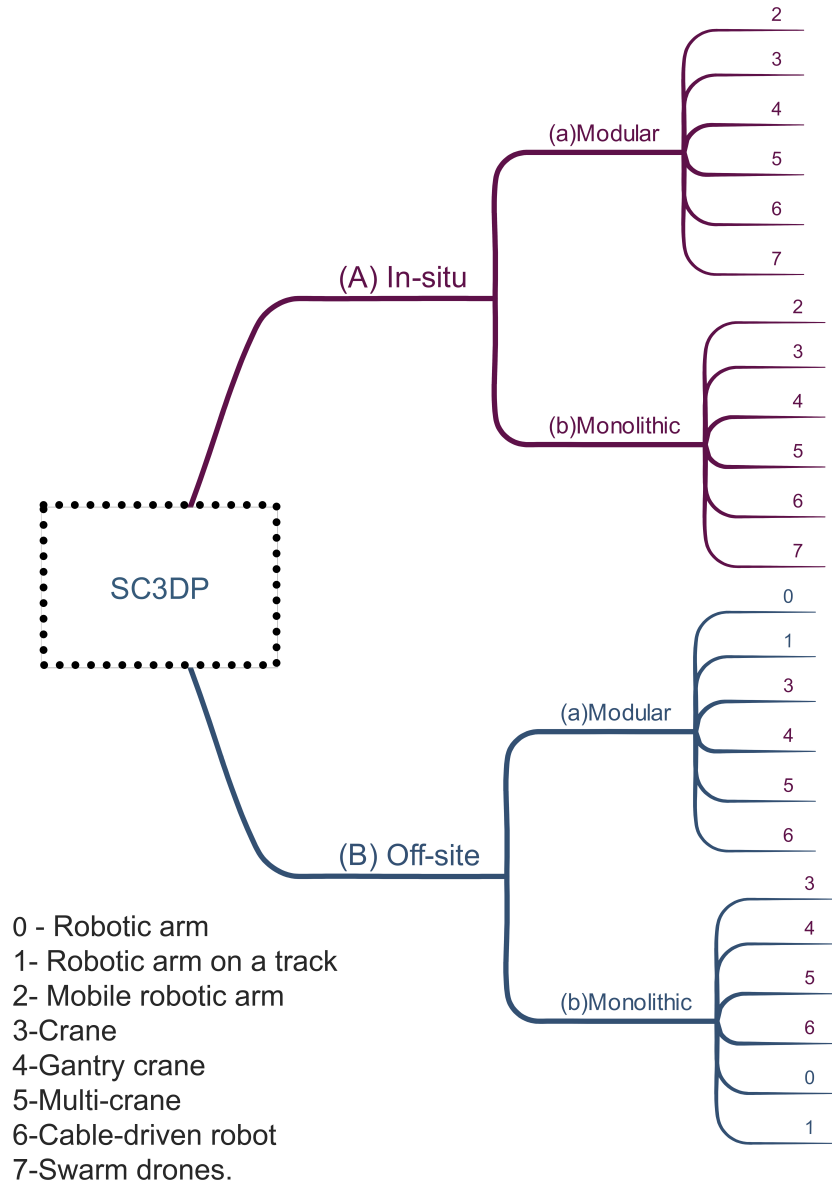


Figure 1.7 – Overview of Various Scenarios for Scaffold-Free 3D Printing Methods, Demonstrating the Range of Applications and Techniques in the Context of Earthen Architecture.

### 1.4.3 Research Methodology

The approach used in this research to develop a design method for SF3DP shells involves deciphering ancient vaulting methods that do not require scaffolding. These methods are then formalised into rule-based design grammar, allowing users to explore numerous design variations within specified boundary conditions. Regarding the investigation of the effect of heat on the buildability and green-strength evolution of earth-based printing mortar, the methodology is as follows:

1. Designing a specific material examination that assesses the impact of wind speed and temperature on the evaporation rate of porous media, such as clay

mixtures.

2. Extracting relevant data from various resources that elucidate the relationship between water quantity and the strength of porous media.

## 1.5 Outline

The second chapter of this dissertation introduces the Patching design grammar for designing shells, specifically earthen shells that can be 3D printed without any scaffolding. The third chapter discusses the required rheological properties of the earth-based paste for 3D printing shell and a method for rapidly increasing the material yield strength after deposition for buildability reasons. The fourth chapter describes the fabrication experiments and discusses challenges and strategies. The last chapter demonstrates outlooks and perspectives and the topics to be further researched in this field.



لكل من خال يرد زر شود...

*L'homme sage ramassant de la terre peut transformer cette terre en or.  
(Djalâl ad-Dîn Rûmî)*

*If a wise man picks up soil, he can turn the soil into gold  
(Rumi)*

# Chapter 2

## Topological & Geometrical Design: Introduction to Patching design grammar

*Reader: So, what will we explore in this chapter?*

*Author: In this chapter, we're delving into the methods to design shells and vaults that can be printed without scaffolding. It's quite an exciting area of study.*

*Reader: That sounds intriguing. Can you tell me more about these methods?*

*Author: Certainly! First, I will present a method to design vaults with convex quad boundaries. It's a fascinating approach that opens up new possibilities.*

*Reader: And what comes next?*

*Author: Later, I will introduce a holistic method called Patching. This approach allows us to design vaults with any boundary condition. While the Patching grammar provides a design framework that's not necessarily printable in all cases, it offers a meaningful design space. We'll explore this space through finite element analysis, considering the properties of printing mortar.*

*Reader: That sounds like a comprehensive approach. I'm looking forward to diving into the details!*

### 2.1 Introduction

The skilled vaulting masters of the past possessed the remarkable ability to construct earthen vaults in arid environments using only natural earth materials. These craftsmen achieved overhangs in their vaults without relying on wooden pallets, formwork, scaffolds, or any temporary structures to support the vaults during construction. Unfortunately, the scarcity of such masters today poses a risk of the specialised vaulting techniques fading into obscurity. However, the emergence of robots provides an opportunity to preserve and carry out the tasks once performed by these vaulting masters.

The advancement of precision hardware, coupled with sophisticated software capable of managing extensive and intricate data, presents a multitude of opportunities for the construction of environmentally conscious and cost-effective structures. Additionally, integrating robots into construction processes can significantly enhance speed, consistency, and structural integrity, resulting in improved strength and thermal efficiency of buildings [152]. Furthermore, the

utilisation of robots can contribute to eliminating the requirement for formwork in construction, specifically the 3D Printing process. This is particularly significant as formwork expenses can account for a substantial portion of total construction costs (35-54%) and consume a significant amount of construction time (50-75%) [45].

This chapter discusses the methods to design shells that could be 3D printed without temporary supports. As Figure 2.1 demonstrates, the idea is to transition from the brick or mud layers of the earthen vaults to print layers of the earthen 3D printed shells. With the aid of six-axis robots, the techniques of the vaulting masters can be imitated. For example, the vaulting masters could lean the brick or mud arch layers with varying inclinations to make the cantilevers. As Figure 2.2 shows, this technique can be performed using the 6-axis robots. Unlike the conventional 3D printers in which the printing nozzle can only move in X, Y, and Z directions (2.5 D printing topology), the six-axis robots can move in space at different angles, making them suitable for imitating the vaulting masters' cantilevering techniques. Figure 2.3 shows the simulation of 2.5 D (a) printing and 3D printing (b) for a semi-sphere geometry. The 2.5D printing topology is simply the vertical extrusion of the printing layers, while 3D printing is the extrusion of the printing layers at different angles. In Printing cantilevers, the 3D printing topology can minimise the local cantilevers between the consecutive layers and maximise the contact surface between them. This matter can increase the chance of achieving higher cantilevers and covering larger spans than 2.5 D printing topology. In 2.5 D printing topology, the local cantilevers are high where the curvature of the geometry increases; consequently, the bound surface between the layers is low. Therefore, the structure of these parts is prone to elastic failure [16].

### 2.1.1 Outline

In this chapter, the discussion begins with an overview of the general concerns of design, including an exploration of form-finding methods and slicing techniques. This is followed by an explanation of how to create suitable geometries that can be printed within specific constraints for convex quad boundaries. Patching design is then introduced, focusing on the grammar for designing geometries that can be printed without support. Two discrete design workflows using Patching design grammar are elaborated, accompanied by examples, and three methods for tuning generated geometries using Patching grammar are explained. The chapter concludes with exploring a common use of Patching design grammar in conventionally 3D printed houses, summarising the key findings and insights.

## 2.2 Funicular Form-Finding

3D printing cantilevers using unreinforced mortars such as high-performance cement or clay must be associated with funicular forms. Funicular forms are the geometries that work only in compression. Since the unreinforced mortars are vulnerable to tensile stress, only 3D Printing of funicular forms can lead to a successful printing process. Historically the funicular forms were massively used by ancient masons to construct earthen shells with large spans [75, 77, 76]. Those masons were used to design such funicular forms by simulating the hanging ropes

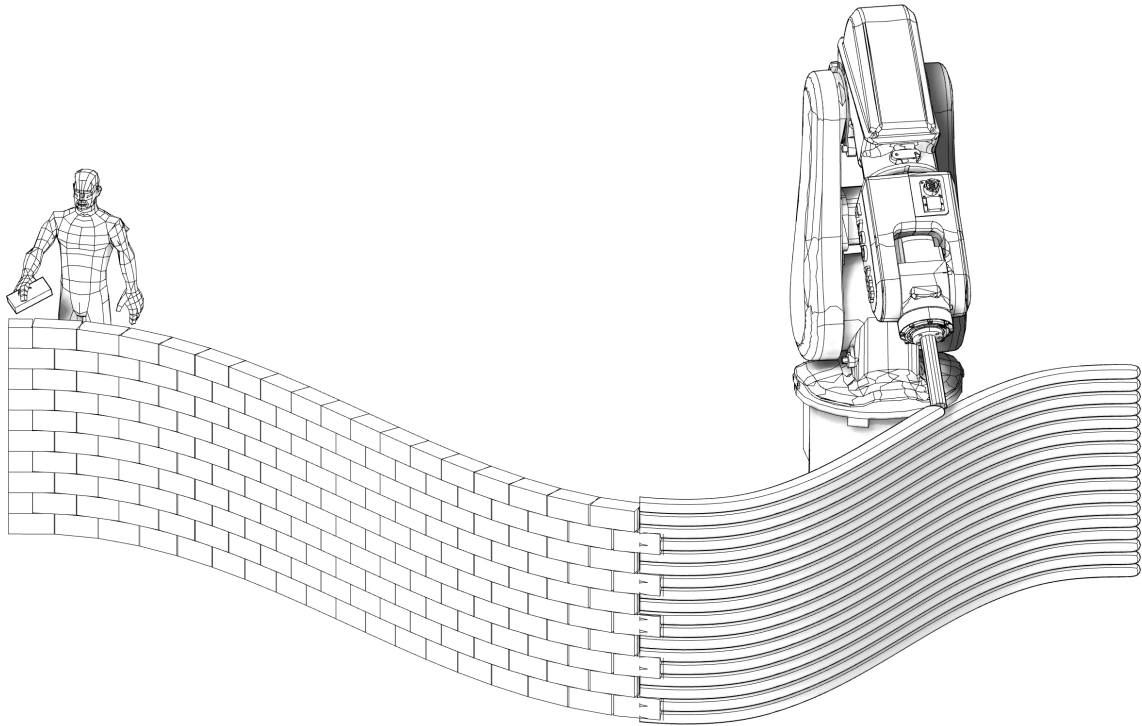


Figure 2.1 – Evolution of Construction Techniques: From Mason-Laid Brick Layers to Six-Axis Robot-Printed Layers. This comparison illustrates the transformative shift towards automation, showcasing advancements in precision and efficiency in building methods.

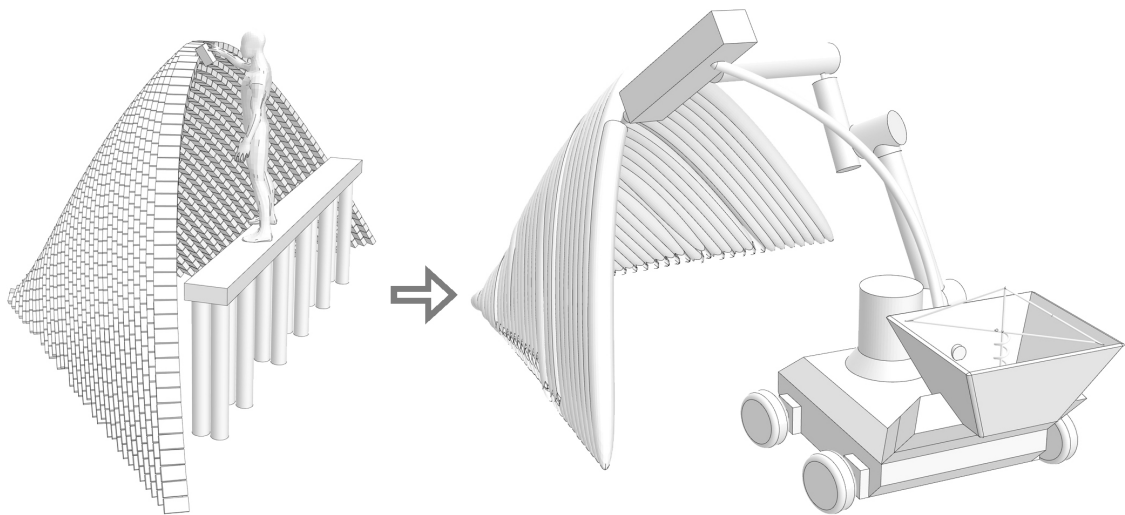


Figure 2.2 – Replicating Vaulting Techniques with a Six-Axis Mobile Robot: Bridging Traditional Craftsmanship and Robotic Precision

or chains. Similarly, the ancient mason’s funicular form-finding techniques have influenced architects and structural engineers such as Antoni Gaudí, Frei Otto and Heinz Isler [85, 124, 21]. They used such a technique with a hanging network of chains models to design the geometry of their buildings. In such a form-finding

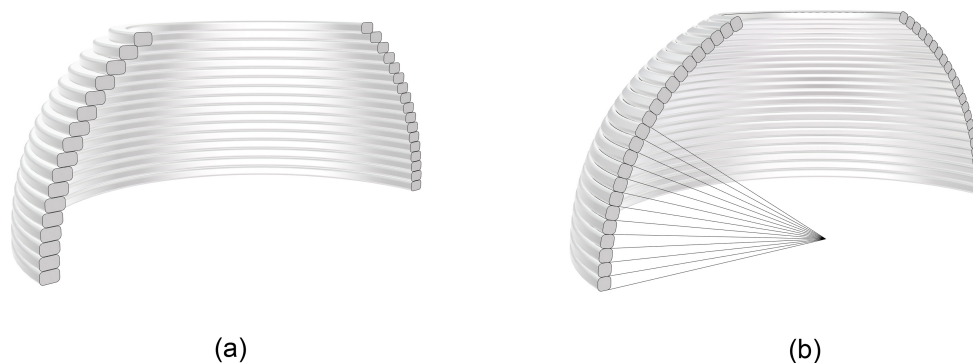


Figure 2.3 – Surface Bond Comparison: (a) 2.5D Printing Topology vs. (b) 3D Printing Topology - Analyzing Layer Adhesion and Structural Integrity

technique, the form follows force. For the design of the funicular forms, one major load condition is usually assumed, and this load condition is typically the self-weight. This means that a form-found funicular form is optimised to transfer a load of its weight [86]. With the advances in computer graphics and 3D modelling software, funicular form-finding does not need to be done with the cumbersome process of simulating hanging chains. One can design a boundary, assign a load condition for optimising the funicular form, and use the user-friendly environment of 3D modelling software to design their geometry. The Force density method[134], Dynamic relaxation[15] and thrust network analysis[10] are the three major techniques that are implemented in the 3D modelling software for engineers and architects. Figure 2.4 shows the general process of funicular form-finding in three main steps. The first step is to design a boundary and the 2D topology of the target geometry. The second step is to assign a load condition to the 2D topology designed in the first step. The third step is to form-find the funicular geometry optimised for the assigned load condition and tailored for the designed boundary and 2D topology.

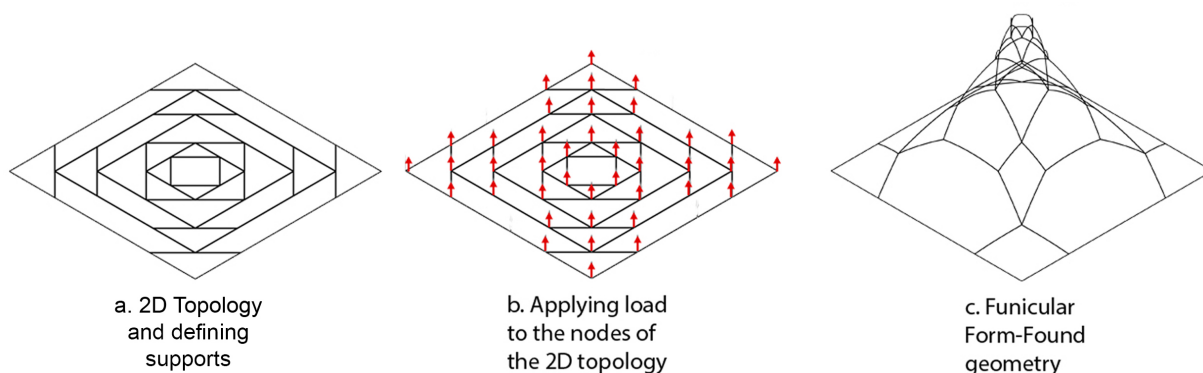


Figure 2.4 – Funicular Form-Finding Process

## 2.3 From Geometry to Robotic Orders

This section explains how a funicular geometry can be transformed into an order for a robotic arm to execute the printing process of that geometry. In the previous section, the methods of funicular form finding using mathematical tools such as the force density method and dynamic relaxation were explained. Once a designer has created their funicular geometry using the mentioned techniques, they must communicate their geometry to a robotic arm using a list of coordinates in space. Then the robot can steer the printing nozzle along the assigned coordinates to deposit the printing mortar through the nozzle and shape the final geometry. There are two main steps to print a funicular geometry using a six-axis robot:

1. Slicing
2. Creation of robotic trajectories

### 2.3.1 Slicing Methods

The slicing approximates a geometry by several consecutive curves representing the original geometry. The slicing can be done through many methods, and it has two main characteristics; the distance and the slicing angle. The distances and angles of slicing planes may be constant or variable. Figure 2.5 shows different slicing strategies for the same geometry. The slicing method can directly influence the mechanical behaviour of the structure during the printing process. This is elaborated more into detail in section 3.6.4

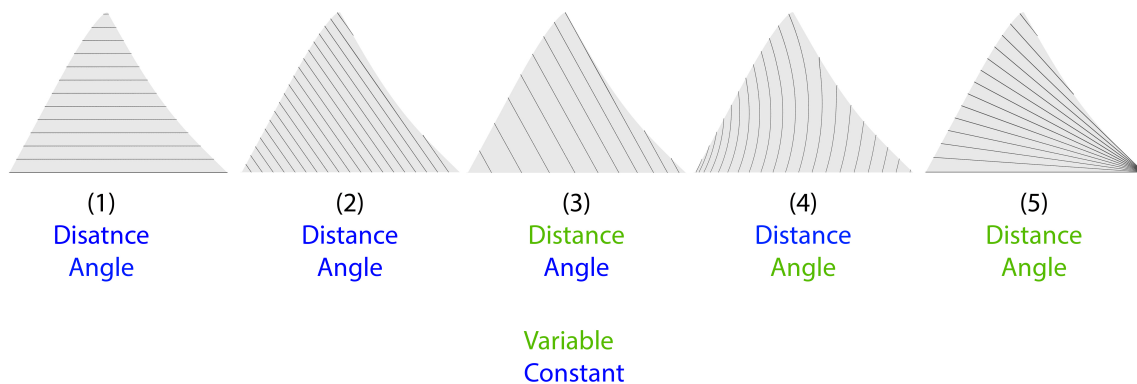


Figure 2.5 – Characteristics of Different Slicing Methods for Geometry - A Comparative Analysis of Techniques and Outcomes

### 2.3.2 Creation of Robotic Trajectories

To order a robot to follow the curves created in the slicing step, one must represent the curves by a list of coordinates. The coordinates convey the curves' point and the printing nozzle's angular orientation at each point. Figure 2.6 shows slicing and creating robotic trajectories for a vault geometry. In figure 2.6 (c), the points (coordinates) on the last curve created in the slicing process are represented. The blue lines are the normal vectors of the built planes on each point. The normal vector of the planes (blue lines) signifies the orientation angle of the printing nozzle at each point. For maximising the structural stability and minimising the local

bending moment at each layer of the structure during the printing process, the best strategy is to set the printing head orientation perpendicular to the previously printed layer. However, due to the robotic joint constraints and reachability, it is not always possible to set the printing head orientation utterly perpendicular to the previous layers. This issue will be discussed later in chapter 4.

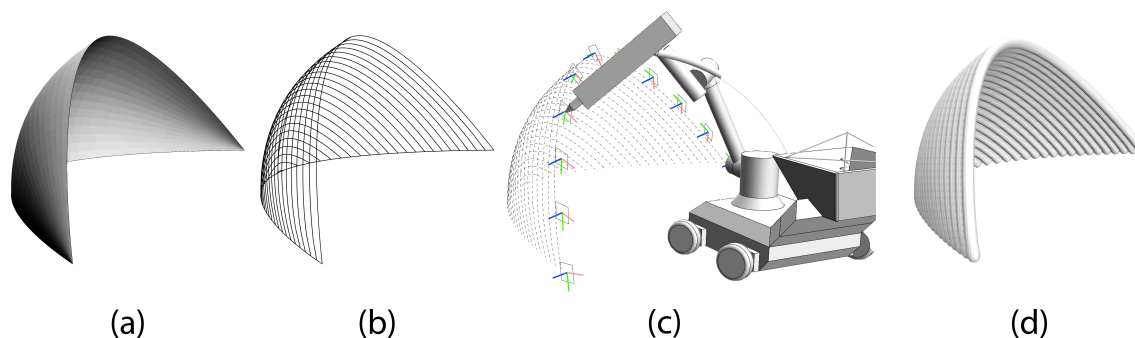


Figure 2.6 – Four-Step Process from Geometry to Printing a Shell: Conceptualization, Design, Slicing, and Fabrication

## 2.4 Developing Vault Designs for Structures with Quadrilateral Boundaries

Historically, the vault masters designed large spans with circular bases to cover those spans using domes while covering the secondary spaces with shorter spans and rectangular bases with vaults. For example, in the design of Isfahan’s central mosque, there are around four hundred and fifty vaults that cover the peripheral spaces and two domes for covering the main halls [100]. The Filpoosh method mentioned earlier in 1.2.7 is the invention of converting quad boundaries into circular ones, as it is shown in figure 2.7. These techniques allowed the masons to cover the quad boundaries with domes. However, in this research, this technique is used to bridge the spans of quad boundaries using squinches and then pendentives as shown in figure 2.8. In this research, bridging the spans of a boundary using self-supporting interconnected elements is called **Patching** [motamedi\_supportless\_2020].

### 2.4.1 Quad Boundaries Typology

Figure 2.8 shows two classical methods for bridging the spans of square boundaries: Method 1 shows the bridging using squinches, and Method 2 shows the bridging with short squinches. The Patching process is not always as straightforward as shown in Figure 2.8. For example, if a quad boundary is skewed or has a short edge, the Patching method must be altered correspondingly. In other words, the Patching strategy must adapt to the configuration of a quad shape. In this section, only the Patching method for convex quads is explained. Section 2.5 discusses a strategy to span advanced boundaries. Figure 2.9 shows four types of convex quads and the Patching process for each type. The quads are sorted by skewness, edge length ratio, or internal facing angle ratio.

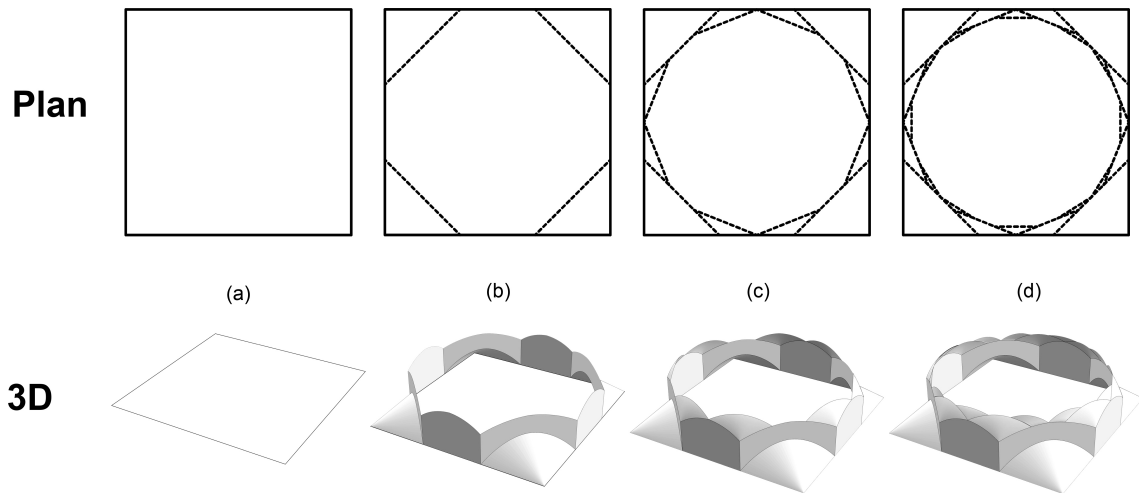


Figure 2.7 – Steps of Converting a Quad Boundary into a Circular Boundary: Sequential Transformation

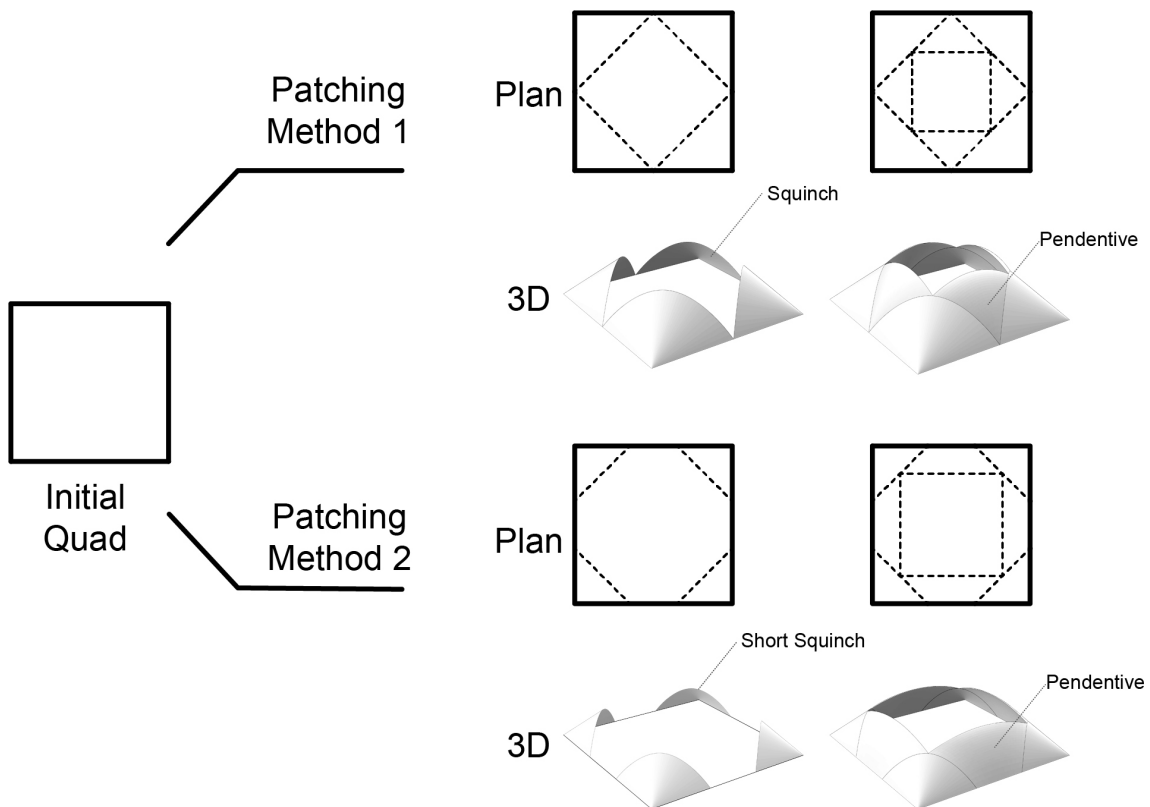


Figure 2.8 – Comparison of Two Patching Methods for Quad Boundaries

Type 1: **Conventional quads** In this type of quadrilaterals, after the first Patching step (a), all four generated triangles should have skewness less than 0.7. These types of quads are closer to squares or rectangles with a low aspect ratio. Hence, they can directly follow the Filpoosh method for the Patching process. The formula for calculating the skewness factor of triangles is shown below, where  $\alpha$  represents the interior angles



of the achieved triangles.

$$\max \left[ \frac{\alpha_{\max} - 60}{120}, \frac{60 - \alpha_{\min}}{120} \right] \leq 0.7$$

Where  $\alpha_{\max}$  is the maximum interior angle and  $\alpha_{\min}$  is the minimum interior angle of the achieved triangle.

**Type 2: Triangle-like quads** These types often have an edge smaller than the average of other edge lengths. To identify such quads, the minimum ratio of the smallest edge length  $\lambda_{\min}$  over the average of edge lengths  $\lambda_{\text{Avg}}$  should be lower than 0.5. Since these quads are close to triangles with a low skewness factor, the smallest segment can be eliminated, and we can reconstruct a new triangle with the first three larger segments.

$$\frac{\lambda_{\min}}{\lambda_{\text{Avg}}} \leq 0.5$$

**Type 3: Stretched quads** These quads resemble stretched rectangles. To identify type 3 quads, the skewness factor for these quads is less than 0.5. The following equation calculates the skewness of quads, where  $\alpha_{\max}$  is the maximum internal angle and  $\alpha_{\min}$  is the minimum angle of a quad.

$$\max \left[ \frac{\alpha_{\max} - 90}{90}, \frac{90 - \alpha_{\min}}{90} \right] \leq 0.5$$

**Type 4: Kite quads** These quadrilaterals are similar to distorted kite quads. To identify such quads, the minimum ratio of the two opposite angles should be less than 0.25, as described in the equation below. The internal angles  $\alpha_{1,2,3,4}$  are sorted clockwise or counterclockwise. In Figure 2.9, type 4, it is demonstrated how an inscribed circle divides the spans of an initial quad.

$$\min \left[ \frac{\min[\alpha_1, \alpha_3]}{\max[\alpha_1, \alpha_3]}, \frac{\min[\alpha_2, \alpha_4]}{\max[\alpha_2, \alpha_4]} \right] \leq 0.25$$

Some quads share common characteristics of two or several types. The user chooses which Patching strategy is more appropriate for the aforementioned quads. In general, the Patching method must be compatible with the rheological properties of printing material, potentials, and constraints of 3D printing set-up and the designers' decision.

## 2.5 Patching Design Grammar

In Section 2.4, the strategies for bridging the spans of convex quad boundaries were explained. However, using such strategies with parametric design is not always straightforward. Especially when the number of spans increases, the definition of parametric modelling gets more complicated and hence harder to control and manipulate. Parametric modelling software often maintains a detailed design development history in the form of a graph. However, as the graph increases

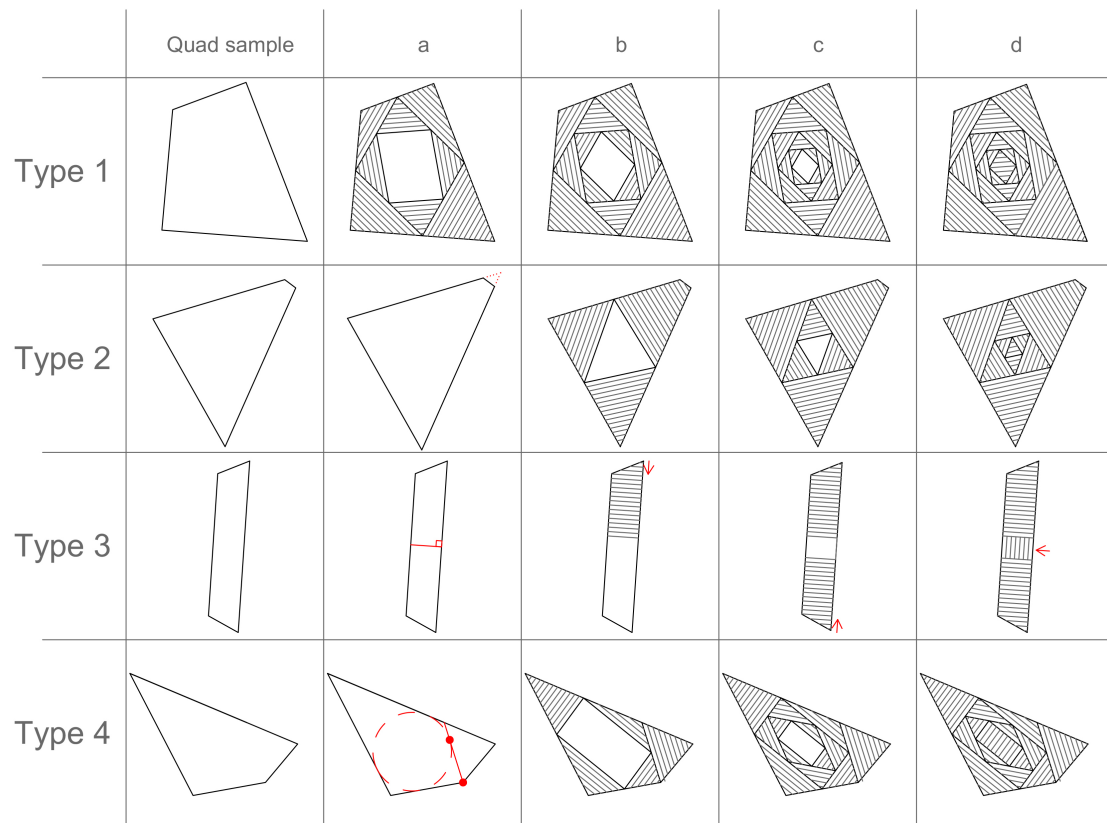


Figure 2.9 – Four Patching Strategies for Different Types of Quads: A Comprehensive Analysis of Techniques and Applications

in complexity, it quickly becomes inflexible and unsuitable for exploring a broad design space. In this section, a grammar-based design workflow is presented. Unlike parametric modelling software, implicit low-level rule systems can offer extensive design exploration thanks to their flexibility [63]. The Patching grammar encapsulates information of a Patch geometry in the form of rules to simplify the design exploration for the users and let them escape the complex graphs of parametric space and focus more on the design rather than the algorithmic process.

### 2.5.1 Introduction

This section introduces the Patching design grammar for not only quad boundaries but also Ngons and advanced boundaries such as periodic (Closed) Nurb curves. Figure 2.10 shows the patching process using the patching grammar for a rectangular boundary. Patching grammar is a tool to design the topology of the Multi-Vaults following the Patching grammar's rules. The Patching method is a design workflow based on the Patching grammar, which includes the four following steps as shown in figure 2.10 :

- (a) Finding the topology of the multi-vaults.
- (b) Funicular form finding of the multi vaults.
- (c) Structural analysis of multi-vaults found in the form.
- (d) Transforming the multi-vaults found in form into 3D printing data.

The Patching design grammar decodes extend and formalise the ancient vaulting techniques. Furthermore, the Patching design grammar utilises numerical tools such as mesh pattern topology and shape topological skeleton to adapt vaulting techniques to 3D Printing data. Finally, this grammar classifies the self-standing interconnected components (Patches) and automatically decomposes the non-traditional boundaries into subdivided spans covered by the classified Patches.

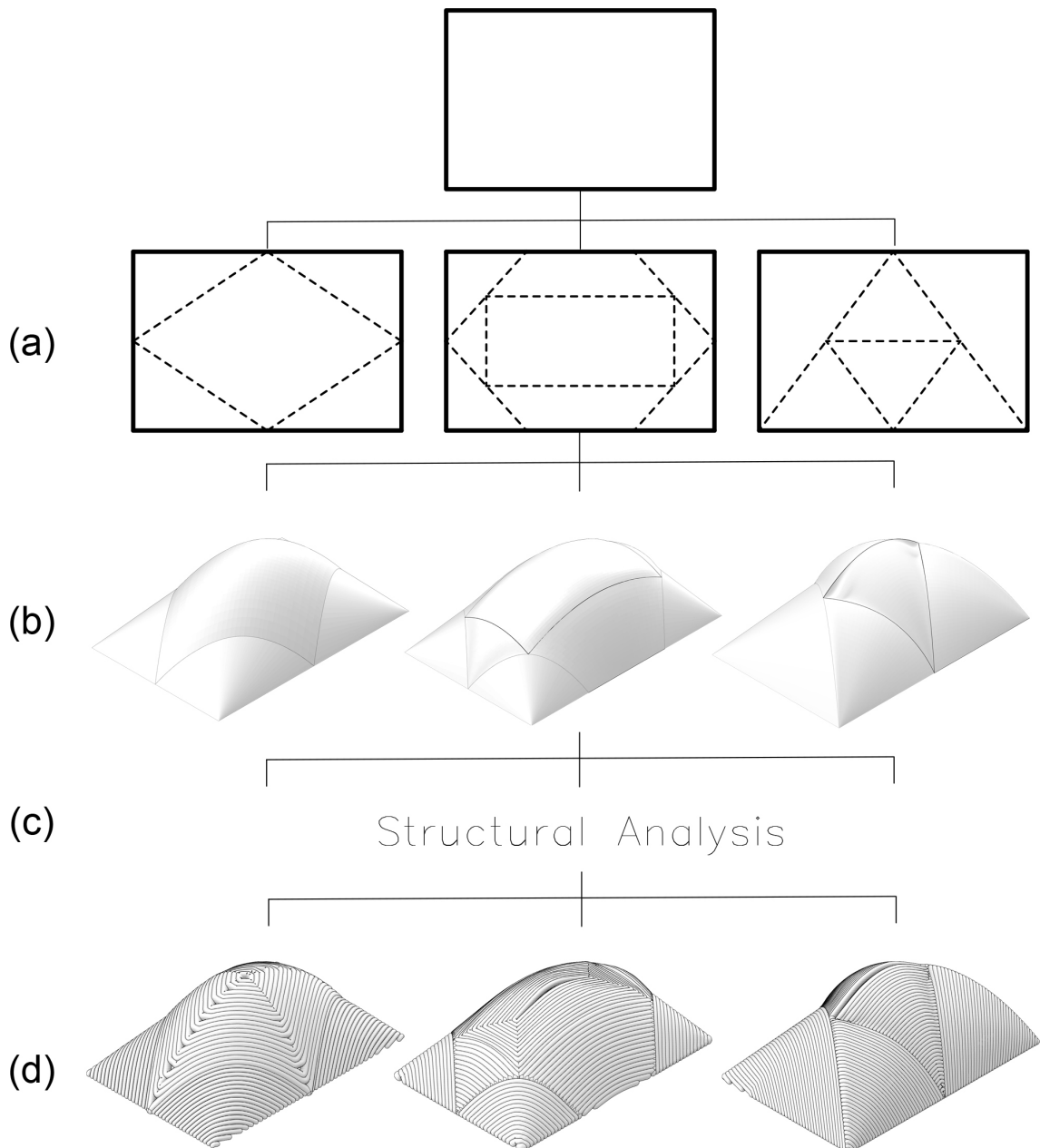


Figure 2.10 – Patching Design Process Overview

## 2.5.2 Grammars vs Parametric Design

Shape grammars generate a design language using concise rules that allow understanding of the diverse styles and designs. These grammars have been

developed to address two primary aspects of design. Firstly, they facilitate the analysis and description of contemporary or historical design styles. Secondly, they support the synthesis and creation of entirely new and original design styles [79].

On the other hand, a set of independent continuous parameters defines a parametric space. For example, a collection of vertex coordinates and their connection order (Mesh topology) describes a specific mesh geometry. Exploring these parameters within their defined ranges enables describing all design instances within the design space (geometry exploration). Parametric modelling software often maintains a detailed design development history in the form of a graph. However, as the complexity of the graph increases, it quickly becomes inflexible and unsuitable for exploring a wide design space. In contrast, implicit low-level rule systems offer greater flexibility, allowing for extensive design exploration [63].

In summary, grammar serves the purpose of creating the topology, while parametric design facilitates geometric exploration based on the established topology. For example, in [5], shape grammar is utilised to simplify the complex task of predicting geometry deformations in the concrete 3D printing process, resulting in compensated shapes. Another example involves using simple rules such as movement and rotation to design interlocking blocks in [53], which are employed in constructing recyclable building elements.

This section introduces the Patching grammar for designing the topology of vault-like structures, specifically to work with funicular form-finding tools. Simple rules are employed to define the support of Patches, as well as the print or slicing direction. In other words, the Patching grammar encapsulates Patch geometry information in the form of rules, simplifying the design exploration process for users and enabling them to navigate complex parametric graphs, thereby focusing more on the design itself rather than the algorithmic process involved.

### 2.5.3 Patching Grammar

The Patching grammar serves as a tool for designing the topology of Multi-Vaults, adhering to the rules defined by the Patching grammar. The Patching method, which is a design workflow derived from the Patching grammar, consists of the following four steps:

1. Topological Design
2. Form-Finding
3. Structural Analysis
4. Geometry Tuning

The Patching grammar offers users a set of rules that enable them to encompass a diverse range of boundaries using the Patching method. Users can use the Patching grammar rules to design a 2D topology covering their desired boundary. It is important to note that designing with the Patching grammar does not guarantee the printability of the resulting design using the SF3DP (Scaffold-Free 3D printing) method. However, the Patching method assists users in generating design instances that have the potential for printability, considering the properties of the printing material.

### 2.5.4 Terms of Patching Grammar

Several terms need to be defined to comprehend the Patching grammar and Patching method. The elements of a Multi-Vault, along with the schematic representation of a Patch and a Lace, are illustrated in Figure 2.11. The definitions of the terms utilised in the Patching grammar and the components depicted in Figure 2.11 are as follows:

1. **Lace:** A Lace is a continuous mortar extruded from the printing nozzle. The Lace is also called the "Print Layer" in additive manufacturing.
2. **Patch:** A Patch is a 3D Printed domain where a lace can be continuously extruded.
3. **Multi-Vault:** Multi-Vaults are vaults composed of several interconnected Patches.
4. **Rule:** The rules in the Patching grammar are the topologically defined Patches that convey information on the support configuration of the Patches and their print direction.

The Squinches and Pendentives are considered Patches since they can be printed continuously. Therefore, the aggregation of nine Patches, including Squinches, Pendentives and other types of Patches in Figure 2.11 represents a Multi-Vault.

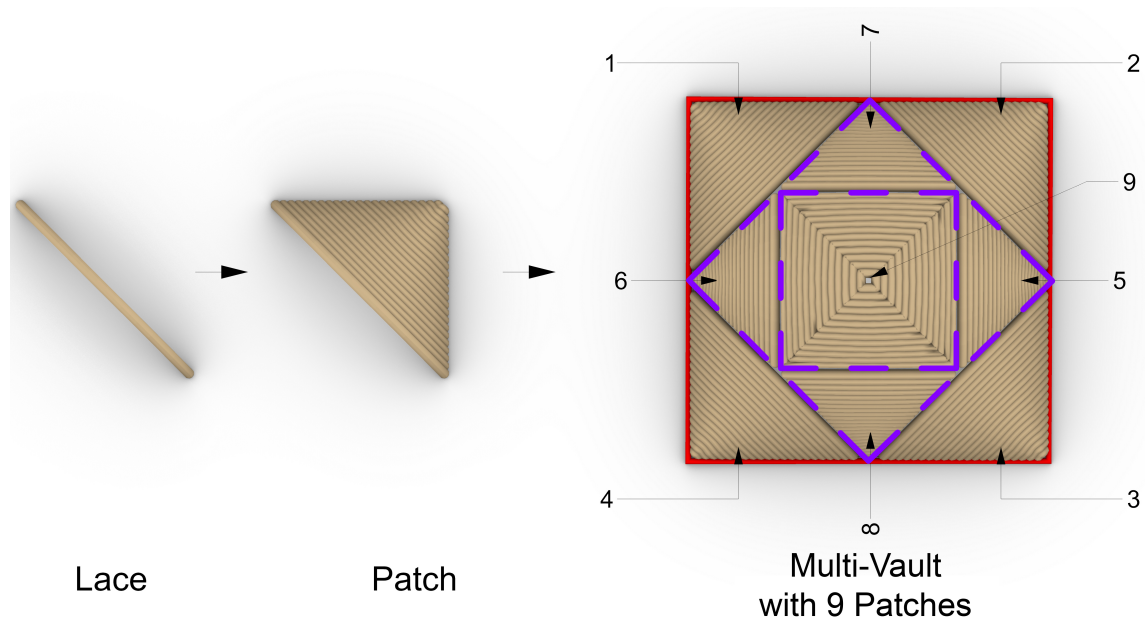


Figure 2.11 – Elements of Multi-Vault Structures: Identifying Key Components and Their Interconnections

### 2.5.5 Support Types

There are two main types of supports for the rules in Patching grammar.

1. Ground support: Ground support is support on the ground or the base of a multi-vault. The ground support is always planar.
2. Patch support (Above ground level):

- (a) When a Patch is supported by another Patch(es), the Patches' intersections are called Patch supports.
- (b) We can consider a wall a Patch since it can be continuously printed in one direction. Thus, the intersection of the Patches with a wall is also a Patch support. The Wall can be straight or curved and planar or non-planar.

Figure 2.12 represents the schematic symbols of support types. The continuous red line stands for Ground support. The dashed purple line stands for the Patch support. The symbols above are used for the support configuration of the Patches for all figures in this paper. The Patches in the Patching grammar are defined as their support condition. The topology of the supports provides information on the printing direction for each Patch. For example, a squinch can be defined in two manners concerning support conditions as shown in figure 2.13. Moreover, the support condition offers details on how the printing direction can be.

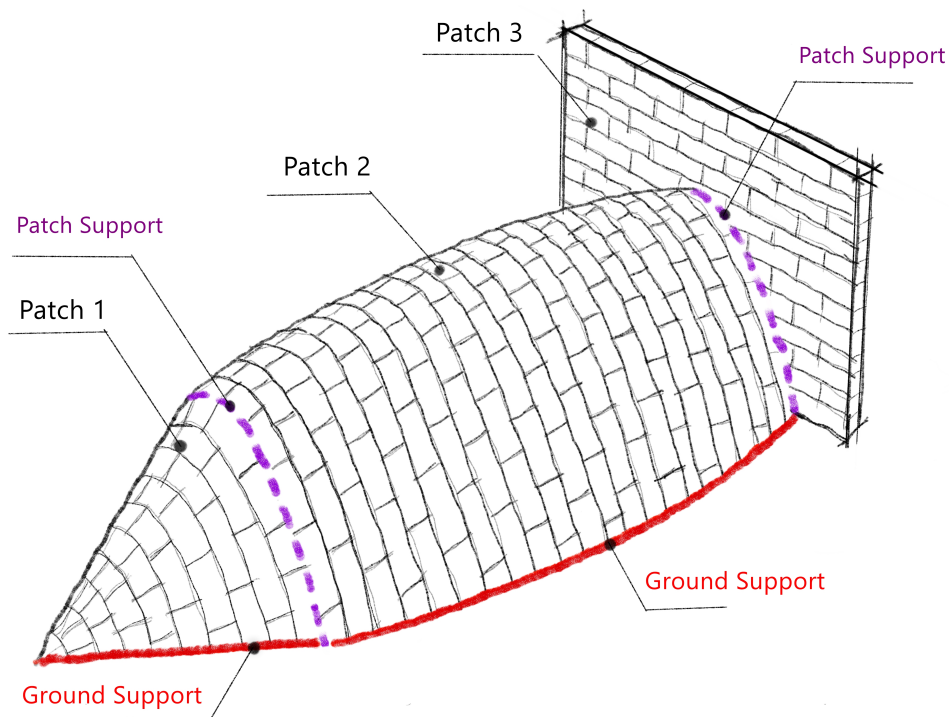


Figure 2.12 – Types of Supports in Patching Grammar - A Detailed Classification and Their Functional Roles

## 2.5.6 Patch Print Direction

Figure 2.13 illustrates two distinct topologies of a squinch, where the print direction is influenced by the supported topology. As discussed in Section 2.5.5, the topology of Patch supports (Boundary condition) impacts the print direction of Patches. If we reconstruct the Patch geometry as a mesh with quad topology, the support condition of the Patches determines the boundary condition and the topology of the quad meshes. To elaborate, if we take the quad mesh representation

of the Patch and slice it into strips, the strip direction corresponds to the printing direction for the laces within a Patch.

In the first row of Figure 2.13, the red curves depict the boundary conditions of each Patch, indicating that the Patches are supported by Ground support. For instance, the first topology exhibits two continuous supporting boundaries, represented by a polyline and a curve, while the second topology features two supporting boundaries with poles. These poles are specific singularities in quad meshes that are adjacent to triangles (known as Pseudo quads). Figure 2.14 illustrates a pole in a quad mesh. The presence of these poles governs the topology of the 2D mesh and, consequently, the print direction or the slicing pattern within the Patches. Further details on discovering quad mesh topology using singularity points are extensively discussed in [110]. Returning to Figure 2.13, the second row showcases the quad meshes created based on the supporting boundary topologies depicted in the first row. The edges of the quad meshes are colour-coded in blue (representing the transverse direction) and red (representing the print direction). Moving on to the third row, the green curves indicate the printing direction within a Patch by filtering the red edges of the quad meshes depicted in the second row. Finally, the fourth row presents a top view of a printed Patch, illustrating the printing trajectories obtained from the third row.

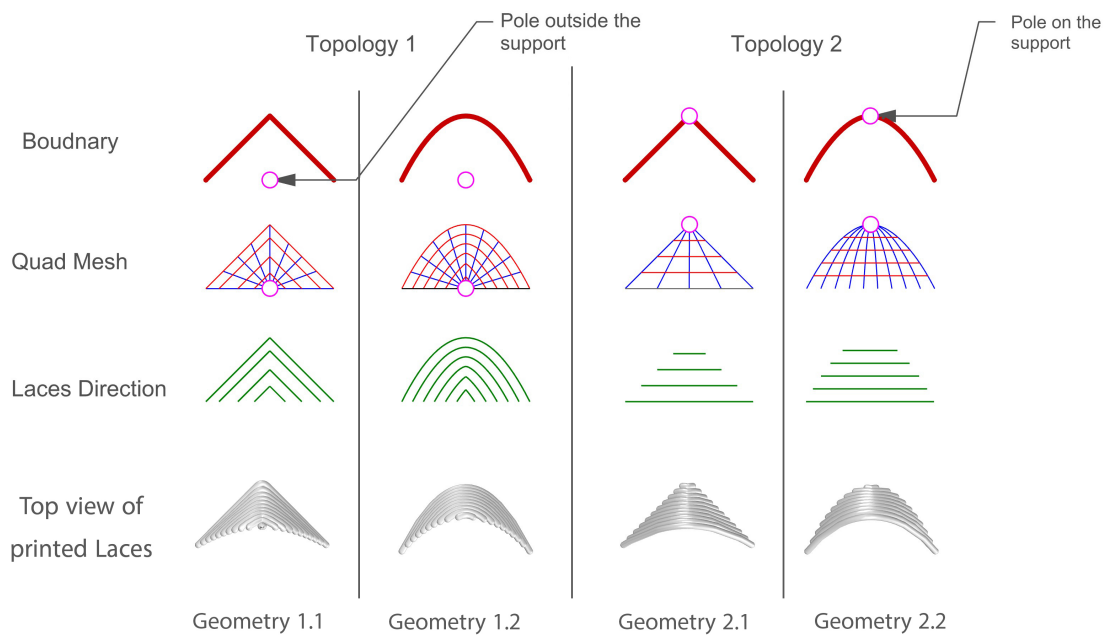


Figure 2.13 – Comparative Analysis of Two Squinch Geometries with Varied Support Conditions: Effects on Print Direction

## 2.5.7 Supports Junctions

Figure 2.15 shows several configurations of the supports combinations. In Section 2.5.5, two types of supports are introduced. These two types can combine differently to shape the Patch support boundary configuration. Finally, Figure 2.16 explains laws concerning the arrangement and combination of supports.

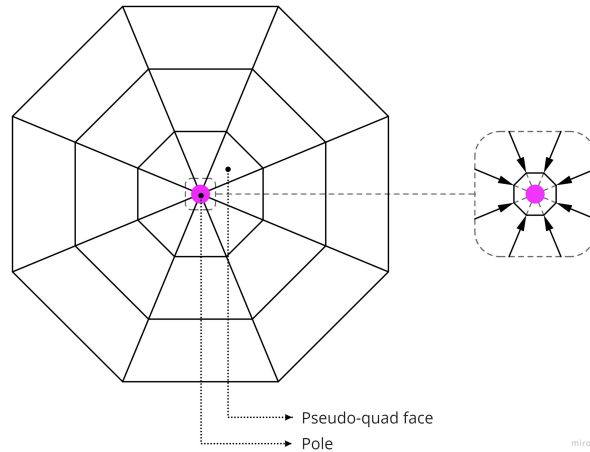


Figure 2.14 – Illustration of a Pole in a Quad Mesh: Highlighting Pseudo Quad Faces and Mesh Topology

1. Regardless of their type, the supports can be a line, polyline or closed. Therefore there are six types of support:
  - (a) Ground line-support
  - (b) Ground polyline-support
  - (c) Ground closed-support
  - (d) Patch line-support
  - (e) Patch polyline-support
  - (f) Patch closed-support
2. If two different support types connect, they will be considered separate. For example, interconnecting a Patch support with one ground support will make a detached polyline support configuration (Figure 2.16, Law 2). In contrast, if two supports with the same type, for example, two Patch-supports connect, they will be considered as one Patch polyline-support.
3. If a pole poses on a support, it splits that support (Figure 2.16, Law 3).
4. The curve-like supports are topologically the same as polylines but geometrically different. Thus, in Patching Design Grammar, wherever there is curve support, it will be titled polyline-support (Figure 2.16, Law 4).

In Section 2.5.9, the subscript and superscripts for the letters (S), representing the support type, and (C), representing the support configuration, adhere to the law described above.

## 2.5.8 Patching Grammar Rules

This section represents the sets of rules that are classified based on their support conditions. The rules are classified into two classes.

1. **Primary rules :**  
*Wall, Squinch, Pendentive, Nubian Vault, Dome* (Figure 2.19).
2. **Hybrid rules:**  
 These rules share the characteristics of two primary rules at the same time.



	Line	Polyline	Polyline-Detached	Closed	Closed-Detached
Ground Support					
Patch Support					
Hybrid Support					

Figure 2.15 – Examples of Support Junctions in Boundary Design: A Visual Guide to Types and Connections

Law 1	Law 2	Law 3	Law 4
Line Support	Two Line Supports	1 Line Support	Polyline
Polyline Support	Two Polyline Supports	2 Line Support	Curve
			Topology 1
Closed Support		1 Polyline Support	
			Polyline
		2 Line Supports	
			Curve
			Topology 2

Figure 2.16 – Laws Governing the Combination of Supports and Their Classification

The list of hybrid rules is as follows:

*Squinch-Pendentive*, *Squinch-Nubian Vault*, *Hybrid-Dome* (Figure 2.20).

The gradient colours in Figures 2.19 and 2.20 show the sequence of printing layers. The layers with pale colour are the initial layers, while the layers with bright pink colour are the last ones. The dark grey layers are meant to understand support

types better and were printed in the previous iteration.

### 2.5.9 Rules Naming

Each rule is named based on its type and support topology configuration. For example  $R_a S_b C_c^d P_e^f$ , R stands for the rule, S stands for support, C stands for support configuration, and P stands for Pole.

- **Rule(R)** : The subscript "a" under the R letter represents the rule type.
  - 0 = Wall
  - 1 = Squinch
  - 2 = Pendentive
  - 3 = Nubian Vault
  - 4 = Dome
  - 5 = Squinch-Pendentive
  - 6 = Hybrid Dome
- **Support(S)**: The subscript "b" under the S letter represents the support type (s).
  - 0 = Ground Support
  - 1 = Patch Support
- **Configuration(C)**:
 

The subscript "c" under the letter C represents the configuration of support(s). Figure 2.17 shows different configurations of supports.

  - 0 = Line
  - 1 = Polyline-Curve
  - 2 = Closed

The superscript "d" above the C letter represents the support(s) kinks. When the support configuration is a Line, the number of kinks always equals zero (The endpoints are not considered kinks). For the polylines, the number of kinks starts from one, and for the closed supports, the number of kinks starts from three. For the curved polylines, the number of kinks is Infinite.

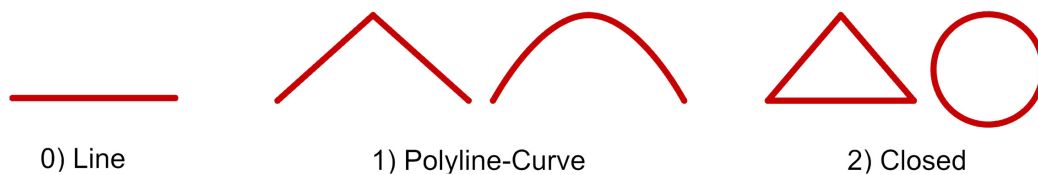


Figure 2.17 – Support Configurations

- **Pole(P)** : The subscript under the P letter represents the pole type (s).
  - 0 = Full pole
  - 1 = Partial Pole

The full poles are adjacent to only triangle faces, whereas the partial poles are adjacent to both triangle and quad faces.

The superscript "f" above the P letter stands for the pole(s) position. Figure 2.18 shows the different possible positions of a pole concerning support

boundary:

- 0 = inside the support
- 1 = outside the support
- 2 = on the support

This letter does not exist for the rule type "Wall" since no pole is needed to define a wall support topology.

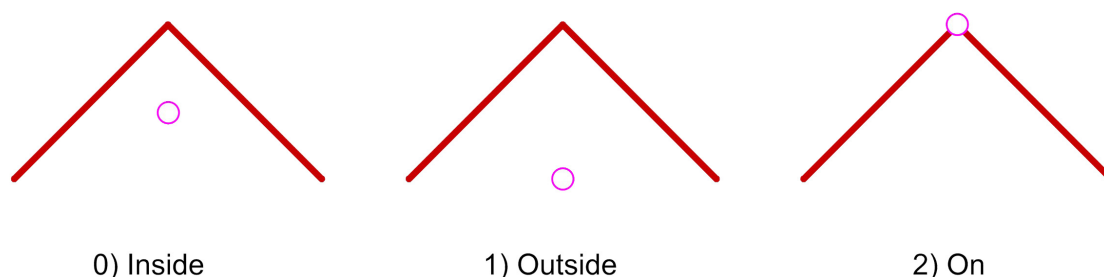


Figure 2.18 – Pole Positioning Strategies in Support Boundary Configuration

The name of each rule following the descriptions above is presented in Figures 2.19 and 2.20.

## 2.6 Design Strategies Utilising Patching Grammar

There are two main approaches to the Patching method.

1. **Generative design approach:** The process of covering a closed boundary with the aggregation of several patches (refer to section 2.6.1).
2. **Analytical design approach:** The process of analysing, splitting and dividing a seamless geometry or a closed boundary into several patches using analytical tools such as Delaunay, Medial axis and heat geodesics. (refer to section 2.6.2).

Figure 2.21 shows two discreet design approaches that users can follow for the design of the multi-vaults. In this section, these two design approaches are explained through examples, showing how a user can integrate the Patching design grammar using these two design approaches to design a Multi-Vault.

### 2.6.1 Generative Design Strategy

Figure 2.21 (A) shows the role of the users in the generative design approach. In this approach, the users will design the initial topology input following the Patching grammar rules and control the Patch geometry by assigning required parameters in a Form-Finding tool. Figure 2.22 represents the steps of topological design by

	Support Topology	Mesh	Geometry		Support Topology	Mesh	Geometry
Wall				Nubian			
	$R_0 S_0 C_0^0$				$R_3 S_0 C_1^3 P_0^1$		
	$R_0 S_0 C_1^1$				$R_3 S_0 C_1^{1.1} P_0^2$		
Squinch	$R_0 S_0 C_2^2$						
Pendentive	$R_1 S_{0,0} C_{0,0}^0 P_0^0$			Dome	$R_4 S_{0,0} C_{1,1}^{\infty} P_{0,0}^{2,2}$		
	$R_1 S_0 C_1^1 P_0^1$				$R_4 S_{1,1} C_{1,1}^{\infty} P_{0,0}^{2,2}$		
					$R_4 S_0 C_2^2 P_0^0$		
	$R_2 S_{1,1} C_{0,0}^0 P_0^0$				$R_4 S_1 C_2^2 P_0^0$		
					$R_4 S_{0,0} C_{1,1}^{\infty} P_{0,0}^{2,0,2}$		
	$R_2 S_1 C_1^1 P_0^1$				$R_4 S_{1,1} C_{1,1}^{\infty} P_{0,0}^{2,0,2}$		
					$R_4 S_0 C_1^1 P_0^0$		
$R_2 S_{1,0,0,1} C_{0,0,0,0}^{0,0,0,0} P_0^0$							
$R_2 S_{1,0,1} C_{0,0,0,0}^{0,0,0,0} P_0^1$							

Figure 2.19 – Catalogue of Primary Rules in Patching Design Grammar

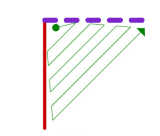
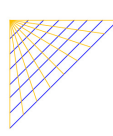
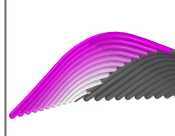
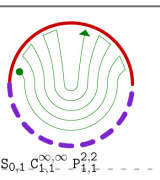
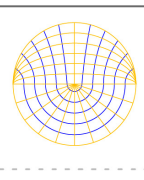
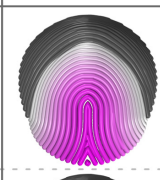

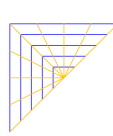
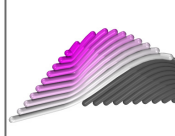
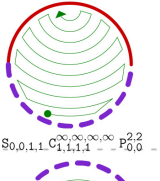
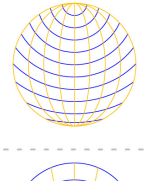
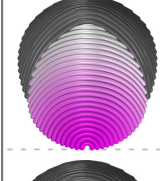
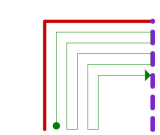

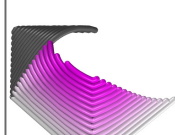
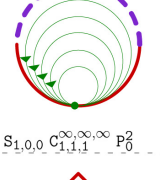
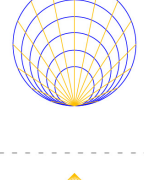
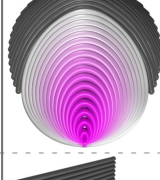
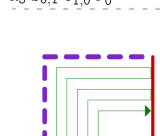
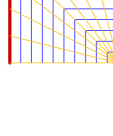
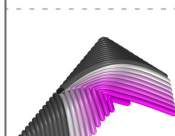
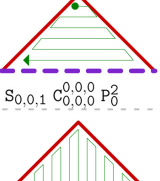
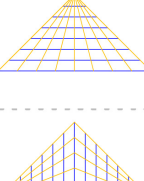
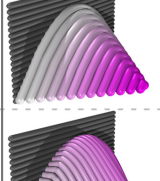
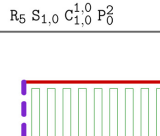
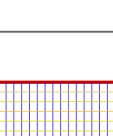
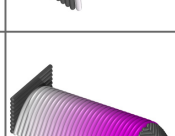
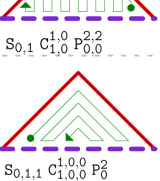

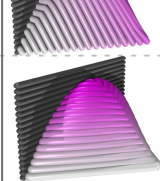
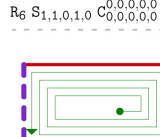
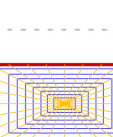
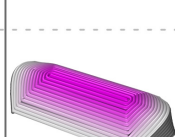
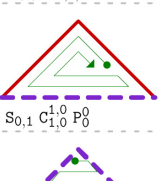
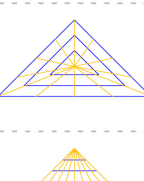
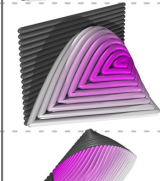
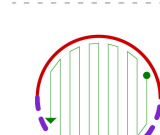
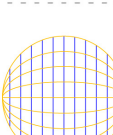
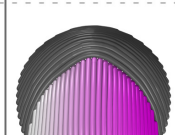
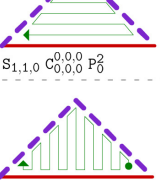
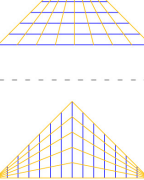
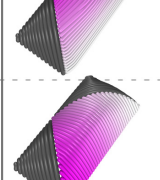
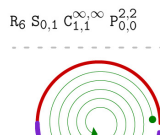
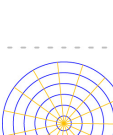
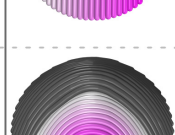
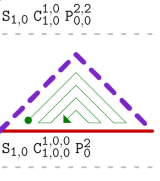
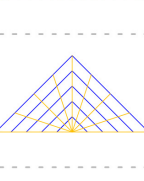
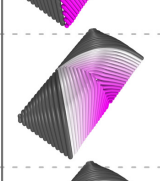
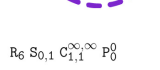


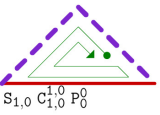
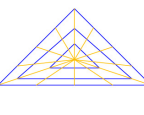
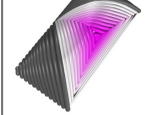






	Support Topology	Mesh	Geometry	Support Topology	Mesh	Geometry
Squinch-Pendentive	 $R_5 S_{0,1} C_{0,0}^0 P_0^2$			 $R_6 S_{0,1} C_{1,1}^{\infty, \infty} P_{1,1}^{2,2}$		
	 $R_5 S_{0,1} C_{0,0}^0 P_1^1$			 $R_6 S_{0,0,1} C_{1,1,1,1}^{\infty, \infty, \infty, \infty} P_{0,0}^{2,2}$		
	 $R_5 S_{0,1} C_{1,0}^1 P_0^2$			 $R_6 S_{1,0,0} C_{1,1,1}^{\infty, \infty, \infty} P_0^2$		
	 $R_5 S_{1,0} C_{1,0}^1 P_0^2$			 $R_6 S_{0,0,1} C_{0,0,0}^0 P_0^2$		
Hybrid Dome	 $R_6 S_{1,1,0,1,0} C_{0,0,0,0,0}^0 P_0^2$			 $R_6 S_{0,1} C_{1,0}^1 P_{0,0}^{2,2}$		
	 $R_6 S_{1,0,1,0} C_{0,0,0,0}^0 P_0^2$			 $R_6 S_{0,1,1} C_{1,0,0}^1 P_0^2$		
	 $R_6 S_{0,1} C_{1,1}^{\infty, \infty} P_{0,0}^{2,2}$			 $R_6 S_{0,1} C_{1,0}^1 P_0^2$		
	 $R_6 S_{1,1,0} C_{0,0,0}^0 P_0^2$			 $R_6 S_{1,0} C_{1,0}^1 P_{0,0}^{2,2}$		
	 $R_6 S_{0,1} C_{1,1}^{\infty, \infty} P_0^2$			 $R_6 S_{1,0} C_{1,0}^1 P_0^2$		
				 $R_6 S_{1,0} C_{1,0}^1 P_0^2$		
				 $R_6 S_{1,0} C_{1,0}^1 P_0^2$		
				 $R_6 S_{1,0} C_{1,0}^1 P_0^2$		

Figure 2.20 – Catalogue of Hybrid Rules in Patching Design Grammar

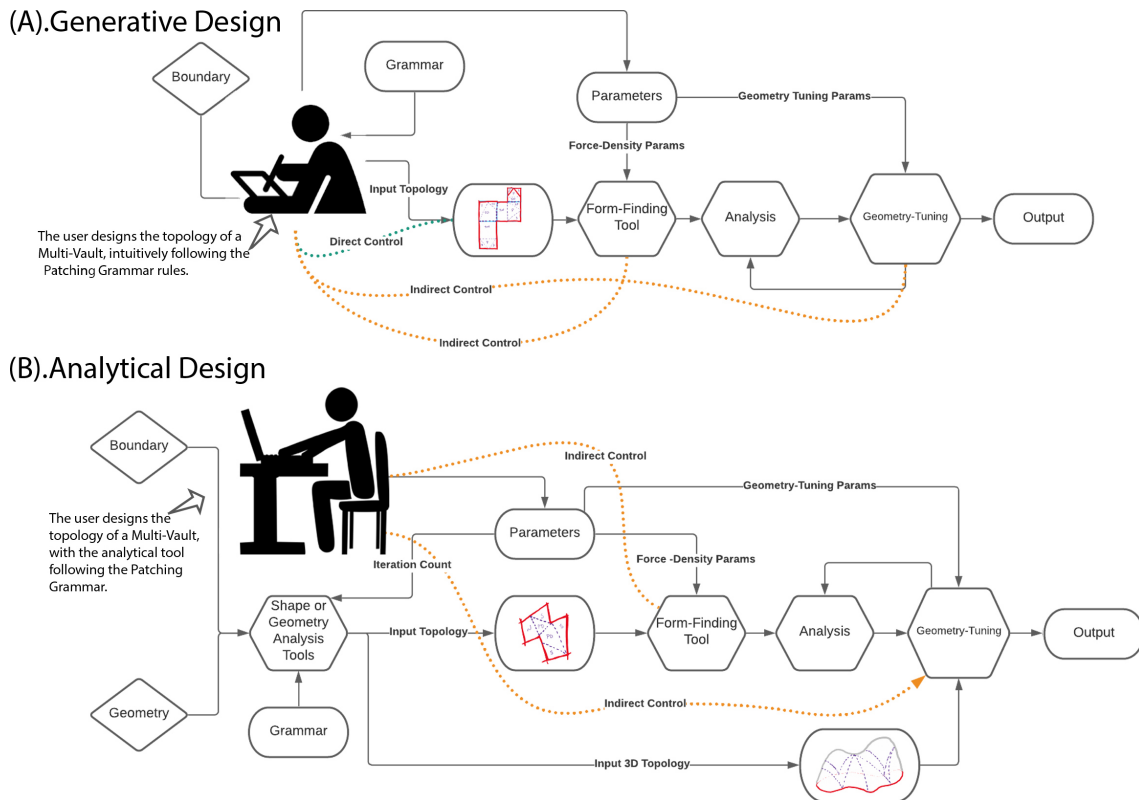


Figure 2.21 – Comparative Analysis of Generative vs. Analytical Design Approaches in Patching Grammar

a user following Patching Grammar and Form-Finding of a Multi-Vault using a Form-Finding tool and evaluation of design outcome using FEA.

The Patching grammar provides the users with the rules to form-find a Multi-Vault tailored for boundary conditions. The design through the Patching Grammar lets the users control the design process directly rather than only inserting parameters in a blind Form-Finding tool. For example, the users can intuitively design a 2D topology for a boundary following the Patching Grammar rules and use that 2D topology in a Form-Finding tool to make a Multi-Vault from that 2D topology. The generative design approach contains two following steps:

### 1. Topology

- (a) Generate a 2D topology (Coarse Mesh) from the proposed boundary. This coarse mesh defines the configuration of Patches and their arrangement in the target boundary to cover the defined boundary in 2D.
- (b) Densify the coarse mesh. Densifying the coarse mesh and geometrical modification of a 2D mesh will smooth the sharp corners of a Patch, such as the examples in Figure 2.23.

### 2. Geometry

- (a) Find a global funicular form from the densified 2D mesh.
- (b) Convert the global geometry to a Multi-Vault by retrieving the Patches from the global funicular form.

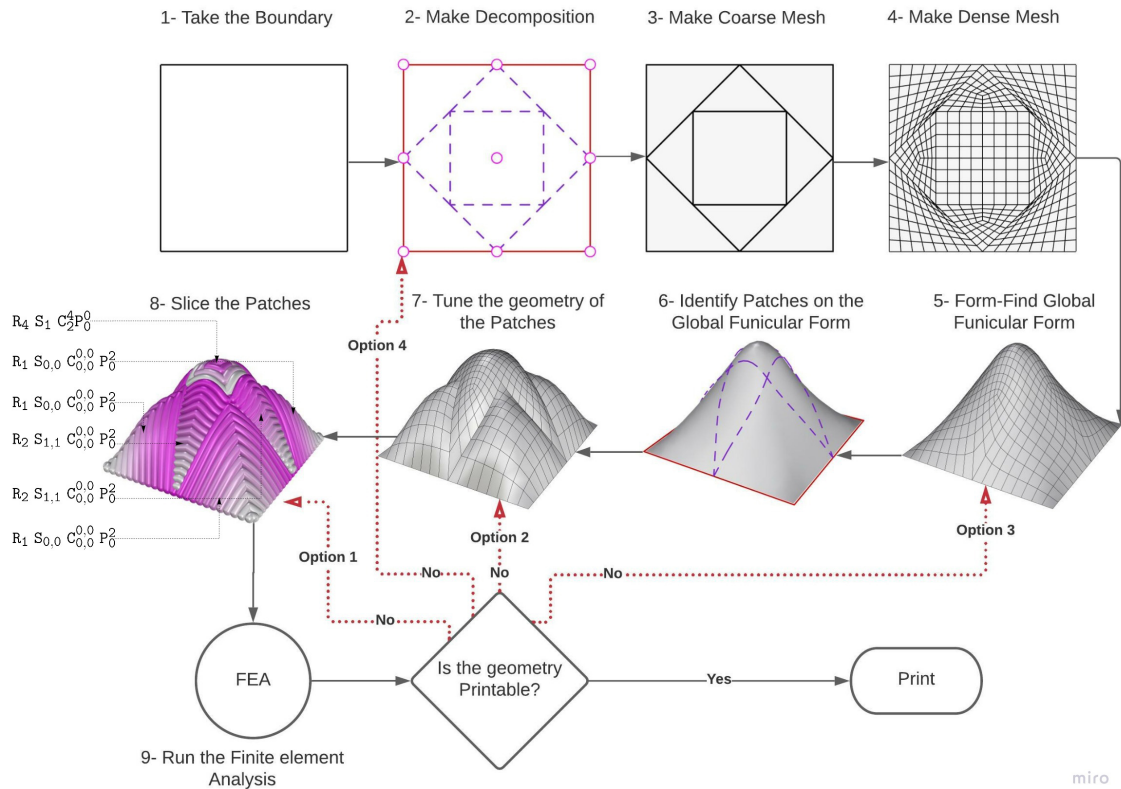


Figure 2.22 – The Generative Design Process: A Step-by-Step Overview

(c) Tune the geometry of the local Patches to increase their stability in the printing process.

Figure 2.23 shows three different 2D topologies proposed for the same boundary and the generated Multi-Vaults from each topology. The numbers inside the faces in the second column from the left (Coarse Mesh) show the printing sequence of the Patches.

### 2.6.2 Analytical Design Strategy

Figure 2.21 (B) illustrates the involvement of a designer within the analytical design approach, highlighting the distinction from the generative design approach. Unlike the latter, users cannot create the initial boundary topology intuitively. Instead, they employ the analytical method to extract essential information about the desired shape of the boundary. This information is then utilised to generate a customised Multi-Vault topology for that specific boundary. Users have two means of manipulating the analytical design approach:

1. **Geometry-based workflow:** In this workflow, users have a specific target geometry, and their objective is to generate patches based on the existing geometry. Additionally, they aim to transform the existing geometry into a Multi-Vault structure.
2. **Boundary-based workflow:** In this workflow, users possess a boundary and seek guidance from the analytical tool to assist them in designing a 2D topology.

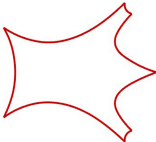
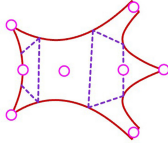
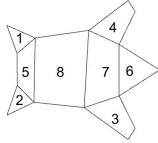
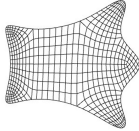
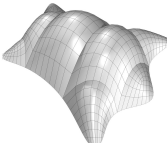
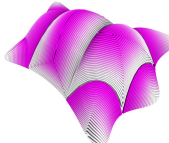
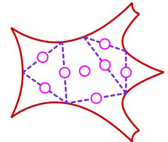
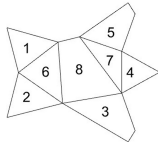
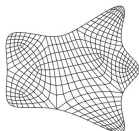
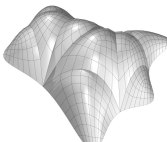
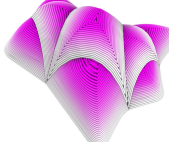
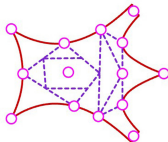
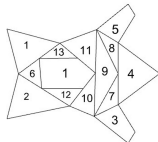
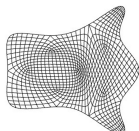
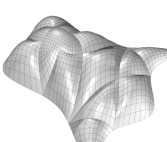
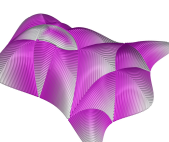
Boundary	Decomposition	Coarse Mesh	Geometrical Enhanced and Densified Mesh	Multi-Vault Geometry	Sliced Geometry
					
					
					

Figure 2.23 – Three Instances of User-Designed Decomposition for Target Boundaries via Generative Design Approach: Showcasing Customisation and Innovation by users through Patching Design Grammar

There are two main analytical methods in the process of analytical design:

1. **Delaunay analytical method:**

This method works with both geometry-based and boundary-based design workflows. Using this method, the users can take the initial boundary or extract the supporting boundary of the existing geometry and find a 2D topology of the Patches on that boundary and Form-Find a multi-vault using the Patching design process. Section 2.6.3 explains the 2D topology finding method through the Delaunay analytical method.

2. **Heat analytical method:**

Through this method, the users practice the Heat distance computing tool to generate the decomposition of the Patches on the existing geometry. The Heat method algorithm, developed and presented by Crane in [27], proposes a robust and fast technique for generating layers with a constant thickness on an arbitrary geometry from defined sources such as point(s), line(s), curve(s). In the analytical design process, the users can use the Heat method to split a seamless geometry into Patches following the Patching grammar's rules and convert that geometry into a Multi-Vault. In addition to the aforementioned function of the Heat distance computing tool, this paper also leverages the Heat method to slice the patch geometries into the laces and generate the robotic tool paths. The Heat analytical method also uses the Delaunay triangulation analytical tool to extract the Heat sources on the boundary of target geometry by extracting the topological skeleton of a boundary. Section 2.6.4 explains the process of Patch topology finding on two target geometries using the Heat analytical method.



### 2.6.3 Topology Finding of the Patches Using the Delaunay Analytical Tool

Figure 2.24 illustrates the Analytical design approach in conjunction with the Delaunay analytical method. In this figure, a user defines the geometry and employs the Analytical design approach to transform it into a multi-vault structure. The Delaunay triangulation method is utilised in this approach to identify expansive areas within the target boundary. These areas are then subdivided into smaller spans following the Patching grammar rules. It's important to recognise that the results obtained through this method may not always be optimal, but they are at least feasible. The definition of an optimal outcome is contingent on specific criteria, including material properties, structural considerations, fabrication constraints, and design requirements.

Another example showcasing the utilisation of the Delaunay analytical method to convert a boundary into a multi-vault is presented in Figure 2.25. In this figure, the user employs a boundary to create a multi-vault, which differs from Figure 2.24, where the user provides an initial geometry. The gradient colours of the layers in Figure 2.24, specifically in step six, indicate the printing layer sequence, ranging from pale to dark brown.

Furthermore, Figure 2.26 illustrates the topology design process using the Delaunay analytical design method for four distinct boundaries. The numbers within the mesh faces in the fifth column from the left (Second Decomposition) indicate the printing sequence order for the displayed patches in the sixth column. Below, the steps illustrated in Figure 2.26 are explained.

1. Divide the perimeter of the target boundary with equally distanced points and make the Delaunay mesh from achieved points.
2. Identify the prominent faces of the Delaunay mesh and merge the prominent faces that share the same segment to set the first decomposition.
3. Iterate steps 1 and 2 on the remaining sub-boundary from the previous decomposition.
4. The number of iterations depends on the designer's decision and the structural and technical necessities. For example, the users can evaluate their design after the first iteration using FEA and simulate the printing process using their printing setup. If the FEA results satisfy the structural necessities and the printing setup can print the generated Patches, there is no need for the designers to do further iteration.

### 2.6.4 Topology Finding of the Patches Using Heat Analytical Tool

Figure 2.27 shows the Analytical design process using the Heat method for two geometries. As mentioned earlier in Section 2.6.2, for identifying the position of Heat sources on the boundary, the topological skeleton<sup>1</sup> of the given boundary at each step of the Patching is extracted. The process of creating the Patch topologies on two geometries in Figure 2.27 is as follows:

- 
1. Medial Axis

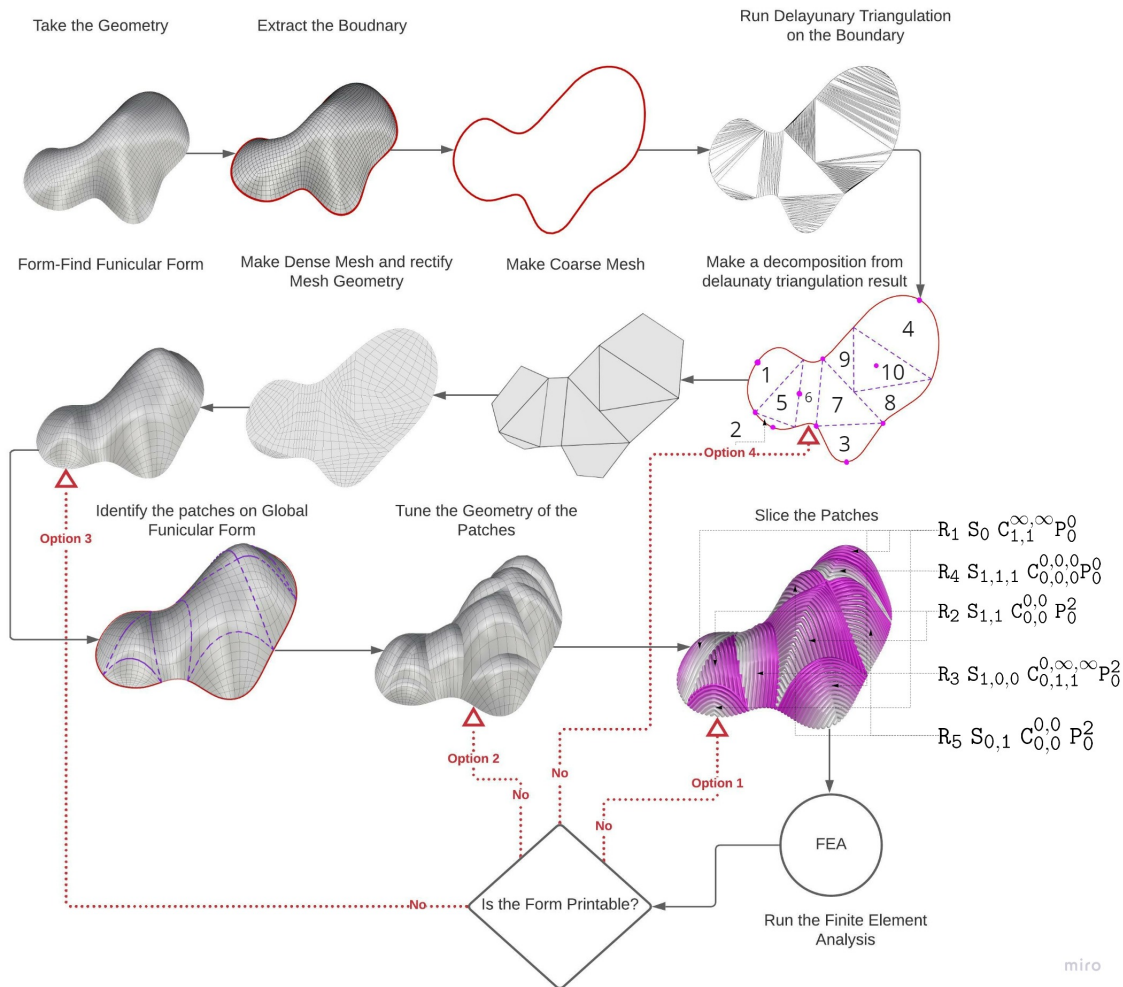


Figure 2.24 – Application of the Analytical Design Approach via Delaunay Method on User-Defined Geometries

1. Take the supporting boundary of the target geometry.
2. Extract the topological skeleton of the boundary. Then, take the endpoints of the topological skeleton and project them onto the boundary. This rule is not all-inclusive and may need some modification for different cases. For example, the Heat sources of the boundary in Figure 2.27(b) were explored with the aid of the target boundary extreme points. The extreme points are the points where the curvature of the boundary is higher or lower compared to adjacent points. The topological skeleton endpoints of the target boundary were compared with the extreme points. Then, the extreme points on the target boundary that corresponded to the endpoints of the topological skeleton were assigned as Heat sources.
3. Compute the distances from the Heat sources on the target geometry.
4. Identify the last generated curves on the target geometry where the generated curves resulting from distance computing from the Heat sources are not intersecting (orange curves).
5. Take the remaining part of the target geometry after splitting and making the first decomposition of the Patches on the target geometry.

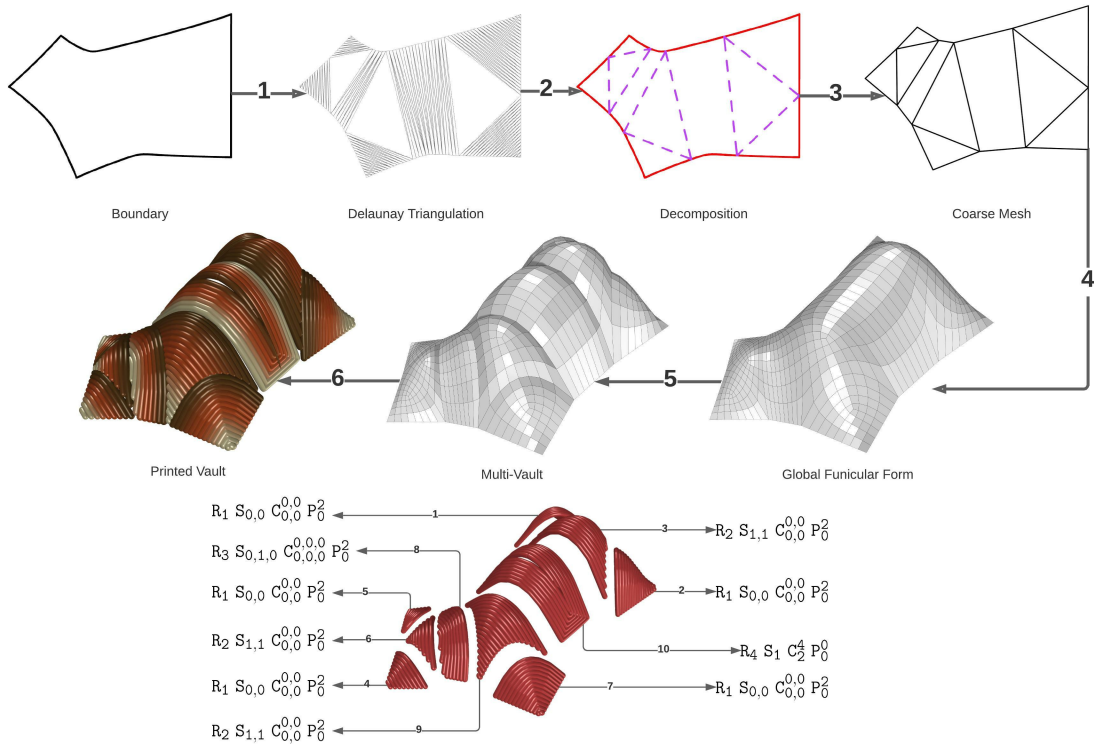


Figure 2.25 – Application of the Analytical Design Approach via Delaunay Method on User-Defined Boundaries

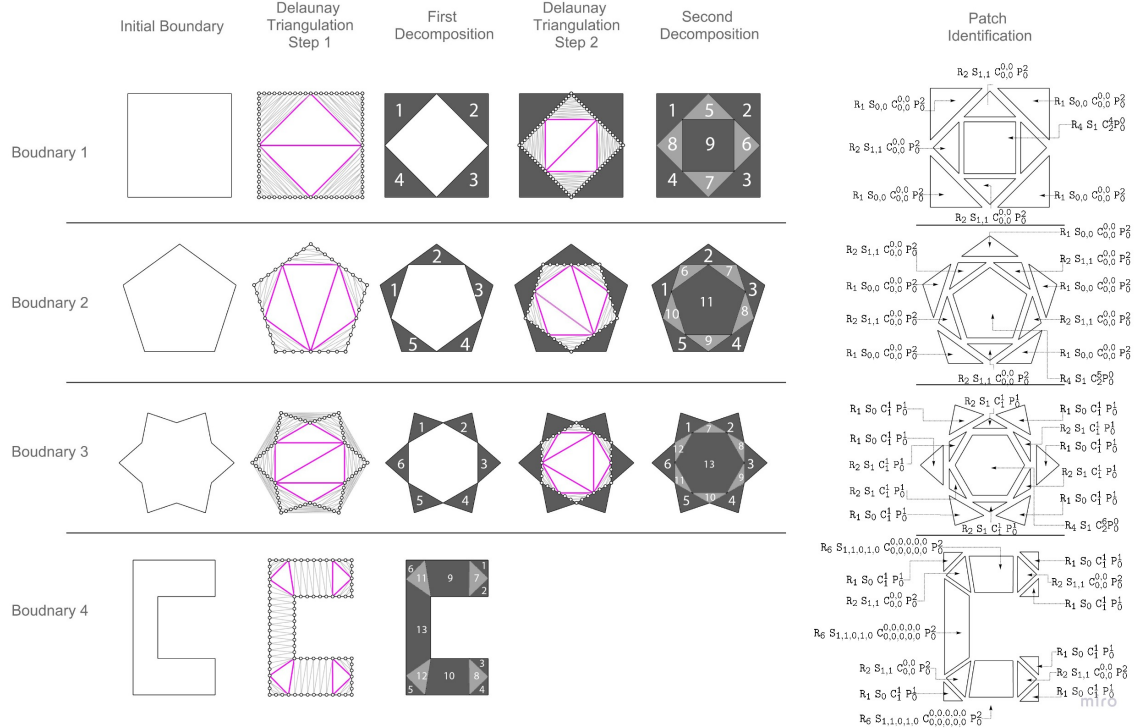


Figure 2.26 – Topology-Finding Process Across Four Different Boundaries Using the Delaunay Analytical Method

6. Iterate.

7. After the decomposition steps, identify the generated Patches on the target geometry based on their boundary condition following the Patching grammar rules.

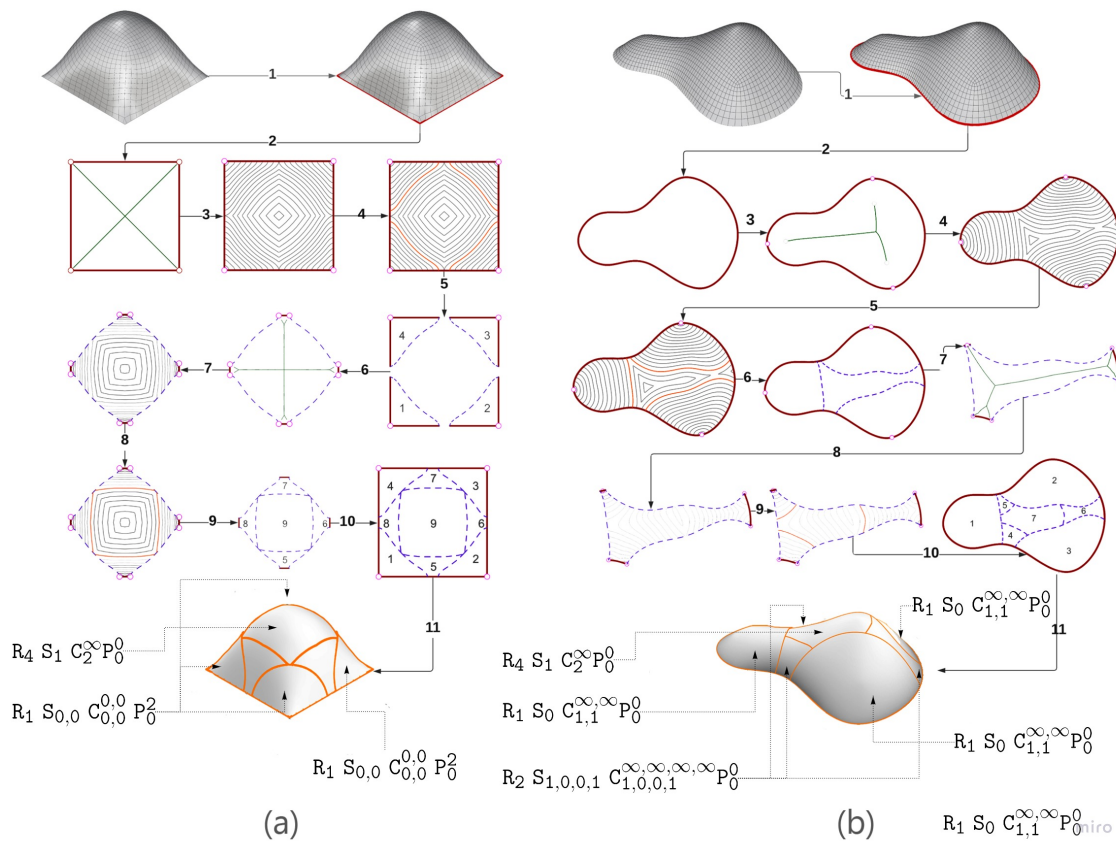


Figure 2.27 – Analytical Design Using the Heat Method for Two Different Boundaries: Application of Heat Method Geodesic Distance in Patching Design Grammar - A Comparative Study

Figure 2.28 provides another example of employing the heat Analytical design approach, where a user defines a geometry containing voids and seeks to transform it into a multi-vault structure with voids. In this specific example, the initial geometry proposed by the user includes two voids. Through the analytical patching process, the geometries of these voids are transformed, along with the initial geometry, to meet the requirements of SF3DP with the Patches.

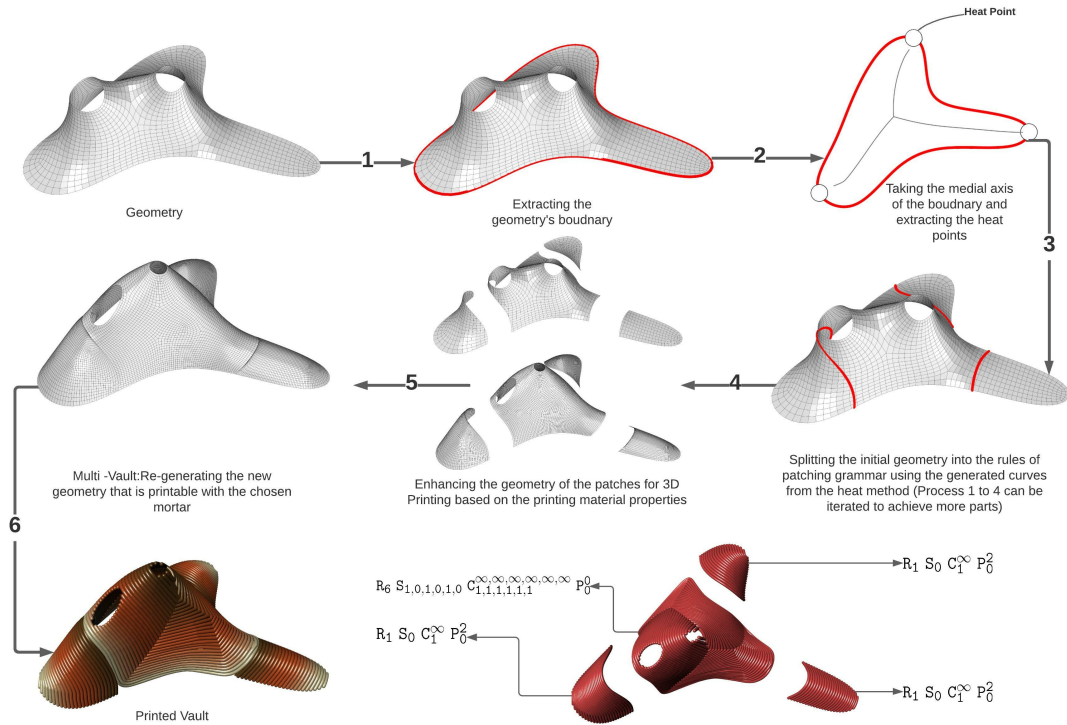


Figure 2.28 – Analytical Design Utilising the Heat Method for Geometries with Voids

## 2.7 Geometry Tuning

If the structure opts to be printed step wisely (Patching technique) rather than continuously, exploration of different geometrical alterations is compulsory. Considering the printing mortar properties such as the Young modulus and the yield strength, and the geometry of the patch and its boundary condition, the user should evaluate the Patches at each step (Lace) of printing regarding their stability both under the self-load and when they become support for the following interconnected Patch(es). During and after the printing process, the Patches of a Multi-Vault experience different stresses such as tensile, compression, and bending moments. To make the Patches more resistant to the applied stresses, the users must tune the curvature of each Patch. Good structural form results in low compressive stresses and reduces the need for bending capacity of a structure, regardless of what material has been chosen [125].

When the users intend to print their target geometry step-wise by the Patches, after converting the initial monolithic geometry into a Multi-Vault, they have to tune the geometry of each Patch to gain local funicular geometries to guarantee successful printing. The geometry tuning can help the printability of the geometry in two ways. First, by reducing the internal forces, and second, by increasing the buckling factor of the geometry. Changes to the global geometry due to local alterations are hard to predict or control since any local change to the hanging model influences the global equilibrium of the network [124]. Naturally, changing the local geometries

(Patches) of a Multi-Vault will transform the global geometry of the Multi-Vault and how the stresses are distributed in the entire structure. To increase the efficiency of the Multi-Vault against compressive stresses, after tuning the geometry of the local Patches, the global geometry of the Multi-Vault must not be very far from a funicular form.

Figure 2.29 shows three different ways of tuning the geometries of a Multi-Vault's Patches. Proposal 1 inflates the Patches by adding forces in the Normal direction to the nodes of the Patches' meshes. Proposal 2 applies forces in the vertical (Z) direction. Proposal 3 performs force density on each Patch by applying loads to the Patches individually to find the funicular geometry under given loads. The user might explore different load coefficient sets to achieve each Patch's minimum stress and maximum buckling capacity. By tuning the curvature of the Patches using the methods mentioned above, the users can reduce the applied stresses to each Patch up to an acceptable level for printing the Patches with selected material. If the user can't achieve such a result, they might alter the topology of the Multi-vault or change the printing material.

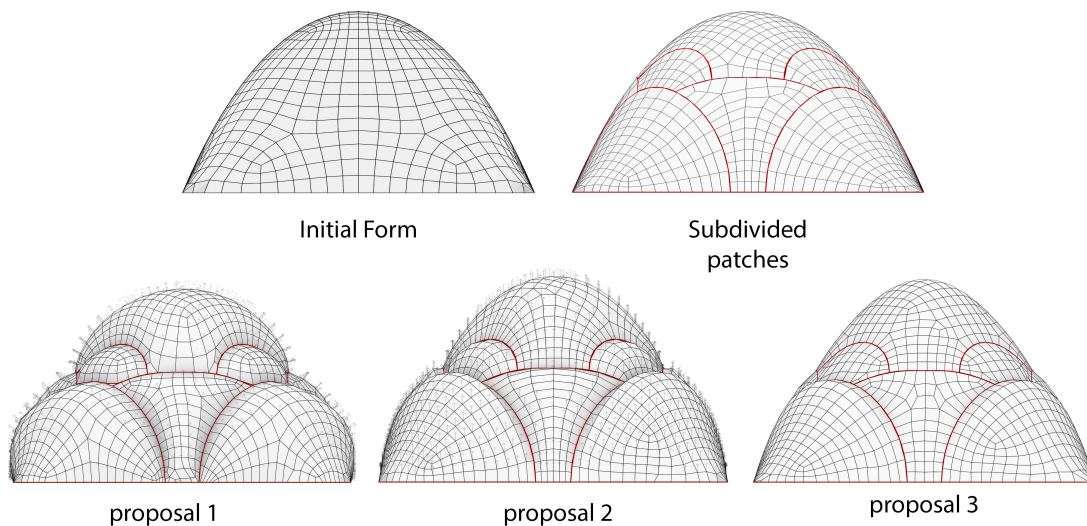


Figure 2.29 – Tuning Multi-Vault Patches' Geometries in Three Different Manners: A Comparative Analysis of Adjustments and Outcomes

Each of the three geometry tuning methods mentioned in Figure 2.29 can result differently in different cases. The users must apply and compare the mentioned methods on their Patch geometry and evaluate which one suits their specific Patch concerning the selected printing material. Accordingly, the users may have to use all three methods for different Patches in a Multi-Vault. Figure 2.30 shows the Patch of a Multi-Vault geometrically tuned with the three methods mentioned above. The input material has a maximum tensile capacity of 5 kPa and a maximum compressive capacity of -4 kPa. The Patch thickness is set at 6 cm for all parts of the Patch geometry. The applied load to the Patch only considered the gravity or the self-weight of the Patch. The Patch dimensions are approximately (50 cm x 50 cm x 48 cm). The results of the FEA on three different geometrically tuned patches are presented in table 2.1. The results indicate that the selected material is unsuitable for printing tuned patches, as they are all susceptible to material failure.

This vulnerability arises because the stresses applied to the patches surpass the material’s yield strength. Additionally, the buckling factor for all three proposals falls below 15, a threshold that typically signifies an unsafe condition. Among the proposals, Proposal 1 exhibits a relatively safer buckling factor and less overall internal stress, reducing maximum displacement. These attributes contribute to its enhanced structural stability compared to the other proposals.

In contrast, Proposal 2 is marked by the lowest buckling factor and greatest maximum displacement, yet it has less internal stress than Proposal 3. This makes Proposal 2 more susceptible to structural buckling but less prone to plastic failure than Proposal 3.

Ideally, a structure’s buckling factor should exceed 15 to ensure safety against buckling. However, given the initial state of common printing mortar, such as the clay mixture utilised in this research with Young’s modulus of 550 kPa, and the dimensions of the printed objects, the buckling factor rarely surpasses 3.27. This observation underscores the limitations of relying solely on geometrical modifications to address the printability problem in the given context.

Nevertheless, certain 3D printing techniques, such as Lace heating (refer to Chapter 3), may offer a solution. Enhancing the stiffness and strength of the fresh material during the printing process without additional substances in the printing paste can bolster the structure’s resistance to both plastic and elastic failure.

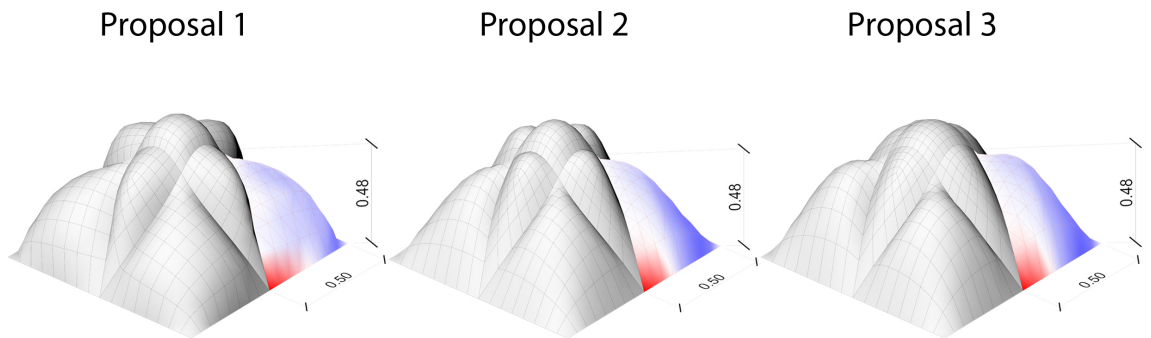


Figure 2.30 – Analytical Comparison of Three Geometry Tuning Methods: Evaluating Structural Integrity

	Proposal 1	Proposal 2	Proposal 3
Buckling	3.27	3.03	3.23
Maximum Displacement (cm)	2.88	3.13	2.91
Mass addition of Utilisation of mesh faces	1646	1683	1765

Table 2.1 – Analytical Comparison of Geometrically Tuned Patches Using Three Different Methods: Assessing Structural Analysis Results

It is important to note that when the curvature of the patch increases, the generated stresses on the ribs between the patches (patch supports) also increase. As an example, Figure 2.31 illustrates a specific patch of the multi-vault structure highlighted by the red boundary in (a) and demonstrates an increase in the patch's curvature by applying pressure load to the normal vectors of its mesh vertices in (b). This increased curvature of the patch leads to a higher utilisation<sup>2</sup> of the exposed (Naked) faces depicted in (c) of the patch, which is the ribs. The patch's curvature is measured using the mean curvatures<sup>3</sup> of the mesh vertices. The results of the Finite Element Analysis (FEA) conducted on the selected patch in Figure 2.31 are presented in Table 2.32. The table clearly shows that an increase in the patch's curvature corresponds to an increase in the utilisation of its ribs. In Table 2.32, the term "Normal vector weighting" refers to the scalar magnitude of the load applied to each vertex of the Patch mesh in the normal direction. In this example, the Kangaroo plugin for Grasshopper is utilised to apply the loads to the vertices of the Patch mesh. The "Mass addition of the mean curvatures of the Patch's mesh vertices" represents the sum of the mean curvatures of the vertices in the Patch's mesh. This value serves as an indicator of how curvy or inflated the Patch geometry is. The "Mass addition of Utilisation of naked faces (Ribs)" refers to the sum of the utilisation values for each naked face in the indicated patch, reflecting the overall magnitude of generated stress in the rib of the Patch. Furthermore, none of the mentioned parameters have units corresponding to a ratio or scalar magnitude.

On the other hand, the curvature reduction in a Patch geometry may grow or lower the stiffness of the Patch geometry against applied stresses. Furthermore, the buckling load of the Patches is also affected by changing the geometry of the Patches since buckling is related to boundary conditions, the geometry of the Patches and the material stiffness. Therefore, the users must find a balance between applied stresses within the acceptable stress range of their material and keep the buckling factor of a Patch at an acceptable level.

## 2.8 Roofing the Conventional 3D Printed Houses

Just like the projects "Casa Covida" and "TECLA" (see 1.2.4) or the experimentation by 3D printing company "ICON 3D" has resulted in the development of a housing campus featuring homes constructed using 3D printing technology. These homes are specifically built in the form of arches and domes using the ICON concrete 3D printing technique [66]. This particular method, referred to as 2.5D printing, utilises a gantry crane-based printing system (introduced in 1.2.3) [40]. However, it is important to note that this approach has not yet gained widespread adoption and is primarily implemented by a limited number of companies at the moment of creating this manuscript due to the 3D printed roof classification in [50].

---

2. The utilisation calculated for shells is the ratio between the tensile or compressive strength and the material's comparative stress in each face of the shell.[1]

3. The mean curvature is the average of the principal curvatures. This is often used to understand the overall bending of the surface. A mean curvature close to zero indicates a relatively flat surface, while a non-zero mean curvature indicates a curved surface.[30]



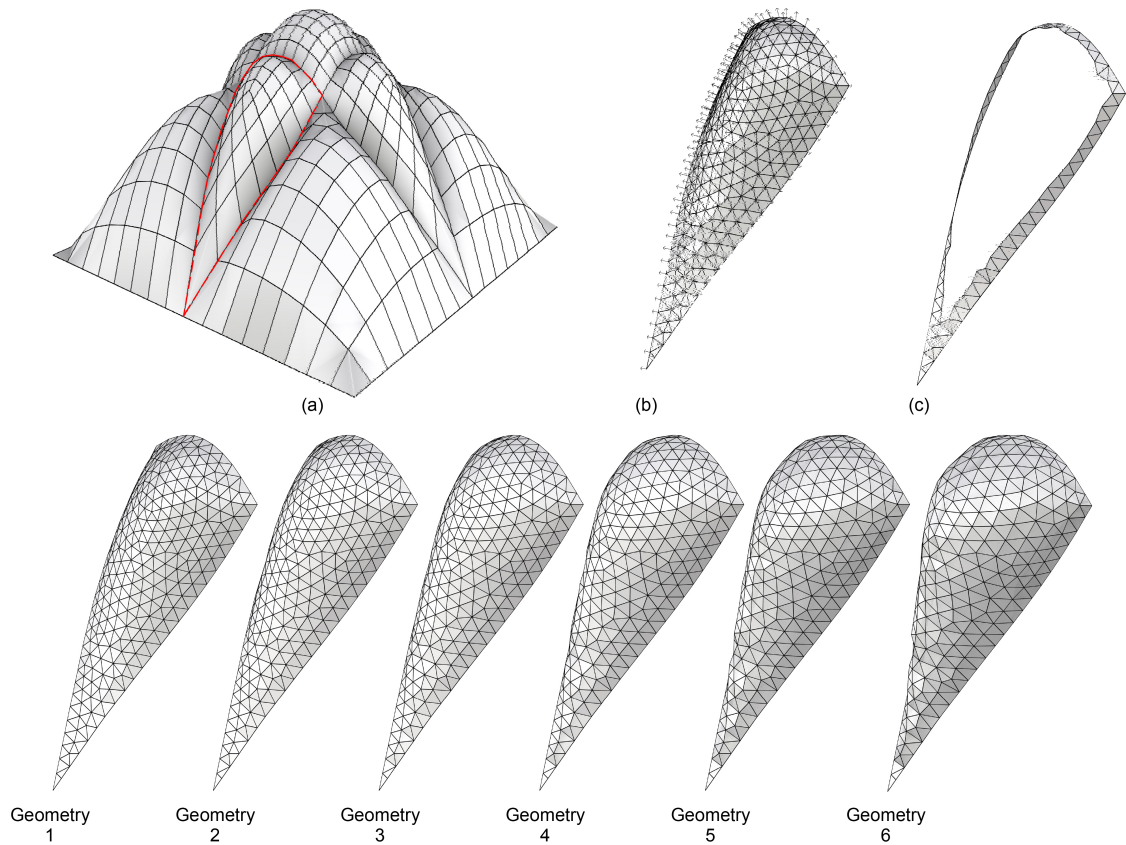


Figure 2.31 – Step-by-Step Increase of Curvature on a Selected Patch of a Multi-Vault by Applying Force in Normal Direction: Process and Structural Transformation

	Geometry 1	Geometry 2	Geometry 3	Geometry 4	Geometry 5	Geometry 6
Normal vector weighting	0.002829	0.008439	0.014577	0.028664	0.042051	0.069961
Mass addition of mean curvatures of the Patch's mesh vertices	1015.54	1214.74	1329.45	1454.71	1513.05	1554.42
Mass addition of Utilisation of naked faces (Ribs)	45.50	48.15	51.46	58.56	64.80	78.19

Figure 2.32 – Effects of Patch Curvature on Stresses Generated in Its Ribs: Analysing the Relationship Between Curvature and Structural Integrity

While using domes and arches in this printing method enables the construction of complete houses without the need for scaffolding, it does impose limitations on the architectural designs, as the shapes are primarily restricted to circular forms. This limitation may present challenges when conforming to standard residential plans and designs.

This study defines "conventional 3D printed houses" as those where the vertical elements are printed, but the roofs are constructed using traditional methods like pitched or sloping wooden roofs. Alternatively, the patching technique allows for printing houses with standard rectangular boundaries without the need for scaffolding. In this approach, 3D printing companies can use patching to cover the

roofs of 3D-printed houses with rectangular boundaries. The exterior and interior walls of the printed buildings serve as the boundary conditions for the patches. If both the interior and exterior walls support the patches, the roof of the building consists of multiple multi-vaults. However, if only the exterior boundary supports the roof, the roof can be 3D printed with just one multi-vault. The house was 3D printed by ICON 3D company in Georgetown, Austin, Texas [71], showcased in Figure 2.33, has its roof fabricated using the conventional method of wood. Figure 2.34 presents the proposal for using the patching technique to print the roof of this house. Figure 2.34 (a) displays the floor plan of the ICON-3D Printed house, while (b) illustrates the proposed roof topology and the decomposition of the patches. The numbers indicate the order in which the patches must be printed. Additionally, (c) shows the printed wall of the ICON-3D Printed house, suggesting arched interior doors to eliminate the need for wooden supports as lintels. Finally, (d) provides a 3D view of the proposed roof for the ICON-3D Printed house. It also demonstrates the possibility of having voids on the roof where the geometry of the voids follows the topology of the patches.

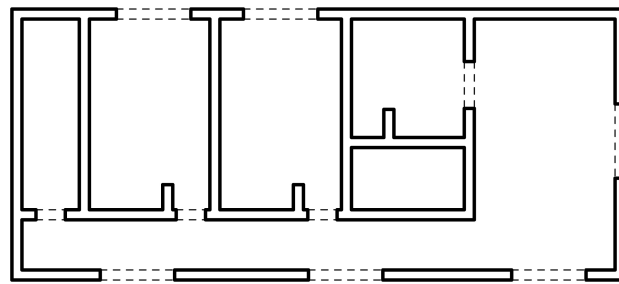


Figure 2.33 – The ICON-3D Printed House: Illustrating the Conventional Use of 3D Printing in Residential Construction with Roofs Constructed by Labour Force

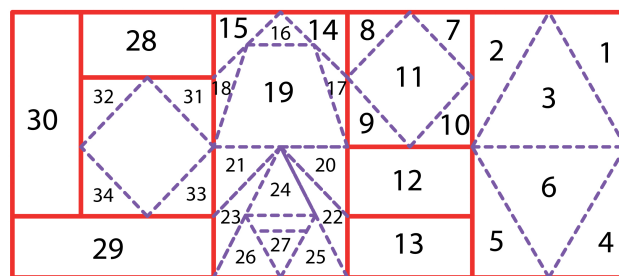
## 2.9 Conclusion

This chapter has presented a new design method for vaults that can be printed without scaffolding. The design methods are inspired by ancient vaulting techniques in desert structures, particularly in Iran’s desert. The chapter introduced a scaffold-free 3D printing (SF3DP) approach for vaults with convex quad boundaries. Additionally, a design grammar called Patching design grammar was presented, allowing users to design SF3DP vaults with various boundaries.

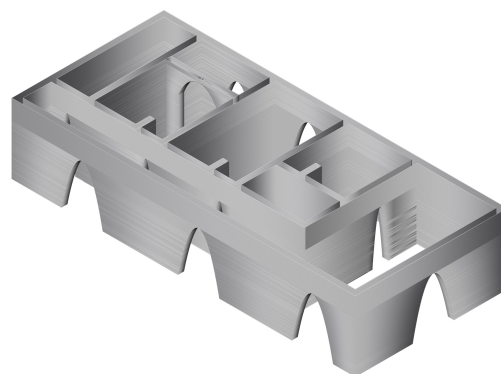
Two discrete design approaches were explained: the generative design approach and the analytical design approach, offering users flexibility based on their design objectives and fabrication constraints. The chapter also presented a step-wise finite element analysis (FEA) method for evaluating the printability of the designed vaults using the Patching design grammar. A method for modifying or tuning the geometry of the design output was also provided, along with an exploration of the impact of slicing patterns and shell cross-section designs on structural stability.



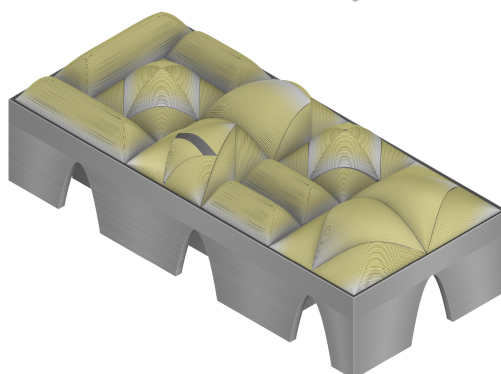
(a)



(b)



(c)



(d)

Figure 2.34 – Proposed Roof Design for the ICON-3D Printed House: Integrating Patching Technique in the 3D Printing Process for Residential Buildings

Furthermore, the chapter listed potential fabrication setups for printing designed shells using the Patching design grammar, categorised based on print strategy (e.g., in-situ/offsite or monolithic/modular) and 3D printing setups. One potential application of the Patching 3D printing system, depicted in the chapter, is the roofing of conventionally 3D-printed houses.

The main question addressed in this chapter was whether it is possible to design buildings that can be 3D printed without the need for temporary support. The objective was to develop a fabrication-aware design method for shells that can be 3D printed without scaffolding. The Patching design grammar, formalising ancient vaulting techniques as a rule-based design grammar, offers a solution.

The Patching design grammar holds the potential to shift 3D printing systems from semi-automated to fully automated, eliminating the need for formworks or temporary supports, even for horizontal elements like roofs and openings' lintels. Moreover, its design flexibility allows for the fabrication of dome-like structures with various boundary configurations beyond circular boundaries, including rectangular or other forms.

The Patching 3D printing method holds practical application potential. It can be utilised in designing shell-like structures for habitats, commercial buildings, or other public constructions. Additionally, it can be employed to print roofs for conventionally 3D-printed buildings, eliminating the need for manually fabricating wooden or steel roofs, thus increasing automation, reducing costs, and relying solely on mortar printing.

Additionally, advancements in 3D printing technology setups, such as drone-based setups, can expand the potential applications of the Patching grammar in different 3D printing scenarios by overcoming fabrication constraints.

The Patching 3D printing method offers significant benefits, including reduced material and labour costs, shorter fabrication times, and expanded design possibilities. Its adoption has the potential to fully harness the advantages of 3D printing in the construction industry.

باد و خال و آب و آذین بند لا اذد  
با من و نور ح لا با حق زند لا اذد

# Chapter 3

## Material, Mechanics & Structural Analysis

### 3.1 Introduction

The material discussed in this chapter regarding the effect of heat on the evolution of the properties of porous media is a culmination of collaborative work between the author of this dissertation, Mahan Motamedi, and a team of material scientists and engineers comprising Romain Mesnil, Anh-Minh Tang, Jean Michel Pereira, and Olivier Baverel. While the full extent of their findings will be published in a future journal article, this chapter incorporates some of the results from this collaboration that are within the scope of this thesis. The previous chapter discussed how one could design potential printable interconnected geometries without formwork regardless of the chosen material. However, with the knowledge of the material and the ability to control the rheological properties of the material, the realisations of the designed structures using Patching grammar is possible.

A successful print is only achievable with material tuning. Fresh earth as an extrusion paste must be fluid enough to be conveyed by the feeding pump (*Pumpability*) to the extrusion nozzle and be extruded by the extrusion system (*Extrudability*). At the same time, as soon as the fresh earth is deposited through a digitally controlled nozzle, it has to be solid enough to maintain its shape (*Workability*) and tolerate the weight of the superposing layer (*Buildability*). The practitioners in additive manufacturing earth-based structures mostly use additives, such as alcohol, in the mixture to accelerate the water evaporation process, consequently increasing the material strength in the 3D printing process.

In addition to the material aspects, this chapter also delves into the structural analysis of the 3D printed objects. The structural stability during the printing process is analysed, focusing on failure modes such as material failure, structural buckling, and global equilibrium failure. The topics of step-wise plastic buckling analysis, step-wise elastic buckling analysis, slicing pattern effect on structural behaviour, cross-section design, and finite element analysis are explored in detail. The effect of heating on the creation of a crust layer and the influence of the environment on raw earth construction are also discussed.

The results of this research are as follows:

- The wind(airflow) speed and the air temperature are significant parameters in

the water evaporation rate from earth-based materials such as the Speswhite kaolin clay mixture.

- The geometry of the printed object influences the drying rate of the porous media such as clay and, consequently, the evolution of the mechanical properties of the earth-based mortar in the 3D Printing process.
- Experiments show that the use of heat guns in the 3D printing process has the best effect on the evolution of the mechanical performance of the material and the success of printing with earth-based mortars, among other heating setups.
- The structural analysis provides insights into the critical aspects of structural failure, material properties, and the effect of slicing patterns, and cross-section design on the stability of 3D printed structures.

### 3.2 Methods to Increase the Mechanical Performance of Earth-Based Mortars

This section discusses different strategies to increase the mechanical performance of the clay mortar after deposition in the 3D printing process. There are two main strategies for increasing the mechanical performance of earth-based materials in the 3D printing process:

1. Chemical method: Applying special additives to accelerate the evolution of the mortar yield stress. This technique is used by other researchers such as Perrot by applying dry alginate to the clay mixture [116]
2. Physical method: Applying wind or heat increases the speed of the water evaporation and consequently increases the speed of the mortar's yield stress evolution.

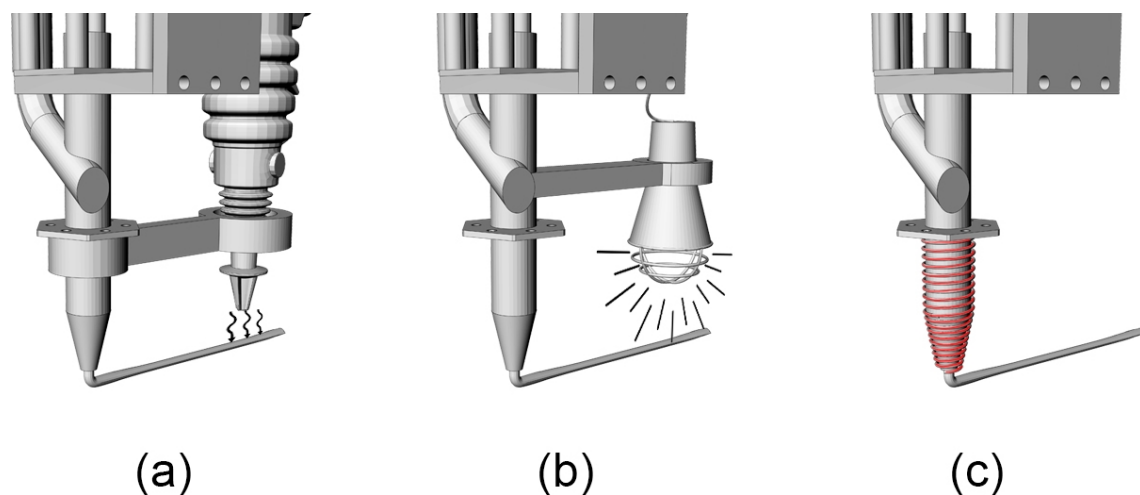


Figure 3.1 – Different Methods of Applying Heat to Fresh Mortar in the 3D Printing Process

This chapter focuses on using the physical method to increase the earth-based material's mechanical performance in 3D printing. Figure 3.1 demonstrates the three main methods of evaporating the water mixture in the 3D printing process.

However, these techniques can be performed using different setups rather than only setups mounted on the robot head. For example, a hot wind ventilator can be positioned in the 3D printing environment during the 3D printing process. It is important to note that while using a hot wind ventilator or similar techniques can effectively achieve evaporation, they may also introduce other variables that can affect the quality of the 3D printed object, such as temperature fluctuations and airflow disturbances. Therefore, it is important to carefully consider the specific requirements of the 3D printing process and select the most appropriate method for achieving evaporation while minimising any potential negative impacts on the printing process.

1. Convection: This method can be performed using a heat gun mounted on the robot head (figure 3.1, a) or hot air ventilators in the 3D printing environment. The use of a regular industrial ventilator can also be a solution.
2. Radiation: A heating lamp can perform this method mounted on the robot head (Figure 3.1, b) or a heating lamp in the printing environment facing the printing object. Using infrared or microwaves to heat the printing mortar is also possible. Regardless of the radiation emitting source, the total amount of radiation that reaches a body per unit area is called irradiation, and it's denoted using the letter "G". The irradiation waves that reach the surface of the printing layer will follow three scenarios:
  - (a) The waves can be absorbed by the printing layer and cause an increase in its temperature
  - (b) The waves can be reflected through the surface of the printing layer
  - (c) The waves can transmit through the printing layer, which is not the case when the printing mortar is clay or any completely opaque material

The black objects function as perfect emitters of radiation and as perfect absorbers. Therefore, incorporating black colour in the printing layer's mixture can significantly enhance radiation absorption from the emitting source, leading to a faster evaporation rate. Absorptivity refers to the amount of radiation absorbed by a surface compared to what a black body absorbs. According to data provided by [140], a red clay brick exhibits an absorptivity of 0.95, while white paint has an absorptivity range of 0.25 to 0.4. Although the Speswhite kaolin clay mixture used for the prototypes in this research appears white, it shares similarities with red brick in terms of porosity and surface roughness. However, the absorptivity of the Speswhite kaolin clay mixture needs to be determined experimentally.

Another crucial factor influencing heating through radiation is the surface geometry of the emitter, as well as its orientation relative to the printing layer. This orientation is known as the view factor. Once the view factor is known, it becomes possible to calculate the heat exchange between the emitter and the printing layer. Subsequently, the net heat transfer between the two surfaces can be calculated by subtracting the radiation from leaving the emitter's surface and reaching the printing layer's surface. It should be noted that this calculation can be exceedingly complex in reality, as mentioned in [142].

3. Conduction: This method can be performed using a hot wire wrapped around the printing nozzle to heat the material in the printing nozzle (Figure 3.1c).



Another possible setup is to print on a hotbed, such as a hot metallic plate. However, it should be noted that these methods may be less effective than radiation and convection when using earth-based materials, as these materials have low thermal conductivity.

4. Hybrid method: The hybrid evaporation method can combine the techniques and setups mentioned above. For example, evaporation can be done by combining a heating lamp and a ventilator.

This research mainly focuses on evaporation using convection utilising configurations such as a heat gun, hot air ventilators, and industrial fans.

### 3.3 Rheological Requirements For Clay 3D Printing

The existing body of literature on 3D printing with concrete and clay-based materials primarily originates from the rheology community, while most published work on the mechanical properties of soils can be found in the soil mechanics community. These two communities employ distinct terminologies, necessitating the introduction of specific definitions and conventions to facilitate effective communication between them.

#### 3.3.1 Pumpability, Workability and Buildability

Soils and cementitious materials can be modelled as yield stress fluids, which behave as solids as long as the shear stress applied to these materials remains below the *yield stress*, noted  $\tau^*$  of the fluid. Once the flow is onset, the material behaves as a viscous fluid. Roussel [129] has identified several quality requirements of printable concrete, which depend on the yield stress. First, the material should be fluid enough to be fed into the pumping system, corresponding to the material's so-called *pumpability*. In practice, there is a threshold value above which clogging will occur. This threshold value depends on viscosity and yield stress, which should remain relatively low, but also on the ability to form a lubrication layer (for extrudability). In the "lubrication layer", only fine particles and water are sheared, and the ability to be pumped or extruded of a given material was reported to depend more on its ability to form such a layer than on its actual bulk rheology [23]. Furthermore, Roussel identifies that mixes with low water content have high yield stress and viscosity and low ability to form a lubrication layer [129]. A first-order approximation can thus be written by limiting the yield stress to critical yield stress depending on the printing system  $\tau_{system}$ .

$$\tau^* < \tau_{system} \quad (3.1)$$

Second, an individual layer should be able to maintain its shape after being extruded (*Workability*). The layer should also maintain its shape under the weight of the layers above it (*buildability*). Writing  $h$  the layer height, it is thus possible to write a criterion for plastic failure<sup>1</sup> of one layer that relates the compressive strength

---

1. Plastic failure, in the context of materials engineering, refers to the failure or deformation of a material that occurs beyond its elastic limit. When a material is subjected to stress, it initially deforms elastically, meaning it can return to its original shape once the load is removed. However, if the stress exceeds the material's elastic limit, it undergoes plastic deformation, resulting in permanent changes to its shape.

$\sigma_c^*$ , the weight density<sup>2</sup>, and the layer height  $h$ . More complex conditions have been proposed for the printability of cantilevers in [16].

$$\sigma_c^* > \rho gh \quad (3.2)$$

According to [18], in reality, the deposition of other layers can result in compressive stress, which is significantly greater in magnitude than the weight of a single layer when the layer is compressed, especially when the ratio between the layer height and the nozzle diameter is low. Moreover, to ensure the stability of the structure, the layer must not deform under the weight of the other layers. Equation 3.3 expresses this requirement and incorporates the robot's vertical speed  $V_z$  and a time parameter  $t$ .

$$\sigma_c(t) > \rho gh \cdot V_z \cdot t \quad (3.3)$$

The compressive strength (green-strength) must rapidly evolve with time due to the pumpability requirement for low-strength fresh material, which strongly restricts the compressive stress of the fresh material (typically below 10kPa). The increase in rheological properties with time is called *build-up* [121] in the following of this article. The build-up of cementitious materials has two main mechanisms identified in [81]: a *reflocculation* phase that lasts less than 120 seconds<sup>3</sup> and a *structuration* phase that is usually due to early hydration<sup>4</sup>. However, in the case of earth-based materials such as clay, the buildability is related to the drying mechanism rather than structuration. However, research in [84] suggests that certain clay suspensions exhibit thixotropic behaviour, especially those with specific additives, which signifies that clay mixtures can also have a reflocculation phase.

### 3.3.2 Stiffness Requirements

So far, the material requirements have only dealt with rheological properties. However, some failures have been observed due to insufficient material stiffness or low stability of the printing geometry, either a settling [4] or a buckling [149]. The settling problem is shown in Figure 3.2 (b): material deformation under self-weight can produce a cumulative deformation that exceeds the layer height, resulting in a free deposition of the layer with little control on its geometry [36].

---

2. Also known as material density and is a measure of how much mass is contained in a given volume of the material  $\rho g$

3. reflocculation is a process where particles come back together to form flocs or clusters after being dispersed or sheared, and this process is particularly significant in the context of 3D concrete printing for maintaining the shape and integrity of the printed structure.

4. The structuration rate is determined over a more extended period, typically in the thousands of seconds, and mainly characterises the increase in static yield stress due to chemical reactions

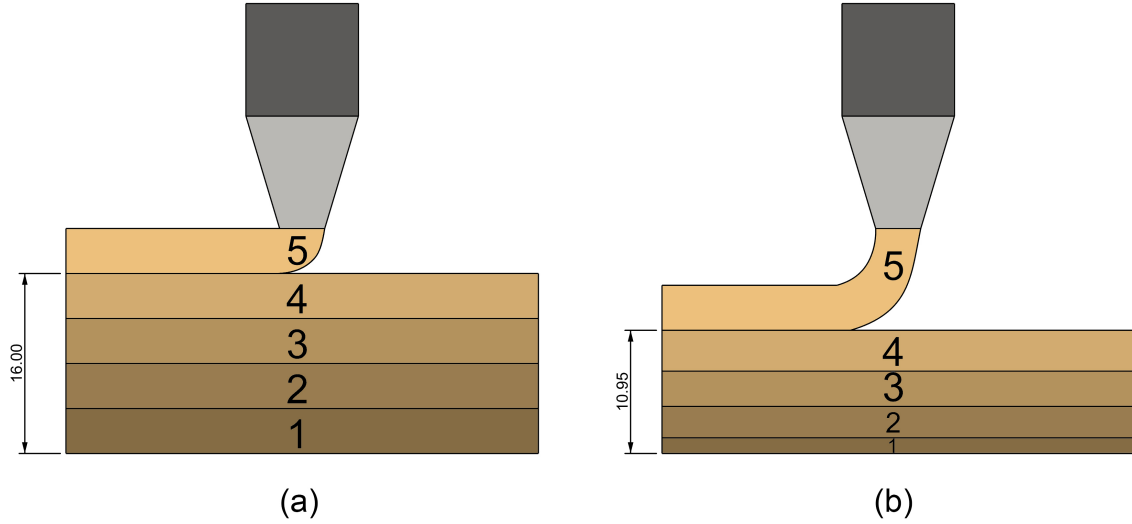


Figure 3.2 – (a) Nominal Printing Regime vs. (b) Free Deposition Due to Material Settling

This problem has been experimentally assessed for printed geopolymers by Archez *et al.* in [4]. The general requirement for rigidity modulus  $E$  to avoid settling of a wall of height  $H$  and thickness  $B$  is given in equation (3.4).

$$\int_0^H \frac{\rho g (H - z)}{E(z)} < h \quad (3.4)$$

in which

- $\rho$  - Density of the material. [kg/m<sup>3</sup>]
- $g$  - Acceleration due to gravity. [m/s<sup>2</sup>]
- $H$  - Height of the wall. [m]
- $z$  - Variable of integration representing the height from the base of the wall. [m]
- $E(z)$  - Rigidity modulus or Young's modulus as a function of height  $z$ . [Unit: Pa or N/m<sup>2</sup>]
- $h$  - Layer height. [m]

A simple formula results in the case of constant Young's modulus is given in equation (3.5).

$$E > \frac{\rho g H^2}{2B} \quad (3.5)$$

in which

- $E$  - Young's modulus, or the modulus of elasticity, represents the stiffness of a material. [Pa or N/m<sup>2</sup>]
- $\rho$  - Density of the material. [kg/m<sup>3</sup>]
- $g$  - Acceleration due to gravity. [m/s<sup>2</sup>]
- $H$  - Height of the wall. [m]
- $B$  - Thickness of the wall. [m]

Buckling is a catastrophic failure resulting from insufficient stiffness. The buckling loads strongly depend on the printed piece's geometry, size and boundary conditions. Roussel [129] proposes an approximation for a straight wall of thickness  $B$  recalled in equation (3.6).

$$E > \frac{3\rho g H^3}{2B^2} \quad (3.6)$$

In which

- $E$  - Elastic or young's modulus (Pa)
- $\rho$  - Density of the material ( $\text{kg}/\text{m}^3$ )
- $g$  - Acceleration due to gravity ( $\text{m}/\text{s}^2$ )
- $H$  - Height of the wall (m)
- $B$  - Thickness of the wall (m)

For example, for a wall with a thickness of 200 mm, height of 2000 mm and length of 1000 mm, and material with a specific weight of 1.6 kg/l, we can calculate the minimum required elastic modulus of the material as below:

$$E > \frac{3 \cdot 1600 \cdot 9.81 \cdot 2^{3/2}}{0.2^2} \approx 3.39 \text{ MPa}$$

It is important to mention that buckling can be independent of the material yield strength since it is unrelated to the material strength. Still, it is related to the material stiffness. Therefore, modification of the printing geometry can significantly alter the buckling capacity of the designed structure. This issue is discussed in more detail in Section 3.6.2.

### 3.3.3 Yield Criterion of Soils and Rocks

The yield criterion of soils is based on the Mohr-Coulomb theory. The Mohr-Coulomb theory is used in civil and geotechnical engineering to predict the strength and behaviour of soils and rocks under stress. The theory states that the shear strength of a material (the resistance to sliding or deformation) is controlled by two factors: the cohesion of the material (the tendency of its particles to stick together) and its internal friction angle (the resistance to sliding between particles). The theory assumes that materials can fail when the shear stress (the force applied to the material parallel to its surface) exceeds the maximum shear stress the material can withstand. The cohesion of the material defines this maximum shear stress plus the product of the normal stress (the force applied perpendicular to the surface) and the tangent of the internal friction angle. The Mohr-Coulomb theory provides a way to calculate the shear strength of soils and rocks based on their cohesion and internal friction angle, which can help engineers design structures and foundations that can withstand different types of loads and stresses [83, 43]. We consider thin shell elements, thus a plane-stress model, which is recalled in equation 3.7.

$$\tau < c_u \quad (3.7)$$

Where

—  $\tau$  - Deviatoric (shear) stress, defined as:

$$\tau = \frac{\sigma_1 - \sigma_2}{2}$$

where  $\sigma_{1,2}$  are principal stresses.

—  $c_u$  - Undrained cohesion, representing the critical shear stress in pure shear conditions. This corresponds to yield stress as mentioned in the 3D concrete printing literature [129].

$$c_u \Leftrightarrow \tau^*$$

Soil undrained cohesion is a term used in geotechnical engineering to describe soil resistance to shear under undrained conditions, meaning there is no water drainage out of the soil during loading. When a load is applied to a soil mass saturated with water and cannot drain, the water pressure within the soil increases, and the soil's strength and stiffness can change. The undrained cohesion is a measure of the shear strength of the soil under these undrained conditions and is often denoted by the symbol  $c_u$ . Furthermore, undrained cohesion is primarily related to the soil particles' characteristics and the pore water's nature [32]. For example, clay soils with smaller particle sizes tend to have different undrained cohesion than sandy soils with larger particles. This research assumes that the earth-based mortars in the 3D Printing process experience undrained conditions since they remain saturated in the printing process. Furthermore, considering the typical printing time for a structure, which is usually less than the time of soil consolidation. Therefore, the printing load may not cause water drainage from the printing mortar. However, this assumption may not be true for very large-scale structures in which printing time exceeds more than 2-3 days. To determine this, It should be examined whether the layers of the earth-based mortar lose water under the pressure of superposing layers in the 3D printing process. Figure 3.3 contrasts two distinct scenarios of superimposing printed layers. In Figure 3.3 (a), the printed layers are under undrained conditions, even when subjected to the pressure from the layers above. Meanwhile, Figure 3.3 (b) depicts a situation where the pressure from the overlying layers causes the water molecules within the printing layers to be extracted, resulting in a completely drained initial layer. The underlying assumption of this research is that the printing process of earth-based fresh mortars is undrained in terms of water drainage caused by the printing load. However, it is not undrained with respect to water evaporation due to environmental conditions.

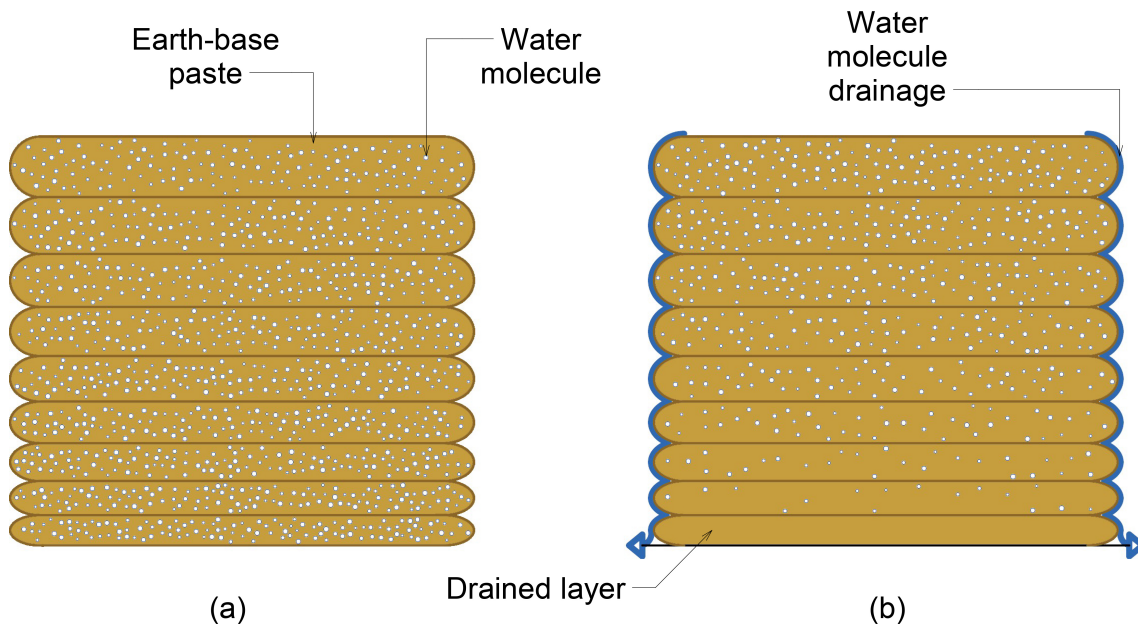


Figure 3.3 – Comparative Representation of Undrained vs. Drained Conditions in the 3D Printing Process

### 3.3.4 Influence of Water Content on the Mechanical Properties of Soils

Soils are porous materials whose mechanical behaviour is significantly influenced by their water content  $w$ , defined as the relationship between water mass and dry material mass  $m_{clay}$ .

$$w = \frac{m_{water}}{m_{clay}} \quad (3.8)$$

Oedometer tests are standard tests in geotechnical engineering, allowing us to measure soil consolidation. A video in [109] shows a brief introduction to oedometer tests on an earth-based sample. Soil consolidation is a process by which the soil gradually undergoes a reduction in volume due to the application of load or weight [8]. This process occurs over a long period and is mainly caused by the expulsion of water from the pores of the soil as the particles are squeezed closer together. When a load is applied to a soil layer, the soil pores' water is expelled immediately, causing some immediate settlement. However, the remaining water in the soil pores has to flow out more slowly through the soil layers, resulting in a gradual reduction in volume and an associated settlement that may continue for a long time. This process is called consolidation and can be modelled mathematically using concepts from soil mechanics.

The oedometer tests can derive earth-based material properties such as Young modulus, bulk modulus, undrained cohesion (Shear Strength), and water content.

The primary formula used in the oedometer test calculates the void ratio, a key parameter in understanding soil compressibility. The void ratio  $e$  is the ratio of the volume of voids to the volume of solids in a soil sample, and it can be expressed as:

$$e = \frac{V_v}{V_s} \quad (3.9)$$

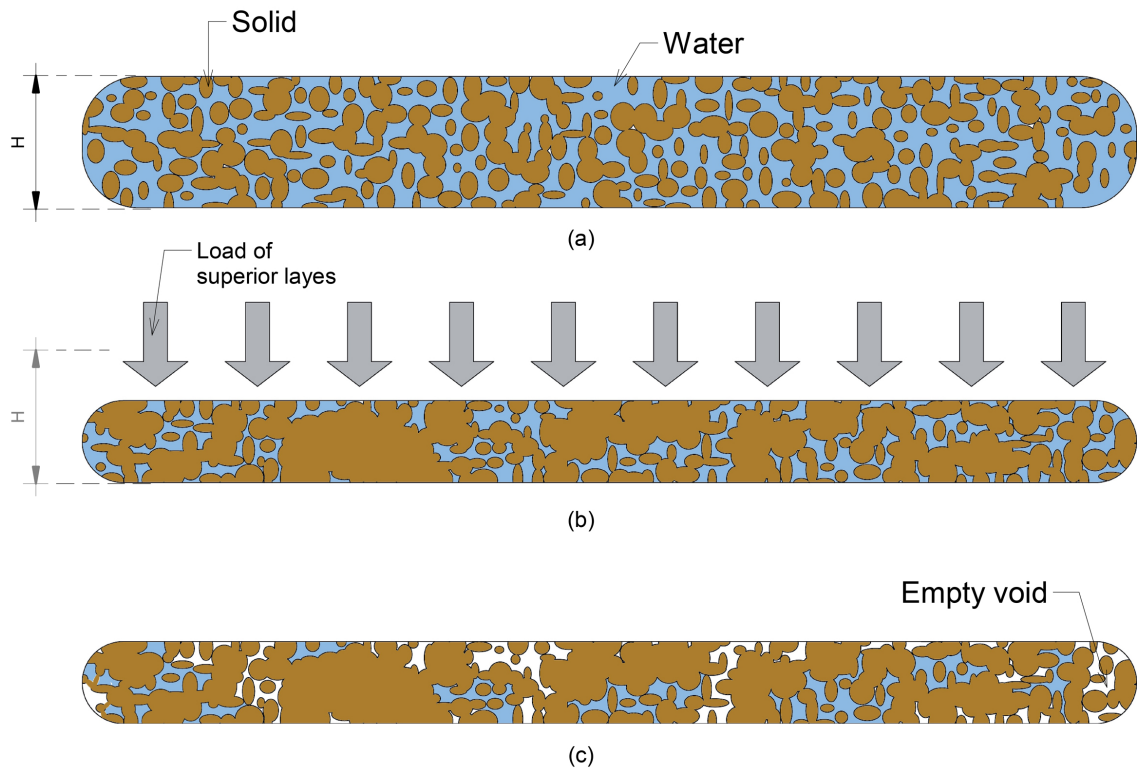


Figure 3.4 – Stages of Water Content and Compaction in a 3D Printed Layer of Kaolin Clay Mixture: Analyzing the Evolution of Material Properties

Where:

- $V_v$  is the volume of voids
- $V_s$  is the volume of solids

This equation applies only to saturated soils where the volume of voids equals the volume of water. Furthermore, for the speswhite kaolin clay, with a water content of more than 26%, the mixture is considered saturated [144]. Figure 3.4 illustrates different stages of a 3D printed layer of Kaolin clay mixture. In part (a), the layer has 58% water content and is fully saturated. Part (b) shows the same layer when compressed under a load of superposed layers, leading to more compacted solid material molecules and a decrease in the volume of voids. Despite the compression, the layer remains saturated with a water quantity of more than 26%. Part (c) depicts the layer when the water quantity falls below 26%, and the volume of voids exceeds the volume of water molecules, resulting in the emergence of empty voids.

The change in void ratio in response to a change in stress (usually vertical stress) is often used to calculate the compression index  $C_c$ , which is a key parameter in predicting settlement:

$$C_c = \frac{\Delta e}{\log \left( \frac{\sigma'_2}{\sigma'_1} \right)} \quad (3.10)$$

Where:

- $\Delta e$  is the change in void ratio
- $\sigma'_1$  and  $\sigma'_2$  are the initial and final effective vertical stresses, respectively

The bulk modulus  $K$  can be related to the compression index and the effective stress applied during the test. It might be expressed as:

$$K = \frac{\sigma'_{\text{mean}}}{C_c \cdot \log_{10}(e_0/e_1)} \quad (3.11)$$

where:

- $\sigma'_{\text{mean}}$  is the mean effective stress, typically in units of pascals (Pa)
- $e_0$  and  $e_1$  are the initial and final void ratios, respectively, and are dimensionless
- $C_c$  is the compression index, also dimensionless
- $K$  is the bulk modulus, typically in units of pascals (Pa)

Using the bulk modulus<sup>5</sup> and the Poisson's ratio  $\nu$ , Young's Modulus  $E$  can be calculated as:

$$E = \frac{3 \cdot K \cdot (1 - 2 \cdot \nu)}{(1 + \nu)} \quad (3.12)$$

Given:

$$\nu = 0.2 \quad (3.13)$$

The Young's Modulus formula:

$$E = \frac{3 \cdot K \cdot (1 - 2 \cdot \nu)}{(1 + \nu)} \quad (3.14)$$

Substituting the value of  $\nu$ :

$$E = \frac{3 \cdot K \cdot (1 - 2 \cdot 0.2)}{(1 + 0.2)} \quad (3.15)$$

$$E = 4.5 \cdot K \quad (3.16)$$

The undrained Young's modulus  $E_u$  may be estimated from the oedometric test. Details of the derivations will be published in a future article.

$$E_u \sim \frac{3 \cdot \ln(10) (1 + e_0) (1 - 2\nu)}{C_c (1 - \nu)} \sigma_{v0} \cdot 10^{\frac{e_0 - e}{C_c}} \quad (3.17)$$

Likewise, it is possible to estimate the undrained cohesion with additional information on the plasticity index. The numerical application for speswhite kaolin is given in equation (3.18).

$$c_u = 0.2 \cdot \sigma_{v0} \cdot 10^{\frac{e_0 - e}{C_c}} \quad (3.18)$$

For speswhite kaolin studied in this article, we may get values from oedometer tests performed in [65]:  $C_c = 0.60$ ,  $\sigma_{v0} = 1$  kPa,  $e_0 = 2.15$ . Therefore, undrained

---

5. The bulk modulus, denoted by  $K$ , measures a material's resistance to uniform compression. It describes how compressible a substance is and is defined as the ratio of the infinitesimal pressure increase to the resulting relative decrease in volume. Simply put, a material with a high bulk modulus is relatively incompressible, meaning it does not change volume significantly under pressure. Conversely, a material with a low bulk modulus is more compressible.



cohesion and Young's modulus depend exponentially on water content, as shown in equation (3.19).

$$\begin{cases} c_u \sim a \cdot 10^{-bw} \\ E_u \sim c \cdot 10^{-bw} \end{cases} \quad (3.19)$$

with  $a = 773$  kPa,  $b = 4.3$ , and  $c = 105.3$  MPa and  $w =$  water quantity of the mixture.

For example, for the Speswhite Kaolin clay mixture with a water content of 58%, the undrained cohesion is equal to

$$\begin{aligned} 773 \times 10^{(-4.3 \times 0.58)} &= 773 \times 10^{-2.494} \\ &\approx 773 \times 0.0031831 \approx 2.4609 \text{ kPa} \end{aligned} \quad (3.20)$$

And Young's modulus is

$$\begin{aligned} 105.3 \times 10^{(-4.3 \times 0.58)} &= 105.3 \times 10^{-2.494} \\ &\approx 105.3 \times 0.0031831 \approx 0.3353 \text{ MPa} \end{aligned} \quad (3.21)$$

### 3.3.5 Drying Mechanism of Soils

Practitioners who operate with concrete or clay in hot weather have experienced the influences of external conditions on the drying rate of these porous media, which can lead to plastic shrinkage cracks. Evaporation nomographs, such as the one found in ACI (American Concrete Institute) 305R-96, estimate the water loss under given meteorological conditions. These nomographs are usually based on experimental measurements on Lake Hefner [62]. However, J.Uno [145] proposed a simplified law to evaluate the evaporation rate  $\Delta_w$  of saturated porous media, which reveals an effective predictor of the drying of mortar at an early age.

$$\Delta_w = 0.313 (e_{s0} - r \cdot e_{sa}) \cdot (0.253 + 0.06V) \text{ kg/m}^2/\text{h} \quad (3.22)$$

where:

- $\Delta w$  - Evaporation rate. [Kg/m<sup>2</sup>hr]
- $e_{s0}$  - Vapour pressure at the clay surface. [kPa]
- $e_{sa}$  - Vapour pressure of air. [kPa]
- $r$  - Relative humidity (RH) expressed as a fraction (e.g., 0.5 for 50%).
- $V$  - Wind speed. [Km/hr]

A simplified equation determines the saturation vapour pressure 3.23, which the World uses with the Meteorological Organisation [145].

$$e_s = 0.61 \cdot e^{\frac{17.3T}{237.3+T}} \quad (3.23)$$

where:

- $s$  - Saturation vapour pressure. [kPa]
- $T$  - Temperature. [°C]

Therefore, the simplified model only requires the measurement of four quantities:

- the relative humidity of the air
- the air temperature
- the water temperature in the clay
- the wind speed

Those quantities can easily be measured, except for water temperature in the clay, which is, in reality, the temperature of the water on its surface.

So for the scenario where the clay temperature is 35 °C, Air temperature is 20 °C and the wind velocity is 32 kph and the relative humidity of the environment is 41%, the evaporation rate will be as follow:

$$\Delta w = 0.313 (e_{s0} - r \cdot e_{sa} \cdot (0.253 + 0.06 \cdot 32))$$

$$e_{s0} = 0.61 \cdot e^{\left(\frac{17.3 \cdot 35}{237.3 + 35}\right)}$$

$$e_{sa} = 0.61 \cdot e^{\left(\frac{17.3 \cdot 20}{237.3 + 20}\right)}$$

therefore :

$$E = 0.313 (5.637 - 0.41 \cdot 2.34) \cdot (0.253 + 0.06 \cdot 32) = 3.181 \text{ kg/m}^2/\text{hr}$$

## 3.4 Analytical Consideration

The previous section has recalled the classical relationships between soil stiffness, water content, and the drying rate of porous media. This section aims to derive an analytical expression for the buildability of a drying vertical 3D-printed wall to capture the basic scaling principles governing its structural build-up.

### 3.4.1 Geometrical Effects

Consider now a printed wall of thickness  $B$ , height  $H$  and length  $L$ , as shown in Figure 3.5.

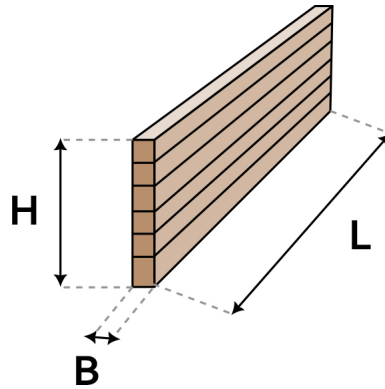


Figure 3.5 – The Wall Considered in This Study

The total mass of water in the wall is :

$$w \frac{\rho_s B H L}{1 + w \gamma} \quad (3.24)$$

And the mass of dry material is :

$$\frac{\rho_s B H L}{1 + w \gamma} \quad (3.25)$$

where:

- $w$  - The water content of the soil. [Typically dimensionless or expressed as a percentage]
- $\rho_s$  - Volumetric mass (or density) of the solid material. [kg/m<sup>3</sup>]
- $B$  - Thickness of the wall. [m]
- $H$  - Height of the wall. [m]
- $L$  - Length of the wall. [m]
- $\gamma$  - Specific gravity of solids. [the ratio of the density of the solid material to the density of water defined as  $\gamma = \frac{\rho_s}{\rho_w}$ ]

The area equals  $2HL$ , and water loss is thus  $2\Delta w HL$ . The water content is given in equation (3.26) Where:

$$w(t) = w_0 - \frac{2\Delta_w \cdot t(1 + \gamma \cdot w_0)}{B \cdot \rho_s} \quad (3.26)$$

- $w(t)$  - Water content of the wall at time  $t$ .
- $w_0$  - Initial water content of the wall.[m<sup>3</sup>]
- $\Delta_w$  - Rate of water evaporation. [kg/m<sup>2</sup>s]
- $t$  - Time. [s]
- $\gamma$  - Specific gravity of solids.
- $B$  - Thickness of the wall. [m]
- $\rho_s$  - Volumetric mass of the solid material. [kg/m<sup>3</sup>]

One may notice that the water content follows a linear decrease with time. This is a natural consequence of the assumption of a constant surface evaporation rate and the definition of water content. Therefore, equation 3.27 identifies a relative drying rate  $d = -dw/dt$

$$d = 2\Delta_w \cdot \frac{(1 + \gamma \cdot w_0)}{\rho_s} \cdot \frac{1}{B} \quad (3.27)$$

Where:

- $d$  - Relative drying rate. [s<sup>-1</sup>]
- $\Delta_w$  - Rate of water evaporation. [kg/m<sup>2</sup>s]
- $\gamma$  - Specific gravity of solids. [Dimensionless, as it's a ratio]
- $w_0$  - Initial water content of the wall. [Typically dimensionless or expressed as a percentage]
- $\rho_s$  - Volumetric mass (or density) of the solid material. [kg/m<sup>3</sup>]
- $B$  - Thickness of the wall. [m]

This rate measures how quickly the water content of the printed wall decreases over time. Furthermore, this rate is influenced by a variety of factors, including **environmental conditions** (e.g., temperature, humidity), **material properties** (e.g., porosity, permeability, density), and the **geometry** of the printed wall (e.g., thickness, surface area). By characterising the relative drying rate of the printed wall, you can gain insights into the drying process and predict how long it will take for the wall to dry completely. Additionally, you can use this information to optimise the printing process by adjusting parameters such as the printing speed, layer thickness, and material composition to achieve the desired drying level. It's important to mention that the assumption of a constant surface evaporation rate may not always hold in practice, as environmental conditions can change over time. However, this assumption is a reasonable starting point for modelling the drying process and can provide valuable insights into the behaviour of the printed wall.

Furthermore, as described by equations 3.26 and 3.27, **the relationship between the water content decrease and the thickness of the printed wall is one of inverse proportionality**, this observation shows why most commercial clay-printing devices are limited to small diameters, usually less than 4mm. Furthermore, it has been demonstrated that **the wall thickness directly influences the evolution of mechanical properties of the printed material**. This finding underscores the significance of the printed structure's geometry in the yield-strength growth of earth-based materials during the 3D printing process.

The relationship between wall thickness and mechanical properties evolution is a balancing act. To elaborate, thicker walls may have higher strength and buckling load capacity due to their increased cross-sectional area, but they have less drying speed, making them prone to plastic failure in the 3D printing process. On the other hand, thinner walls may have less strength and stability in buckling load capacity, but they may have less internal self-weight stress and can gain strength faster due to the higher drying rate, making them less likely to fail due to plastic failure. Determining the optimal wall thickness for a given application requires considering the specific mechanical requirements of the printed part and the printing process itself. To illustrate, a printed part aiming for robustness and stability would necessitate thicker walls, whereas a printing setup utilising a low-strength mixture might call for thinner walls. Likewise, a printing process prioritising rapid print speeds would find advantages in thinner walls that dry swiftly, while a process prioritising post-printing structural stability over speed may require thicker walls. Figure 3.6 showcases three distinct wall configurations. The primary objective is to identify the best configuration for wall printing in terms of stability, given a set amount of material. Walls with greater surface areas experience faster evaporation rates, leading to a rapid increase in the material's undrained cohesion. Yet, based on boundary conditions and global geometry, each wall presents varying buckling load factors. Ideally, a wall with the most extensive surface area and the highest buckling load factor would be selected. The analytical results for these walls are detailed in Table 3.7.

Specifically:

- Wall 1, despite having the smallest surface area, has the highest buckling load factor. This results in a gradual rise in its material shear strength.
- Wall 2, augmented with interior infill layers, has a larger surface area than Wall 1. However, its buckling load factor is less impressive.

- Wall 3 possesses the largest surface area but disappoints with the lowest buckling factor.

For these configurations, Speswhite kaolin clay with 58% water content was chosen, resulting in Young’s modulus of 550 kPa. Given the results, a clear trade-off emerges between the increase in material yield strength and the buckling load factor. It’s a balancing act, requiring users to weigh these elements to arrive at the most optimal configuration – a decision that’s far from straightforward.

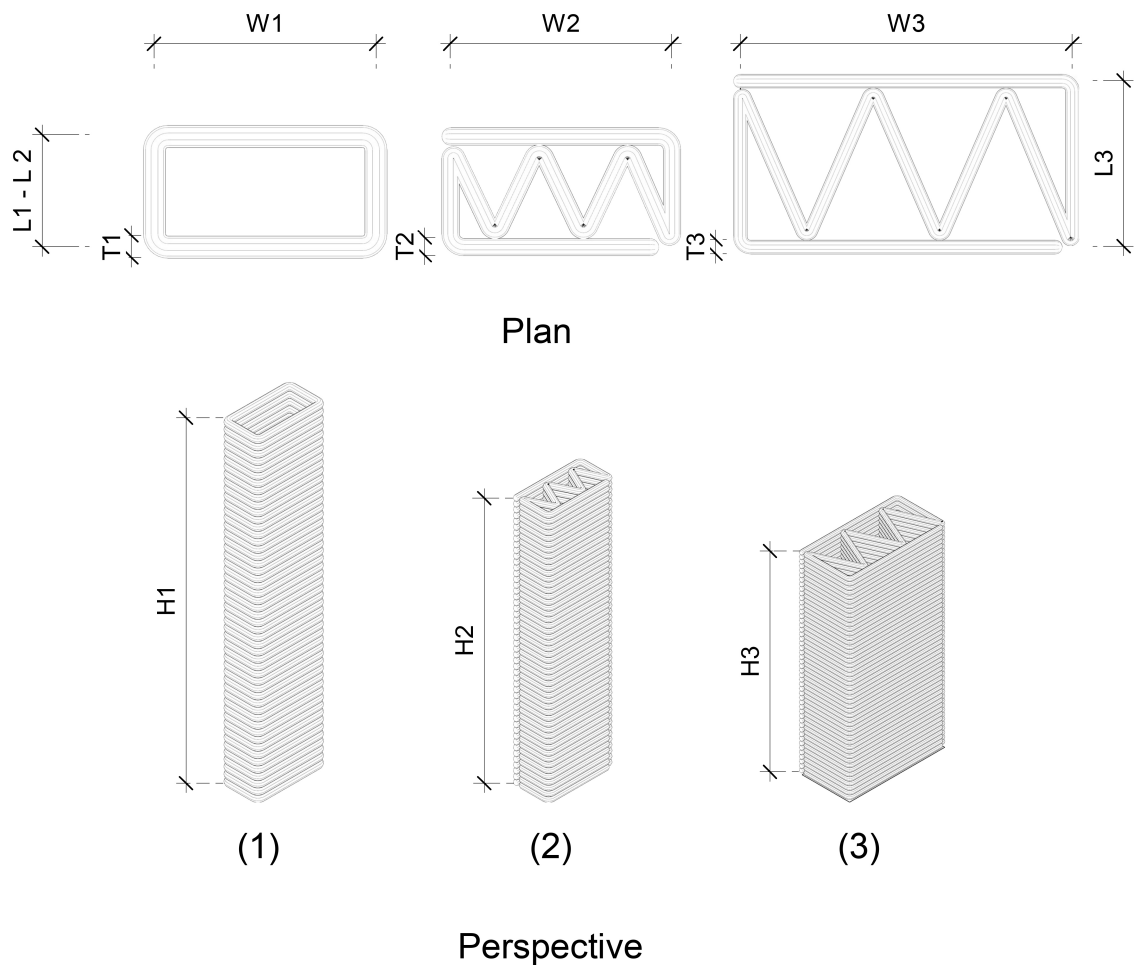


Figure 3.6 – Comparative Analysis of Three Walls with Equivalent Material Volume: Assessing Design Efficiency, Structural Performance

Wall	Buckling Load (B)	Maximum Displacement (cm)	Layer Thickness (cm)	Wall Height (cm)	Wall Surface (m <sup>2</sup> )	Mass (kg)	Width (cm)	Length (cm)
1	B1 = 0.51	1.41	T1 = 2	H1 = 100	S1 = 1.15	18	W1 = 10	L1 = 20
2	B2 = 0.26	0.89	T2 = 1.58	H2 = 79	S2 = 1.50	18	W2 = 10	L2 = 20
3	B3 = 0.56	0.56	T3 = 1.23	H3 = 61.5	S3 = 1.91	18	W3 = 15	L3 = 30

Figure 3.7 – Structural Analysis Data for Three Walls with Equivalent Material Volume

### 3.4.2 Drying and Increase in Mechanical Performance

We have now explicitly derived a linear relation between the age of the material and its water content. We may now estimate the strength of the material thanks to equation (3.28).

$$c_u(t) = a \cdot 10^{-bw_0 + bdt} \quad (3.28)$$

Where:

- $c_u(t)$  - Undrained cohesion of the material at time  $t$ . It represents the strength of the material. [Pa or N/m<sup>2</sup>]
- $a$  - 773 kPa
- $b$  - constant 4.3
- $w_0$  - Initial water content
- $d$  - Relative drying rate. [Unit: s<sup>-1</sup>]
- $t$  - Time. [Unit: s]

Figure 3.8 shows the plot of equation (3.28) for a Speswhite kaolin mixture with an initial water content of 58%  $\frac{\text{Water}}{\text{Kaolin}}$  and a surface evaporation rate of 2kg/m<sup>2</sup>/hour. The wall thickness was varied between 15 mm and 30 mm to highlight the sensitivity of the consolidation phenomenon to the geometry of the sample. This dependency is not considered a common practice for cementitious materials.

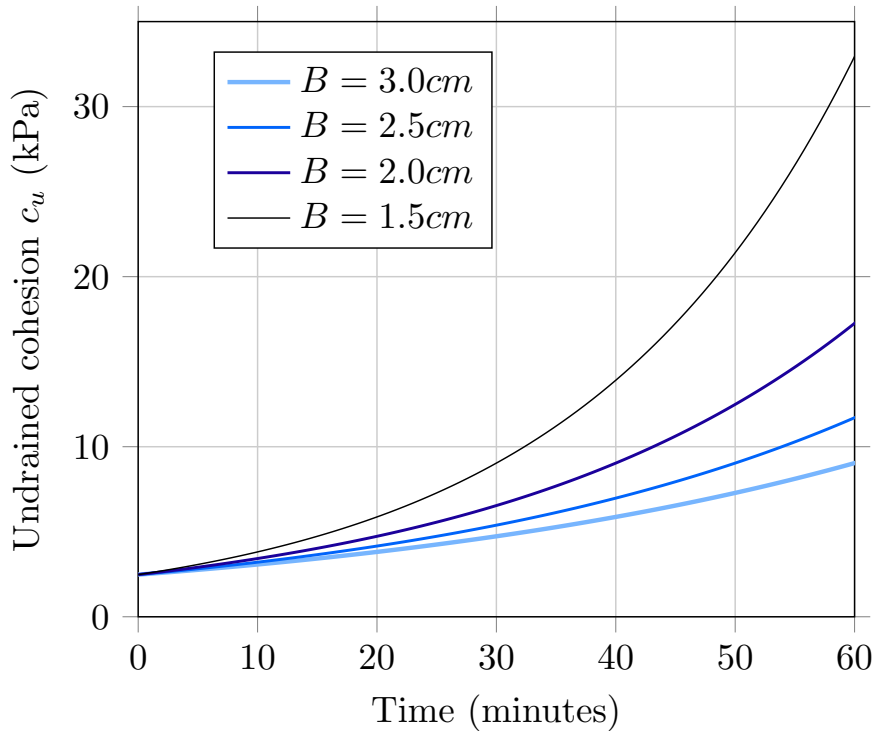


Figure 3.8 – Strength Evolution of Speswhite Kaolin Clay Over Time with a Drying Rate of  $\Delta = 2\text{kg}/\text{m}^2/\text{hour}$ .

We consider now that the wall is printed with a vertical velocity  $V_z$ . We assume that the material dries at a constant rate  $d$ , as explained in the previous paragraph,

and we aim to determine the critical vertical velocity. The buildability requirement at the bottom of the wall reads as follows:

$$c_{u,0} \cdot 10^{bdt} > \frac{\rho g t V_z}{2} \quad (3.29)$$

The buildability criterion is always fulfilled if equation (3.30) is satisfied. This equation depends on material parameters ( $b$ ,  $\rho$  and  $c_{u,0}$ ), environmental conditions and geometry ( $d$ ), but also process parameters ( $V_z$ ).

$$\frac{c_{u,0} \cdot bd}{\rho g V_z} > \frac{1}{2e \ln 10} \sim 0.08 \quad (3.30)$$

where  $e$  is Euler's constant,  $e \approx 2.718$  (Not to be mistaken by the void ratio discussed earlier).

### 3.4.3 Characteristic Structuration Time

We now consider the required time  $t_n$  to multiply the undrained cohesion by a factor  $n$ . The ratio between the strength of the material is given in equation (3.31).

$$\frac{c_u(t)}{c_u(0)} = 10^{bdt} \quad (3.31)$$

This time,  $t_n$  is found by replacing  $d$  with the result from equation 3.27. The result is shown in equation (3.32): it is proportional to the wall thickness  $B$ , which means that the mechanical properties of thinner walls increase much faster than thicker ones.

$$t_n = \frac{B \cdot \rho_s \cdot b}{2\Delta_w (1 + \gamma \cdot w_0)} \log_{10} n \quad (3.32)$$

The time  $t_n$  is inversely proportional to the surface evaporation rate  $\Delta_w$ . A small change in evaporation rate may thus lead to drastic changes in the load-bearing capacity of a 3D printed structure. Notice that equation (3.32) is only valid while there is no drying front (Crust layer) in the clay.

### 3.4.4 Impact of Heating on Crust Layer Formation

This chapter delves into the role of heat in the evaporation of saturated porous media during 3D printing. Real-world observations, however, show that excessive heating, such as that from a heat gun, can reduce the evaporation rate. This reduction occurs due to the formation of a crust layer on the exposed surfaces. This crust inhibits water within the layers from evaporating at the same rate as during the initial stages of the printing process, where no crust exists. Insufficient evaporation of this water can compromise the material's strength, potentially leading to plastic failure in the printed structure. Figure 3.9 illustrates the impact of overheating (b) on crust layer formation and its resistance to the evaporation of water molecules within the printed layers.

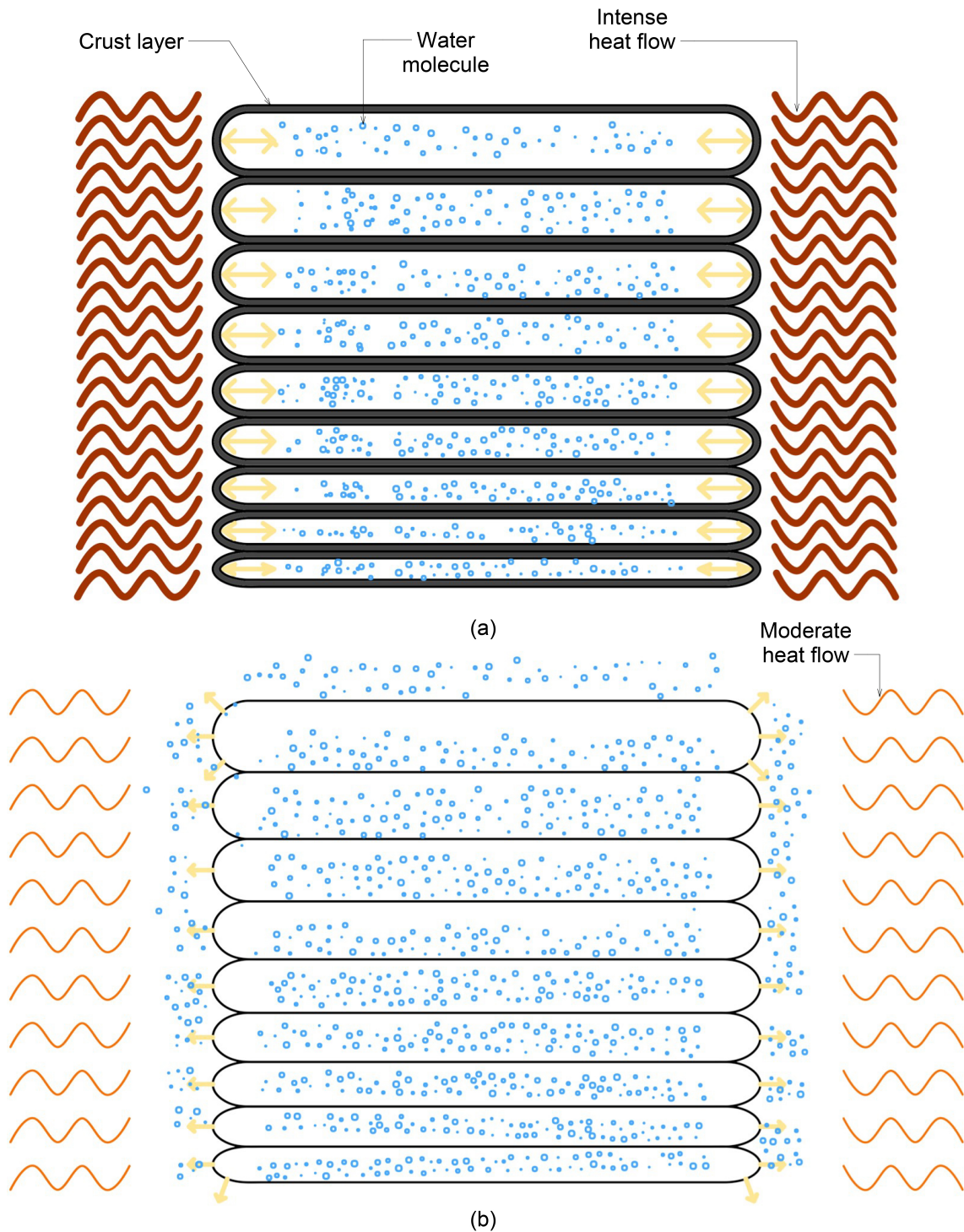


Figure 3.9 – Appearance of Crust Layer Due to Overheating

### 3.4.5 Effect of Environment and Energy Consumption

Raw earth construction can be found in many regions of the globe but seems biased towards hotter areas. The drying model of equation (3.22) shows a strong dependency of the drying rate on temperature. For example, air pressure and temperature can significantly affect the water evaporation rate from the porous media. For example, the drying rate is zero for a humidity of 100% when clay and



air have the same temperature. Therefore, it is concluded that printing in hot and high-pressure environments with low altitudes, such as the Sahara Desert in North Africa, Death Valleys in California, USA, the Australian Outback, the Arabian Peninsula or the low-lying areas of India can be the best options for reducing the energy consumption for layer heating method.

## 3.5 Experiments

In the 3D printing process, assessing the rheological properties of the printing mortar is crucial for accurately analysing the structural behaviour of the intended geometry. Four material experiments were performed to evaluate the mechanical performance of the earth-based printing mortar in the 3D Printing process, both under heat conditions and without. The following is a list of the material experiments utilised in this research. These terms are defined in the following sections.

- (a) Wind-tunnel experiment
- (b) Squeeze test
- (c) Slug test
- (d) Vane test

### 3.5.1 Wind-Tunnel Experiment

As seen in the previous section, there are well-established models to predict the evaporation rate of a porous medium. This model depends on wind speed (convection effect) and air and water temperature at the free surface. The aim of this experiment is thus to provide an experimental set of results that remains close to actual printing conditions. The mixture studied in this experiment consists of 37% water and 63% Speswhite kaolin ( $\frac{Water}{Clay} = 58\%$ ). The material was kept in a sealed reservoir to ensure the same amount of humidity during the material experimentation, which lasted approximately one month. However, later the actual water quantity of the material was measured according to ASTM D2216 [139] (Since the material could change due to temperature and humidity over time). Nine samples on three different days of the experiment (three samples per day) were kept for 48 hours in an oven with 105°C. The material, average water quantity was conceived as the same amount of the mixing time, which is ( $\frac{Water}{Clay} = 58\%$ ).

A wind tunnel with three channels was fabricated to have three samples for each experiment (See Figure 3.10). Each channel is equipped with a similar computer fan. A regulator could change the speed of the fans. Inside each channel, a space was predicted for positioning a material sample with the dimensions of  $18cm \times 4cm \times 2(h)cm$ . A depth of 2cm was selected to represent the thickness of a printed lace. First, the wind tunnel parts were 3D Printed with PLA<sup>6</sup>. Then at a temperature higher than 50 C°, it was observed that the PLA could not keep its shape, and it started deforming. Therefore the wind tunnel was re-fabricated with a 3mm MDF board. Next, the material containers were 3D Printed with PLA material to guarantee the similarity of the reservoirs. Unlike the wind tunnel box,

---

6. Polylactic acid

the material sample reservoirs could withstand temperatures higher than 50 C° since the material inside kept them cool and held their shape. However, since we had to wash the reservoirs with water and reuse them for several experiments, they were not fabricated by a 3mm MDF board vulnerable to humidity. Another reason for not using MDF containers was that the MDF could absorb the material water and cause imprecision in evaporation measurement results. In addition to the material container, a cap with the same material (PLA) was 3D printed for each material container to preserve the water evaporation from the material inside the reservoir before being exposed to the wind tunnel. The caps were designed to have a 1 mm gap between the top surface of the reservoir and the surface of the cap to avoid contacting the material inside the reservoir and causing imprecision in the mass measurement.

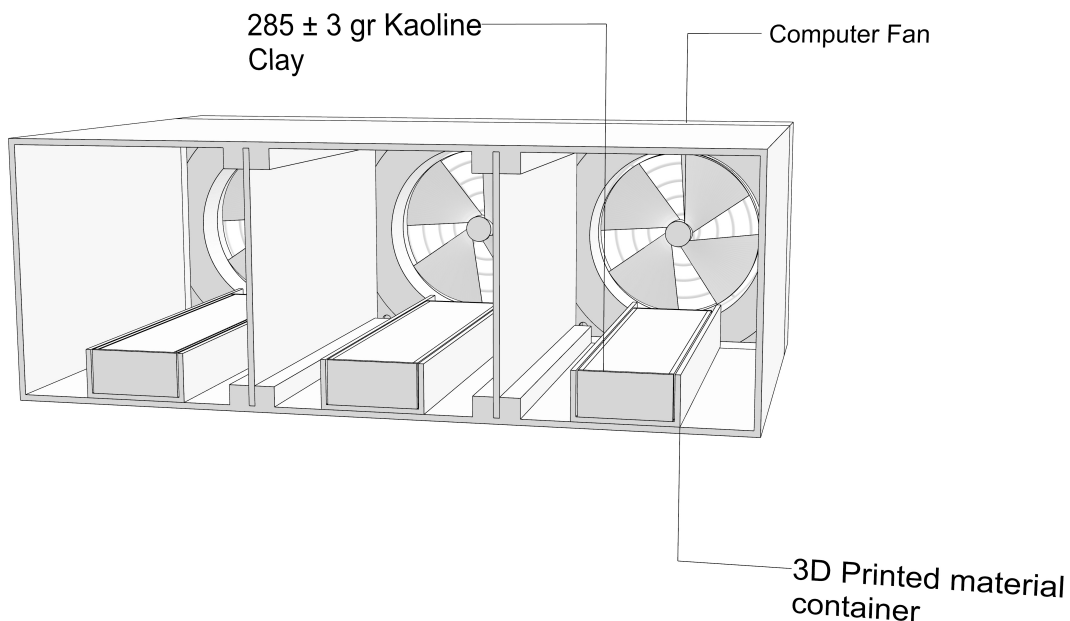


Figure 3.10 – Wind Tunnel Setup for Clay Evaporation Experiment

### 3.5.1.1 Experimentation Environment

The experimentation was done in March and April 2022 at Champs-sur-Marne, France, in a laboratory with an average related humidity (RH) of 50% and 2 meters above the ground. The average air pressure was conceived as 30.5 103 kPa. The air humidity and pressure were collected from the climate data in [92]

### 3.5.1.2 Experiment Protocol

Figure 3.11 shows clay heating experimentation equipment and the environment. Figure 3.12 shows the fabricated wind tunnel with 3mm MDF inside an oven. Below, the experiment protocol is described:

1. Measure the empty mass of three reservoirs.
2. Fill up three reservoirs with clay material using a steel spatula.
3. Put a plastic cover on the reservoir to avoid the material humidity evaporation while transferring the material and wind tunnel in the oven.

4. Measure the mass of the filled reservoirs with their cap(Initial weight).
5. Put the three samples in the wind tunnels, remove the material cap, and put the wind tunnel inside the oven. The wind speed of the wind tunnel and the oven's temperature are fixed in advance.
6. Open the oven door and take out the samples from the wind tunnel, put back the reservoir cover, and measure the mass of the samples after applying wind under a fixed temperature for a certain amount of time (Secondary weight).
7. Register the measured data in an Excel sheet.

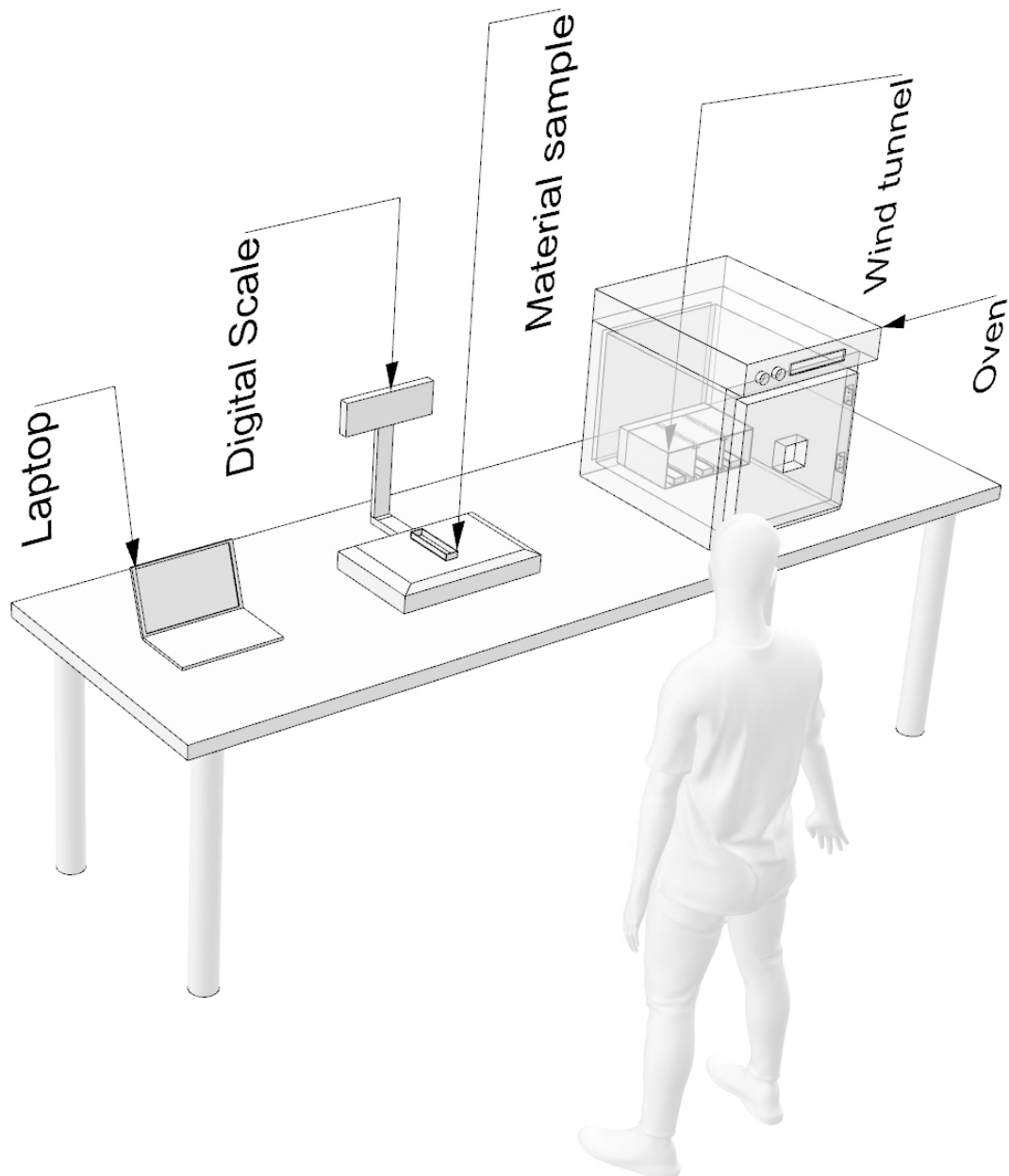


Figure 3.11 – Wind-Tunnel Experimentation Setup

### 3.5.1.3 Experiment Results

The experiment was performed by varying three main parameters:



Figure 3.12 – Fabricated Wind Tunnel Inside an Oven

- (a) Time (10, 20, 40 ) Minutes (Chosen to be representative of a printing time of a meter-scale component.)
- (b) Temperature (35, 55, 65) C°
- (c) Wind speed (0.1, 0.3, 0.5)  $\frac{M}{S}$

The wind speeds inside the channels of the experimental tunnel are measured using a Trotec digital anemometer. However, their result might not be precise as the wind speed was high compared to the exposing objects' dimensions. We expect this

turbulence and uncertainty on the precise value of the wind speed. This problem would certainly occur on a large printed piece. Three samples were experimented with for each set of parameters, ensuring the data precision. Twenty-seven sets of parameters were tested. Figure 3.13 visually represents the experimental results.

Table 3.1 displays the drying rate of the samples for the nine combinations of parameters considering the drying rate is linear. The observation is that evaporation rate is positively correlated with wind speed and temperature, in qualitative agreement with drying models for mortars.

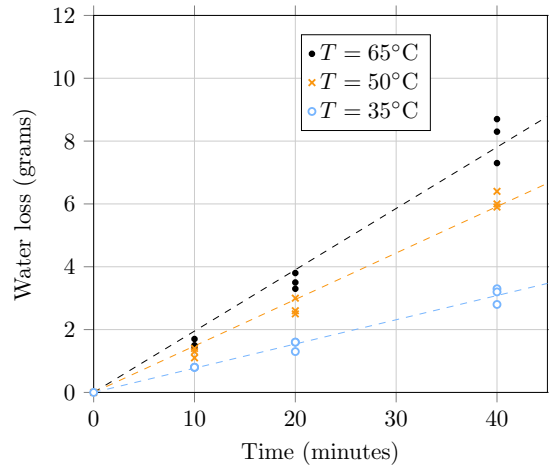
Table 3.1 – Drying rate of Speswhite kaolin clay in the wind tunnel experiment (in  $\frac{gr}{min}$ ).

	<b>V = 0.3 m/s</b>	<b>V = 1.1 m/s</b>	<b>V = 1.9 m/s</b>
<b>T = 35 C</b>	0.0771	0.1073	0.1254
<b>T = 50 C</b>	0.1479	0.169	0.2724
<b>T = 65 C</b>	0.1952	0.236	0.3705

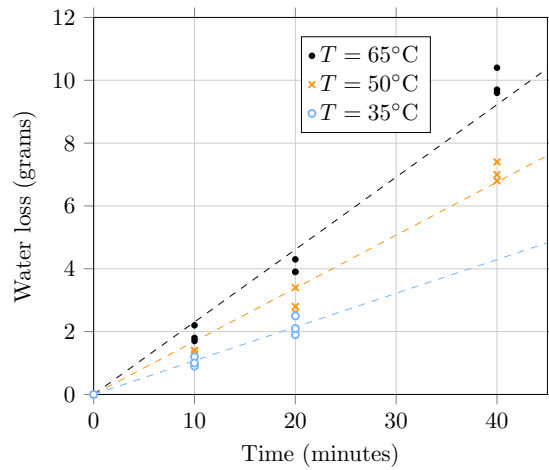
Finally, the surface evaporation rate can be computed by dividing the absolute drying rate presented in Table 3.1 by the sample's surface area ( $72 \text{ cm}^2$ ). The value is compared to the Uno formula with the following assumption:

- The air and water temperature are considered to be equal to the oven temperature
- Relative humidity in the clay is 100% (the sample remains saturated at any time)
- Relative humidity in the air is computed from absolute humidity in the room ( $8.5\text{g}/\text{m}^3$ )

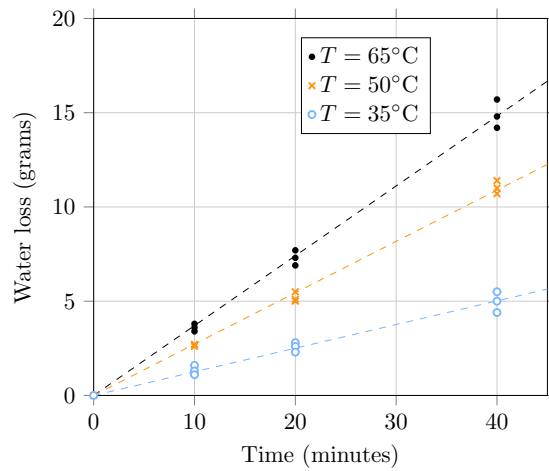
Figure 3.14 compares the theoretical model and the experiments. The dashed line is the best linear fit of the data, with the equation  $y = 0.823x$ . It can be noticed that the experimental drying rate is larger than the theoretical formula. The experimental setup can partially explain this trend: the evaporation does not stop once the sample is removed from the oven. It is thus possible that additional evaporation occurs during step 6, which typically lasts 1 minute. The reference time is the time spent in the oven. We expect this to overestimate the evaporation rate slightly. This overestimation should, however, remain limited, as the measurement time is small compared to the drying time. Other factors may explain the differences between experiments and theory, like turbulence in the wind tunnel, irregular wind speeds, or inaccuracies in the temperature set point of the oven. However, the correlation remains satisfying from a practical perspective and shows a good qualitative agreement between theory and experiments representative of printing conditions.



(a)  $V = 0.3 \text{ m/s}$



(b)  $V = 1.1 \text{ m/s}$



(c)  $V = 1.9 \text{ m/s}$

Figure 3.13 – Results of the Drying Experiment

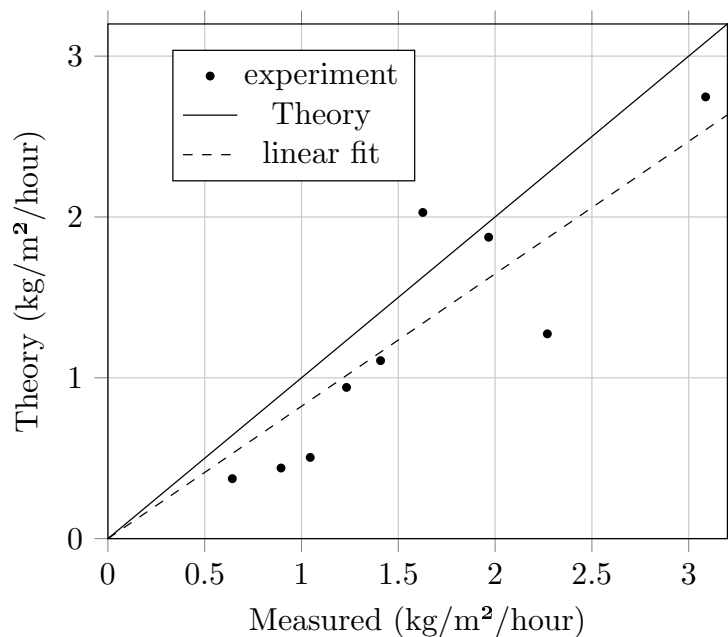


Figure 3.14 – Comparison Between Theoretical Predictions and Experimental Results

### 3.5.2 Squeeze Test

To measure the compressive strength of a Kaolin mixture, two material samples in the form of cylinders (7 cm in diameter and 8 cm in height), one sample with 5 cm of diameter and 3.5 cm of height and one sample with 12 cm of diameter and 3.5 cm of height (Four samples overall) were put in the squeeze test device. Perrot in [117] has used a cylinder sample with a 6 cm diameter and 3.5 cm height for a cement-based material squeeze test. A mould (See figure 3.15) was 3D printed with PLA material to cast the cylindrical samples. Due to the high viscosity of the Kaolin mixture, the samples had some deformations in detaching the mould. Afterwards, the material samples were put in the compression test device to measure the displacement of the applied stress. Figure 3.16 shows the steps of the material squeezing with the squeezing device. Table 3.2 shows the squeeze test results and achieved young modulus for the mixture. The average compressive strength is conceived as -4 kPa. The other possible test for obtaining the yield stress of the clay-based mixtures can be the plunger test as it is proposed in [143] or the oedometer test, which is discussed earlier in section 3.3.4.

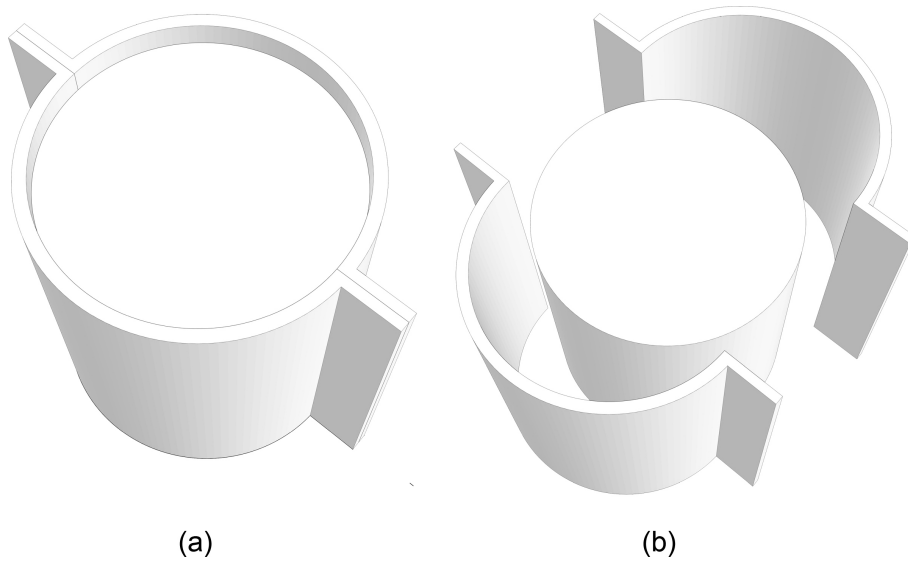


Figure 3.15 – Mould for Casting Material Samples for Squeeze Test

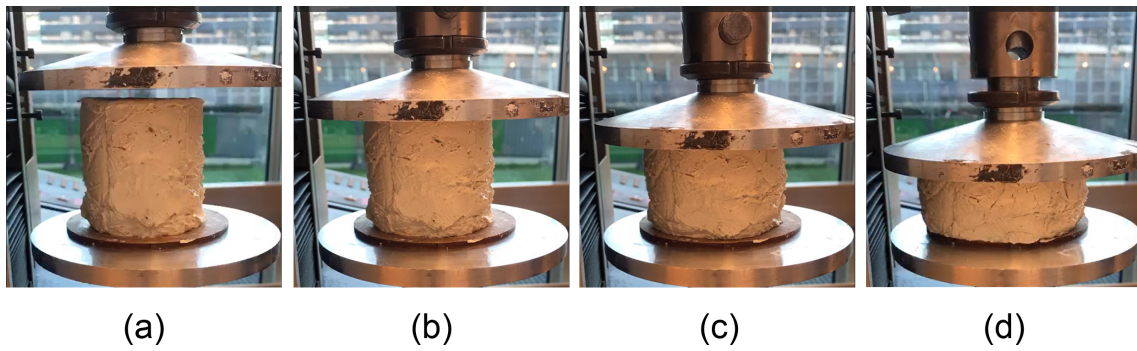


Figure 3.16 – Squeeze Steps of a Material Sample

Table 3.2 – Results of the Squeeze Test on Four Cylindrical Speswhite Kaolin Clay Mixture samples. (Water content = 56%)

Test No	Rho.g [N/m <sup>3</sup> ]	Sample height [m]	Sample diameter [m]	Sample cross section area (Pi * Sample diameter <sup>2</sup> ) [m <sup>2</sup> ]	F [N]	Displacement [m]	epsilon (Strain = Displacement / Sample height) [ - ]	Stress (F/Sample cross section area) [kPa]	Stress with self-weight (Stress + Rho* g*Sample height) [kPa]	Young Modulus (Stress / epsilon) [kPa]
Test 1	16660	0.035	0.06	0.002827433	10	0.005	0.14285714	3.5	4.1	25
Test 2	16660	0.035	0.12	0.011309734	50	0.002	0.05714286	4.4	5.0	77
Test 3	16660	0.08	0.07	0.003848451	10	0.003	0.0375	2.6	3.9	69
Test 4	16660	0.08	0.07	0.003848451	10	0.003	0.0375	2.6	3.9	69
Test 5	16660	0.08	0.07	0.003848451	6	0.004	0.05	1.6	2.9	31
Average									4.0	54.4
Standard deviation									0.8	24.4
Confidence interval (lower bound)									3.3	33.0



### 3.5.3 Slug Test

The yield stress of the fresh clay was also evaluated with the so-called *slugs tests*, first proposed by [39]. The test is identified as a promising research direction in the 3D printing community [108]. The test relies on the extrusion of a yield stress fluid at a constant rate, which naturally forms drops or "slugs". The weight of those drops is directly related to the yield stress. Coussot indeed showed that the time of separation of the drop remains small compared to the time before necking occurs. The drop separation is due to a tensile failure of the material [70]. The critical tensile strength reads thus as follows:

$$\sigma_T = \frac{4mg}{\pi D^2} \quad (3.33)$$

Where:

- $\sigma_T$  - Stress or force per unit area, typically measured in Pascals (Pa) or  $\text{N/m}^2$ .
- $m$  - Slug mass of the object or material. A slug is a unit of mass in the Imperial system, typically used in the U.S. for objects in motion.
- $g$  - Acceleration due to gravity, typically  $9.81 \text{ m/s}^2$  on the surface of the Earth.
- $D$  - Diameter of the nozzle, typically measured in millimetres (mm) or centimetres (cm), depending on the context.

Ducoulombier *et al.* proposed a Von Mises criterion to estimate the yield stress. Using the fact that the stress is uniaxial before necking, we may estimate the undrained cohesion:

$$c_u = \frac{2mg}{\pi D^2} \quad (3.34)$$

Where:

- $c_u$  - Undrained cohesion, typically measured in Pascals (Pa) or  $\text{N/m}^2$ .
- $m$  - Mass of the object or material, typically measured in kilograms (kg) or slugs, depending on the context.
- $g$  - Acceleration due to gravity, typically  $9.81 \text{ m/s}^2$  on the surface of the Earth.
- $D$  - Diameter of the nozzle, typically measured in millimetres (mm) or centimetres (cm).

The slug test was performed for various extrusion speeds on a large-scale extruder, with  $D = 8\text{mm}$ . The material was a Speswhite kaolin with  $w = 58\%$  ( $\frac{\text{Water}}{\text{Kaolin}}$ ). The drop masses are shown in figure 3.17. The results showed no relationship between the extrusion flow rate and the tensile strength<sup>7</sup>. Furthermore, the average tensile strength achieved was 5.3 kPa. Interestingly, the tensile stress approximately equals the compressive strength (refer to section 3.5.2), which may seem unusual. The results showed that the slug mass is independent of the flow rate, which confirms that viscous effects are negligible.

---

7. This may signify that the mixture of Speswhite kaolin and water does not form a thixotropic material as the viscosity of the material remains the same while increasing the shear strength (The extrusion speed)

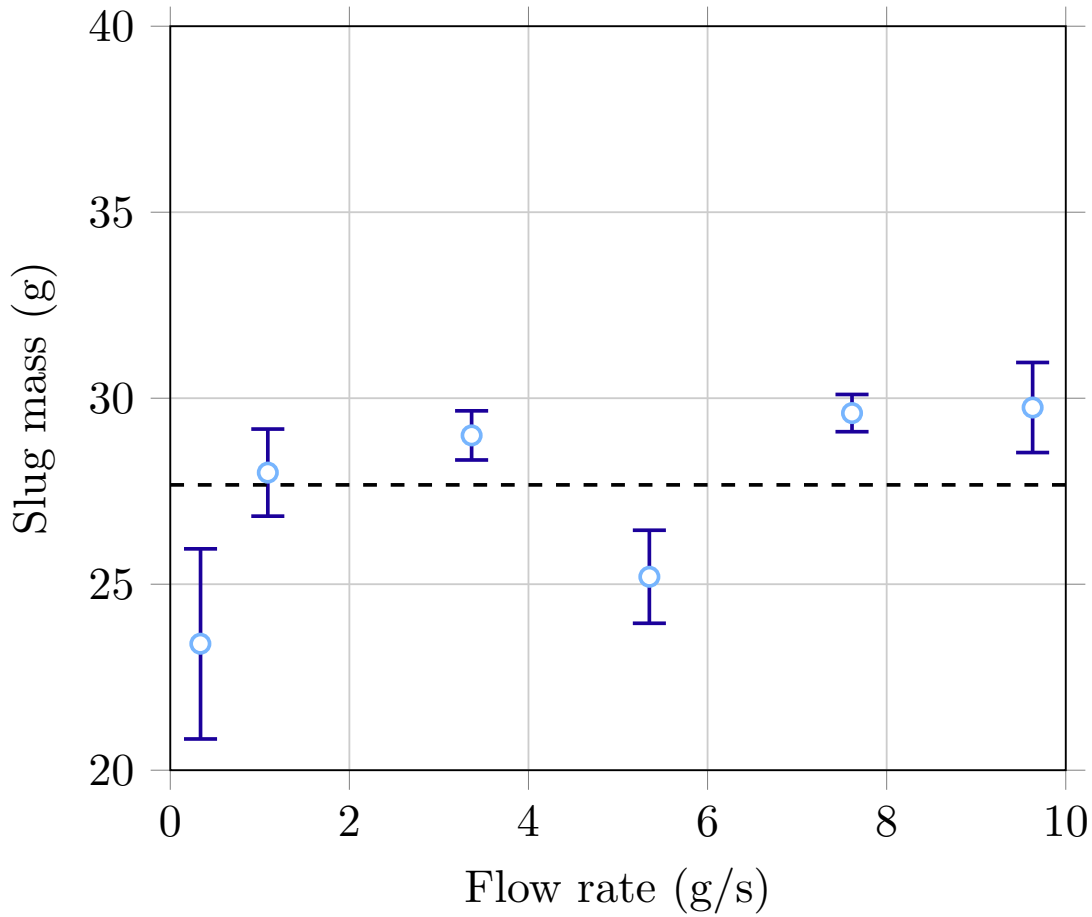


Figure 3.17 – Slug mass measurements as a function of flow rate. Error bars indicate standard deviation, and the dashed line corresponds to the average of all measurements.

### 3.5.4 Vane Test

Figure 3.18 show how a vane test setup can measure the critical shear strength of printing mortar. The Vane Test is a geotechnical test used to determine the undrained shear strength of cohesive soils, particularly soft clays. The test involves inserting a cylindrical vane into the soil and rotating it constantly while measuring the torque required to maintain the rotation.

The vane is typically a thin-walled cylindrical tube with four blades attached to the bottom. The vane is constantly pushed into the soil and rotated until the material shears. As the vane rotates, the soil deforms, and the torque required to maintain the rotation is measured. The undrained shear strength is then calculated based on the maximum torque measured during the test. The Vane Test is particularly useful for soft clay soils that are sensitive to disturbance, as the test does not require the extraction of undisturbed samples. However, the test is generally not recommended for more dense or granular soils, as the vane may not provide a reliable measure of shear strength in these materials. The vane test is a good candidate for in-field measurement since it is a fast and easy experiment to measure the strength of the material for printing purposes. The brief video in [105] demonstrates how the vane test for the prototypes of this dissertation measures the

critical shear strength of the printing mortar.

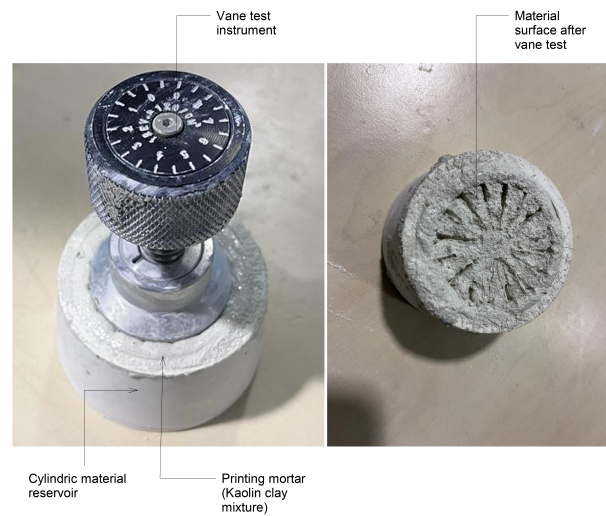


Figure 3.18 – Vane Test for In-Field Measurement of Critical Shear Strength

### 3.5.5 Printing Cylinders with Different Heating Methods

This experiment aims to assess the yield strength evolution of a Speswhite kaolin clay mixture (Speswhite kaolin 33%, fine sand 33%, Water 34%,  $d = 2140 \frac{Kg}{m^3}$ ) through various heating methods. The objective is to determine the most effective heating/blowing setup for successfully printing a vertical cylinder by measuring the number of printed layers before encountering plastic failure. To achieve this, a cylinder with a diameter of 400 mm is designed, and a printing extrusion head with a nozzle diameter of 16.5 mm is utilised for the test. To enhance the cylinder’s resistance against buckling failure, two layers are printed at each cylinder level (3.20). The layer height is 13 mm, and the achieved layer width is  $16 \times 2 = 32mm$ . The relative humidity of the printing environment is measured as an average of 40%. This test comprises four distinct printing scenarios. Figure 3.19 shows the printed cylinder in four different tests, one layer before they collapsed due to material strength.



Figure 3.19 – 3D Printed Cylinders Using Different Heating Methods

**Test 1:** *Printing with no wind or heat*

For this test, no wind-blowing or heat-generating device was used. Table 3.3 shows the results and measured data of test 1.

Table 3.3 – Printing Process Without Heat or Wind Flow

TEST 1	NO VENTILATION OR HEAT
Environment temperature°C	19
Print bed (Table) temperature°C	19
First layer (Inside the layer) temperature°C during the printing process	18.9
RH(Environment relative humidity)	40%
Layer width (MM)	16.8 (Single) - (29 Double)
Layer height (MM)	12.6
Cylinder height (Achieved before material failure) (CM)	21
Number of layers (Achieved before failure)	17
Robot speed mm/s	48
Vertical speed (Time for printing one layer) (s)	25.21
Total printing time before the collapse (s)	429

**Test 2:** *Printing Process with two ventilators*

For this test, two industrial ventilators were used during the 3D printing process. The industrial ventilator’s features are as follows:

Wind Flow Rate	$3900 \frac{\text{m}^3}{\text{h}}$
Wind Speed	$2920 \frac{\text{r}}{\text{min}}$
Power	500 W
Voltage	220 – 240 V

Table 3.4 shows the results and measured data of test 2.

Table 3.4 – Printing Process with Two Ventilators

TEST 2	2 air ventilators
Environment temperature°C	19
Print bed (Table) temperature°C	19
First layer (Inside the layer ) temperature during the printing process	19
RH(Environment relative humidity)	40 %
Layer width (MM)	(21.25 Single) - ( 43.19 Double)
Layer height (MM)	13.3
Cylinder height (Achieved before material failure) (CM)	25
Number of layers (Achieved before failure)	18
Robot speed mm/s	48
Vertical speed (Time for printing one layer) (s)	25.21
Total printing time before the collapse (s)	454

**Test 3:** *Printing two industrial heaters*

For this examination, two industrial heaters were used during the 3D printing process. The industrial heaters’ features are as follows:

Power	3000 W
Dimensions	$26.5 \times 29 \times 21 \text{ cm}$
Air debit or Flow rate	$280 \frac{\text{m}^3}{\text{h}}$
Voltage	220 – 240 V

Table 3.5 shows the results and measured data of test 3.

Table 3.5 – Printing Process with Two Industrial Heaters

TEST 3	2 Hot air ventilators
Environment temperature°C	20
Print bed (Table) temperature°C	33-37
First layer (Inside the layer) temperature°C during the printing process	25.5-26
RH(Environment relative humidity)	41 %
Layer width (MM)	(16 Single) - (31 Double)
Layer height (MM)	13.3-14.5
Cylinder height (Achieved before material failure) (CM)	25
Number of layers (Achieved before failure)	19
Robot speed mm/s	48
Vertical speed (Time for printing one layer) (s)	25.21
Total printing time before the collapse (s)	479

**Test 4:** Printing with one heat gun. A heat gun was used in the 3D Printing process for this test. The features of the employed heat gun are as follows:

Power 1800 W  
 Air debit or Flow rate  $500 \frac{1}{\text{min}} = 31.25 \frac{\text{m}^3}{\text{h}}$   
 Voltage 220 V

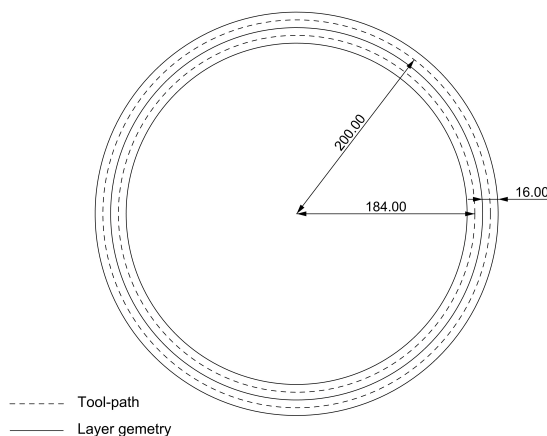


Figure 3.20 – Designed Cylinder for Layer Heating Experiment

Table 3.6 shows the results and measured data of test 4.

Table 3.6 – Printing Process with One Heat Gun

TEST 4	Heat gun
Environment temperature°C	20
Print bed (Table) temperature°C	20-46
First layer (Inside the layer) temperature°C during the printing process	25.5-26
RH(Environment relative humidity)	40 %
Layer width (MM)	(22.76 Single) - (43 Double)
Layer height (MM)	13.4
Cylinder height (Achieved before material failure) (CM)	31
Number of layers (Achieved before failure)	22
Robot speed mm/s	52 mm/s
Vertical speed (Time for printing one layer) (s)	23.52
Total printing time before the collapse (s)	517.44

By comparing the obtained results, it becomes apparent that using a heat gun significantly impacts yield strength development in the 3D printing process, allowing for the creation of 22 layers before experiencing plastic collapse. On the other hand, the absence of heat or airflow demonstrates the least potential for yield strength enhancement, resulting in only 19 layers before encountering plastic collapse. However, the presented results can vary due to the material formulation inconsistency while using pump MAI (Explained in 4.5. During test 2, the printed cylinder experienced curvature on two sides due to the wind pressure generated by the industrial ventilators (See figure 3.19, Test 2). In future attempts, it is recommended to position the ventilators at a greater distance from the object during printing. However, it is essential to note that the failure occurred due to the collapse of the first layer.

In test 4, the heat gun could only heat one side of the cylinder at a time. Consequently, certain cylinder areas became more solid than others, resulting in an asymmetrical geometry (See figure 3.19, Test 4). To address this issue, two heat guns can provide a solution by evenly and symmetrically distributing heat across the cylinder surface.

### 3.6 Structural Analysis

To understand the shell's structural stability during the printing process, one must analyse structural failure's critical aspects at each step(layer) of printing. A compression shell is subjected to the following failure modes:

1. Material failure (Plastic failure)
2. Structural buckling (Elastic failure)
3. Global equilibrium failure

Figure 3.21 shows the schematic of the above-mentioned failure modes. Furthermore, the video in [26] demonstrates the difference between elastic and plastic collapse in cement mortar printing cylinders.

To evaluate the structure behaviour, one must analyse the above factors at each step (Layer) of Printing. When the users slice their geometry into very thin layers, all the intermediary geometries' analysis becomes costly and time-consuming. Therefore one can reduce the analysis into a few steps by approximating the printing process.

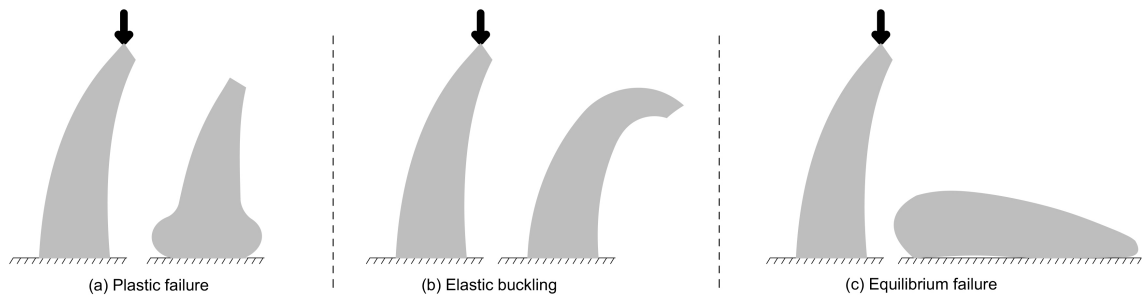


Figure 3.21 – Possible Failure Modes During the 3D Printing Process of Funicular Forms with Fresh Unreinforced Mortars

### 3.6.1 Mixture Properties

The material properties play a crucial role in ensuring structural stability during the 3D printing process, as the yield strength of the material dictates the amount of stress the printed object can withstand before experiencing plastic failure (refer to section 3.6.3). In this research, the primary mixture utilised for the fabrication of medium-scale prototypes (refer to Chapter 4) consisted of 0.58 mass units of water for each mass unit of Speswhite kaolin clay. To achieve the desired properties of this mixture, we conducted several material experiments, including squeezing (inspired by [143]), plunger, and vertical extrusion.

The material's maximum compressive strength is -4 kPa, while its maximum tensile capacity reaches 5 kPa (Refer to sections 3.5.2 and 3.5.3). Additionally, the young modulus has been determined to be 550 kPa. These material characteristics are essential in ensuring successful and reliable 3D printing outcomes.

### 3.6.2 Step-Wise Elastic Buckling Analysis

Buckling is a loss of stability that occurs when the applied compressive load reaches a certain critical value, causing a change in the shape of the structure and large displacements. This does not always result in yielding or fracture of the material (Plastic failure), but buckling is still considered a failure mode since the buckled structure can no longer support a load in the way it was designed to. The signs of buckling in a structure are as follows:

- (a) Sudden deformation
- (b) Large displacements
- (c) Member can no longer carry a load as intended

Buckling can lead to catastrophic structural failure. In 1744, Euler developed a new method for analysing functions. The Euler's equation 3.35 for buckling is a simple formula which is still in use by the engineers to design columns and other members of a structure that are in pure compression [142].

$$P_{cr} = \frac{\pi^2 EI}{(KL)^2} \quad (3.35)$$

Where:

- $P_{cr}$  is the critical buckling load (the maximum load the column can carry before buckling).

- $E$  is the modulus of elasticity (or Young’s modulus) of the material.
- $I$  is the moment of inertia of the column’s cross-sectional area.<sup>8</sup>
- $L$  is the effective length of the column.
- $K$  is the column effective length factor, which depends on the boundary conditions (how the column is supported at its ends).

The effective length factor,  $K$ , values for common boundary conditions are:

1. Pinned-Pinned:  $K = 1$
2. Fixed-Fixed:  $K = 0.5$
3. Fixed-Pinned:  $K = \sqrt{2}$
4. Fixed-Free:  $K = 2$

Structural buckling is primarily influenced by material stiffness rather than material strength (refer to Section 3.3.2). Buckling occurs when a slender structure, such as a column or beam, undergoes compressive loads that cause it to buckle out of its straight and stable configuration. Generally, higher-restricting materials are more buckling-resistant because they can better withstand bending and deflection under compressive loads. On the other hand, materials with high strength but low stiffness, like certain plastics, may still experience buckling even if they can support high loads without breaking (Plastic Failure).

Euler’s formula suggests that an element’s support condition significantly impacts its susceptibility to buckling. This principle is particularly relevant for shells and vaults, where boundary conditions are critical in determining the structure’s resistance to elastic buckling. The geometry of the printed element also contributes significantly to the structure’s stability against structural buckling.

Figure 3.22 illustrates two distinct methods for modifying the geometry of a squinch and two separate techniques for adjusting the squinch’s supporting boundary. The effects of these modifications on the structure’s buckling factor are also depicted. In this scenario, the material used is Speswhite kaolin clay with a water content of 58%. The shell’s thickness is assumed to be 8 cm, the squinch’s supporting sides are 50 cm long, and the squinch spanning arch’s apex height is consistently 30 cm.

The first geometric manipulation modifies the squinch spanning arch configuration from a catenary curve (a) to an arc (b) and finally to a three-point interpolation (c). The second geometric manipulation adjusts the spanning arch plane’s orientation degree. In (a), it is oriented 15 degrees backwards; in (b), it remains fixed; and in (c), it is oriented 15 degrees forward.

The first boundary manipulation modifies the supporting boundary of the squinch. In (a), it has a sharp corner; in (b), it has a rounded corner with a fillet of 15 cm; and in (c), it has a rounded corner with a fillet of 30 cm. The second boundary manipulation changes the angle degree between the two sides of the supporting lines. In (a), it is 60 degrees; in (b), it is 90 degrees; and in (c), it is 120 degrees.

---

8. The quadratic moment of inertia, also known as the second moment of area or area moment of inertia, is a property of a shape that can be used to predict its resistance to bending and deflection. The calculation depends on the specific geometry of the shape. For a rectangle with base  $b$  and height  $h$ :  $I = \frac{b \cdot h^3}{12}$



The impact of these geometric and boundary modifications on the structure's buckling factor underscores the importance of geometry and boundary conditions in determining a structure's stability.

There are some similarities between the fabrication of masonry vaults and the 3D printing of funicular shells. Heyman developed the theorem of yield design for masonry construction problems in 1995 [64]. Based on the Masonry safety theory, an arch will buckle when the stress thrust line crosses the arch's extrados or intrados. This fact applies to the network of arches (i.e. Double curvature funicular forms). The funicular geometries are proper forms for 3D printing with earth-based materials. Suppose we design a funicular target geometry and slice it into several consecutive layers. In that case, the layers' aggregation from the first to the last layer before the printing completion produces the same number of intermediate geometries as the number of layers. These geometries are not necessarily funicular as the target geometry. In other words, the final equilibrium of a shell structure does not guarantee the equilibrium of the geometry at the intermediate steps of 3D Printing. Therefore, to design a printable structure, one must design a locally funicular and globally functional geometry as funicular as possible. This approach applies to thin shells, such as studies in [16]. However, the 3D printing of cantilevered earthen structures with no formwork due to the low initial yield strength and slow green-strength (Refer to section ) evolution is subjected to increase the shell's thickness to compensate for the material's low stiffness and strength. However, later in chapter3, it's proved that the thinner the clay shell, the faster the evolution of its mechanical performance using the layer heating method. Therefore the best solution might be increasing the cross-section thickness of the shell to increase the buckling capacity of the shell, at the same time, reduce the thickness of the printing layer and hold as much cavity as possible inside the cross-section of the shell (Infill cavity) to decrease the shells internal forces (To resist plastic failure) and increasing the evaporation rate (refer to chapter 3 and consequently increasing the green-strength evolution speed. Therefore, based on the masonry safety theorem, which is a simple geometric criterion, one can design a thick target funicular geometry compared to thin shells and verify if the thrust stress networks at each step of printing cross the shell's extrados and intrados, as mentioned in the Figure 3.23.

Heyman's safe theorem is based on three hypotheses :

- (a) The tensile capacity of the material is zero
- (b) The compressive capacity of the material is infinite
- (c) There is no sliding between the masonry structure blocks

The hypotheses mentioned above are only partially true for the case of 3D printed funicular forms with fresh mortars such as clay and earth. The first assumption of Heyman's theorem adapts to 3D printed structures with soil and concrete since these materials have low tensile strength. However, the second and third hypotheses for the 3D Printed systems are invalid. In the 3D printing process of funicular forms with earth or concrete, at the initial state of the material deposition, the material has a low compressive strength compared to the blocks of the brick or stones in masonry structures. Furthermore, the sliding between the consecutive layers of the 3D printed structures can happen if the contacting surface between the layers is improper or the printing angle is so high that the internal shear stress between the layers exceeds the material capacity.

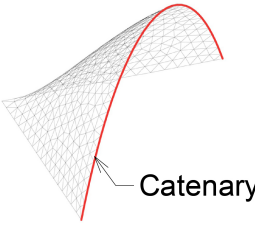
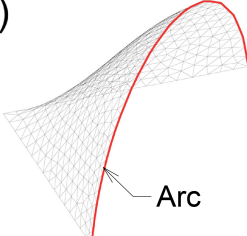
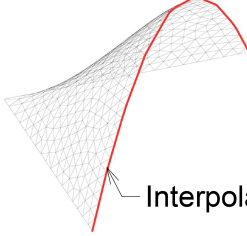
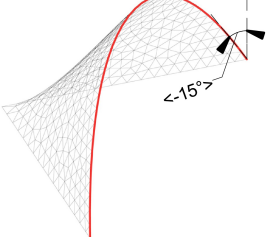
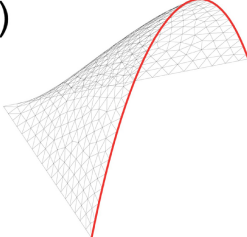
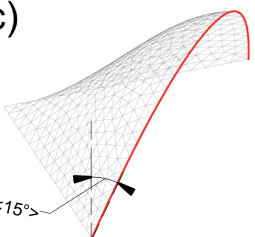
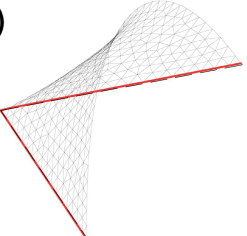
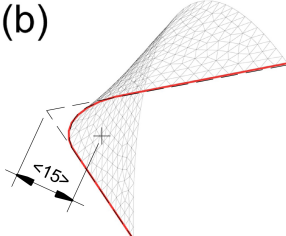
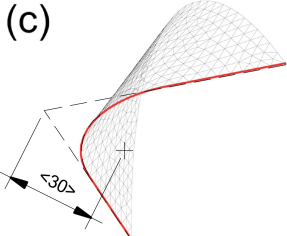
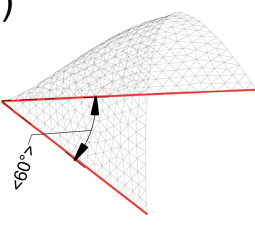
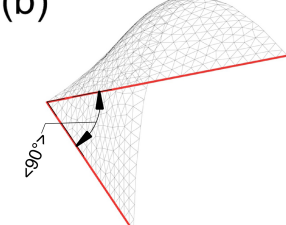
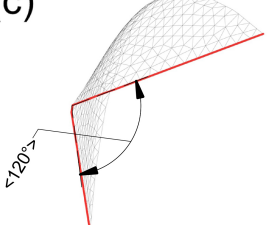
Geometry manipulation 1		
(a)  Catenary	(b)  Arc	(c)  Interpolate
Buckling: 12.02	Buckling: 11.45	Buckling: 12.83
Geometry manipulation 2		
(a)  $\langle 15^\circ \rangle$	(b) 	(c)  $\langle 15^\circ \rangle$
Buckling: 17.73	Buckling: 12.02	Buckling: 8.79
Boundary manipulation 1		
(a) 	(b)  $\langle 15^\circ \rangle$	(c)  $\langle 30^\circ \rangle$
Buckling: 17.74	Buckling: 17.25	Buckling: 12.38
Boundary manipulation 2		
(a)  $\langle 60^\circ \rangle$	(b)  $\langle 90^\circ \rangle$	(c)  $\langle 120^\circ \rangle$
Buckling: 24.69	Buckling: 17.19	Buckling: 17.86

Figure 3.22 – Impact of Geometry and Boundary Modifications on the Structural Buckling of a Squinch: Comparative Analysis of Design Variations and Their Effects

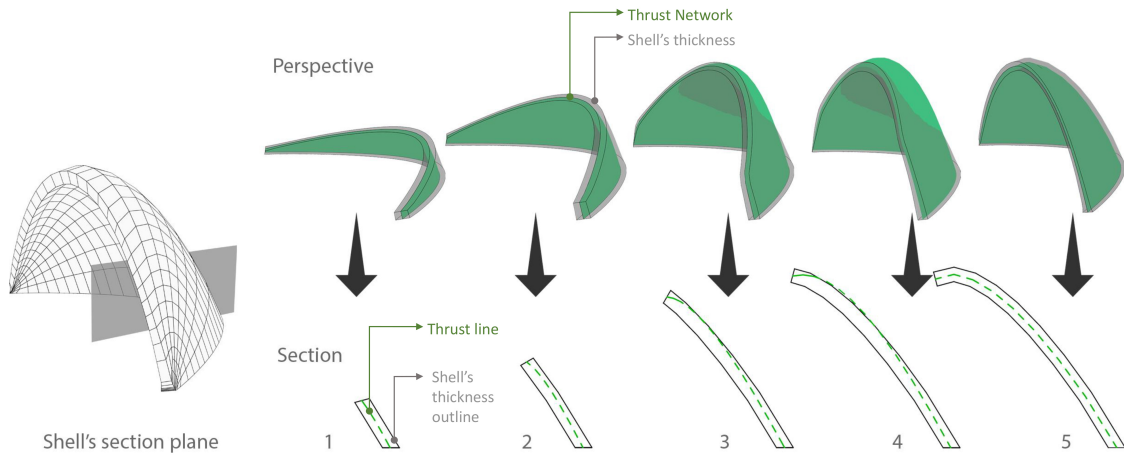


Figure 3.23 – Step-Wise Analysis of Thrust Network in the Section of a Shell

### 3.6.3 Step-Wise Plastic Buckling Analysis

To assess the plastic failure during the printing process, choosing the correct failure theory is crucial. At this step, we analyse the structural failure due to material collapse under self-weight. Observations revealed that the fresh Speswhite kaolin clay mixture has a ductile behaviour in compression and a brittle behaviour in tension. Therefore, the Rankine failure can predict the plastic failure at each printing step, which happens when one of the two principal stresses applied to the material surpasses the material tensile or compression capacity  $\sigma_1, \sigma_2 > \sigma_T$  or  $\sigma_1, \sigma_2 < \sigma_C$ . Equations 1 and 2 define the Rankine failure theory criterion with the following:

$$\sigma_c < \sigma_1 < \sigma_t \quad (3.36)$$

$$\sigma_c < \sigma_2 < \sigma_t \quad (3.37)$$

It is important to mention that failure theories such as Von Mises or Tresca are more conservative and provide safer estimations of material plastic failure in the 3D printing process. However, these failure theories are valid for ductile materials [142]. Since the fresh Speswhite kaolin clay mixture exhibited ductile behaviour in compression and brittle behaviour in tension, the Mohr-Coulomb failure theory remains the most suitable for predicting the plastic failure of fresh earth-based materials in 3D printing. Nevertheless, implementing the Mohr-Coulomb failure theory is more complex than the Rankine failure theory and falls outside the scope of this research.

### 3.6.4 Slicing Pattern Effect on Structural Behaviour

The slicing pattern can affect the success of printing in two manners:

- (a) By effecting the appearance of local stresses in between consecutive print layers

- (b) By effecting the intermediate geometries of the structure before print completion and consequently the structural buckling capacity.

Figure 3.24 shows how a slicing pattern can affect the generated internal stresses between the layers of a printed cantilever. (a) has only bending moment between the layers, (b) has the combination of bending moment and shear stress between the layers, and (c) has only shear stress showing the advantage of 3D printing in the direction tangent to the target geometry surface. On the other hand, Figure 3.25 shows three different slicing patterns applied to the same geometry with the same cross-section with equal thickness. The buckling load factor at each printing step for each pattern indicates that the slicing pattern directly influences the structural stability. Indeed, the slicing pattern participates in structural stability during the printing process through the following aspects:

1. The slicing pattern indicates the local cantilevers in between the laces
2. The slicing pattern indicated the applied load's orientation to the progressing structure through each Lace's deposition.
3. The slicing pattern defines how many layers are supported by the printing base.

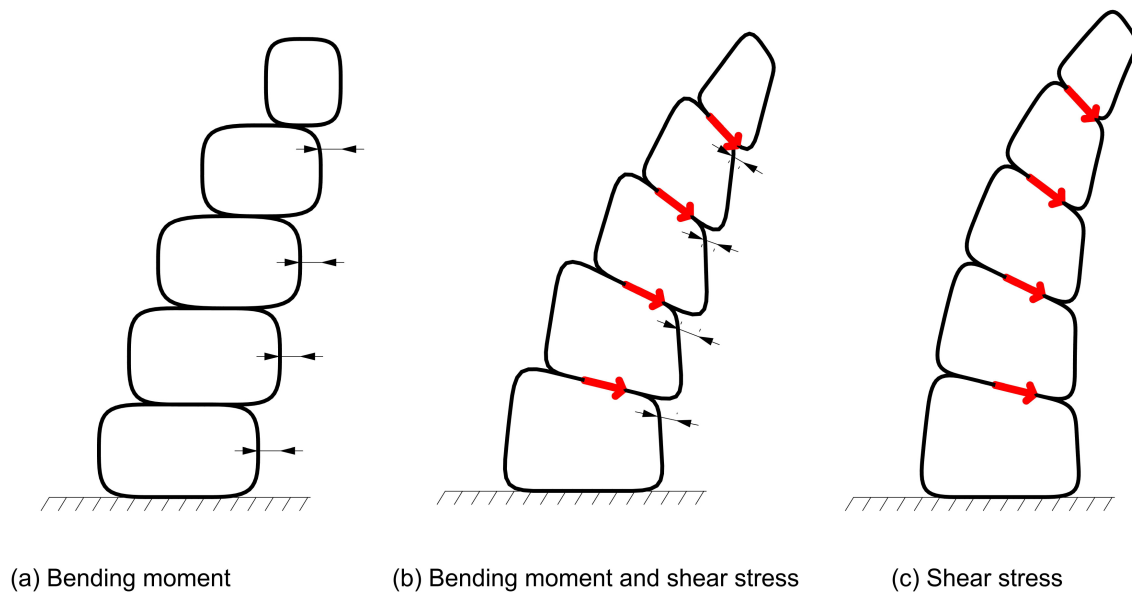


Figure 3.24 – Impact of Slicing Patterns on the Inter-Layer Bonding of a Printed Overhang Structure

### 3.6.5 Cross-Section Design

The cross-section of the shell plays a vital role in its structural stability. 3D Printing technology makes it possible to control material deposition and reduce

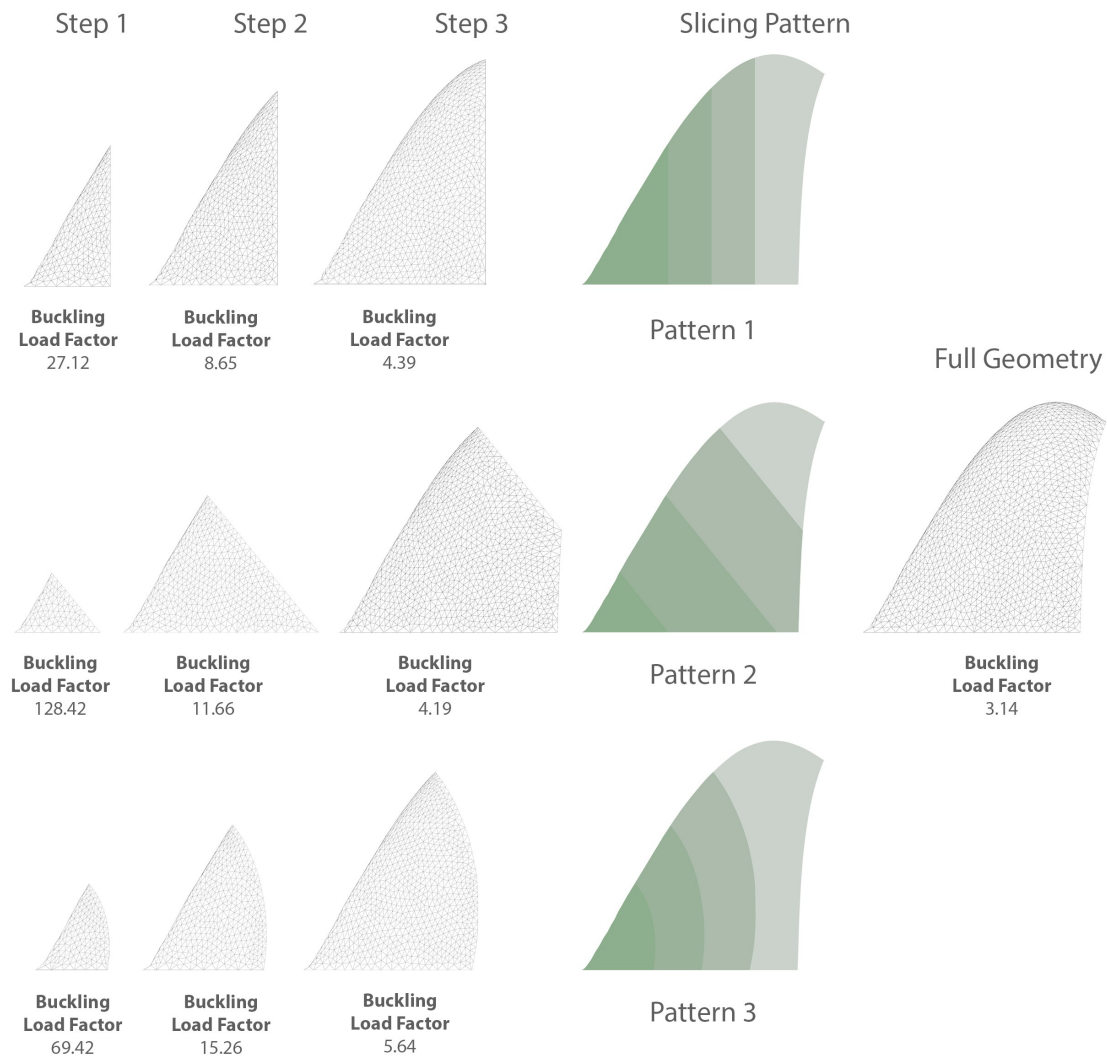


Figure 3.25 – Slicing Patterns and Their Effect on Structural Integrity

material consumption. A shell’s cross-section can be designed to minimise its self-weight while maintaining structural stability. The main principle is to deposit more material where the compressive stresses are higher. Traditionally, the masonry domes and vaults had thicker skin at the bottom and thinner skin at the top since the compression stresses at the base of these structures are at maximum. Firstly, we can narrow the shell’s thickness from the bottom to the top to optimise the cross-section of a funicular shell for the 3D Printing process (Figure 3.26(a)). Second, remove material from the shell’s cross-section (Figure 3.26(b)). Figure (Figure 3.26(b)) shows a zigzag infill between the shell’s outer and inner skin. As such, the stresses due to the self-weight are reduced while the stiffness is maintained thanks to the bracing between the two skins. A cross-section’s infill can be designed with different pattern topologies and densities (Figure 3.27) to be optimal for structural stability and material consumption, such as the work of Rodiftsis in [126]. However, using surface-based FEA software such as Karamba, it is impossible to simulate the effect of the cross-section’s infill pattern on structural stability as the software assumes the shell cross-section is always solid. Alternatively, geometry-based FEA software such as Abaqus or ANSYS Workbench can evaluate the effect of the infill pattern

and its density on the stability of a shell. A recent study [90] aimed to optimise the infill topology of 3D printed shells using a density-based method. Furthermore, the researchers at the Concrete3D Lab in Ghent developed the Voxel Print plugin for Grasshopper [31] that enables the simulation of the 3D printing process and analysis of the structural stability of 3D printed concrete objects through layer-wise mesh generation [26]. A video demonstrating this simulation is provided in [25]. The plugin generates data from the 3D-printed object for further analysis in Abaqus. Implementing such a process for 3D printing earth-based materials can significantly enhance the precision of finite element analysis by considering the geometry of the infill within the shells.

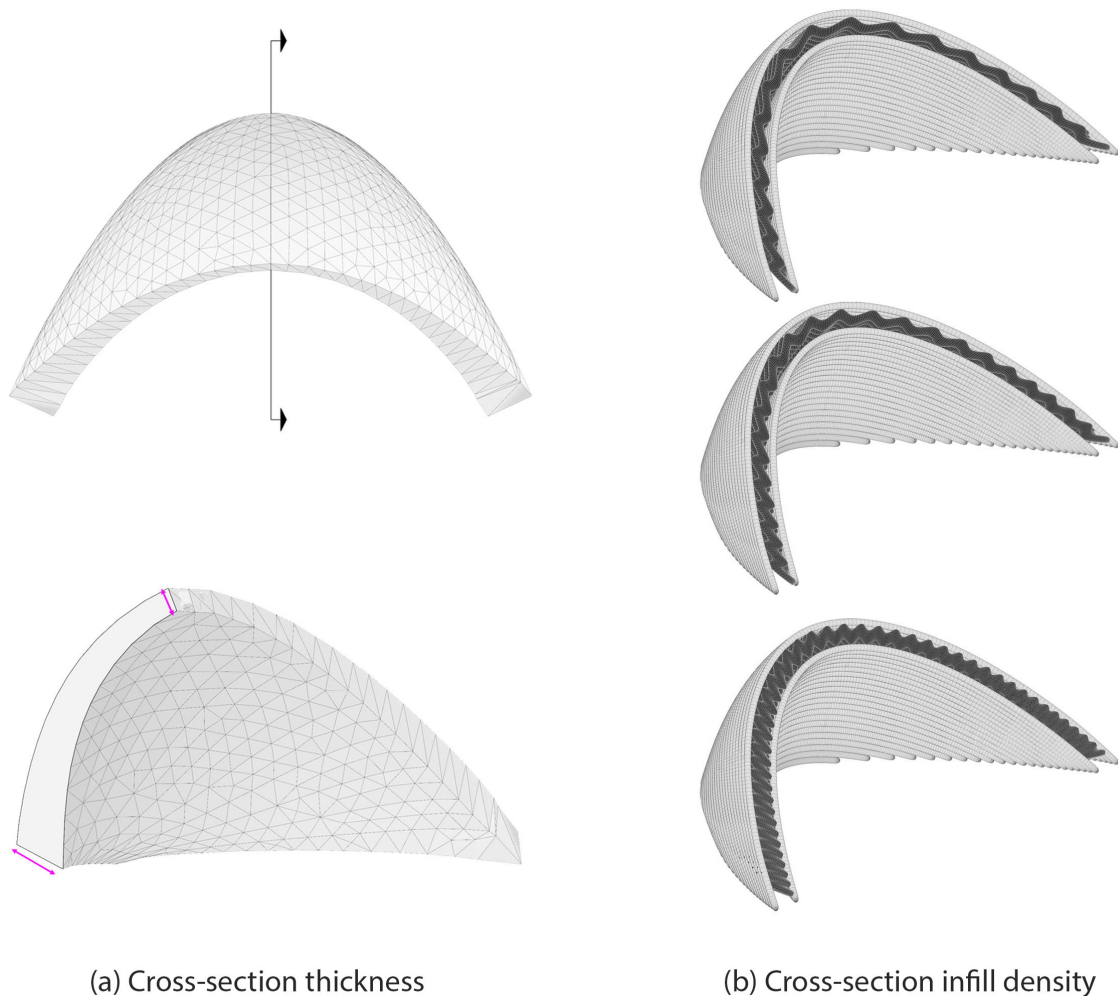


Figure 3.26 – Characteristics of a Shell's Cross-Section Design

### 3.6.6 Finite Element Analysis

In this research, the Karamba FEA plugging for grasshopper was used to analyse the printability and stability of 3D-printed shells. Figure 3.28 shows the steps and process of FEA using Karamba software.

To accurately evaluate the structural behaviour, it is crucial to precisely define the printing material's properties. Figure 3.29 shows a screenshot of the Grasshopper

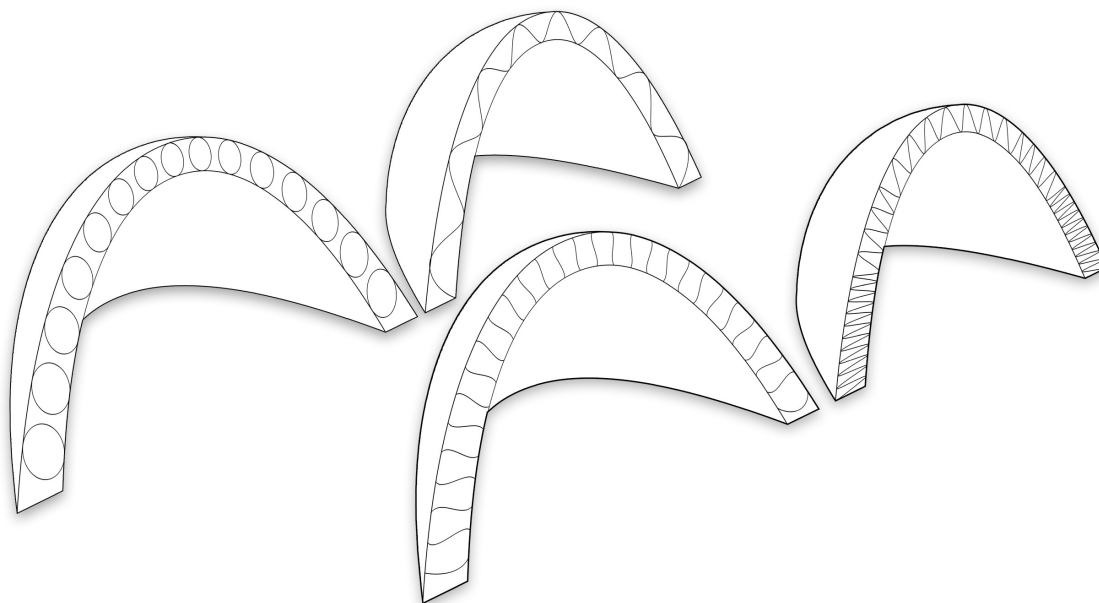


Figure 3.27 – Different Infill Patterns for the Cross-Section of a Shell

environment, illustrating the material component from the Karamba plugin. The following is a summary of how these parameters are determined:

- 1 **Young's Modulus:** This value can be obtained from the squeeze test. For the Speswhite kaolin clay mixture ( $\frac{\text{Water}}{\text{Kaolin}} = 0.58$ ), Young's modulus is 550 kPa (see section 3.5.2).
- 2 **In-plane Shear Modulus:** This parameter refers to the material's deformation response to shear stress within its plane. The relationship between Young's modulus ( $E$ ) and the in-plane shear modulus ( $G$ ) for isotropic materials can be expressed using Poisson's ratio  $\nu$  as:

$$G = \frac{E}{2(1 + \nu)}$$

where:

$G$  : In-plane shear modulus, in Pascals (Pa)

$E$  : Young's Modulus, in Pascals (Pa)

$\nu$  : Poisson's ratio, dimensionless

For the given Speswhite kaolin clay mixture, considered partially saturated, the Poisson ratio is 0.3.

- 3 **Transverse Shear Modulus:** This relates to the material's deformation response to shear stress applied perpendicular to its plane. Since the kaolin mixture is considered isotropic, the transverse shear modulus equals the in-plane shear modulus.
- 4 **Specific Weight:** The specific weight of the kaolin mixture is  $1.6 \frac{Kg}{L}$ , equivalent to  $15.68 \frac{KN}{m^3}$ , and can be measured using a balance.
- 5 **Tensile Strength:** The tensile strength of the fresh kaolin mixture is 5 kPa, as measured by a slug test (see section 3.5.3).

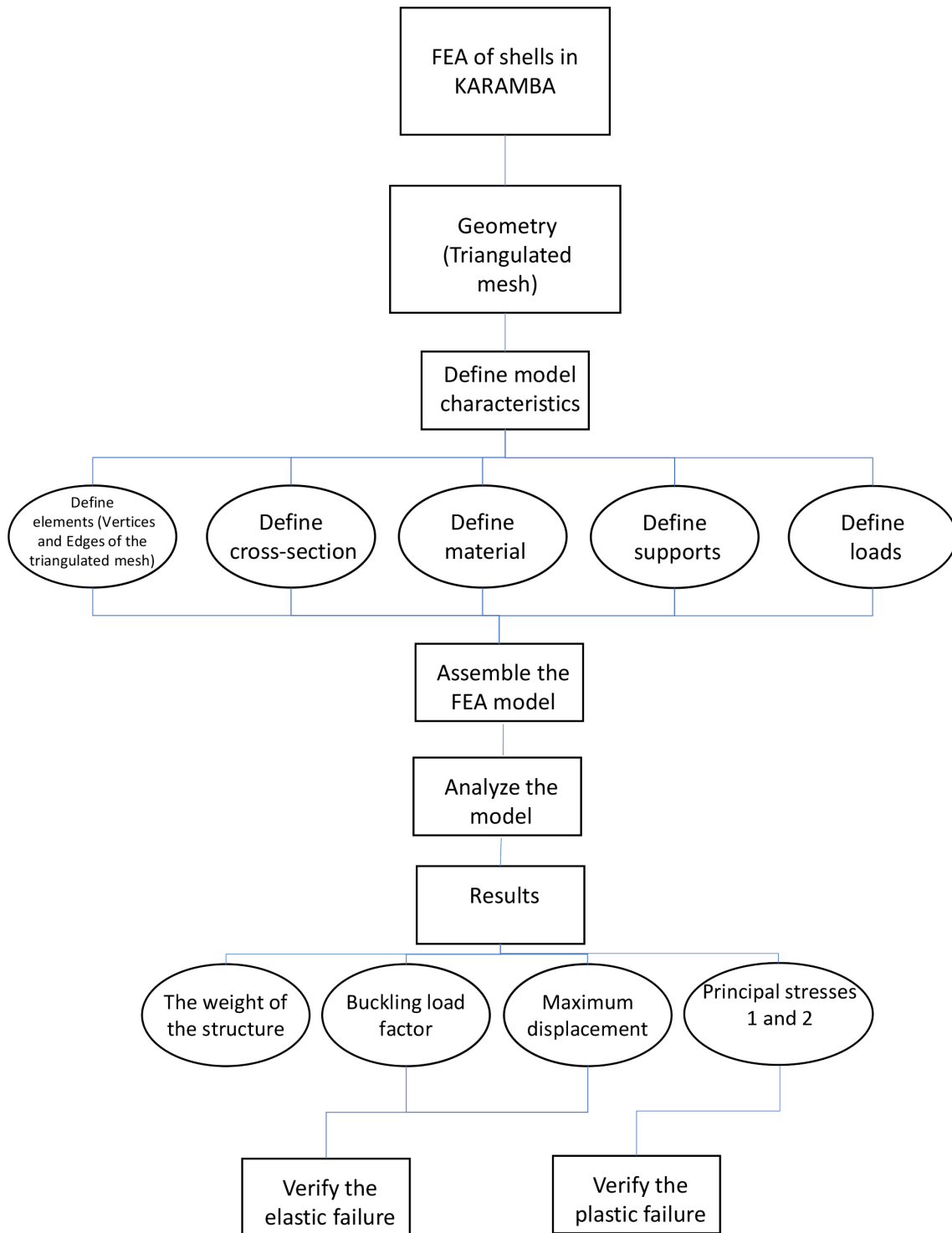


Figure 3.28 – The FEA process in KARAMBA

**6 Compressive Strength:** The compressive strength of the fresh Speswhite kaolin clay is -4 kPa, as measured by the squeeze test (see section 3.5.2).

**7 Strength Hypothesis:** In this dissertation, the Rankine failure theory is employed to predict the plastic failure of the material.



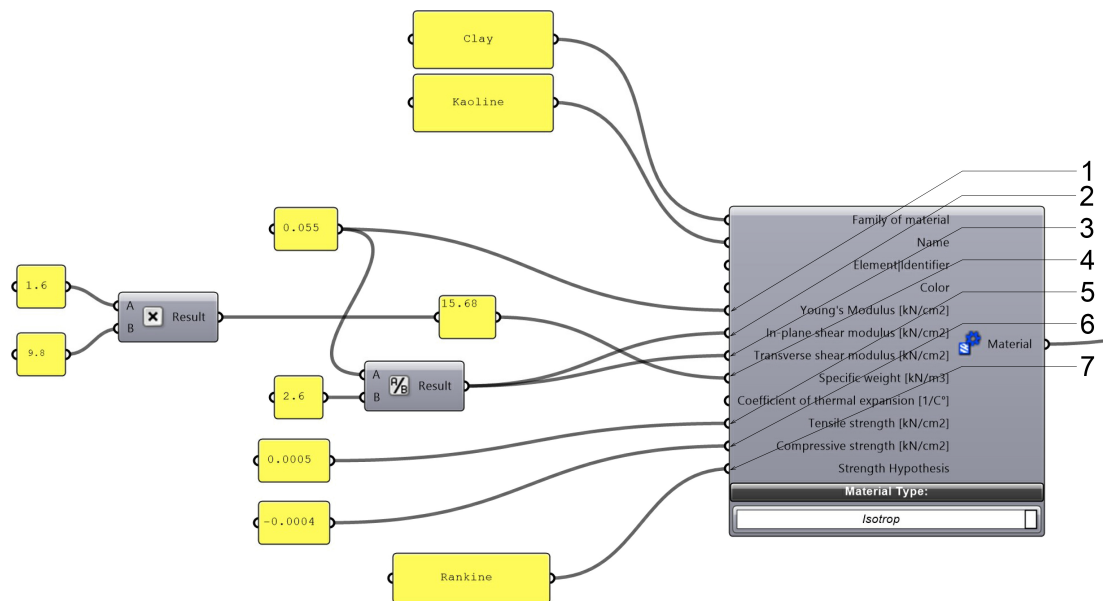


Figure 3.29 – Material Component of Karamba Plugin and the Input Parameters

### 3.7 Conclusion

This chapter focused on layer-heating methods to enhance earth-based materials' compressive capacity in 3D printing. The main question addressed was how to increase the yield strength of earth-based mortars by applying heat to the printed layers after deposition from the extrusion head. The objective was to evaluate the impact of heat on the mechanical behaviour of saturated porous media and its application to 3D printing.

The significance of this chapter lies in recognising that controlling the mechanical behaviour of the material is crucial for achieving successful 3D printing of cantilever structures using earth-based materials. The findings presented contribute to a better understanding of the effect of heat on the mechanical properties of such materials, enabling practitioners to enhance their printing experiences based on these insights.

The chapter began by introducing techniques to enhance the yield strength of earth-based materials, including additives and water evaporation from the printing paste. Various heating setups were presented, encompassing convection, conduction, radiation, and hybrid methods, focusing on layer heating through convection. The rheological requirements for a printing mortar were outlined: pumpability, workability, and buildability. The importance of material stiffness for 3D printing purposes was discussed, highlighting the potential buckling failure resulting from geometric and material stiffness factors.

Furthermore, the chapter delved into the yield criterion for earth-based materials based on the Mohr-Coulomb theory, emphasising cohesion and material internal friction angle. The assumption of undrained cohesion in the earth-based printing mortar during the printing process was addressed, introducing the oedometer test as a geotechnical method for measuring undrained cohesion. The influence of water

content on the mechanical properties of soils and the consolidation phenomena relevant to compacting material for increased density and strength were also explored.

Moreover, the chapter highlighted the drying mechanism of soils and introduced Uno's formula, a simplified equation for the evaporation rate of saturated porous media. It discussed how the printing geometry could impact the yield strength evolution of earth-based materials in the 3D printing process through evaporation. The chapter then presented four material experiments, including a wind tunnel, slug test, squeeze test, and vane test, to evaluate water evaporation rate, pure tensile strength, compressive strength, and shear strength of the printing mortar, respectively. Additionally, printing cylinders with different heating methods were examined to assess the effectiveness of convection-based heating setups in achieving successful 3D printing with earth-based materials. Finally, the layer heating method's printing environment and energy consumption were discussed.

Later in the chapter, the method of Finite Element Analysis (FEA) for structures using earth-based mortar, with Speswhite kaolin clay as a case study, is demonstrated through the Karamba plugin for Grasshopper. This section elucidates the failure modes and explains the impact of slicing patterns and shell cross-sections on structural stability. It's important to recognise that the FEA method, grounded in the Rankine failure criterion, offers a foundational approach that can be further refined. By incorporating more sophisticated failure theories, such as the Mohr-Coulomb failure theory, a more precise evaluation of the structural stability of SF3DP shells could be achieved. This enhancement would facilitate the exploration of more complex and ambitious geometries.

The contributions of this chapter can be summarised as follows:

1. Introduction of layer heating method as a passive approach to enhance the yield strength of materials in the 3D printing process.
2. Introduction of the wind tunnel experiment to evaluate the effect of heat on saturated porous media in 3D printing.
3. Evaluation of the impact of printing geometry on the evolution of saturated porous media in the 3D printing process under heat conditions.

Future studies should investigate the influence of crust layer formation on the evaporation rate of saturated porous media in the 3D printing process and examine at each level the crust layer emerges.

This material chapter has shed light on the layer heating methods to increase the yield strength of earth-based materials in 3D printing. It has provided valuable insights and experimental findings that contribute to advancing knowledge in the field, enabling practitioners to improve their 3D printing experiences and achieve tremendous success in constructing robust structures using earth-based materials.

# Chapter 4

## Fabrication & Automation

### 4.1 Introduction

In this chapter, through the presentation of different prototypes in different scales (small, medium and large), the concerns about prototyping and using 3D printing setups and the technical problems one might face are discussed. The scales classify the prototypes because as the prototype scales grow, different issues and challenges will arise. Therefore, the user must adapt their design and fabrication technique thoroughly. Based on the classification in [35], the object's scale in 3D Printing systems can vary from objects less than a meter to those in the scale of a full tall building. The object scale can be classified into four categories as follows:

- (a). Objects with a size of less than a meter and a thickness layer of less than 8 mm.
- (b). Constructive element of size around 1 to 4 meters (Typically beam, column or a part of a slab) with a thickness layer between 8 mm and 5 cm.
- (c). Object around 5-10 meters, typically a living unit or a one-story house with a thickness layer between 5 cm and 30 cm.
- (d). Full tall building.

In this chapter, the prototype scales are classified in the following order:

- (S) The objects of size less than 30 cm with a layer thickness less than 5 mm.
- (M) The objects of size larger than 30 cm and less than 1 meter with a layer thickness of 5mm to 2 cm.
- (L) The objects of a size more than 1 m and a layer thickness between 2-4 cm.

The relevance and progress of Patching grammar, described in chapter 2, has a direct relationship with the advances in fabrication setup technologies. The more sophisticated the fabrication technologies are, the more freedom of design the users can have based on the patching grammar. This chapter describes the workflow and process of communication with robotic arms to transform the 3D printing data into robotic orders. Second, the prototype of a small-scale (Max  $20 \times 20 \times 20$  CM) multi-vault using a wooden strand and a 3D doodler mounted on a mini ABB arm is described. Third, the prototype of a medium scale (Max  $50 \times 100 \times 50$  CM) squinch and a multi vault with three Patches printed with Kaolin clay is demonstrated. Lastly, the attempt to prototype large-scale shells ( Max  $100 \times 100 \times 200$  CM) is depicted.

## 4.2 Geometric Data to Robotic Commands

Using conventional robotic arms, an intermediate software between the design software and robot controlling software is needed to convert the designed geometry and 3D printing data, such as the movement speed and extrusion flow speed. In this dissertation, the Hal Robotics plugin for Grasshopper [60] is used to create the robotic procedures for all the prototypes. Figure 4.1 shows the process of creating a robotic procedure using the Hal Robotics plugin. In the first place, the user has to transform their geometry into the sliced curve and then transform the curves into planes in the space. However, one can directly transform the geometry into planes in space. The optimal orientation of the planes in the space is to have the Z vector of each plan aligned with the tangent vector of that plane's origin point onto the Target geometry. However, due to the robotic kinematic constraints, this is not always possible to set the planes tangent to the target geometry. Therefore, the users might have to compromise this feature to have a reachable target for a robot to execute the print process. The next step after setting the planes and their orientation into space is to set the robotic actions. The robotic action defines how a robot should reach a certain plane in space. For example, a robot can use the Joint motion setting or Cartesian motion setting to reach a plane. It's up to the user to determine which type of movement is proper for their action. In addition to the motion setting, the robot speed and other custom actions, such as the extrusion flow speed at each plane, must be defined at this step. After creating the sets of robotic actions, one must combine those actions and solve the procedure in the solve component. The solve component will notify the user if their action is feasible. The solve component also shows the user at which plane the robot has kinematic (Singularity) or reachability constraint. Therefore, the user can modify their plane correspondingly. In general, the user must control that their target geometry is positioned in the right place, not so far that the robot can not reach the object (Figure 4.2). Not too close, so the robot won't have difficulty in terms of its joint orientation to reach the planes that are very close to the robot or have clashed with its tool (Figure 4.3). Furthermore, the orientation of the planes into space has a direct influence on the kinematic freedom of the robot (Figure 4.4). Finally, the user can simulate their action and export it in the form of RAPID<sup>1</sup> code for communicating with the robot. Figure 4.4 shows a case in which the robot has a joint constraint and self-clash with its tool, and figure 4.2 shows a case in which the robot has difficulty reaching a target since its too far from the robot.

## 4.3 Small

In the early investigation of the SF3DP methods, small-scale prototypes were practised to simulate the feasibility of the 3D Printing process of shells with overhangs without using temporary supports. The idea behind using the small setup without a real construction material was to put it one step further from theoretical discourses and see how a robot behaves while printing overhangs. Furthermore, the proportion of the robot to the size of the printed object was a concern to determine. The setup used for small scale prototypes (Figure 4.5) comprises the

---

1. RAPID code is a sophisticated language for the ABB robotic arms.

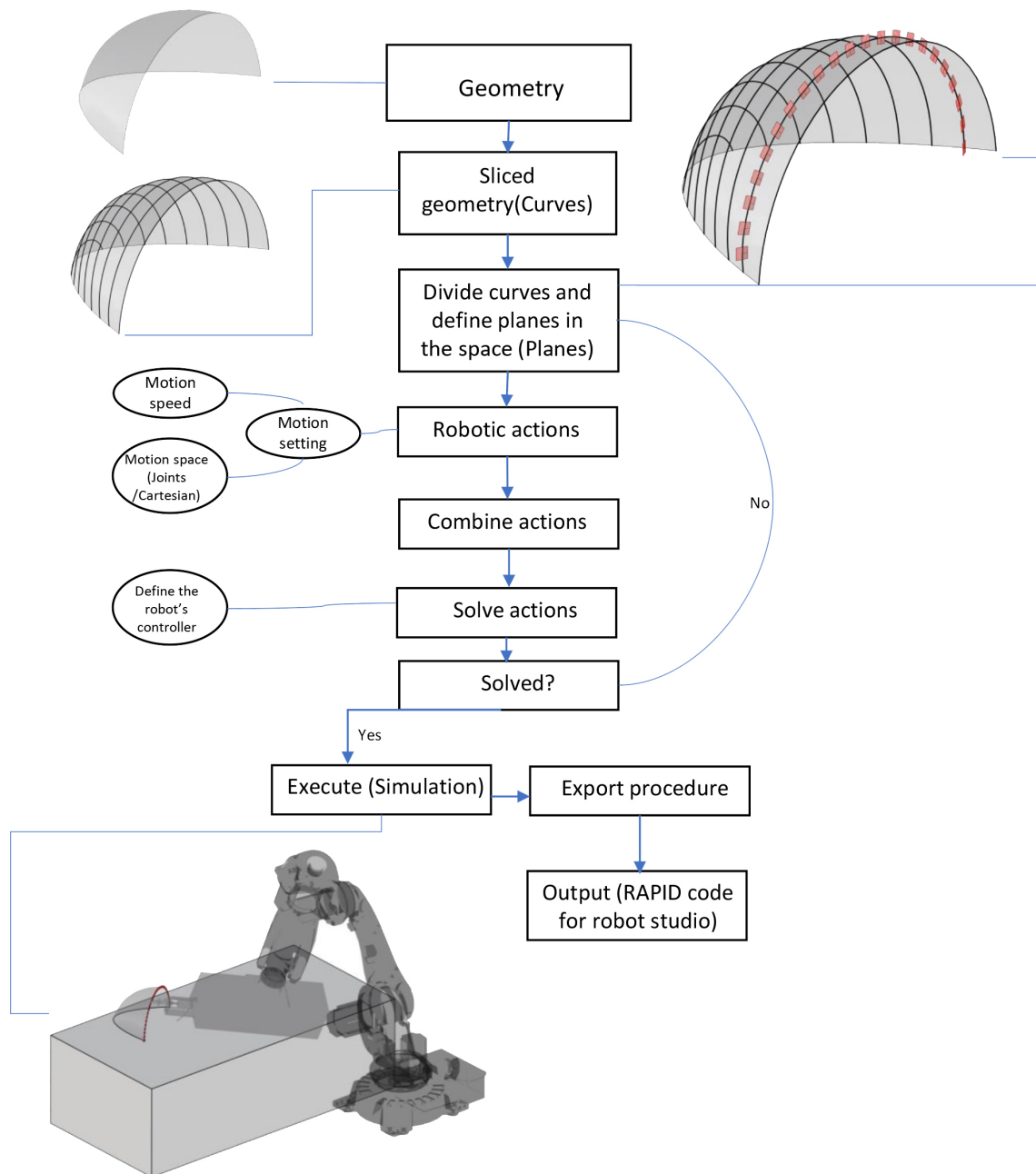


Figure 4.1 – Creating Robotic Procedures in the Hal Robotics Plugin for Grasshopper: A Step-by-Step Workflow Illustration

following elements :

- (a). Robot: ABB IRB 1200, 6-axis arm (5 kg of payload)  
This is a small-scale robot that is very handy for variant applications. The reachability distance is 700 mm.
- (b). Tool : 3Doodler Pro  
This advanced 3D printing pen can print various materials and set different extrusion speeds and nozzle temperatures. The nozzle is circular and has a diameter of 2 mm.
- (c). Gripper : Custom 3D Printed gripper This is a custom-designed gripper for holding a 3Doodler pen and mounting it on the tool-changer of the ABB

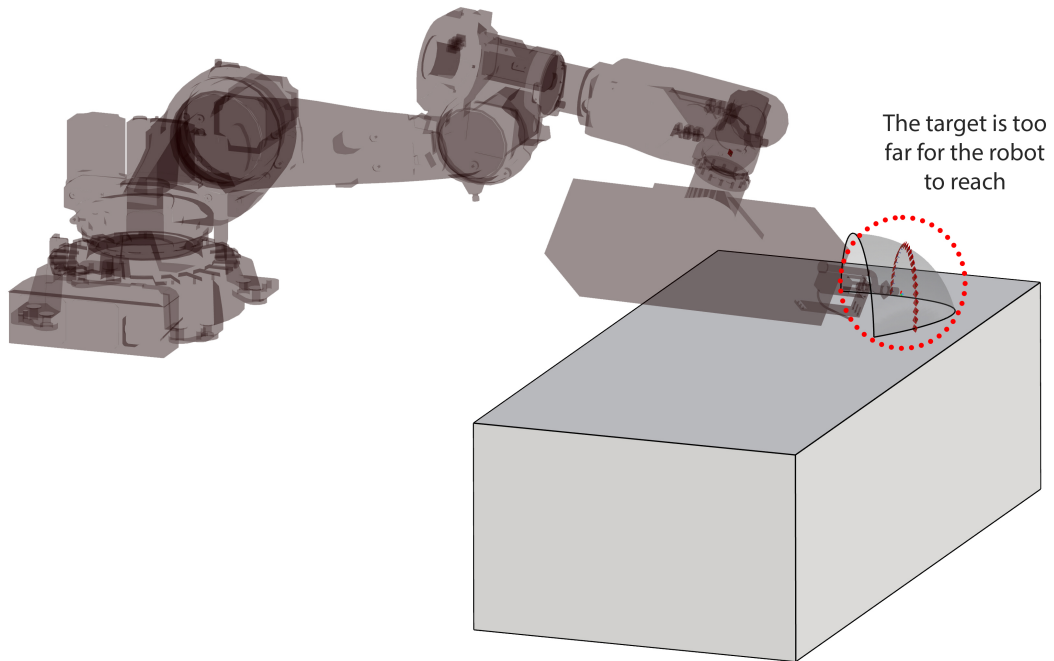


Figure 4.2 – Robot’s Inability to Reach the Target Plane

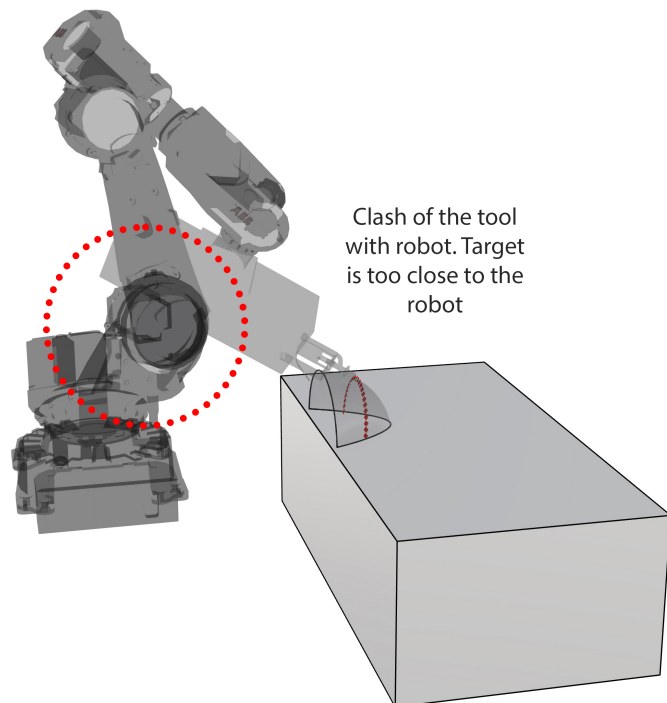


Figure 4.3 – Robot Self-Clashes Due to Close Target Constraint

IRB 1200. It is 3D-printed with ABS material and high infill intensity to ensure stability.

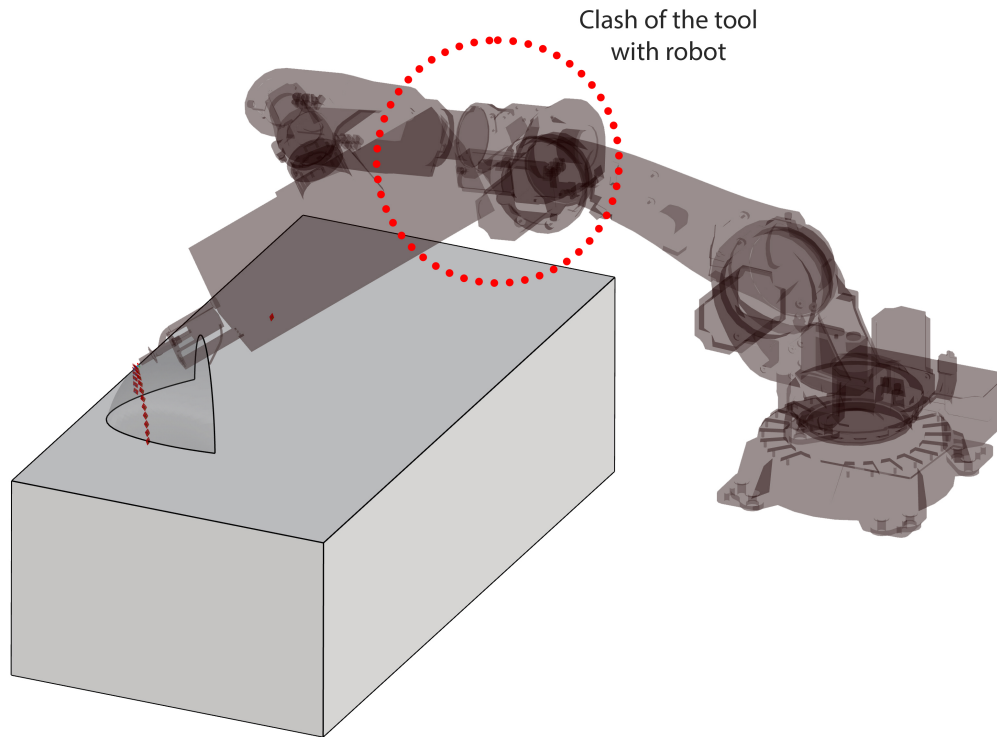


Figure 4.4 – Robot-Tool Clashes Due to Improper Orientation of the Target Plane

(d). Material : Wooden strand This material is fabricated by the 3Doodler company and comes in the form of strands.

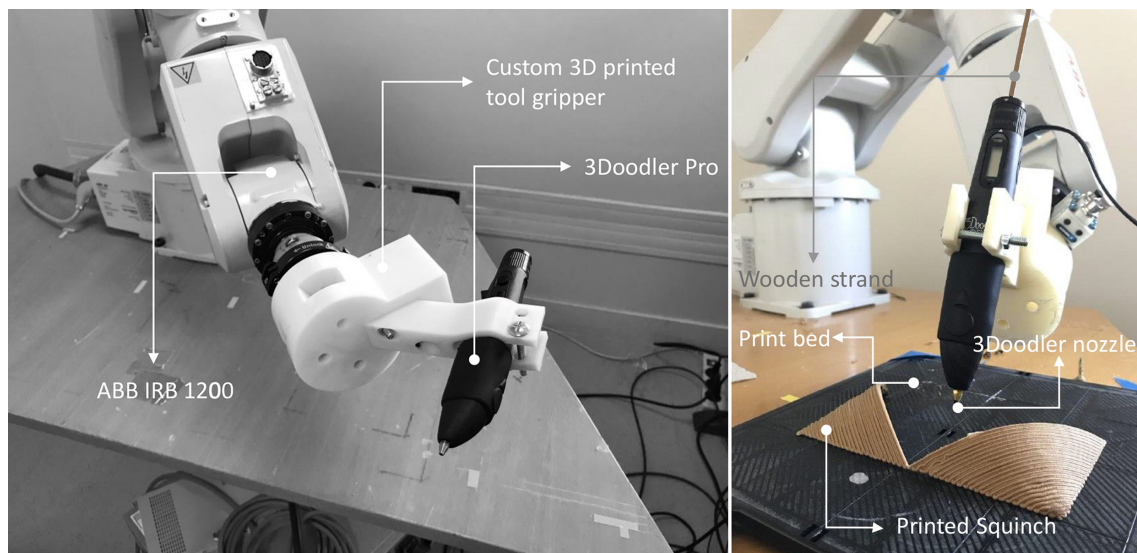


Figure 4.5 – Small Prototyping Setup

### Multi-Vault with a Square Boundary

The prototype of a multi-vault with a square boundary was 3D printed using this setup. The size of the boundary is  $15 \times 15\text{cm} \times 15\text{cm}$ . The full video of the

robotic 3D Printing simulation and the actual process of printing using the setup mentioned above are accessible in [97]. The 3doodler is a flexible pen that can extrude multi-materials such as ABS, PLA and aluminium by melting the material in the preheated nozzle. The same company provides the material in the form of strands, such as spaghetti strands, before it's cooked. The wooden strand is chosen among other materials due to its similar behaviour to materials such as clay or cement paste in the deposition process. Another material, such as PLA or ABS, has a high tensile strength that behaves differently from clay, cement or melted wooden strands, not representing the realistic simulation for full-scale prototyping. The 3Doodler can set different nozzle temperatures and different extrusion speeds. The user can set the nozzle temperature and extrusion speed based on the chosen material, the robot movement speed, and the desired layer and height. Therefore these parameters are tested with different robot speeds for an optimal set of printing parameters. One should tackle several challenges while prototyping with such a precise robot in small dimensions. First, the model printing base should be precisely calibrated. Otherwise, accumulating printing errors will lead to unsuccessful printing after printing several layers. Second, the tool's centre point(TCP), which is considered the centre of the 3Doodler nozzle, must be precisely defined in the world coordinates and assigned to the corresponding tool components in the robotic procedure simulating program such as HAL Robotics mentioned in the previous section. This will guarantee that the independent Patches will be printed precisely on the printing bed corresponding to the digital model. Therefore the interconnecting Patches (Pendentives) can be supported by the lateral Patches in the correct location. Lastly, the printing process must be as continuous as possible, meaning there should be no or at least very few interruptions in the printing process due to the sensibility of the robot to the vibration. The vibration is due to human activities besides the robot working environment or even the shock vibration from starting and stopping the robot engine. Lastly, the printing using such a setup is significantly constrained by the robot working area, reachability, and robot constraint for arriving at a particular target in space with a special joint angle. The width and height of the layers in this prototype is about 2mm. Due to the reasons above, the prototype of the presenting multi-vault is done in many steps with many trials. Finally, it was possible to print all the Patches except the last part, a Dome, due to accumulated calibration errors (Figure 4.6. However, finishing this prototype with some manual adjustment and re-calibration is possible.

## 4.4 Medium

After gaining experience with small prototyping and seeing how a robot can 3D print overhangs, it was decided to put it one step further in real construction scenarios by printing with earth-based material. In the previous section, using wooden strands instead of earth-based material prevents us from considering the issues arising from the material properties. The wooden strand is a very flexible material that can easily melt and be extruded from the 3doodler nozzle and gain its strength very fast after deposition, which makes it able to print many complex geometries without confronting material failure. However, this is not the same scenario when we use earth-based materials. As mentioned in detail in chapter 3 The clay must be mixed with a certain amount of water to be fluid enough to be pumped



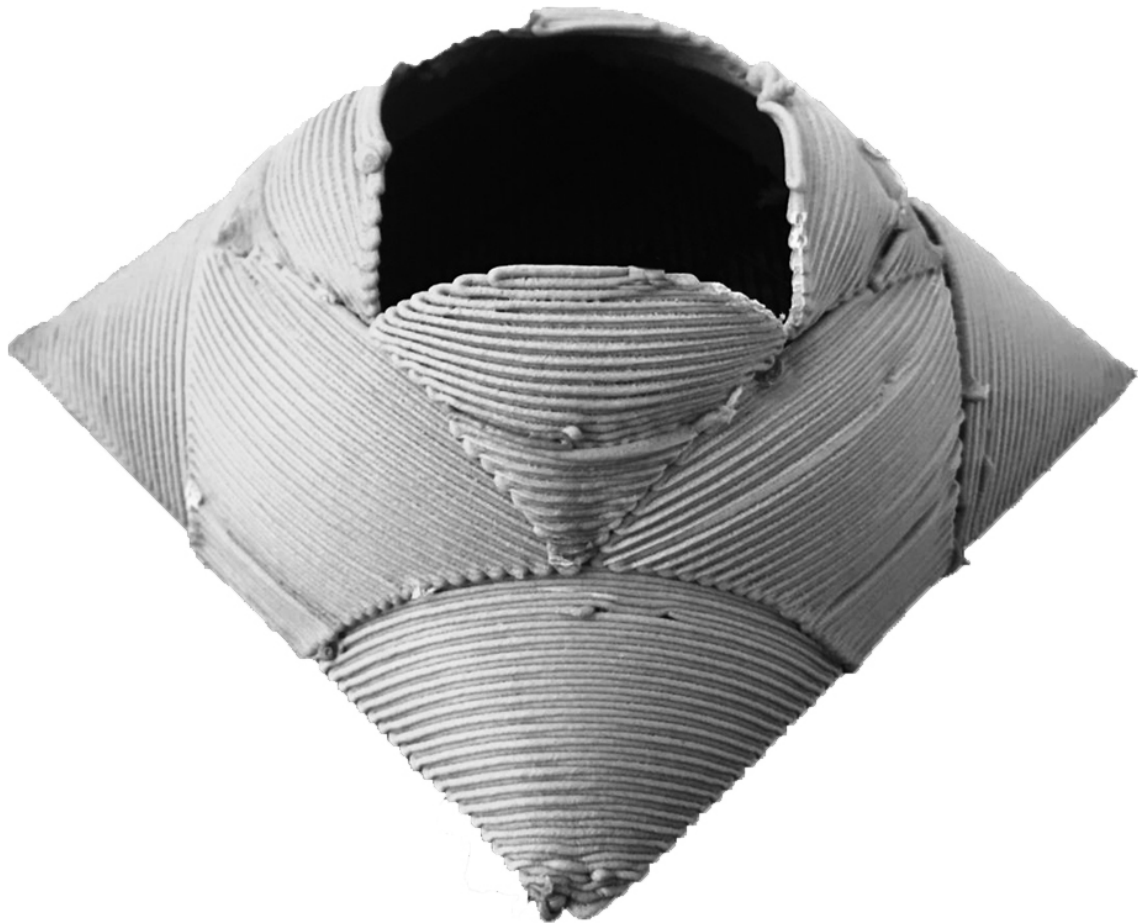


Figure 4.6 – Prototype of a Multi-Vault Constructed Using a Small Prototyping Setup and Wood-Based Material

(Sheared) and extruded, making it a low-strength material and can fail during the deposition. In contrast to cement-based material in concrete 3D printing or wooden strands, the clay does not gain strength very fast after the deposition. Therefore, techniques such as Lace Heating (Refer to 3 must accompany the 3D printing process to compensate for the long strength evolution time for the earth-based material. Although the medium-scale prototyping with earthy material can show us the issues coming from the material behaviour, it still does not fully demonstrate the real size fabrication issues of 3D printing a living unit. However, in terms of scale, the objects of medium scale can be considered a component of a construction element, such as a part of a post-tension column. In this dissertation, two prototypes were printed on a medium scale. The first is the prototype of a "squinch", and the second is the prototype of a "multi-vault with three Patches".

## Medium Prototyping Setup and Environment

Figure 4.7 show the environment in which the medium scale. The medium-scale prototypes of this dissertation are performed. This lab is called Halle Freyssinet, which belongs to *Build'in* lab and is located at *Ecole des Ponts et chausset*. As presented in figure 4.7, this lab comprises a cage with a 6-six-axis ABB IRB 6620 robot installed on a track (7-axis). The robot can move along the track, making

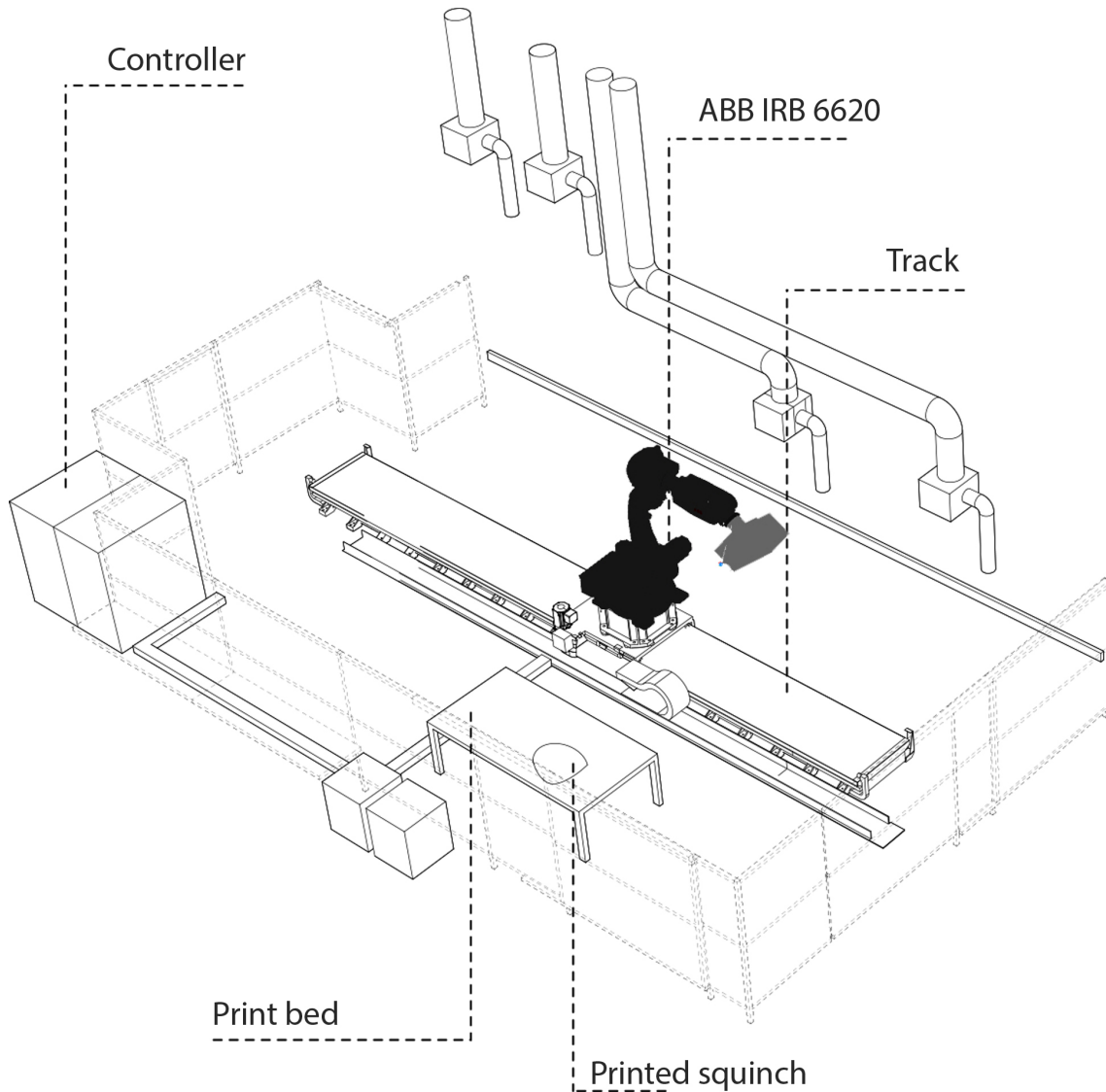


Figure 4.7 – The Medium Scale Prototyping Environment

it possible to print on a large area compared to fixed robots. Figure 4.8 shows the extruding system used for medium-scale prototyping. This custom-made pneumatic extruder works with a hydraulic jack with 5 bar power. However, the extruder is made by *Wasp*. Furthermore, a set of nozzles is 3D Printed with different end diameters and geometries to serve different printing scenarios. The clay reservoir has 5 litres capacity and is made from a 7 mm transparent Plexiglass tube.

### Double Layer Squinch ( $66 \times 37 \times 27h$ cm)

Figure 4.9 shows The prototype of a double-layered squinch with a parabolic base. The full prototyping video of this squinch can be found in [95]. This prototype is successfully printed using a Kaolin clay mix. The prototype consumed around 35 litres of Kaolin clay mixture. The mixture is the kaolin clay powder mixed with water with the proportion of  $0.56 \frac{\text{Water}}{\text{Kaolin}}$ . The slicing technique used for this prototype is the successively increased angle slicing method (Refer to figure 2.5-5). The starting slicing plane is tilted  $20^\circ$ , and the ending slicing plane is tilted  $75^\circ$ . Using the

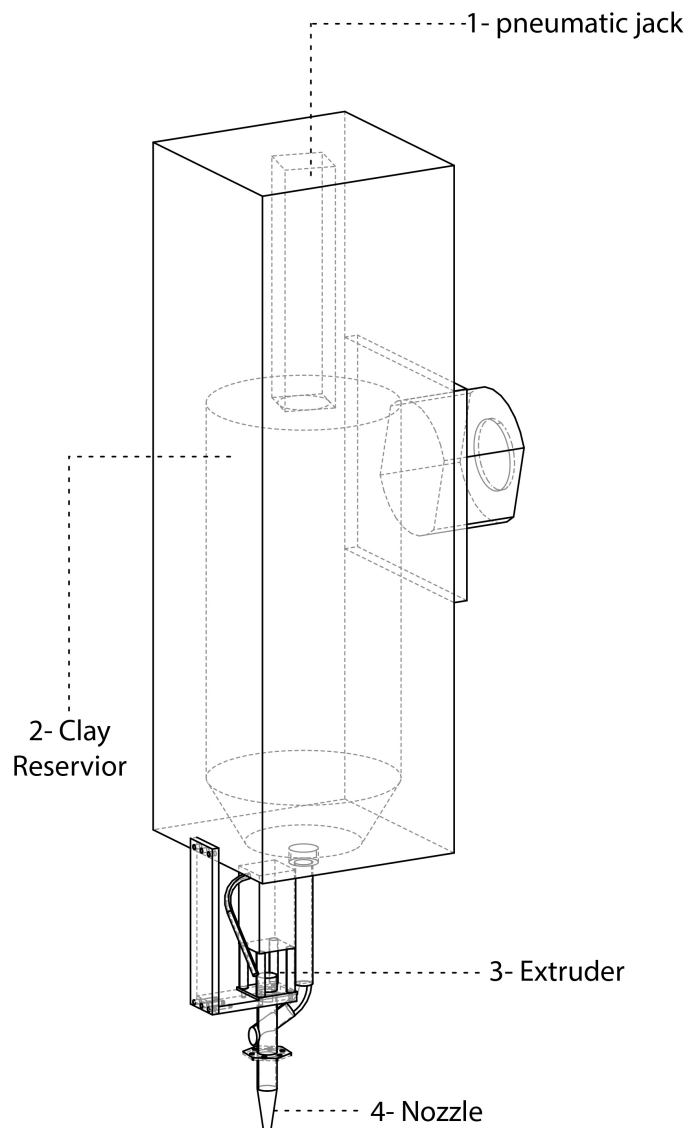


Figure 4.8 – Schema of the Clay Extruding System

aforementioned slicing method, the maximum achieved height of the layers is 4 mm. The nozzle used for this prototype has a 10 mm diameter. Therefore, the printing technique used for this prototype is the layer pressing technique. This technique is elaborated in detail in [17]. The extrusion speed is set to 8080 rps. The achieved width of the layers corresponding to the speed of the robot ( $R_v$ ) is as follows:

$R_v$  41 mm/s: 12 mm

$R_v$  50 mm/s: 11 mm

$R_v$  65 mm/s: 10 mm

At the beginning of the printing process, the robot speed was set to 41 mm/s. However, after printing several layers, to reduce the layer's width, the robot speed was increased to 50 mm/s and later 65 mm/s. Furthermore, the speed of 70 mm/s also was tested, and the material tearing was observed at this speed.

The cross-section of this squinch is designed to be 7 cm thick at the bottom of the Patch and 2 cm thick at the top. The digital model of the cross-section of this squinch is presented earlier in figure 3.26. Furthermore, the density of the

cross-section infill of this squinch is designed to be less dense in the part of the shell (With more space or cavity) with lower compressive stress (Upper part) and more dense in the part where the compressive stress is maximum (Bottom).

Finally, from the execution of this prototype, it is observed that the success of the printing process for a cantilevered geometry using fresh clay is related to the following items:

### **Geometry**

The geometry of the squinch must be designed in a way that the squinch geometry has maximum tensile or compressive stress less than the material's capacity to prevent plastic failure. Furthermore, the geometry of the squinch directly influences maximum displacement and the buckling behaviour of the structure.

### **Cross-section**

It is observed that the cross-section geometry and topology directly influence the geometry's stability during the printing process.

### **Slicing method**

The slicing method has a great impact on the structural behaviour of the geometry during the evolution process, as successive layers are deposited.

The 3D printing process of this squinch using the mentioned setup takes several hours since stopping the print process and filling the clay reservoir is time-consuming. The prototype has 35 litres volume, and the material reservoir (4.8 has only 5 litres capacity). This means the printing process is interrupted up to seven times. Furthermore, figure 4.10 shows the displacement that appeared at the top part of the printed squinch, which could end up with elastic buckling if the printing process continued. The reason for the aforementioned displacement is the low stiffness of the material in its early age. This issue can be eliminated using the lace heating technique with sufficient heating intensity, as mentioned in chapter 3. For this prototype, the Lace Heating method is not employed. Figure 4.11 shows one of the failed attempts for printing a squinch prototype due to the buckling failure. This geometry is buckled under its self-load due to geometrical issues, support condition (Polyline base instead of parabola) and low material stiffness. The next prototype demonstrates that printing a squinch with a polyline base is possible using the lace heating method.

## **Multi-Vault with Three Patches ( $100 \times 36 \times 27h$ cm)**

Figure 4.12 shows a multi-vault with three patches. The multi-vault has two identical squinches and one intermediate pendentive. The mixture formula for this prototype is the same as the first medium prototype. The fabrication of this prototype is done in four days. In the first two days, the first squinch is printed (In two days). On the third day, the second squinch is printed (In one day), and on the fourth day, the third patch (pendentive) is successfully 3D printed connecting two independent identical squinches. Patch number one (First Squinch) was printed in two parts since after printing the half part, the material had to dry for one day long and became stronger and stiffer to handle the weight of the remaining half of the Patch since the Layer Heating strategy (Refer to section 3.6.2) was not used for this patch. Later, the Layer Heating strategy was used to print Patch number

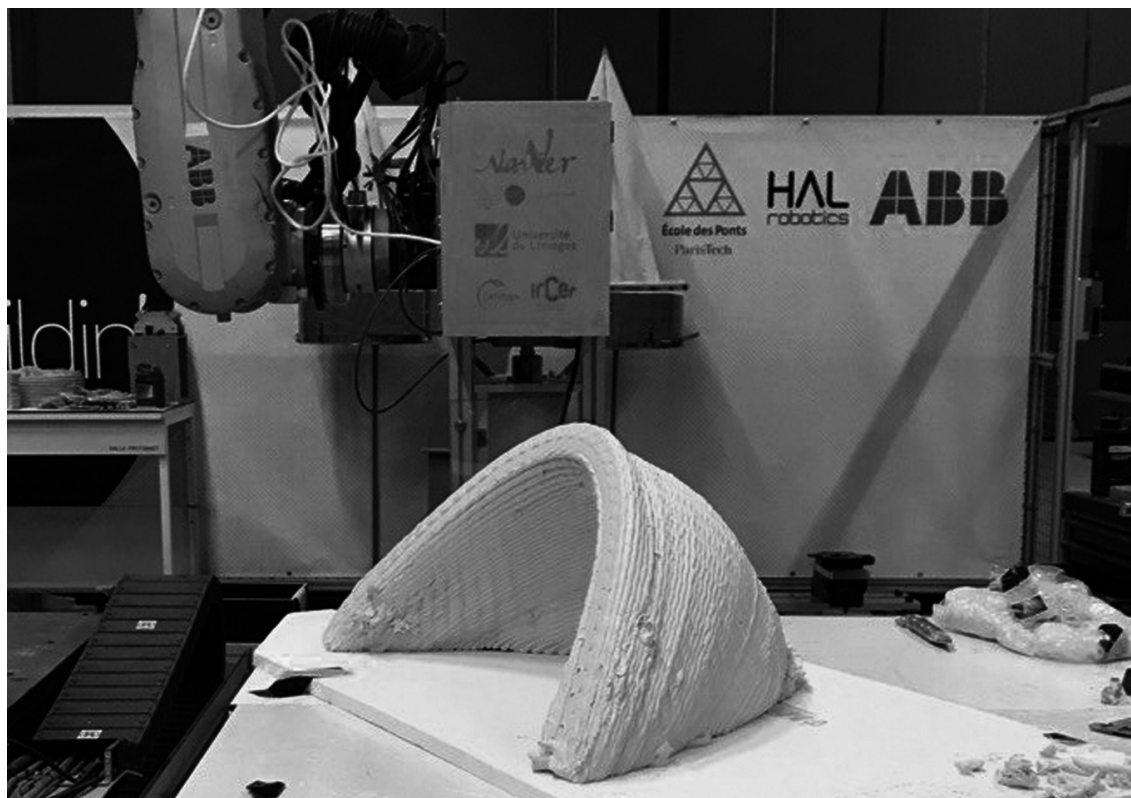


Figure 4.9 – The First Medium Prototype: A Double-Layered Squinch - Detailed View of Construction and Layering Technique

two (Second Squinch) entirely on the third day. Finally, Patch number three was printed on the fourth day using the layer heating strategy as patch number two. The limitations in the actual fabrication practice are mostly related to fabrication setup limits and material formulation. The cross-section design of the patches for this multi-vault incorporates doubly layered patches with a zigzag-shaped infill. This design serves two purposes: first, it ensures the stability of the shell structure, and second, it reduces the overall self-weight of the shell by creating cavities within the patches' cross-sections.

#### **Material related challenges:**

- *Material Strength:* the low stability of the material prevents us from printing fast and large. Due to the necessity of having low-yield strength material for the extrudability reason, it is necessary to use the lace heating method to increase the material strength while the geometry is being printed.
- *Shrinkage detachment:* After having three Patches printed and dried, the cold joints between the Patches occurred, and the Patches became detached. The assumption is that this is due to the reason that the Patches were printed on different days. If the Patches are printed not with a very long delay before the prior Patches become dry and the material becomes less viscous, the problem of the cold joints may be solved. However, the hypothesis above has not been experimented with yet at the stage of this prototype. Furthermore, the material formulation is vital in reducing or increasing shrinkage amount. Since shrinkage in

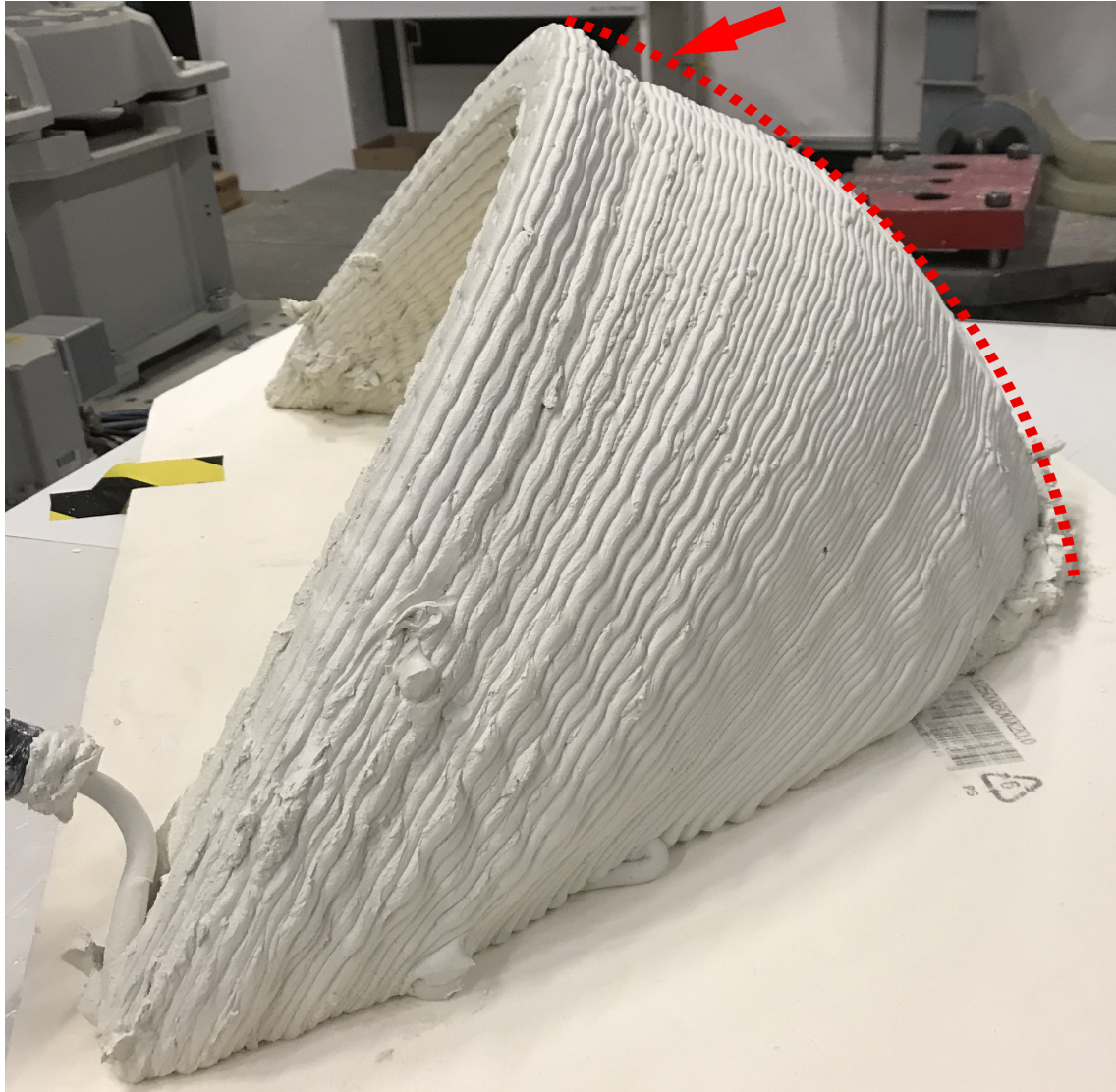


Figure 4.10 – Displacement Occurring in the Last Layers of the Printing Process

clay depends on the amount of water lost by evaporation, it is preferable to reduce the water content of the clay mixture to reduce the shrinkage deformation intensity. However, the less water in the mixture, the harder it is for the extrusion setup to extrude the material. The other possible solution is to use sand or gravel to create a granular skeleton, reducing shrinkage strains and the time needed for water evaporation from the material.

**Fabrication setup constraints:**

- Clay Reservoir: As mentioned in the experience of the first medium prototype, the limitation of clay reservoir capacity (5 litres) increases the print time considerably. Furthermore, recharging the clay reservoir in the printing process can also contribute to the loss of tool calibration. Consequently, imprecision in the printing process can occur, especially when printing the multi-vaults in which the position of the patches corresponding to the digital model is vital for the excellent connection of intermediate patches with supporting ones. A setup with a continuous



Figure 4.11 – The Buckled Squinch

material pumping system can eliminate the mentioned problem.

- *Shrinkage deformation:* As the patches within this multi-vault were not printed simultaneously and considering their interconnected nature, sharing the same edges in the supporting parts, it became necessary to modify the geometry of the third intermediate patch (Pendentive) to align with the new geometries of the initial squinches after shrinkage. This adjustment was crucial to ensure optimal support for the pendentive, allowing it to be perfectly supported by the two lateral squinches. In this process, the robot head is employed to trace the revised geometry of the squinches after shrinkage. Subsequently, the geometry of the pendentive is re-imagined, taking into account the updated supporting position derived from the traced squinch geometry.
- *Robotic-arm collision with the printed patches:* This problem did not occur for this research experiment since the robot tool path was carefully and patiently simulated before each patch's printing process. However, due to simulations using the robotic procedure solvers, the printing head collision with the printed Patches when the robot attempts to print the intermediary is a common problem. Hence, the users might have to re-modify their robotic procedure for printing each new patch and corresponding to the existence of the previously printed patches to avoid any collision. Furthermore, as the number of patches increases, this can be time-consuming to solve each patch's procedure individually.
- *Robotic arm reachability and movement constraints:* In the 3D printing of cantilevered structures workflow, orienting the printing head following the tangent direction of target printing geometry is prevalent. However, in some cases, a six-axis robot might have difficulty orienting the printing head as the users had set a specific target. In this research, the problem of robotic arm reachability and orientation constraints was addressed by

designing and fabricating a set of custom-made nozzles, such as the nozzle presented in Figure 4.13.

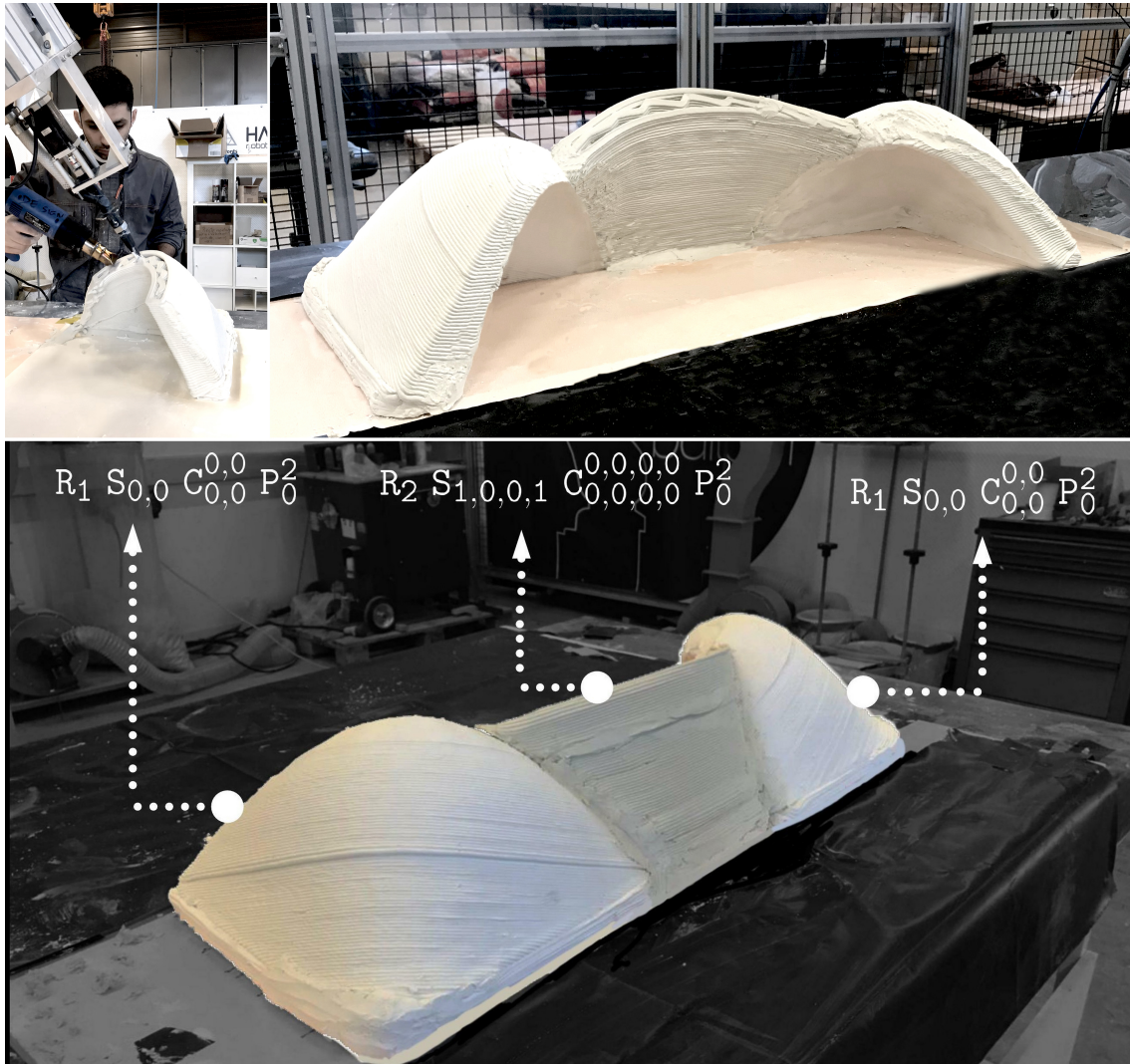


Figure 4.12 – Second Medium Prototype: A Multi-Vault with Two Squinches and One Pendentive

## 4.5 Large

Prototyping on a small scale showed how a robot could bend and print cantilevers differently from simple 2.5 D printing, where a CNC can move only on the x,y and z-axis. Prototyping on the medium scale with a kaolin clay mixture demonstrates the challenges one can face with material behaviour and how to tackle such problems using the lace-heating method. However, large-scale prototyping can fully represent the challenges of printing multi-vaults or any shells in the scale of a living unit, opt to be printed without scaffold using earth-based material. Furthermore, since the scale of the laboratory robotic arm is smaller than the scale of a habitat, therefore we consider the large-scale elements that we print as the components of a building rather than a full building. However, as it is mentioned in the medium-scale printing



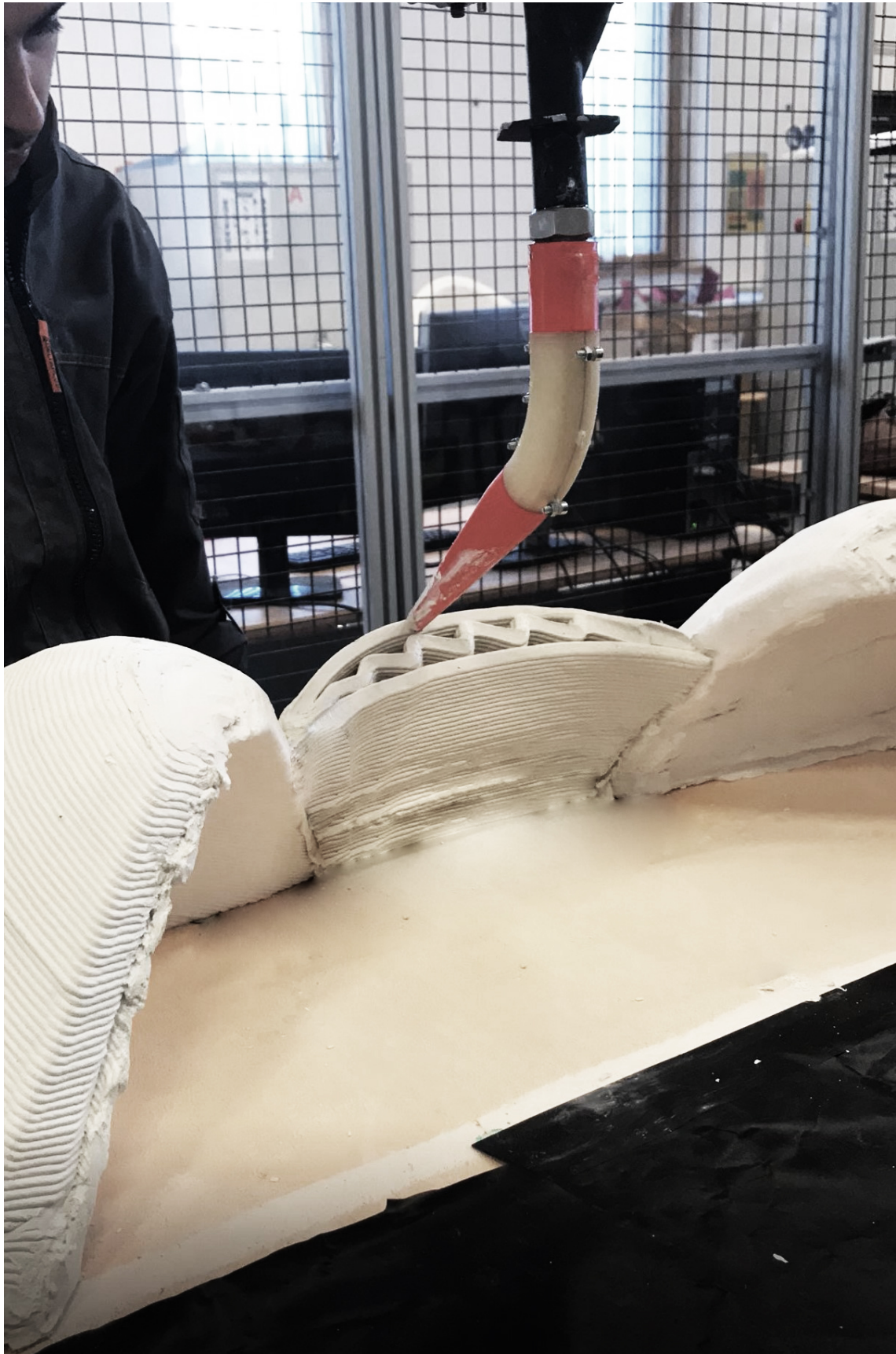


Figure 4.13 – 3D Printing of an Intermediate Patch (Pendentive) Between Self-Supporting Independent Patches (Squinches): Fabrication of a Custom-Made Nozzle to Minimize Robot Movement Constraints

section, the medium prototypes could also be considered as smaller components of a full-scale printed building. The large-scale prototyping needed a printing setup different from the one used for medium-scale printing. The medium-scale printing setup had a limited capacity for the material reservoir, making it unsuitable for large-scale fabrication where the continuous flow of the material is needed. Therefore, it was decided to prototype the large-scale model in another laboratory of the *Build'in* lab, which is also located at *ecole des Ponts et chausset*. This laboratory is equipped primarily for concrete 3D Printing setup. The mounted extrusion system on the ABB 6620 arm is fabricated by *XtreeE* company for the extrusion of high-performance cement mixture mainly. However, it was adapted to extrude the Kaolin clay mixture for the large-scale prototypes of this dissertation by connecting the material hose from the MAI pump directly to the extrusion head nozzle input pipe. Therefore the *XtreeE* extrusion head was only used to carry the material hose from the pump, as demonstrated in figure 4.15. Figure 4.14 shows the concrete printing lab environment where the large-scale prototype is 3D printed. The large-scale prototyping comprises the following units:

- (a) ABB IRB 6600, fixed on a cylindrical pedestal
- (b) *XtreeE* concrete extrusion head
- (c) MAI 4MultiMix 3D pump (440GE - Worm pump-MP4L)

The MAI 4Multimix 3D pump is a mortar mixing pump capable of continuously creating the material mixture and pumping the material to the extrusion head. This pump has a fairly high power capacity of 40 bar for pumping the material. Furthermore, the maximum allowed particle size of the mortar is 4 mm, and the maximum flow rate of this pump is  $25.5 \frac{L}{S}$ . This pump has a different set of extrusion rotors for different extrusion flow speeds. Using this pump and the standard rotor, it was possible to pump a kaolin clay mixture with 3.5 kPa resistance.

- (d) Heat gun (1800 W, 600°)

## Experience Using MAI 4MultiMix 3D Pump

Figure 4.16 illustrates the different parts of the Pump MAI. Our experience with the Pump MAI had both positive and negative aspects. On the positive side, the pump efficiently extruded mixtures with high power, even when the mixture was very solid, throughout the printing process. However, we faced challenges related to material consistency due to various factors, such as the weight of the material in the reservoir. To maintain the consistency of the mixture, we had to keep the Dry Powder mixing reservoir always full. Another issue we faced was the need for a large amount of material at the beginning of the printing process for calibration purposes, which was both costly and environmentally unfriendly. To solve this, we reserved the not calibrated material from the calibration process and stored it in unsealed plastic bags to evaporate the extra water from the mixture. We also hacked the pump by removing the hopper cover to feed the hopper with reused material from previously printed objects instead of feeding the dry powder-feeding reservoir with pristine material. This allowed us to reuse the material from the previous calibration process and add extra clay powder to the mixture to solidify it further and directly

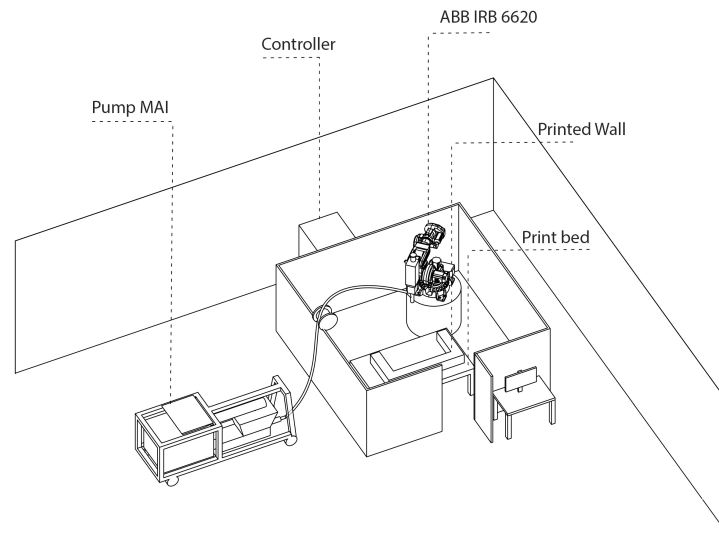


Figure 4.14 – The Large-Scale Prototyping Environment

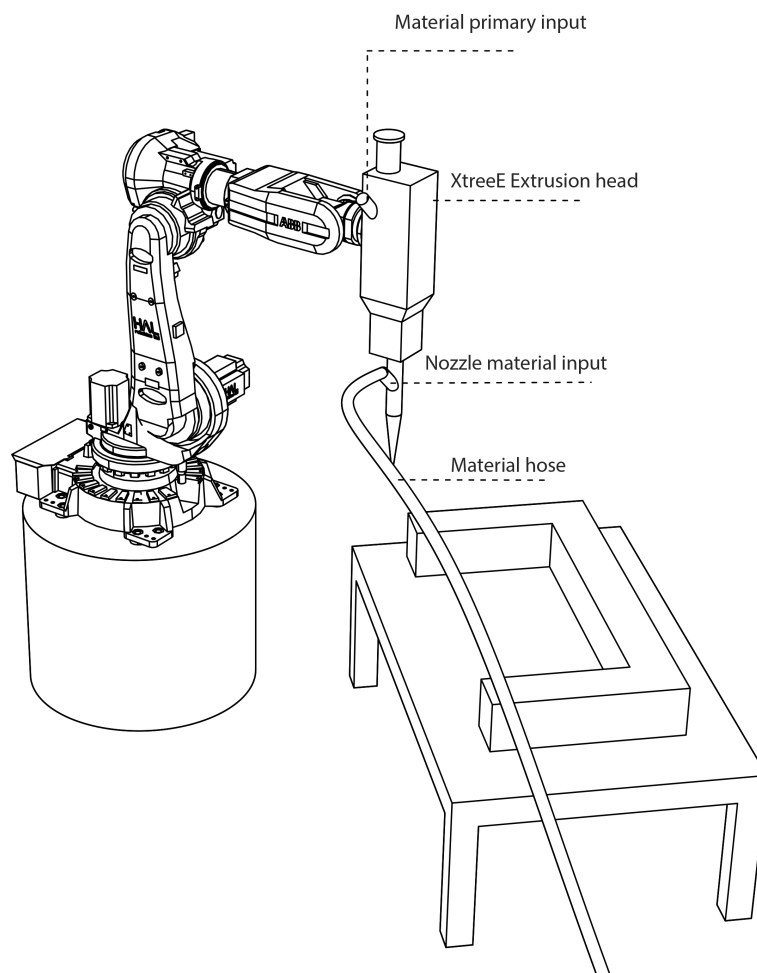


Figure 4.15 – The Material Extrusion System

extrude the material from the secondary pump reservoir. In this dissertation, we needed more solid material, so we replaced the default conveying screw with a larger

one. We also replaced the default rotator and stator with larger ones to control the Flow rate of the pump and have a higher Flow rate when extruding materials with a higher yield strength of 4 kPa. However, we sometimes used the small rotator and stator to reduce the printing speed for buildability reasons. Overall, the Pump MAI is a good option for extruding materials during 3D printing, but it does have some limitations and challenges that need to be considered for optimal use. It is also worth noting that reusing the material with the Pump MAI is not its intended use, and it requires some hacks and adjustments to do so.

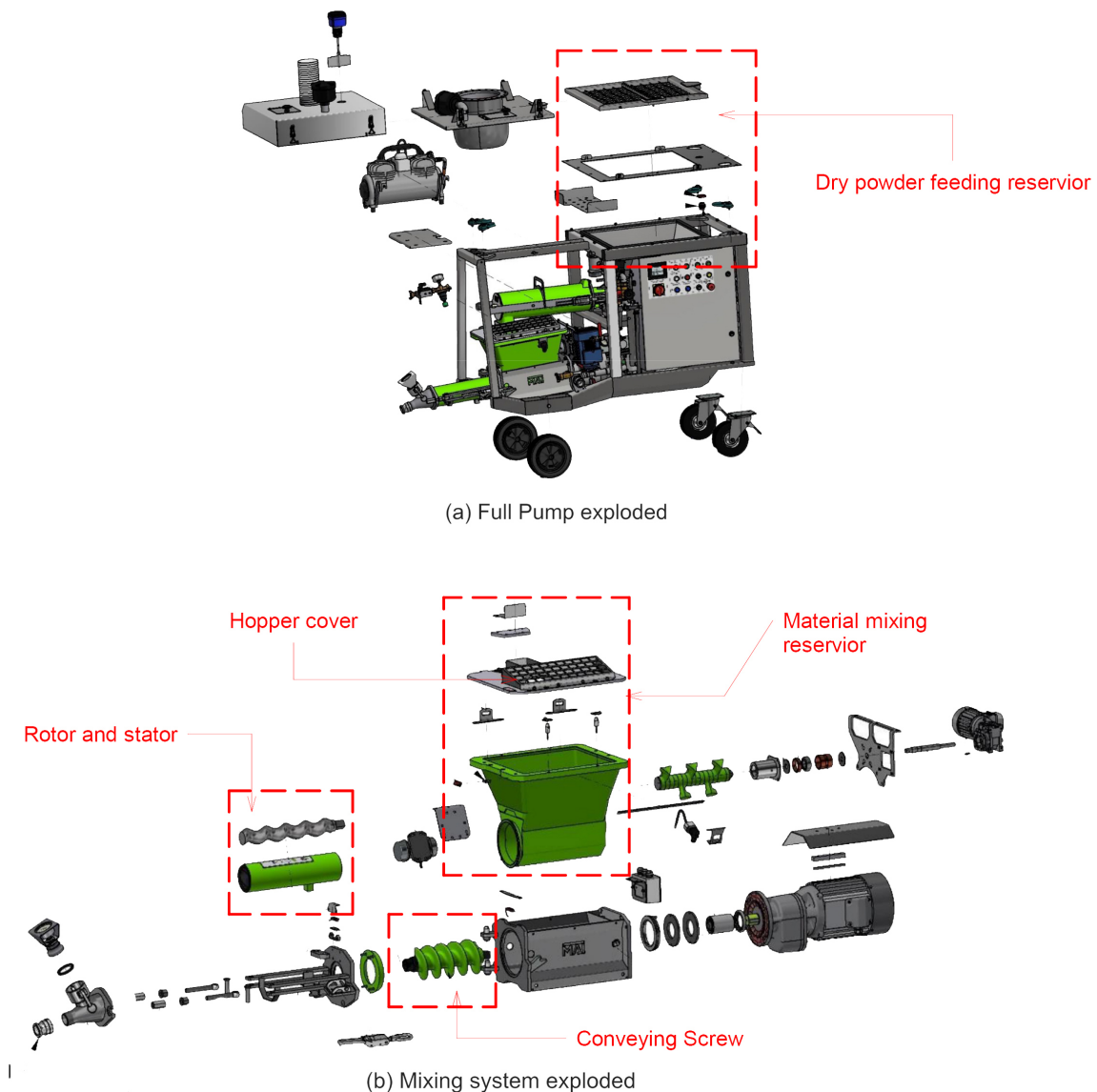


Figure 4.16 – Components of the MAI 4MultiMix 3D Pump: An Exploded View Diagram Highlighting Key Parts

#### 4.5.1 U Shape Wall ( $120 \times 90 \times 23h$ cm)

To overcome the challenges of scaling up printing prototypes using a Kaolin clay mixture, an attempt was made to create a U-shaped wall prototype. The video of the fabrication of this prototype is available at [103]. After adjusting the

print parameters, including the pump extrusion flow speed and the robot movement speed, a layer width of 12 mm was achieved. The digital model of the wall was 100 cm in height, but after printing 23 layers, each 1 cm in height, the structure deformed significantly. This was because the mixture used for this prototype had less strength than the one used for medium-scale printing, as we had limited experience in controlling the Pump MAI for mixing materials. In addition, the Lace Heating method was performed in this prototype. Still, the heating intensity was insufficient to consider the wall's scale and the water quantity of the material. The material water quantity was not the same as the material used in medium-scale prototypes because the material was automatically mixed using the Pump MAI, and we had not fully controlled the exact water addition. Moreover, our lack of experience using the Pump MAI caused the material formulation to be inconsistent during the printing process. However, we later gained more control over the consistency of the material and the formulation of the mixture by troubleshooting our Pump MAI problem. After the printing process was stopped, the printed wall was kept in the cell for several days to evaluate its deformation due to shrinkage. The structure had shrunk from different sides, and the wall was cracked at the sharp corners due to the shrinkage. In this prototype, only Kaolin powder was mixed with water. However, for later prototypes, plastic fibres were added to the mixture to reduce shrinkage deformation and increase the material's tensile strength. Figure 4.17 illustrates the printed wall before and after shrinkage. The FEA analysis of the model previously revealed that the structure would fail considering the initial material yield strength. The initial material young modulus was estimated to be the same as the material we used for the medium-scale prototyping ( $0.0055 \frac{KN}{CM^2}$ ). However, the goal for printing this wall was to evaluate the effect of the Lace-Heating method on the success of large-scale printing and see how far it was possible to print.

### 4.5.2 Squinch on a Wooden Wall

Figure 4.19 shows a wooden L-shaped wall as a representative of a printed wall positioned in front of a robotic arm to be covered by a squinch. The idea of this prototype was to present the possibility of covering the spans of a building using patches as the roof. Therefore, this prototype can be considered a component of the real-scale building. The dimensions of this wall from the plan view are  $100 \times 100 \times 141$ . The complete video of the fabrication process for this prototype is available in [104]. Furthermore, unlike the previously presented prototypes, plastic fibres were used in the mixture of this prototype with a proportion of 1% of the admixture. The study in [61] suggests that cellulose microfibrils increase both the tensile and compression capacity of the material, which seems also to be more environmentally friendly than plastic fibres. It is important to mention that this prototype was completed fully with reused material from earlier prototypes to emphasise the recyclability potential of earth-based materials in the 3D printing process, which is a great promise for sustainable construction. The Squinch prototype for the wooden wall was created in two attempts. Firstly, a squinch with a straight crest was developed, followed by a positive curvature crest. Figure 4.18 compares the two squinch geometries. Surprisingly, FEA analysis revealed that the straight squinch had greater stability than the squinch with a positive curvature crest, as determined by the buckling factor and the maximum internal



(a) U-Shape wall after printing process (wet)



(b) U-Shape wall after shrinkage (dry)

Figure 4.17 – Prototype of The U-Shape Wall

stresses resulting from self-weight. Therefore, the initial prototype of the squinch with a straight crest was 3D printed. However, it failed approximately three layers before completion. The print process of the squinch with a straight crest is shown in Figure 4.20, and the weak bond between two layers of the printed squinch can be seen in Figure (4.20- b). This geometry was attempted twice, but the structure failed for the same reason and location. The failure may have been due to partial structural buckling and shearing. The structure sheared from a certain part, as shown in Figure (4.20- e), which is assumed to be due to a weak bond between the sheared part and the rest of the squinch. This caused the structure to deform from that part, leading to the rest of the squinch buckling, as seen in Figures 4.20-c).

Therefore, It was decided to alter the geometry, and a squinch with a positive

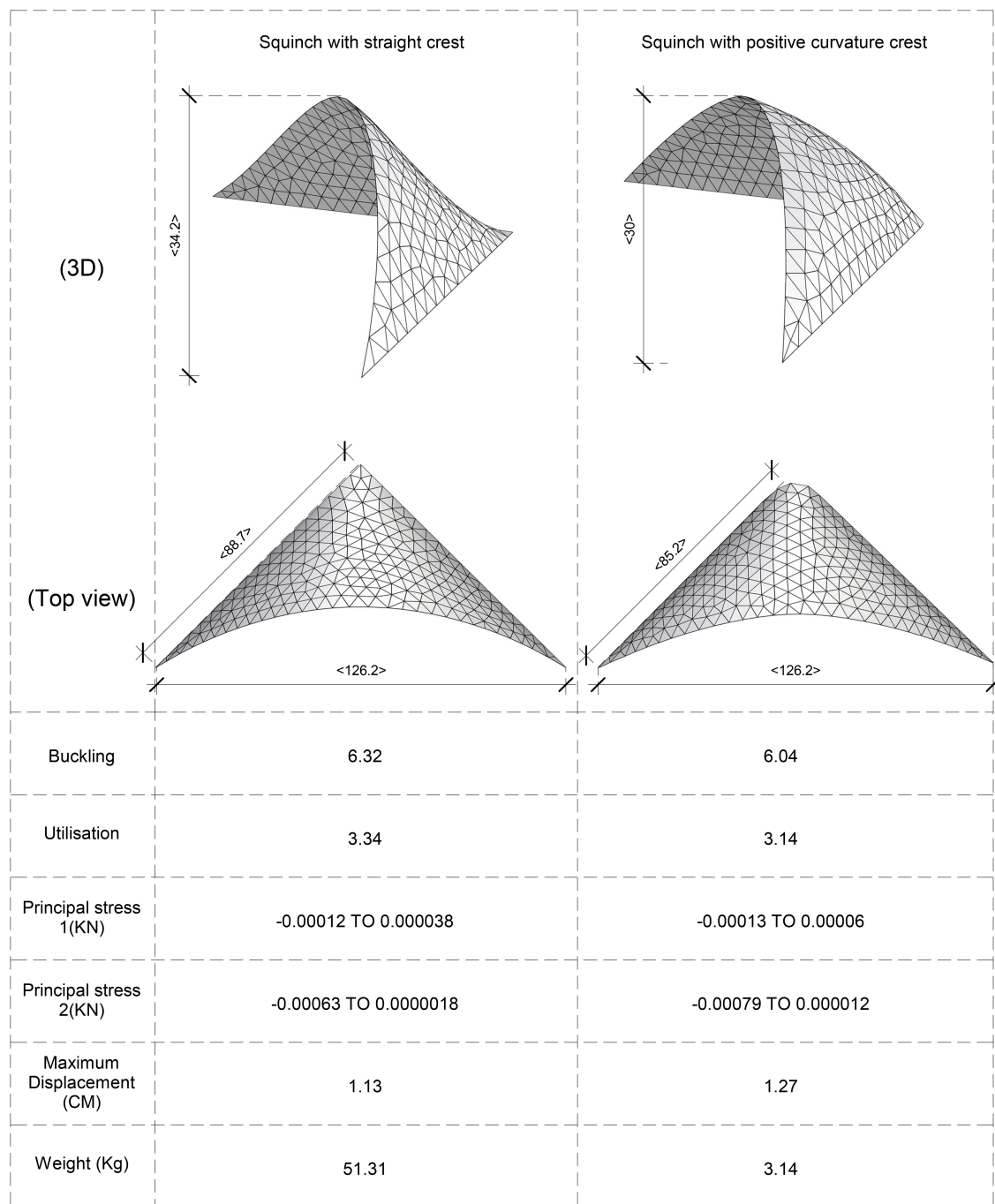


Figure 4.18 – Comparison of Two Squinch Geometries

curvature crest was printed. Figure 4.21 shows the print process of this prototype. This prototype also encountered the same problem as the squinch with the straight crest. After printing a certain number of layers (Figure 4.21-a), the structure started to detach from the part with a weak bonding between two layers. This may have been caused by overheating that layer due to printing interruptions. Therefore, the decision was made to print the second prototype in two parts. The first part was printed until cracks where weak bonding between the layers was observed (figure 4.21-b), and the structure was left to dry for two weeks. Furthermore, it was decided to manually fill the gap between the two layers using the same mortar where the detachment appeared 4.21-c). After the drying process, the tool path

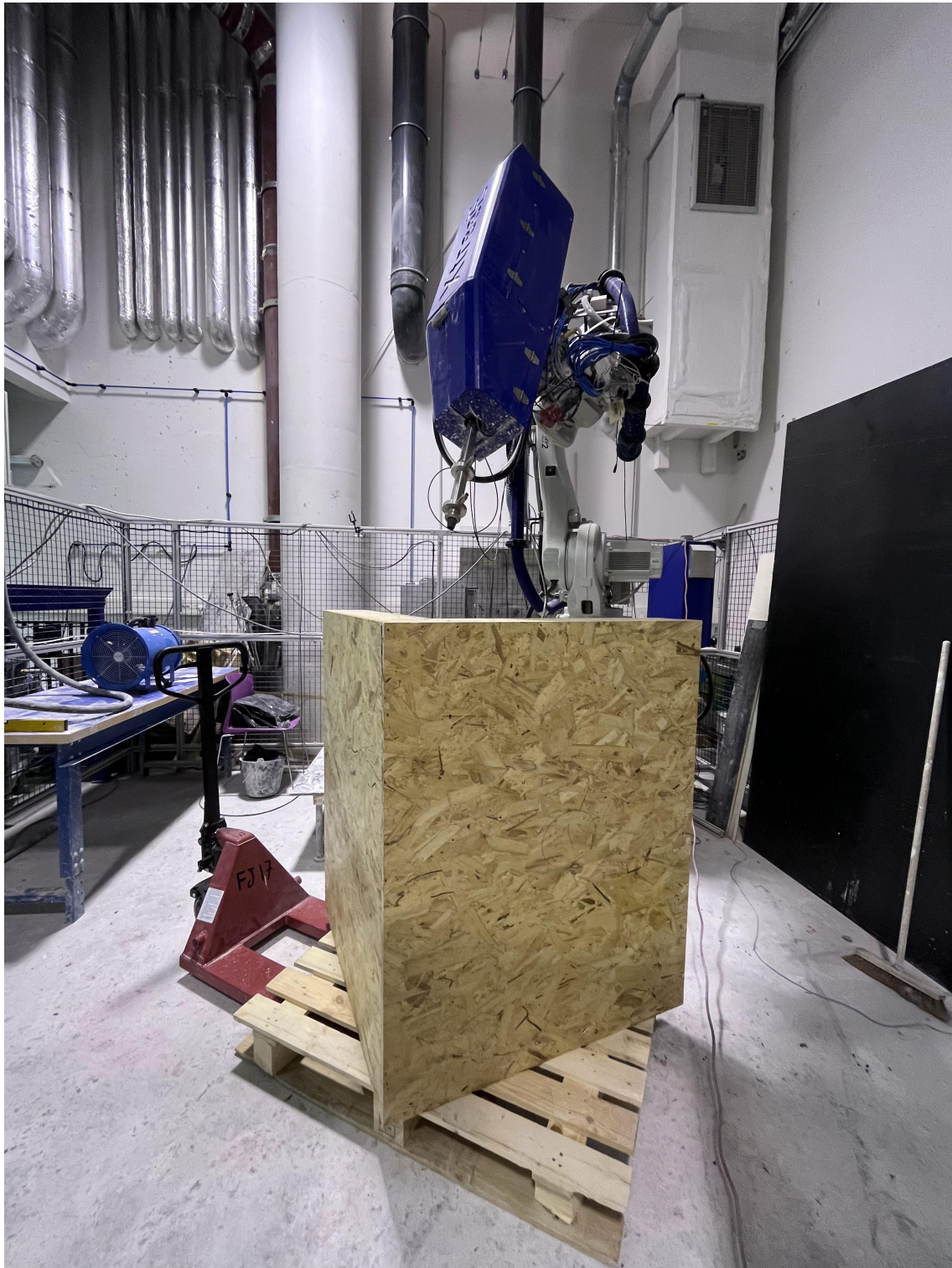


Figure 4.19 – Wooden Wall as Support for Squinch Prototype

was re-calibrated to accommodate the deformed object due to shrinkage. To do this, pins were implanted in the corners of the squinch just after the termination of the printing process of the first part, and the position of those points in space was recorded using the printing head. After two weeks, the position of the points was recorded again to evaluate the shrinkage deformation. A tool path was then created for the second part, adapted to the deformed object, and printing was attempted.





Figure 4.20 – Print Process of the Squinch with Straight Crest

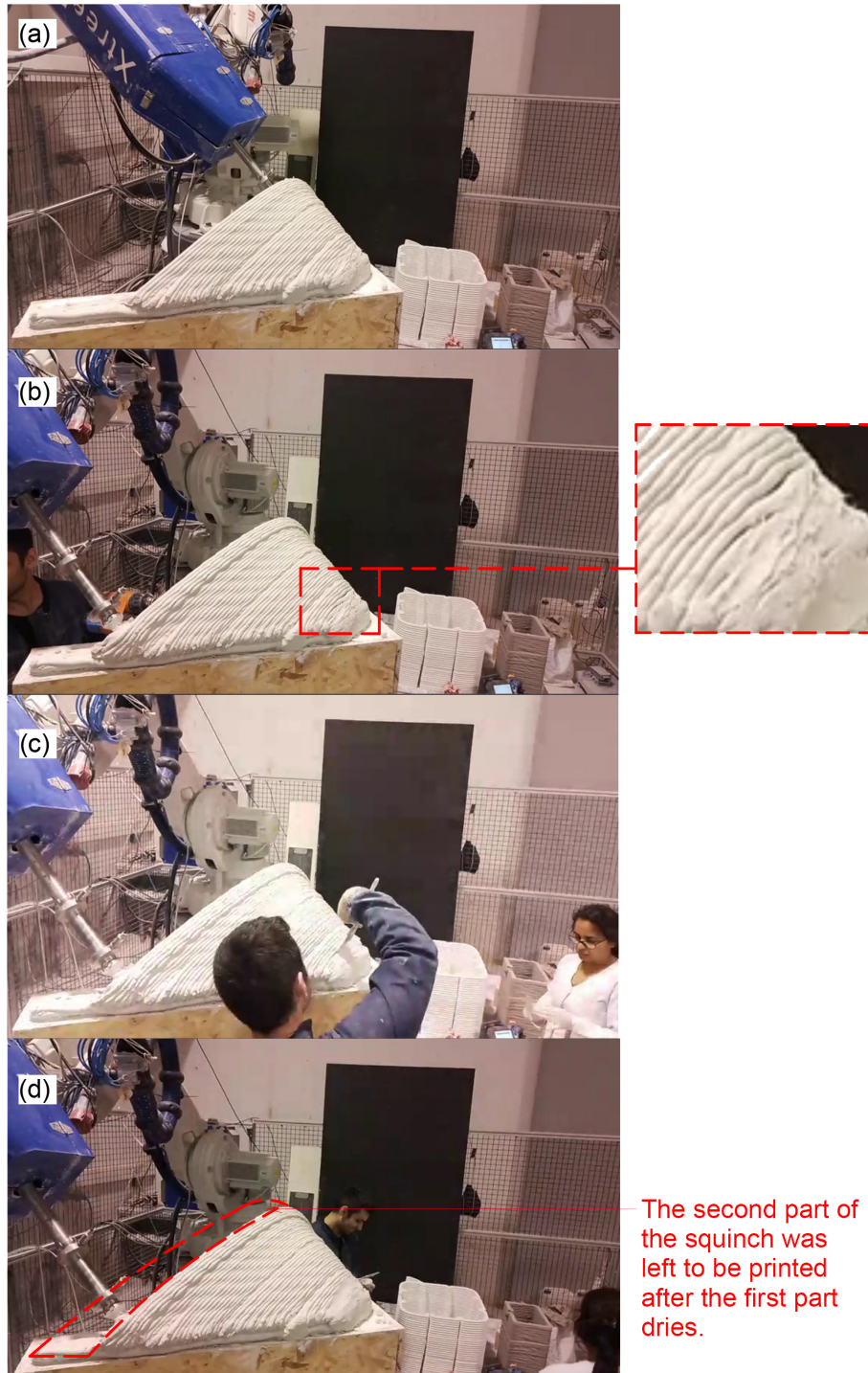


Figure 4.21 – Print Process of the Squinch with Positive Curvature Crest

Figure 4.22 shows this prototype's 3D printing steps and shrinkage deformation. Figure 4.22 (a) shows the first 3D printed part of the squinch up to the point where a detachment occurred between two layers of the printed model, causing the print to be stopped until the model could dry. Figure 4.22 (b) shows the projection of the first layer of the second part of the squinch onto the last layer of the first printed part (before shrinkage) to represent the amount of shrinkage deformation. It is observed that the model shrunk by 17 mm in height after it became dry. Figure 4.22 (c) displays the first 3D printed part after shrinkage alongside the second printed part before shrinkage. Finally, in Figure 4.22 (d), the first 3D printed part after shrinkage is shown alongside the second printed part after shrinkage. Here it is observed that the model shrunk 47 mm from the height, much higher than the shrinkage of the first 3D printed part. This might be due to the material formulation inconsistency we had during the printing session for the second part.

Two strategies were implemented to prevent the occurrence of a cold joint between the dry and fresh sections. Initially, the final layer of the dry object was moistened by applying water with a sponge. Additionally, screws were inserted into the final layer to secure the second part once it had dried, as depicted in figure 4.23. However, after two days of printing the second part, the screws proved ineffective in maintaining its position, leading to deformation. Moreover, the saturation of the final layer did not yield the desired results as the dry object absorbed all the water, remaining dry. The successful bonding of two layers relies on the ability of both layers to exchange water, which is achieved when they possess similar water content. Unfortunately, this exchange was not feasible between the dry-printed object and the freshly printed part at their intersection layer, even with saturating the intersecting layer using a soaked sponge.

### 4.5.3 Interlocking Module

This prototype was created as part of the 3D Printing course for Digital Building Design, for which the author of this dissertation served as a supervisor and teaching assistant. The course was taught by Nicolas Ducoulombier, and the geometry of this model was designed by "Stive Kousseifi", a student of the "Digital Building Design" program at Ecole des Ponts et Chaussées. The purpose of this model was to serve as a module in a larger system constructed by interconnecting modules. The aim of presenting this prototype is to demonstrate the effect of the layer heating method in the 3D printing process for earth-based materials. The model was printed twice: first with a layer heating method using one heat gun 1800w, and then with a layer heating method using two heat guns - one 1500 W and the other 1800 W. The first print attempt failed before completion (25th layer) due to plastic failure, highlighting the low yield strength of the material and the insufficient speed of yield strength growth. The video of the plastic collapse can be found in [37]. Without altering the geometry, the model was printed using the layer heating method with two heat guns. The video of the second print attempt with two heat guns can be found in [38], and this time, the print was successful. Figure 4.24 shows the collapsed model of the first attempt and the successfully printed model for the second attempt (30 layers).

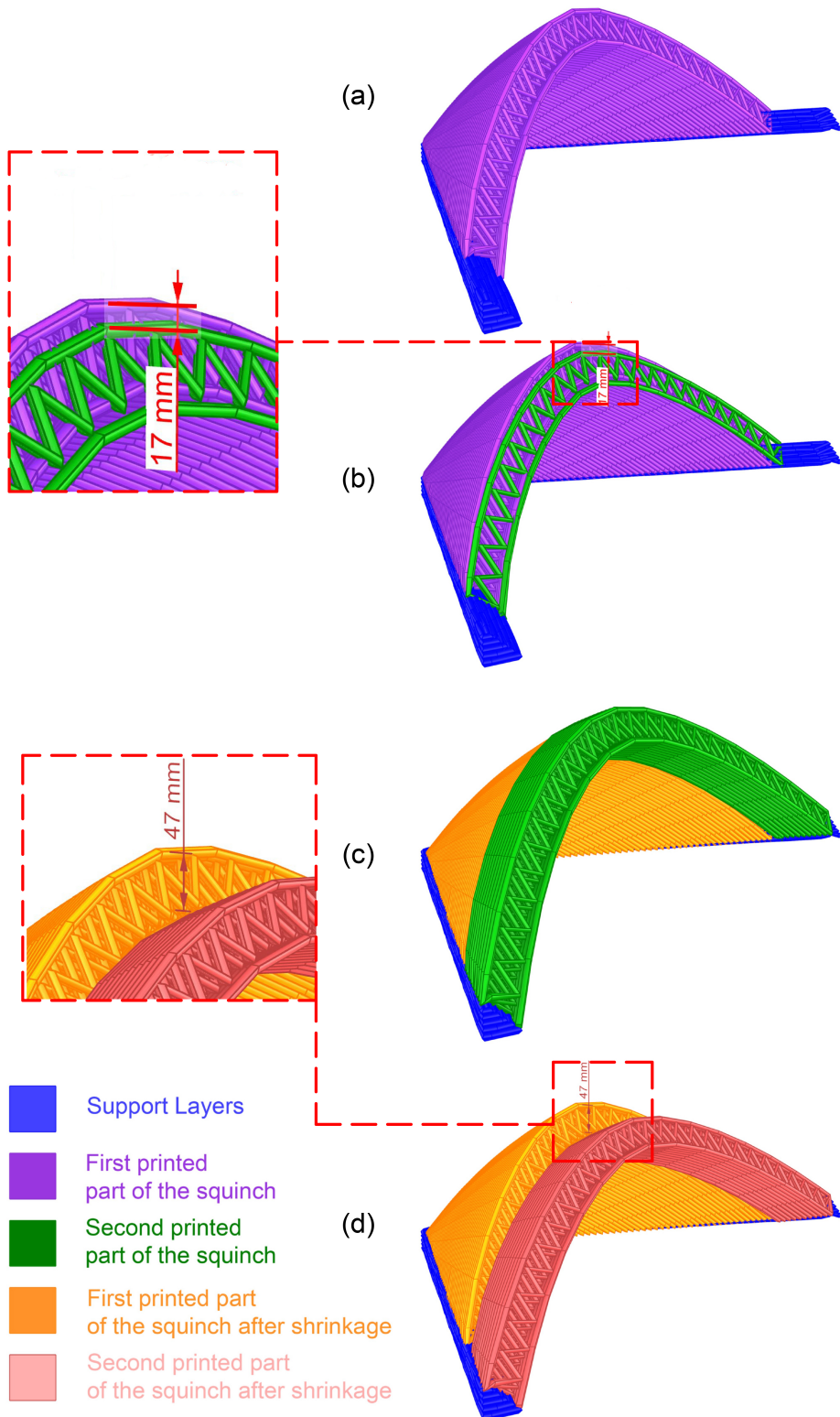


Figure 4.22 – 3D Representation of the Printing Process for the Squinch with Positive Curvature Crest



Figure 4.23 – Process of Planting Screws to Prevent The Layers Detachment

#### 4.5.4 How to Bind Fresh Clay to an Air-Dried Clay?

During the 3D Printing process of two prototypes of 1-Multi-vault with three Patches 2- Squinch on the wooden wall, it was observed that due to the shrinkage and the occurrence of the cold joints, the clay pieces could not bind together, which led to the structure collapse after the structure dries. To address this problem, more studies must be done on solving the problem of binding two clay pieces when they don't have the same humidity level. Practitioners in the field of pottery and ceramics use the following techniques to stick objects with different humidity levels together:

1. One approach is to use specialised types of glue such as PVA Glue, Epoxy Resin, or Gorilla Glue. However, it has been found that PVA glue does not work well with polymer clay [146].
2. Another method is to bind the layers together when they have similar humidity levels. To achieve this, the timing of printing the patches and the environmental conditions should be controlled to ensure that the interconnected patches connect with similar humidity levels. However, the maximum allowable difference in the quantity of water between the patches must be tested.
3. A third technique involves wrapping a wet newspaper around the dry clay to absorb moisture and make it wet. However, for the prototype of the squinch on the wooden wall in this dissertation, a wet sponge was used instead, and even after applying 2 litres of water, the dry clay did not become saturated. Therefore, it seems that using a wet newspaper can gradually and effectively

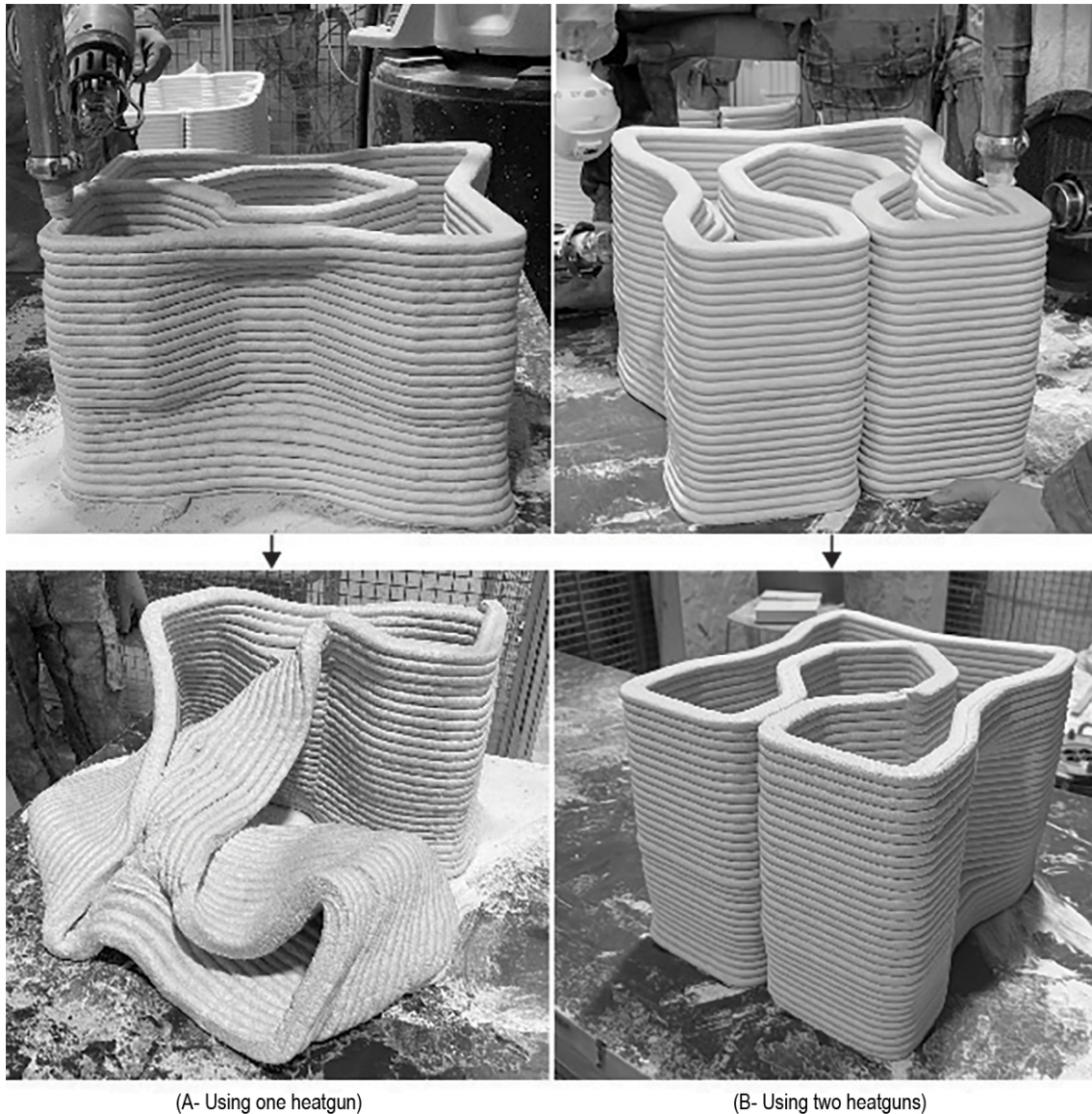


Figure 4.24 – 3D Printing an Interlocking Module with Heat Assistance: A Comparative View Using One vs. Two Heat Guns for Enhanced Structural Build-Up

insert the water inside the thickness of the dry clay.

4. Designing the interlocking patches. In this technique, the patches border are designed to be interlocked together. However, this technique can hold the Patches together, but it does not guarantee the layer fusion binding between the border of the Patches.

Moreover, when printing patches using concrete, it is important to integrate starter rebars to ensure the interconnected patches can establish a robust connection with the preceding ones.

#### 4.5.5 Conclusion

In this chapter, the technical aspects of the SF3DP process were explored by creating seven prototypes of different sizes, including small, medium, and large

scales. The advantages and challenges of printing at each scale were examined, focusing on the setup required for each.

Using a small-scale robotic arm (ABB IRB 1200) and a wooden strand material, the team was able to successfully print cantilevers in an inclined manner, which was a breakthrough in demonstrating that 3D printing of cantilevers at the living unit scale is possible if certain issues such as robot scalability, material constraints, and structural mechanics are addressed properly.

Printing with the wooden strand material allowed for eliminating constraints such as low green strength and plastic failure, which enabled the team to create more ambitious prototypes in terms of geometry while being less ambitious in terms of scale. However, issues such as cold joints and robot joint position and orientation constraints were identified when creating a multi-vault with a square boundary using the small-scale setup.

Medium-scale prototypes of a double-layer squinch and a multi-vault with three patches were created using a more realistic material for construction, a Kaolin clay mixture ( $\frac{Water}{Clay} = 0.58$ ). The prototypes were made with an ABB IRB 6620 installed on a track (7-axis) and equipped with a clay extrusion setup with a pneumatic jack. While the setup had high accuracy and consistency in extruding the material, the limited size of the reservoir significantly constrained the fabrication speed and prototyping scale.

The effect of geometry and cross-section optimisation on the success of SF3DP was demonstrated in the prototype of a double-layer clay shell. At the same time, the multi-vault with three patches was the first attempt to print a multi-vault with real material (Kaolin clay). The issue of cold joints between the patches was identified in this prototype for the first time.

In large-scale prototyping, the team transitioned from a reservoir-based extrusion system to a direct pumping system, using the MAI 4MultiMix 3D pump connected to the XtreeE concrete extrusion head mounted on the ABB IRB 6600 installed on a pedestal (6-axis). However, the material was directly pumped to the extrusion nozzle and did not pass through the XtreeE extrusion system. To promote the recyclability of the earth-based material for the SF3DP workflow, the MAI 4MultiMix 3D pump was hacked to reuse material from earlier prototypes, which helped to save on material cost and waste.

The experience using the MAI 4MultiMix 3D pump demonstrated that while print speed can increase significantly due to the direct continuous pumping, the consistency of the material formulation (water quantity) was not as accurate as the reservoir-based extrusion system used in medium printing. The prototypes of the U-shape wall, Squinch on the wooden wall, and an interlocking module highlighted the importance of optimising heat and wind flow based on the prototype scale in the layer heating technique to prevent structure collapse during the printing process. Furthermore, the addition of the plastic short fibres to the Kaolin mixture with a proportion of 1% proved the effectiveness of this technique on shrinkage deformation and cracking decrease. In general, in the 3D printing process of the patches using earth-based material on medium and large scales, the following aspects are identified to be crucial for the successful result:

In general, in the 3D printing process using earth-based materials on a medium and large scale, the following aspects are identified to be crucial for achieving successful results:

- 1 Patch's boundary condition.
- 2 Geometry of the first 3D printed layers (support layers) as demonstrated in Figure 4.22 (blue part).
- 3 Slicing method (angle, distance, direction).
- 4 Robot head orientation angle compared to the geometry of the printing object at each layer of printing. Aligning the robot head tangent to the surface of the printing object is always the best solution, especially when printing cantilevers. However, this is not always possible due to the robotic joint constraints.
- 5 Geometry of the printing object.
- 6 Parameters of the layer heating method (heat temperature and wind speed).
- 7 Material properties (yield strength, green strength, and stiffness).
- 8 Printing regime (Refer to Table 1.4).
- 9 Printing parameters include the vertical speed  $V_z$ , nozzle diameter, nozzle distance from the printing base or previously printed layer and extrusion flow rate.

Finally, the chapter addresses potential techniques for solving the cold-joint and shrinkage detachment issues and emphasises that future work on SF3DP should focus on this topic.



# Chapter 5

## Conclusion

In this research, we explored the potential of ancient vaulting techniques as a valuable resource for sustainable development in modern construction, particularly in combination with the advancements in 3D printing technology. By investigating the adaptation of scaffold-free vaulting techniques to 3D printing and the use of earth-based materials, our objective was to establish a design method that enables the creation of highly sustainable, efficient, and affordable structures for various types of buildings.

### 5.1 Key Findings

The key findings of this research are as follows:

1. Scaffold-Free 3D Printing Method: The introduction of a scaffold-free 3D printing (SF3DP) approach for vaults with convex quad boundaries is a significant finding. This method allows for the 3D printing of vaults without needing temporary support or scaffolding, which can reduce costs and simplify the construction process.
2. Patching Design Grammar: The development of the Patching design grammar, inspired by ancient vaulting techniques, offers a flexible and formalised rule-based design grammar. It enables users to design SF3DP vaults with various boundary configurations beyond circular boundaries. This finding expands the design possibilities for 3D printed structures and allows for creation of dome-like structures with different shapes.
3. Practical Application Potential: The potential practical applications of the Patching 3D printing method are crucial findings. This method can design shell-like structures for habitats, commercial buildings, or public constructions. Additionally, it can be used to print roofs for conventionally 3D-printed buildings, leading to reduced material and labour costs and increased automation in the construction industry.
4. Layer Heating Method for Yield Strength Enhancement: This research introduced the layer heating method as a passive approach to enhance the yield strength of earth-based materials in the 3D printing process. This finding is significant because it offers a practical and effective way to improve the mechanical properties of printed structures using earth-based materials, thereby increasing their strength and durability.

5. **Impact of Printing Geometry on Yield Strength Evolution:** This research explored how the geometry of the printing object can influence the green-strength evolution of earth-based materials in the 3D printing process under heat and wind conditions. This finding provides valuable insights into the relationship between the design of printed structures and the effectiveness of the layer heating method, enabling practitioners to optimise their printing processes for better results.
6. **Experimental Evaluation of Material Properties:** This research presented several material experiments, including wind tunnel, slug test, squeeze test, and vane test, to evaluate the water evaporation rate, pure tensile strength, compressive strength, and shear strength of the printing mortar, respectively. These experimental findings contribute to a better understanding of the mechanical behaviour of saturated porous media in the 3D printing process, helping researchers and practitioners make informed decisions about material manipulation and geometry design.
7. **Challenges of Printing on Different Scales:** This research presented the challenges, constraints, and potentials of printing scale prototypes using different printing setups categorised by their scale to small, medium, and large. Practitioners can extract the experience of printing cantilever structures using the described printing setups and build their knowledge on them.
8. **Identifying Key Contributing Aspects in Successful 3D Printing:** Research identifies key factors that play a role in successful 3D printing using the SF3DP method for earthen shells. These aspects include the boundary conditions of the patch (support condition), the geometry of the initial supporting layers, the slicing method, the printing orientation angle, the geometry of the printing object, parameters of the layer heating method, properties of printing mortar, printing regime, and 3D printing parameters.

## 5.2 Limitations and Future Work

While this research developed and presented a novel design method and 3D printing technique for fabricating earthen structures without any temporary support, several limitations should be addressed in future studies. These limitations include:

1. **Enrichment of the Patching Design Grammar:** The proposed design grammar can be further enriched with new rules and embedded in a user-friendly interface, such as BIM-based architectural software or as a plugin in CAD software like Rhinoceros and Grasshopper. This enhancement will facilitate the design process for users and expand the possibilities for designing complex structures.
2. **Advancing FEA Methods:** Although the proposed FEA method based on the Rankine failure theory is efficient, developing a step-wise FEA method based on the Mohr-Coulomb criterion can extend the exploration of geometries, especially after the elastic region of the material. Solid-based FEA software like ANSYS Abaqus can account for the topology of the shell's cross-sections, leading to more precise evaluations of the structures' behaviour during the 3D printing process. such as the study in [48] on the effect of the infill pattern on

the tensile strength of the 3D printed specimen using experimental data and ANSYS analysis data.

3. Utilising Mobile Robots and Drones: Investigating the use of setups such as mobile robots and drones for 3D printing multi-vaults can leverage the full potential of SF3DP through the patching method and design grammar. These setups can offer greater flexibility and versatility in printing large and complex structures.
4. Addressing the problem of cold joints: The problem of cold joints between the Patches must be addressed either by using special additives to the material mixture by optimising the printing speed and the interval between printing interconnected Patches or by using particular dry joints between the Patches or designing the geometry of the Patches in a way that they can be interlocked.
5. Exploring Modularity for Circular Construction: Given the challenges posed by the formation of cold joints between patches, we can aim to transform these 3D-printed multi-vault structures into modular units by the use of specific joints. This not only enhances off-site transportability but also promotes a circular economy by turning a potential limitation into a strength.
6. Investigating the sequence of construction for patches and its impact on stability: In the examples of designing multi-vaults described in Chapter 2, the sequences of the Patches were ordered in a way the initial Patched become support for the upper Patched. However, following the same principle, different orders of sequences can be defined. This order can eventually impact the structural stability of the multi-vaults during the printing process. The leverage of a sequential form-finding approach that accounts for the sequence of the Patched print order is necessary to guarantee a successful 3D Printing process. The theoretical approaches to study the impact of the sequence of the Patching printing order on the stability of the multi-vaults can be as follows:
  - **Computational Modelling:** Use Finite Element Analysis (FEA) or other computational methods to simulate the construction sequence and evaluate its impact on structural stability.
  - **Algorithmic Form Finding:** Develop algorithms that can optimise the sequence of patch assembly to meet specific stability criteria. This could involve genetic algorithms, machine learning, or other optimisation techniques.
  - **Analytical Models:** Develop mathematical models that can predict the behaviour of the structure based on the sequence of patch assembly. This could involve equations that account for material properties, joint behaviour, and other relevant factors.
7. Adaptability to Various Construction Materials: While the research primarily focuses on the Patching design grammar for earthen structures, the technique is adaptable to other materials like concrete and geopolymers, each with its own set of considerations. Adapting the Patching method to different materials can broaden its applicability, especially in environments where earth is not the most suitable construction material or in structures that require materials other than earth.

8. Study of Heat Transfer Effects: Extending the study of the effect of heat on the structural build-up of 3D printed earthen shells to include heat transfer through radiation and conduction can provide valuable insights into efficient methods for increasing the green strength of earth-based mortars in the 3D printing process.

This research has successfully demonstrated the promising potential of scaffold-free 3D printing techniques inspired by ancient vaulting methods and the use of earth-based materials. The findings presented here can significantly impact the future of sustainable construction in the AEC industry, enabling the creation of cost-effective, resource-efficient, and aesthetically unique structures. By addressing the identified limitations and following future research directions, implementing these techniques can be further refined and lead to substantial advancements in the construction field.

# Bibliography

- [1] *3.7.7: Utilization of Elements*. en. URL: <https://manual.karamba3d.com/3-in-depth-component-reference/3.6-results/3.6.6-utilization-of-elements#utilization-of-shells> (visited on 08/06/2023).
- [2] Sigrid Adriaenssens et al. *Shell Structures for Architecture: Form Finding and Optimization*. en. Routledge, Mar. 2014. ISBN: 978-1-317-90938-5.
- [3] Javier Alonso Madrid et al. « 3D Claying: 3D Printing and Recycling Clay ». en. In: *Crystals* 13.3 (Mar. 2023). Number: 3 Publisher: Multidisciplinary Digital Publishing Institute, p. 375. ISSN: 2073-4352. DOI: 10.3390/cryst13030375. URL: <https://www.mdpi.com/2073-4352/13/3/375> (visited on 03/10/2023).
- [4] Julien Archez et al. « Strategy to shape, on a half-meter scale, a geopolymer composite structure by additive manufacturing ». In: *Open Ceramics* 5 (2021). Publisher: Elsevier, p. 100071. DOI: 10.1016/j.oceram.2021.100071. URL: <https://hal.archives-ouvertes.fr/hal-03146651> (visited on 10/09/2022).
- [5] Negar Ashrafi et al. « A grammar-based algorithm for toolpath generation: Compensating for material deformation in the additive manufacturing of concrete ». en. In: *Additive Manufacturing* 55 (July 2022), p. 102803. ISSN: 2214-8604. DOI: 10.1016/j.addma.2022.102803. URL: <https://www.sciencedirect.com/science/article/pii/S2214860422002044> (visited on 03/02/2023).
- [6] Carlos Balaguer and Mohamed Abderrahim. *Robotics and Automation in Construction*. en. Google-Books-ID: ogehDwAAQBAJ. BoD – Books on Demand, Oct. 2008. ISBN: 978-953-7619-13-8.
- [7] Eric Barnett and Clément Gosselin. « Large-scale 3D printing with a cable-suspended robot ». en. In: *Additive Manufacturing* 7 (July 2015), pp. 27–44. ISSN: 2214-8604. DOI: 10.1016/j.addma.2015.05.001. URL: <https://www.sciencedirect.com/science/article/pii/S2214860415000263> (visited on 07/30/2022).
- [8] K. Been and G. C. Sills. « Self-weight consolidation of soft soils: an experimental and theoretical study ». en. In: *Géotechnique* (May 2015). Publisher: Thomas Telford Ltd. DOI: 10.1680/geot.1981.31.4.519. URL: <https://www.icevirtuallibrary.com/doi/10.1680/geot.1981.31.4.519> (visited on 05/07/2023).

- [9] Lola Ben-Alon and Alexandra R. Rempel. « Thermal comfort and passive survivability in earthen buildings ». en. In: *Building and Environment* 238 (June 2023), p. 110339. ISSN: 0360-1323. DOI: 10.1016/j.buildenv.2023.110339. URL: <https://www.sciencedirect.com/science/article/pii/S0360132323003669> (visited on 06/10/2023).
- [10] Philippe Block and John Ochsendorf. « THRUST NETWORK ANALYSIS: A NEW METHODOLOGY FOR THREE-DIMENSIONAL EQUILIBRIUM ». en. In: *JOURNAL OF THE INTERNATIONAL ASSOCIATION FOR SHELL AND SPATIAL STRUCTURES* 48.3 (2007), p. 9.
- [11] *Block Research Group*. URL: <https://block.arch.ethz.ch/brg/project/striatus-3d-concrete-printed-masonry-bridge-venice-italy-2021> (visited on 08/01/2022).
- [12] Thomas Bock. « The future of construction automation: Technological disruption and the upcoming ubiquity of robotics ». en. In: *Automation in Construction* 59 (Nov. 2015), pp. 113–121. ISSN: 0926-5805. DOI: 10.1016/j.autcon.2015.07.022. URL: <https://www.sciencedirect.com/science/article/pii/S092658051500165X> (visited on 07/26/2022).
- [13] Freek P. Bos et al., eds. *Second RILEM International Conference on Concrete and Digital Fabrication: Digital Concrete 2020*. en. Vol. 28. RILEM Bookseries. Cham: Springer International Publishing, 2020. ISBN: 978-3-030-49915-0 978-3-030-49916-7. DOI: 10.1007/978-3-030-49916-7. URL: <http://link.springer.com/10.1007/978-3-030-49916-7> (visited on 03/10/2023).
- [14] B. a. G. Bossink and H. J. H. Brouwers. « Construction Waste: Quantification and Source Evaluation ». EN. In: *Journal of Construction Engineering and Management* 122.1 (Mar. 1996). Publisher: American Society of Civil Engineers, pp. 55–60. ISSN: 0733-9364. DOI: 10.1061/(ASCE)0733-9364(1996)122:1(55). URL: <https://ascelibrary.org/doi/10.1061/%28ASCE%290733-9364%281996%29122%3A1%2855%29> (visited on 02/26/2023).
- [15] Jane Burry et al. « Dynamical Structural Modeling: A Collaborative Design Exploration ». en. In: *International Journal of Architectural Computing* 3.1 (Jan. 2005), pp. 27–42. ISSN: 1478-0771, 2048-3988. DOI: 10.1260/1478077053739595. URL: <http://journals.sagepub.com/doi/10.1260/1478077053739595> (visited on 03/27/2021).
- [16] Paul Carneau et al. « Additive manufacturing of cantilever - From masonry to concrete 3D printing ». en. In: *Automation in Construction* 116 (Aug. 2020), p. 103184. ISSN: 0926-5805. DOI: 10.1016/j.autcon.2020.103184. URL: <http://www.sciencedirect.com/science/article/pii/S0926580519308568> (visited on 01/11/2021).
- [17] Paul Carneau et al. « Characterisation of the Layer Pressing Strategy for Concrete 3D Printing ». en. In: *Second RILEM International Conference on Concrete and Digital Fabrication*. Ed. by Freek P. Bos et al. RILEM Bookseries. Cham: Springer International Publishing, 2020, pp. 185–195. ISBN: 978-3-030-49916-7. DOI: 10.1007/978-3-030-49916-7\_19.

- [18] Paul Carneau et al. « Layer pressing in concrete extrusion-based 3D-printing: Experiments and analysis ». en. In: *Cement and Concrete Research* 155 (May 2022), p. 106741. ISSN: 00088846. DOI: 10.1016/j.cemconres.2022.106741. URL: <https://linkinghub.elsevier.com/retrieve/pii/S0008884622000321> (visited on 07/17/2022).
- [19] Jean-François Caron et al. « 3D printing of mortar with continuous fibres: Principle, properties and potential for application ». en. In: *Automation in Construction* 129 (Sept. 2021), p. 103806. ISSN: 09265805. DOI: 10.1016/j.autcon.2021.103806. URL: <https://linkinghub.elsevier.com/retrieve/pii/S0926580521002570> (visited on 05/05/2023).
- [20] Shareen S.L. Chan et al. « 3D printing of clay for decorative architectural applications: Effect of solids volume fraction on rheology and printability ». en. In: *Additive Manufacturing* 35 (Oct. 2020), p. 101335. ISSN: 22148604. DOI: 10.1016/j.addma.2020.101335. URL: <https://linkinghub.elsevier.com/retrieve/pii/S2214860420307077> (visited on 12/11/2021).
- [21] John Chilton and Heinz Isler. *Heinz Isler: the engineer's contribution to contemporary architecture*. en. Google-Books-ID: pKhbsrIc8IkC. Thomas Telford, 2000. ISBN: 978-0-7277-2878-4.
- [22] Alberto Chiusoli. *3D printed house TECLA - Eco-housing - 3D Printers / WASP*. URL: <https://www.3dwasp.com/en/3d-printed-house-tecla/> (visited on 07/30/2022).
- [23] Myoungsung Choi et al. « Lubrication layer properties during concrete pumping ». en. In: *Cement and Concrete Research* 45 (Mar. 2013), pp. 69–78. ISSN: 0008-8846. DOI: 10.1016/j.cemconres.2012.11.001. URL: <https://www.sciencedirect.com/science/article/pii/S0008884612002566> (visited on 10/09/2022).
- [24] *Clay & Glass Gallery showcases 3D printed façades by University of Waterloo students*. en-US. Section: News. May 2019. URL: <https://www.canadianarchitect.com/clay-glass-gallery-showcases-3d-printed-facades-by-university-of-waterloo-students/> (visited on 08/01/2022).
- [25] Concre3DLab Ghent. *CobraPrint - a Grasshopper plug-in for 3D concrete printing numerical simulation in Abaqus*. Jan. 2021. URL: [https://www.youtube.com/watch?v=c8ZcY-4\\_gU4](https://www.youtube.com/watch?v=c8ZcY-4_gU4) (visited on 07/09/2023).
- [26] Concre3DLab Ghent. *Elastic buckling vs plastic collapse in concrete printing*. Aug. 2020. URL: [https://www.youtube.com/watch?v=2Fd1Rk\\_79x4](https://www.youtube.com/watch?v=2Fd1Rk_79x4) (visited on 01/01/2023).
- [27] Keenan Crane, Clarisse Weischedel, and Max Wardetzky. « The heat method for distance computation ». en. In: *Communications of the ACM* 60.11 (Oct. 2017), pp. 90–99. ISSN: 0001-0782, 1557-7317. DOI: 10.1145/3131280. URL: <https://dl.acm.org/doi/10.1145/3131280> (visited on 01/08/2022).
- [28] *CRATerre :: Accueil*. URL: <http://craterre.org/> (visited on 03/03/2023).

- [29] Flávio Craveiro et al. « Additive manufacturing as an enabling technology for digital construction: A perspective on Construction 4.0 ». en. In: *Automation in Construction* 103 (July 2019), pp. 251–267. ISSN: 09265805. DOI: 10.1016/j.autcon.2019.03.011. URL: <https://linkinghub.elsevier.com/retrieve/pii/S0926580518310781> (visited on 07/25/2022).
- [30] *Curvature of a triangle mesh, definition and computation*. - Rodolphe Vaillant's homepage. en. URL: <http://rodolphe-vaillant.fr/entry/33/curvature-of-a-triangle-mesh-definition-and-computation> (visited on 08/06/2023).
- [31] *Digital fabrication / 3D concrete printing*. en. Page. URL: <https://www.ugent.be/ea/structural-engineering/en/research/clusters/themes/digitalfabrication> (visited on 07/09/2023).
- [32] Bojana Dolinar and Ludvik Trauner. « The impact of structure on the undrained shear strength of cohesive soils ». en. In: *Engineering Geology* 92.1-2 (June 2007), pp. 88–96. ISSN: 00137952. DOI: 10.1016/j.enggeo.2007.04.003. URL: <https://linkinghub.elsevier.com/retrieve/pii/S0013795207000877> (visited on 05/07/2023).
- [33] Kathrin Dörfler et al. « Additive Manufacturing using mobile robots: Opportunities and challenges for building construction ». en. In: *Cement and Concrete Research* 158 (Aug. 2022), p. 106772. ISSN: 0008-8846. DOI: 10.1016/j.cemconres.2022.106772. URL: <https://www.sciencedirect.com/science/article/pii/S0008884622000631> (visited on 07/30/2022).
- [34] R. Duballet, O. Baverel, and J. Dirrenberger. « Building systems in robotic extrusion of cementitious materials ». In: *Université Paris Est, Paris* (2019).
- [35] R. Duballet, O. Baverel, and J. Dirrenberger. « Classification of building systems for concrete 3D printing ». en. In: *Automation in Construction* 83 (Nov. 2017), pp. 247–258. ISSN: 0926-5805. DOI: 10.1016/j.autcon.2017.08.018. URL: <https://www.sciencedirect.com/science/article/pii/S0926580516302977> (visited on 03/16/2023).
- [36] Romain Duballet et al. « Free deposition printing for space truss structures ». In: *RILEM International Conference on Concrete and Digital Fabrication*. Springer, 2020, pp. 873–882.
- [37] Nicolas Ducoulombier and Mahan Motamedi. *Plastic collapse of an interlocking clay module*. Ecoles-des ponts Paris-Tech, Aug. 2023. URL: [https://youtu.be/VF\\_PXdXAAS4](https://youtu.be/VF_PXdXAAS4).
- [38] Nicolas Ducoulombier and Mahan Motamedi. *Printing an interlocking clay module with two heat guns*. Ecoles-des ponts Paris-Tech, Aug. 2023. URL: <https://youtube.com/shorts/2D-7z2HzFYs?feature=share>.
- [39] Nicolas Ducoulombier et al. « “The Slug Test”: Inline Assessment of Yield Stress for Extrusion-Based Additive Manufacturing ». en. In: *Second RILEM International Conference on Concrete and Digital Fabrication*. Ed. by Freek P. Bos et al. RILEM Bookseries. Cham: Springer International Publishing, 2020, pp. 216–224. ISBN: 978-3-030-49916-7. DOI: 10.1007/978-3-030-49916-7\_22.



- [40] *El Cosmico*. en. URL: <https://www.iconbuild.com/projects/el-cosmico> (visited on 05/23/2023).
- [41] *ELstudio, » 3D printed shelter*. en-US. URL: <https://www.elstudio.nl/?p=1639> (visited on 08/01/2022).
- [42] *Esfahk mud institute*. URL: <https://esfahkmudcenter.org/en/> (visited on 06/14/2023).
- [43] *Essai sur une application des règles de Maximis & Minimis à quelques Problèmes de Statique, relatifs à l'Architecture. - Physics - Shop | Herman H.J. Lynge & Søn A/S*. en. URL: <https://lynge.com/en/physics/44922-essai-sur-une-application-des-regles-de-maximis-minimis-a-quelques-problemes-de-statique-relatifs-a-larchitecture/> (visited on 05/07/2023).
- [44] Mehdi Farahbakhsh et al. « Impact of robotic 3D printing process parameters on interlayer bond strength ». en. In: *Automation in Construction* 142 (Oct. 2022), p. 104478. ISSN: 0926-5805. DOI: 10.1016/j.autcon.2022.104478. URL: <https://www.sciencedirect.com/science/article/pii/S092658052200351X> (visited on 07/29/2022).
- [45] Michael Fiske et al. *The Disruptive Technology that is Additive Construction: System Development Lessons Learned for Terrestrial and Planetary Applications*. Sept. 2018. DOI: 10.2514/6.2018-5127.
- [46] Laetitia Fontaine and Romain Anger. *Bâtir en terre : du grain de sable à l'architecture*. fr-FR. 70115204-05. Belin, Cite sciences et industrie, 2020. ISBN: 978-2-7011-5204-2. (Visited on 03/03/2023).
- [47] Lee Chin Foo et al. « Classification and Quantification of Construction Waste at Housing Project Site ». en. In: 1.1 (2013).
- [48] S. Ganeshkumar et al. « Investigation of Tensile Properties of Different Infill Pattern Structures of 3D-Printed PLA Polymers: Analysis and Validation Using Finite Element Analysis in ANSYS ». en. In: *Materials* 15.15 (July 2022), p. 5142. ISSN: 1996-1944. DOI: 10.3390/ma15155142. URL: <https://www.mdpi.com/1996-1944/15/15/5142> (visited on 07/06/2023).
- [49] Borja García de Soto et al. « Productivity of digital fabrication in construction: Cost and time analysis of a robotically built wall ». en. In: *Automation in Construction* 92 (Aug. 2018), pp. 297–311. ISSN: 0926-5805. DOI: 10.1016/j.autcon.2018.04.004. URL: <https://www.sciencedirect.com/science/article/pii/S092658051731124X> (visited on 01/08/2022).
- [50] Rodrigo García-Alvarado, Ginnia Moroni-Orellana, and Pablo Banda-Pérez. « Architectural Evaluation of 3D-Printed Buildings ». en. In: *Buildings* 11.6 (June 2021). Number: 6 Publisher: Multidisciplinary Digital Publishing Institute, p. 254. ISSN: 2075-5309. DOI: 10.3390/buildings11060254. URL: <https://www.mdpi.com/2075-5309/11/6/254> (visited on 06/10/2023).
- [51] Dominique Gauzin-Müller. *Architecture En Terre D'Aujourd'Hui*. French. MUSEO. 2017. ISBN: 978-2-37375-028-7.

- [52] Seyed Hamidreza Ghaffar, Jorge Corker, and Mizi Fan. « Additive manufacturing technology and its implementation in construction as an eco-innovative solution ». en. In: *Automation in Construction* 93 (Sept. 2018), pp. 1–11. ISSN: 0926-5805. DOI: 10.1016/j.autcon.2018.05.005. URL: <https://www.sciencedirect.com/science/article/pii/S0926580517309731> (visited on 06/10/2023).
- [53] Pierre Gilibert, Romain Mesnil, and Olivier Baverel. « Rule-based generative design of translational and rotational interlocking assemblies ». en. In: *Automation in Construction* 135 (Mar. 2022), p. 104142. ISSN: 0926-5805. DOI: 10.1016/j.autcon.2022.104142. URL: <https://www.sciencedirect.com/science/article/pii/S0926580522000152> (visited on 03/03/2023).
- [54] Mohamed Gomaa et al. « 3D printing system for earth-based construction: Case study of cob ». en. In: *Automation in Construction* 124 (Apr. 2021), p. 103577. ISSN: 09265805. DOI: 10.1016/j.autcon.2021.103577. URL: <https://linkinghub.elsevier.com/retrieve/pii/S0926580521000285> (visited on 07/18/2022).
- [55] Mohamed Gomaa et al. « Digital manufacturing for earth construction: A critical review ». en. In: *Journal of Cleaner Production* 338 (Mar. 2022), p. 130630. ISSN: 0959-6526. DOI: 10.1016/j.jclepro.2022.130630. URL: <https://www.sciencedirect.com/science/article/pii/S0959652622002712> (visited on 07/31/2022).
- [56] Mohamed Gomaa et al. « Thermal performance exploration of 3D printed cob ». In: *Architectural Science Review* 62.3 (May 2019). Publisher: Taylor & Francis \_eprint: <https://doi.org/10.1080/00038628.2019.1606776>, pp. 230–237. ISSN: 0003-8628. DOI: 10.1080/00038628.2019.1606776. URL: <https://doi.org/10.1080/00038628.2019.1606776> (visited on 06/10/2023).
- [57] *Gramazio Kohler Research*. URL: <https://gramaziokohler.arch.ethz.ch/web/d/projekte/430.html> (visited on 07/31/2022).
- [58] Linda N Groat and David Wang. « Architectural Research Methods ». en. In: ().
- [59] Norman Hack et al. « Structural stay-in-place formwork for robotic in situ fabrication of non-standard concrete structures: A real scale architectural demonstrator ». en. In: *Automation in Construction* 115 (July 2020), p. 103197. ISSN: 0926-5805. DOI: 10.1016/j.autcon.2020.103197. URL: <https://www.sciencedirect.com/science/article/pii/S0926580519303607> (visited on 08/08/2022).
- [60] *HAL Robotics / Unique Automation · Simplified*. en-GB. URL: <https://hal-robotics.com/> (visited on 01/08/2023).
- [61] Mohamad Hanifa, Bruno Figueiredo, and Paulo Mendonca. « Additive Manufacturing Earth-Based Composite: Strategical and Computational Methodology for Building Shell Geometries ». In: Apr. 2023, pp. 61–71. ISBN: 978-3-031-25794-0. DOI: 10.1007/978-3-031-25795-7\_5.

- [62] Guy Earl Harbeck. *Water-loss investigations: Lake Mead studies*. 298. US Government Printing Office, 1958.
- [63] John E. Harding and Paul Shepherd. « Meta-Parametric Design ». English. In: *Design Studies* 52 (Sept. 2017), pp. 73–95. ISSN: 0142-694X. DOI: 10.1016/j.destud.2016.09.005. URL: <https://researchportal.bath.ac.uk/en/publications/meta-parametric-design> (visited on 06/26/2021).
- [64] Jacques Heyman. « The stone skeleton ». en. In: *International Journal of Solids and Structures* 2.2 (Apr. 1966), pp. 249–279. ISSN: 00207683. DOI: 10.1016/0020-7683(66)90018-7. URL: <https://linkinghub.elsevier.com/retrieve/pii/0020768366900187> (visited on 08/06/2023).
- [65] Osama Al-Hussaini. « Volume change behaviour of some geomaterials under combined influence of freeze-thaw and wet-dry cycles: An experimental investigation ». en. phd. Cardiff University, Dec. 2017. URL: <https://orca.cardiff.ac.uk/id/eprint/110778/> (visited on 10/09/2022).
- [66] *ICON (@icon3dtech)* • Instagram photos and videos. URL: <https://www.instagram.com/p/CscA-JX0mjZ/> (visited on 08/06/2023).
- [67] Innovative Techs. *WORLD'S FIRST 3D PRINTED CLAY HOUSES*. May 2023. URL: <https://www.youtube.com/watch?v=20jovj6IHcw> (visited on 06/10/2023).
- [68] *Iran – EARTH ARCHITECTURE*. en-US. Feb. 2021. URL: <https://eartharchitecture.org/?cat=41> (visited on 06/14/2023).
- [69] Jean-Baptiste Iazard et al. « Large-scale 3D printing with cable-driven parallel robots ». en. In: *Construction Robotics* 1.1 (Dec. 2017), pp. 69–76. ISSN: 2509-8780. DOI: 10.1007/s41693-017-0008-0. URL: <https://doi.org/10.1007/s41693-017-0008-0> (visited on 01/16/2022).
- [70] Yohan Jacquet et al. « Gravity induced flow to characterize rheological properties of printable cement-based materials ». en. In: *RILEM Technical Letters* 5 (Dec. 2020), pp. 150–156. ISSN: 2518-0231. DOI: 10.21809/rilemtechlett.2020.128. URL: <https://letters.rilem.net/index.php/rilem/article/view/128> (visited on 10/28/2022).
- [71] Jarett Gross. *ICON 3D PRINTING 100 HOMES ACTIVE SITE*. Feb. 2023. URL: <https://www.youtube.com/watch?v=WzI8ZV5KyfQ> (visited on 05/23/2023).
- [72] Roozbeh Kangari and Tetsuji Yoshida. « Automation in construction ». en. In: *Robotics and Autonomous Systems* 6.4 (Oct. 1990), pp. 327–335. ISSN: 0921-8890. DOI: 10.1016/S0921-8890(05)80014-4. URL: <https://www.sciencedirect.com/science/article/pii/S0921889005800144> (visited on 07/26/2022).
- [73] Laurence Keefe. *Earth Building: Methods and Materials, Repair and Conservation*. en. Google-Books-ID: odt\_AgAAQBAJ. Routledge, May 2012. ISBN: 978-1-134-35017-9.

- [74] Emmanuel Keita et al. « Weak bond strength between successive layers in extrusion-based additive manufacturing: measurement and physical origin ». en. In: *Cement and Concrete Research* 123 (Sept. 2019), p. 105787. ISSN: 00088846. DOI: 10.1016/j.cemconres.2019.105787. URL: <https://linkinghub.elsevier.com/retrieve/pii/S0008884618313760> (visited on 07/18/2022).
- [75] Nader Khalili. *Ceramic Houses: How to build your own*. 1986.
- [76] Nader Khalili. *Racing alone: a visionary architect's quest for houses made with earth and fire*. 1983.
- [77] Nader Khalili. *Sidewalks on the Moon: The Journey of a Mystic Architect Through Tradition, Technology, and Transformation*. en. Cal-Earth Press, 2002. ISBN: 978-1-889625-02-7.
- [78] Harald Kloft et al. « TRR 277: Additive manufacturing in construction ». en. In: *Civil Engineering Design* 3.4 (2021). \_eprint: <https://onlinelibrary.wiley.com/doi/pdf/10.1002/cend.202100026>, pp. 113–122. ISSN: 2625-073X. DOI: 10.1002/cend.202100026. URL: <https://onlinelibrary.wiley.com/doi/abs/10.1002/cend.202100026> (visited on 07/25/2022).
- [79] Terry W. Knight. « Designing with grammars ». In: *CAAD futures*. Vol. 91. Vieweg Wiesbaden, 1992, pp. 19–34.
- [80] Branko Kolarevic. « Digital Fabrication Manufacturing Architecture in the Information Age ». en. In: Buffalo (New York), USA, 2001, pp. 10–12. DOI: 10.52842/conf.acadia.2001.010. URL: <http://papers.cumincad.org/cgi-bin/works/paper/cfd8> (visited on 06/10/2023).
- [81] Jacques Kruger, Stephan Zeranka, and Gideon Van Zijl. « 3D concrete printing: A lower bound analytical model for buildability performance quantification ». en. In: *Automation in Construction* 106 (Oct. 2019), p. 102904. ISSN: 09265805. DOI: 10.1016/j.autcon.2019.102904. URL: <https://linkinghub.elsevier.com/retrieve/pii/S0926580519301852> (visited on 07/02/2023).
- [82] Nathalie Labonnote et al. « Additive construction: State-of-the-art, challenges and opportunities ». en. In: *Automation in Construction* 72 (Dec. 2016), pp. 347–366. ISSN: 0926-5805. DOI: 10.1016/j.autcon.2016.08.026. URL: <https://www.sciencedirect.com/science/article/pii/S0926580516301790> (visited on 07/25/2022).
- [83] Joseph F. Labuz and Arno Zang. « Mohr–Coulomb Failure Criterion ». en. In: *Rock Mechanics and Rock Engineering* 45.6 (Nov. 2012), pp. 975–979. ISSN: 0723-2632, 1434-453X. DOI: 10.1007/s00603-012-0281-7. URL: <http://link.springer.com/10.1007/s00603-012-0281-7> (visited on 05/07/2023).

- [84] Gnanli Landrou, Coralie Brumaud, and Guillaume Habert. « Clay particles as binder for earth buildings materials: a fresh look into rheology of dense clay suspensions ». en. In: *EPJ Web of Conferences* 140 (2017). Ed. by F. Radjai et al., p. 13010. ISSN: 2100-014X. DOI: 10.1051/epjconf/201714013010. URL: <http://www.epj-conferences.org/10.1051/epjconf/201714013010> (visited on 07/22/2023).
- [85] Ian Liddell. « Frei Otto and the development of gridshells ». en. In: *Case Studies in Structural Engineering* 4 (Dec. 2015), pp. 39–49. ISSN: 22143998. DOI: 10.1016/j.csse.2015.08.001. URL: <https://linkinghub.elsevier.com/retrieve/pii/S2214399815300011> (visited on 03/27/2021).
- [86] YABF Liem. « Graphic statics in funicular design: calculating force equilibrium through complementary energy ». In: (2011).
- [87] S. Lim et al. « Developments in construction-scale additive manufacturing processes ». en. In: *Automation in Construction* 21 (Jan. 2012), pp. 262–268. ISSN: 0926-5805. DOI: 10.1016/j.autcon.2011.06.010. URL: <https://www.sciencedirect.com/science/article/pii/S0926580511001221> (visited on 06/10/2023).
- [88] Zhongjie Lin. « Nakagin Capsule Tower: Revisiting the Future of the Recent Past ». en. In: *Journal of Architectural Education* 65.1 (2011). \_eprint: <https://onlinelibrary.wiley.com/doi/pdf/10.1111/j.1531-314X.2011.01158.x>, pp. 13–32. ISSN: 1531-314X. DOI: 10.1111/j.1531-314X.2011.01158.x. URL: <https://onlinelibrary.wiley.com/doi/abs/10.1111/j.1531-314X.2011.01158.x> (visited on 09/17/2022).
- [89] Thomas Linner. « Automated and Robotic Construction: Integrated Automated Construction Sites ». PhD thesis. Technische Universität München, 2013. URL: <https://mediatum.ub.tum.de/1131018> (visited on 07/26/2022).
- [90] Yichang Liu et al. « Topology optimization of shell-infill structures considering buckling constraint ». en. In: *Computers & Structures* 283 (July 2023), p. 107055. ISSN: 00457949. DOI: 10.1016/j.compstruc.2023.107055. URL: <https://linkinghub.elsevier.com/retrieve/pii/S0045794923000858> (visited on 05/06/2023).
- [91] Ena Lloret-Fritschi et al. « Additive Digital Casting: From Lab to Industry ». en. In: *Materials* 15.10 (Jan. 2022). Number: 10 Publisher: Multidisciplinary Digital Publishing Institute, p. 3468. ISSN: 1996-1944. DOI: 10.3390/ma15103468. URL: <https://www.mdpi.com/1996-1944/15/10/3468> (visited on 09/15/2022).
- [92] *Location - Weather Forecast Maps | Ventusky*. en-us. URL: <https://www.ventusky.com/48.851;2.603> (visited on 05/26/2022).
- [93] Dirk Lowke et al. « Particle-bed 3D printing in concrete construction – Possibilities and challenges ». en. In: *Cement and Concrete Research*. SI : Digital concrete 2018 112 (Oct. 2018), pp. 50–65. ISSN: 0008-8846. DOI: 10.1016/j.cemconres.2018.05.018. URL: <https://www.sciencedirect.com/science/article/pii/S000888461731267X> (visited on 08/08/2022).

- [94] M. Luzuriaga. « Replicating Candela's Los Manantiales ». In: *History of Construction Cultures*. CRC Press, 2021, pp. 382–391.
- [95] Mahan Motamedi. *Double Layered Squinch Full video*. Jan. 2023. URL: <https://www.youtube.com/watch?v=oqYdj-8gtes> (visited on 01/13/2023).
- [96] Mahan Motamedi. *Mahan Motamedi's PhD Defense: Scaffold-Free 3D Printing of Earthen Shells*. Dec. 2023. URL: <https://www.youtube.com/watch?v=rcU2kqXnnsQ> (visited on 04/07/2024).
- [97] Mahan Motamedi. *Scaffold Free 3D Printing of a Shell*. Champs-sur-marne, Apr. 2020. URL: <https://www.youtube.com/watch?v=2KnedWnyenw> (visited on 01/11/2023).
- [98] *Maker Economy Starter Kit*. URL: [https://www.3dwasp.com/en/maker-economy-starter-kit/?utm\\_term=&utm\\_campaign=GLOBAL-en-SE-DSA-Sito&utm\\_source=adwords&utm\\_medium=ppc&hsa\\_acc=3352968755&hsa\\_cam=16280182754&hsa\\_grp=139246202851&hsa\\_ad=583042531321&hsa\\_src=g&hsa\\_tgt=dsa-19959388920&hsa\\_kw=&hsa\\_mt=&hsa\\_net=adwords&hsa\\_ver=3&gad=1&gclid=CjwKCAjwvpCkBhB4EiwAujULMoPS4j2RIoS0Tyzw8\\_aj9CV06\\_Y7fGTLXRjcpbsY4Ud6z-5Epw-1ZR0CyMQQAvD\\_BwE](https://www.3dwasp.com/en/maker-economy-starter-kit/?utm_term=&utm_campaign=GLOBAL-en-SE-DSA-Sito&utm_source=adwords&utm_medium=ppc&hsa_acc=3352968755&hsa_cam=16280182754&hsa_grp=139246202851&hsa_ad=583042531321&hsa_src=g&hsa_tgt=dsa-19959388920&hsa_kw=&hsa_mt=&hsa_net=adwords&hsa_ver=3&gad=1&gclid=CjwKCAjwvpCkBhB4EiwAujULMoPS4j2RIoS0Tyzw8_aj9CV06_Y7fGTLXRjcpbsY4Ud6z-5Epw-1ZR0CyMQQAvD_BwE) (visited on 06/10/2023).
- [99] Vasilios Maniatidis and Peter Walker. « A review of rammed earth construction ». In: *Innovation Project "Developing Rammed Earth for UK Housing", Natural Building Technology Group, Department of Architecture & Civil Engineering, University of Bath* 12 (2003).
- [100] Gh Memariam. *[The Persian architecture, construction]*. Farsi. 1st ed. Iran, Tehran: Naghme-no-andish.
- [101] Russ Miller-Johnson. « Fabric Formwork—An Alternative Concrete Construction System ». In: *Structures Congress 2009: Don't Mess with Structural Engineers: Expanding Our Role*. 2009, pp. 1–5.
- [102] J.C Morel et al. « Building houses with local materials: means to drastically reduce the environmental impact of construction ». en. In: *Building and Environment* 36.10 (Dec. 2001), pp. 1119–1126. ISSN: 03601323. DOI: 10.1016/S0360-1323(00)00054-8. URL: <https://linkinghub.elsevier.com/retrieve/pii/S0360132300000548> (visited on 12/11/2021).
- [103] Mahan Motamedi. *"U" Shape wall*. EN. Apr. 2023. URL: <https://youtu.be/Pv12ovWs3Z8>.
- [104] Mahan Motamedi. *Squinch on the wooden wall*. EN. Apr. 2023. URL: <https://youtu.be/LA-NW5cirIQ>.
- [105] Mahan Motamedi. *Vane test*. URL: <https://youtu.be/aMEjvE1Nc88>.
- [106] Mahan Motamedi and Seyed Yahya Islami. « From the Primitive Hut to Architectural RepRaps: The Impact of Additive Manufacturing on the Evolution of Architecture ». In: *Rahpooye Memari-o Shahrsazi* 1.3 (Feb. 2023). Publisher: Soore University, pp. 7–18. ISSN: 2821-1758. DOI: 10.22034/rau.2023.1975774.1019. URL: [http://rau.soore.ac.ir/article\\_703227\\_en.html](http://rau.soore.ac.ir/article_703227_en.html) (visited on 05/10/2023).

- [107] Kumar Neeraj. *Formwork For Concrete Structures*. en. New Delhi, India: Tata McGraw Hill Education Private Limited, 2012. ISBN: (13): 978-1-25-900733-0. (Visited on 07/29/2022).
- [108] Roussel Nicolas et al. « Assessing the fresh properties of printable cement-based materials: High potential tests for quality control ». en. In: *Cement and Concrete Research* 158 (Aug. 2022), p. 106836. ISSN: 0008-8846. DOI: 10.1016/j.cemconres.2022.106836. URL: <https://www.sciencedirect.com/science/article/pii/S0008884622001272> (visited on 10/28/2022).
- [109] *oedometer test - Google Search*. URL: [https://www.google.com/search?rlz=1C1UEAD\\_enFR973FR973&sxsrf=AB5stBjMEkhrG8sD3DBeKqki9sCA0vBjrA:1690039460595&q=oedometer+test&tbm=vid&sa=X&ved=2ahUKEwig09HNz6KAAxV4UKQEhdjiBpwQOpQJegQIDBAB&biw=1620&bih=961&dpr=2#fpstate=ive&vld=cid:ef53d102,vid:5kuw6-axQIw](https://www.google.com/search?rlz=1C1UEAD_enFR973FR973&sxsrf=AB5stBjMEkhrG8sD3DBeKqki9sCA0vBjrA:1690039460595&q=oedometer+test&tbm=vid&sa=X&ved=2ahUKEwig09HNz6KAAxV4UKQEhdjiBpwQOpQJegQIDBAB&biw=1620&bih=961&dpr=2#fpstate=ive&vld=cid:ef53d102,vid:5kuw6-axQIw) (visited on 07/22/2023).
- [110] Robin Oval et al. « Feature-based Topology Finding of Patterns for Shell Structures ». In: *Automation in Construction* (Feb. 2019). DOI: 10.1016/j.autcon.2019.02.008.
- [111] Alexander Paolini, Stefan Kollmannsberger, and Ernst Rank. « Additive manufacturing in construction: A review on processes, applications, and digital planning methods ». en. In: *Additive Manufacturing* 30 (Dec. 2019), p. 100894. ISSN: 2214-8604. DOI: 10.1016/j.addma.2019.100894. URL: <https://www.sciencedirect.com/science/article/pii/S2214860419309029> (visited on 07/25/2022).
- [112] Stefana Parascho et al. « Robotic vault: A cooperative robotic assembly method for brick vault construction ». In: *Construction Robotics* 4.3 (2020). Publisher: Springer, pp. 117–126.
- [113] Suvash Chandra Paul et al. « A review of 3D concrete printing systems and materials properties: current status and future research prospects ». In: *Rapid Prototyping Journal* 24.4 (Jan. 2018). Publisher: Emerald Publishing Limited, pp. 784–798. ISSN: 1355-2546. DOI: 10.1108/RPJ-09-2016-0154. URL: <https://doi.org/10.1108/RPJ-09-2016-0154> (visited on 07/29/2022).
- [114] *Pennacchi a tromba nell'architettura islamica | Dalla Realtà al Progetto - Dal Progetto alla Realtà*. URL: <https://smart.seieditrice.com/materiali/contenuti-digitali/disegno-bien/html-dalla-realta-al-progetto/da-geometrie-rette-curve/pennacchi-tromba-nellarchitettura-islamica.html> (visited on 06/14/2023).
- [115] PERI. *PERI Group - Formwork, Scaffolding, Engineering*. en. URL: <https://www.peri.com/en> (visited on 08/01/2022).
- [116] A. Perrot, D. Rangeard, and E. Courteille. « 3D printing of earth-based materials: Processing aspects ». en. In: *Construction and Building Materials* 172 (May 2018), pp. 670–676. ISSN: 09500618. DOI: 10.1016/j.conbuildmat.2018.04.017. URL: <https://linkinghub.elsevier.com/retrieve/pii/S0950061818308079> (visited on 01/16/2022).

- [117] A. Perrot, D. Rangeard, and A. Pierre. « Structural built-up of cement-based materials used for 3D-printing extrusion techniques ». en. In: *Materials and Structures* 49.4 (Apr. 2016), pp. 1213–1220. ISSN: 1871-6873. DOI: 10.1617/s11527-015-0571-0. URL: <https://doi.org/10.1617/s11527-015-0571-0> (visited on 10/28/2022).
- [118] Alban Pinel et al. « Earthen construction: Demonstration of feasibility at 1/2 scale of poured clay concrete construction ». en. In: *Construction and Building Materials* 312 (Dec. 2021), p. 125275. ISSN: 0950-0618. DOI: 10.1016/j.conbuildmat.2021.125275. URL: <https://www.sciencedirect.com/science/article/pii/S0950061821030166> (visited on 07/30/2022).
- [119] C. S. Poon, Ann T. W. Yu, and L. Jaillon. « Reducing building waste at construction sites in Hong Kong ». In: *Construction Management and Economics* 22.5 (June 2004). Publisher: Routledge \_eprint: <https://doi.org/10.1080/0144619042000202816>, pp. 461–470. ISSN: 0144-6193. DOI: 10.1080/0144619042000202816. URL: <https://doi.org/10.1080/0144619042000202816> (visited on 02/26/2023).
- [120] Ronald Rael and Virginia San Fratello. « Clay Bodies: Crafting the Future with 3D Printing ». en. In: *Architectural Design* 87.6 (Nov. 2017), pp. 92–97. ISSN: 00038504. DOI: 10.1002/ad.2243. URL: <https://onlinelibrary.wiley.com/doi/10.1002/ad.2243> (visited on 07/18/2022).
- [121] Lex Reiter et al. « The role of early age structural build-up in digital fabrication with concrete ». en. In: *Cement and Concrete Research* 112 (Oct. 2018), pp. 86–95. ISSN: 00088846. DOI: 10.1016/j.cemconres.2018.05.011. URL: <https://linkinghub.elsevier.com/retrieve/pii/S0008884617312930> (visited on 07/18/2022).
- [122] Carlos F. Revelo and Henry A. Colorado. « 3D printing of kaolinite clay ceramics using the Direct Ink Writing (DIW) technique ». en. In: *Ceramics International* 44.5 (Apr. 2018), pp. 5673–5682. ISSN: 02728842. DOI: 10.1016/j.ceramint.2017.12.219. URL: <https://linkinghub.elsevier.com/retrieve/pii/S0272884217329280> (visited on 07/18/2022).
- [123] M. J. Rietema. *Design of a solar sand printer*. en. Internship report. Publisher: University of Twente. Oct. 2013. URL: <http://essay.utwente.nl/69808/> (visited on 08/08/2022).
- [124] Matthias Rippmann. « Funicular Shell Design: Geometric approaches to form finding and fabrication of discrete funicular structures ». en. Doctoral Thesis. ETH Zurich, 2016. DOI: 10.3929/ethz-a-010656780. URL: <https://www.research-collection.ethz.ch/handle/20.500.11850/116926> (visited on 01/17/2022).
- [125] Matthias Rippmann and Philippe Block. « Rethinking structural masonry: unreinforced, stone-cut shells ». en. In: *Proceedings of the Institution of Civil Engineers - Construction Materials* 166.6 (Dec. 2013), pp. 378–389. ISSN: 1747-650X, 1747-6518. DOI: 10.1680/coma.12.00033. URL: <http://www.icevirtuallibrary.com/doi/10.1680/coma.12.00033> (visited on 12/03/2020).



- [126] Athanasios Rodiftsis. « From the ground up: Robotic Additive Manufacturing (RAM) of a structurally optimized earthen shell through computational design ». en. PhD Thesis. Delft, Netherlands: Delft University of Technology (TU Delft), 2020. URL: <https://repository.tudelft.nl/islandora/object/uuid%3A1d54f0e4-be53-4fe0-9dee-bbad9a09635f> (visited on 01/11/2021).
- [127] Ulrich Röhlen and Christof Ziegert. *Construire en terre crue - Construction-Rénovation-Finitions*. fr. Paris: LE MONITEUR, 2013. ISBN: 978-2-281-11567-3. URL: [www.editionsdumoniteur.com](http://www.editionsdumoniteur.com).
- [128] Rael Ronald. *Casa Covida*. en-US. 2021. URL: <https://www.rael-sanfratello.com/made/casa-covida> (visited on 01/08/2022).
- [129] Nicolas Roussel. « Rheological requirements for printable concretes ». en. In: *Cement and Concrete Research* 112 (Oct. 2018), pp. 76–85. ISSN: 00088846. DOI: 10.1016/j.cemconres.2018.04.005. URL: <https://linkinghub.elsevier.com/retrieve/pii/S000888461830070X> (visited on 07/18/2022).
- [130] Nicolas Roussel et al. « Numerical simulations of concrete processing: From standard formative casting to additive manufacturing ». en. In: *Cement and Concrete Research* 135 (Sept. 2020), p. 106075. ISSN: 0008-8846. DOI: 10.1016/j.cemconres.2020.106075. URL: <https://www.sciencedirect.com/science/article/pii/S0008884620301083> (visited on 03/10/2023).
- [131] Moshe Safdie. « Habitat '67-Towards the Development of a Building System ». In: *PCI JOURNAL* 12 (1967), pp. 60–66.
- [132] Valentino Sangiorgio et al. « The New Boundaries of 3D-Printed Clay Bricks Design: Printability of Complex Internal Geometries ». en. In: *Sustainability* 14.2 (Jan. 2022), p. 598. ISSN: 2071-1050. DOI: 10.3390/su14020598. URL: <https://www.mdpi.com/2071-1050/14/2/598> (visited on 07/18/2022).
- [133] S. El-Sayegh, L. Romdhane, and S. Manjikian. « A critical review of 3D printing in construction: benefits, challenges, and risks ». en. In: *Archives of Civil and Mechanical Engineering* 20.2 (Mar. 2020), p. 34. ISSN: 1644-9665. DOI: 10.1007/s43452-020-00038-w. URL: <https://doi.org/10.1007/s43452-020-00038-w> (visited on 07/24/2022).
- [134] H. -J. Schek. « The force density method for form finding and computation of general networks ». en. In: *Computer Methods in Applied Mechanics and Engineering* 3.1 (Jan. 1974), pp. 115–134. ISSN: 0045-7825. DOI: 10.1016/0045-7825(74)90045-0. URL: <https://www.sciencedirect.com/science/article/pii/0045782574900450> (visited on 04/03/2021).
- [135] Marcel Schweiker et al. « Ten questions concerning the potential of digital production and new technologies for contemporary earthen constructions ». en. In: *Building and Environment* 206 (Dec. 2021), p. 108240. ISSN: 03601323. DOI: 10.1016/j.buildenv.2021.108240. URL: <https://linkinghub.elsevier.com/retrieve/pii/S0360132321006417> (visited on 12/12/2021).
- [136] Clare Scott. *Apis Cor 3D Prints a House in 24 Hours and Creates a Technological Showcase*. en-US. Feb. 2017. URL: <https://3dprint.com/166389/apis-cor-3d-printed-house-russia/> (visited on 06/10/2023).

- [137] *Solar Sinter*. en-US. URL: <https://kayserworks.com/798817030644> (visited on 06/10/2023).
- [138] Borja Garcia de Soto and Mirosław J. Skibniewski. « Future of robotics and automation in construction ». In: *Construction 4.0*. Num Pages: 18. Routledge, 2020. ISBN: 978-0-429-39810-0.
- [139] *Standard Test Methods for Laboratory Determination of Water (Moisture) Content of Soil and Rock by Mass*. en. URL: <https://www.astm.org/d2216-19.html> (visited on 02/06/2024).
- [140] *Surface Radiation Absorptivity*. URL: [https://www.engineeringtoolbox.com/radiation-surface-absorptivity-d\\_1805.html](https://www.engineeringtoolbox.com/radiation-surface-absorptivity-d_1805.html) (visited on 07/04/2023).
- [141] Yeşim Tarhan et al. « Sustainable Materials for Additive Manufacturing: Earth-Based Concrete ». In: May 2021, pp. 708–716. ISBN: 978-3-030-75314-6. DOI: 10.1007/978-3-030-75315-3\_75.
- [142] The Efficient Engineer. *Understanding Thermal Radiation*. Nov. 2021. URL: [https://www.youtube.com/watch?v=FDmYCI\\_xY1A](https://www.youtube.com/watch?v=FDmYCI_xY1A) (visited on 07/04/2023).
- [143] Julia Tourtelot et al. « Yield stress measurement for earth-based building materials: the weighted plunger test ». en. In: *Materials and Structures* 54.1 (Feb. 2021), p. 6. ISSN: 1359-5997, 1871-6873. DOI: 10.1617/s11527-020-01588-4. URL: <http://link.springer.com/10.1617/s11527-020-01588-4> (visited on 03/28/2021).
- [144] Snehasis Tripathy, Mohd Yuhyi M. Tadza, and Hywel Rhys Thomas. « Soil-water characteristic curves of clays ». In: *Canadian Geotechnical Journal* 51.8 (Aug. 2014). Publisher: NRC Research Press, pp. 869–883. ISSN: 0008-3674. DOI: 10.1139/cgj-2013-0089. URL: <https://cdnsiencepub.com/doi/full/10.1139/cgj-2013-0089> (visited on 08/10/2023).
- [145] Paul J. Uno. « Plastic shrinkage cracking and evaporation formulas ». In: *ACI Materials Journal* 95 (1998). Publisher: AMERICAN CONCRETE INSTITUTE, pp. 365–375.
- [146] Valentin. *How to Glue Clay: Including Air-Dry Clay And Polymer Clay*. en-US. Section: Air dry clay. May 2020. URL: <https://craftknight.com/how-to-glue-clay-including-air-dry-clay-and-polymer-clay/> (visited on 05/13/2023).
- [147] Henri Van Damme and Hugo Houben. « Earth concrete. Stabilization revisited ». en. In: *Cement and Concrete Research* 114 (Dec. 2018), pp. 90–102. ISSN: 00088846. DOI: 10.1016/j.cemconres.2017.02.035. URL: <https://linkinghub.elsevier.com/retrieve/pii/S0008884616308365> (visited on 03/28/2021).
- [148] Diederik Veenendaal and Philippe Block. « Design process for prototype concrete shells using a hybrid cable-net and fabric formwork ». en. In: *Engineering Structures* 75 (Sept. 2014), pp. 39–50. ISSN: 0141-0296. DOI: 10.1016/j.engstruct.2014.05.036. URL: <https://www.sciencedirect.com/science/article/pii/S0141029614003344> (visited on 08/08/2022).

- [149] R. J. M. Wolfs, F. P. Bos, and T. A. M. Salet. « Early age mechanical behaviour of 3D printed concrete: Numerical modelling and experimental testing ». en. In: *Cement and Concrete Research* 106 (Apr. 2018), pp. 103–116. ISSN: 0008-8846. DOI: 10.1016/j.cemconres.2018.02.001. URL: <https://www.sciencedirect.com/science/article/pii/S000888461730532X> (visited on 10/09/2022).
- [150] Kaufui V. Wong and Aldo Hernandez. « A Review of Additive Manufacturing ». en. In: *ISRN Mechanical Engineering* 2012 (Aug. 2012), pp. 1–10. ISSN: 2090-5130. DOI: 10.5402/2012/208760. URL: <https://www.hindawi.com/journals/isrn/2012/208760/> (visited on 07/25/2022).
- [151] Hao Wu et al. « Digital Design and Fabrication of a 3D Concrete Printed Funicular Spatial Structure ». en. In: Sydney, Australia, 2022, pp. 71–80. DOI: 10.52842/conf.caadria.2022.2.071. URL: [http://papers.cumincad.org/cgi-bin/works/paper/caadria2022\\_406](http://papers.cumincad.org/cgi-bin/works/paper/caadria2022_406) (visited on 05/10/2023).
- [152] Guang-Zhong Yang. « Digital architecture and robotic construction ». In: *Science Robotics* 2.5 (Apr. 2017). Publisher: American Association for the Advancement of Science, ean3673. DOI: 10.1126/scirobotics.aan3673. URL: <https://www.science.org/doi/full/10.1126/scirobotics.aan3673> (visited on 09/18/2022).
- [153] Dianjin Zhang et al. « 3D printing lunar architecture with a novel cable-driven printer ». en. In: *Acta Astronautica* 189 (Dec. 2021), pp. 671–678. ISSN: 0094-5765. DOI: 10.1016/j.actaastro.2021.09.034. URL: <https://www.sciencedirect.com/science/article/pii/S009457652100518X> (visited on 01/08/2022).
- [154] Xu Zhang et al. « Large-scale 3D printing by a team of mobile robots ». en. In: *Automation in Construction* 95 (Nov. 2018), pp. 98–106. ISSN: 0926-5805. DOI: 10.1016/j.autcon.2018.08.004. URL: <https://www.sciencedirect.com/science/article/pii/S0926580518304011> (visited on 07/30/2022).